AD-A122 025 GROUND RUNUP NOISE SUPPRESSION PROGRAM PART 3 DRY SUPPRESSOR TECHNOLOGY BASE(U) NAVAL OCEAN SYSTEMS CENTER SAN DIEGO CA R GLASS ET AL. 20 JUN 82 1/3

UNCLASSIFIED NOSC/TR-674 F/G 20/1 NL

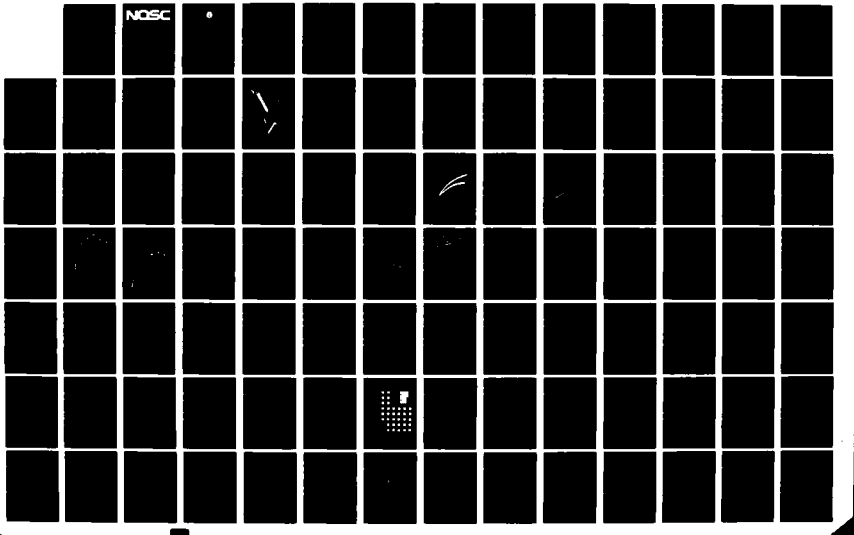

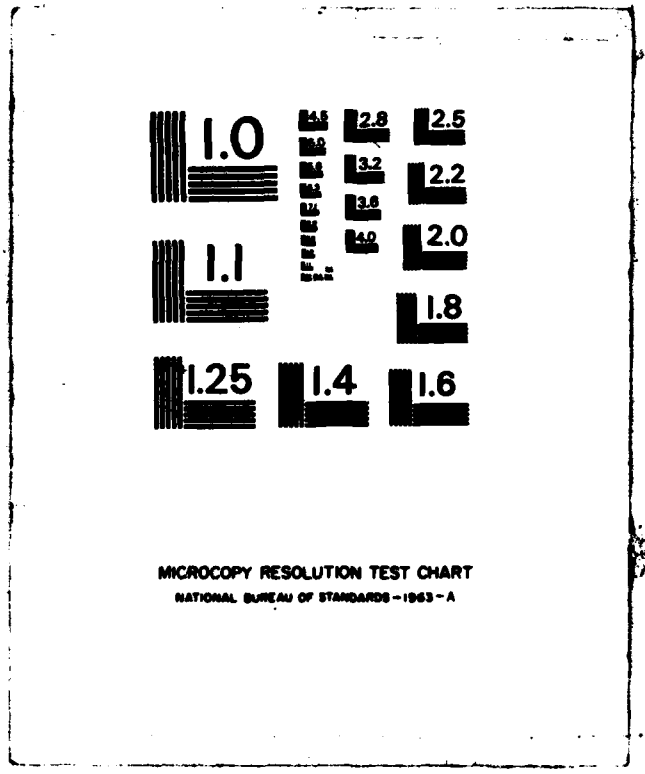
1.0
1.1
1.25
1.4
1.6
1.8
2.0
2.2
2.5
2.8
3.2
3.6
4.0
4.5
MICROCOPY RESOLUTION TEST CHART
NATIONAL BUREAU OF STANDARDS-1963-A

AD A122025

NOSC

NOSC TR 674

NOSC TR 674

Technical Report 674

GROUND RUNUP NOISE SUPPRESSION PROGRAM

Part 3 – Dry Suppressor Technology Base

R Glass
M Lepor

20 June 1982

Final Report: July 1974 - October 1980

Prepared for
Naval Facilities Engineering Command
NAVFAC 032P

"Original contains color plates: All DTIC reproductions will be in black and white"

DTIC FILE COPY

Approved for public release; distribution unlimited

NAVAL OCEAN SYSTEMS CENTER
SAN DIEGO, CALIFORNIA 92152

DTIC
ELECTE
DEC 1 1982
A

82 12 01 037

NAVAL OCEAN SYSTEMS CENTER, SAN DIEGO, CA 92152

AN ACTIVITY OF THE NAVAL MATERIAL COMMAND

SL GUILLE, CAPT, USN
Commander

HL BLOOD
Technical Director

ADMINISTRATIVE INFORMATION

Work was conducted by personnel of the Naval Ocean Systems Center, San Diego, as part of the Ground Runup Noise Suppression Program of the Naval Facilities Engineering Command under NAVFAC Element 63721N, Project Y0817-SL, Task Area Y0817-SL, Work Unit 512-MB06. This report, Part 3, summarizes the dry suppressor technology data base developed from July 1974 to October 1980 and was approved for publication on 20 June 1982.

Overall program guidance and review were provided by SM Hurley (NAVFAC 032P) of the Naval Facilities Engineering Command.

Released by
S Yamamoto, Head
Marine Sciences Division

Under authority of
HO Porter, Head
Biosciences Department

METRICATION

To convert from	to	multiply by
inch	meter	0.025 4
lb/ft^2	kg/m^2	4.882 4
pound	kg	0.453 5
ft^2	m^2	0.092 9
inch of water (60°F)	Pa	248.84

UNCLASSIFIED

SECURITY CLASSIFICATION OF THIS PAGE (When Data Entered)

REPORT DOCUMENTATION PAGE		READ INSTRUCTIONS BEFORE COMPLETING FORM
1. REPORT NUMBER NOSC Technical Report 674 (TR 674)	2. GOVT ACCESSION NO. AD-A122025	3. RECIPIENT'S CATALOG NUMBER
4. TITLE (and Subtitle) GROUND RUNUP NOISE SUPPRESSION PROGRAM Part 3 - Dry Suppressor Technology Base		5. TYPE OF REPORT & PERIOD COVERED Final Report July 1974 - October 1980 6. PERFORMING ORG. REPORT NUMBER
7. AUTHOR(s) R Glass M Lepor		8. CONTRACT OR GRANT NUMBER(s)
9. PERFORMING ORGANIZATION NAME AND ADDRESS Naval Ocean Systems Center San Diego, CA 92152		10. PROGRAM ELEMENT, PROJECT, TASK AREA & WORK UNIT NUMBERS 63721N, Y0817-SL Y0817-SL, 512-MB06
11. CONTROLLING OFFICE NAME AND ADDRESS Naval Facilities Engineering Command 032P Alexandria, VA 22332		12. REPORT DATE 20 June 1982 13. NUMBER OF PAGES 194
14. MONITORING AGENCY NAME & ADDRESS(if different from Controlling Office)		15. SECURITY CLASS. (of this report) UNCLASSIFIED 15a. DECLASSIFICATION/DOWNGRADING SCHEDULE

16. DISTRIBUTION STATEMENT (of this Report)

Approved for public release; distribution unlimited

17. DISTRIBUTION STATEMENT (of the abstract entered in Block 20, if different from Report)

18. SUPPLEMENTARY NOTES

19. KEY WORDS (Continue on reverse side if necessary and identify by block number)

Aircraft engine noise	Air pollution
Aircraft exhaust	Noise pollution
Noise reduction	Test cells

20. ABSTRACT (Continue on reverse side if necessary and identify by block number)

In Part 1 of this report (Executive Summary, 25 March 1981) the technology for augmenter tube and Coanda/refraction air-cooled suppressors is summarized. Use of scale-model tests for aerothermal and acoustic parameter evaluation is discussed. Results of material and material fabrication testing in full-scale air-cooled suppressors are presented. Use of air-cooled suppressor technologies for augmenter tube and Coanda/refraction designs versus existing water-cooled technology is evaluated.

Part 2 describes program progression between July 1974 and October 1980, providing objectives and background information, a chronological summary of suggested efforts, requested and actual funding levels, and a listing of associated NOSC-sponsored research projects. (Continued)

DD FORM 1 JAN 73 1473 EDITION OF 1 NOV 65 IS OBSOLETE

S/N 0102-LF-014-6601

UNCLASSIFIED

SECURITY CLASSIFICATION OF THIS PAGE (When Data Entered)

20. Continued.

Part 3 summarizes the dry suppressor technology base.

CONTENTS

FINAL REPORT — GROUND RUNUP NOISE SUPPRESSION PROGRAM

PART 3 — DRY SUPPRESSOR TECHNOLOGY BASE

DDC QUALITY INSPECTED 2

Dist. Special
A

CONTENTS (Continued)

CONTENTS (Continued)

CONTENTS (Continued)

LIST OF FIGURES

CONTENTS (Continued)

CONTENTS (Continued)

CONTENTS (Continued)

CONTENTS (Continued)

LIST OF TABLES

SUMMARY

The Ground Runup Noise Suppression Final Report consists of three documents. The first document, Part 1, is an executive summary which provides a brief, technical description and overview of the program conducted at the Naval Ocean Systems Center (NOSC). The second document, Part 2, provides a documented history of NOSC's participation in the Dry Jet Noise Suppression Program. This document, Part 3, is a technical summary of the information and data developed during the program.

This report integrates predictive techniques, scale-model test results, and full-scale test results for the new air-cooled noise suppressor technology. All program data are summarized to assist the architect/engineer in the design of air-cooled noise suppressors. Included are aerothermal, aeroacoustic, and pressure data in addition to acoustic material life cycle information. Cost/benefit techniques are included to aid in the selection of air-cooled or water-cooled facilities based on operational requirements.

FINAL REPORT — GROUND RUNUP NOISE SUPPRESSION PROGRAM

PART 3 — DRY SUPPRESSOR TECHNOLOGY BASE

I. INTRODUCTION

The Navy has developed a technology base for jet aircraft ground runup noise suppressors using air-cooled exhaust. The Navy has applied the technology primarily to full-scale aircraft acoustic enclosures (Hush Houses). The technology is also applicable to gas turbine engine test cell design. Scale-model tests and full-scale evaluations were used to design four acoustic enclosures and one demonstration exhaust section.

This report provides a summary of aerothermal/acoustic scale-model tests and full-scale evaluations. Data from five design/construction programs and problem-specific research efforts form the basis of this report. Data presented apply to air-cooled exhaust technology for full acoustic enclosures, hybrid acoustic enclosures, and gas turbine engine test cells. The intention of this document is to provide, in one place, the technology base, the source documents which identify that technology base, and the scale-model test hardware available for further research efforts.

The Navy supported development of two technologies for air-cooled jet engine noise suppression. The augmenter tube technology uses a round or obround tube of varying lengths lined with acoustic material. The Coanda/refraction technology uses a curved surface where jet exhaust flow attaches to the turning surface and noise separates at 90 degrees from the hot exhaust gas. Acoustic absorption is achieved by lining a plenum which encloses the curved surface.

The Naval Facilities Engineering Command (NAVFAC) led the development of the augmenter tube technology. The augmenter tube technology has been tested in Fleet operation at the Naval Air Station, Miramar. Fluidyne Engineering Corporation, Bolt Beranek and Newman Incorporated, and Gustav Getter Associates performed analytical, scale-model, and full-scale design evaluations.

The Naval Air Engineering Center (NAEC) led the development of the Coanda/refraction technology. The Coanda technology has not been tested in Fleet operation. The Boeing Wichita Company performed analytical, scale-model and full-scale demonstration unit design/construction efforts under the direction of NAEC.

The Naval Ocean Systems Center (NOSC) served as an independent technical evaluator of the two air-cooled suppressor technologies. Under an advanced development research effort NOSC evaluated acoustical lining materials and updated acoustic design considerations. The Navy Civil Engineering Laboratory, Naval Regional Medical Center, San Diego, Naval Air Test Center Patuxent River, Rohr Industries, Science Applications Inc, and Western Electro Acoustics Laboratory performed research efforts under the direction of NOSC. These efforts investigated suppressor unique noise environments, sonic/thermal fatigue potential, and cost/risk considerations.

II. AUGMENTER TUBE TECHNOLOGY

The augmenter tube air-cooled dry exhaust technology was developed as part of the Navy's Acoustical Enclosure (Hush House) Program. The efforts included analytical, scale-model (1/15 scale) and full-scale evaluation of aerothermal/acoustical parameters. Scale-model tests predicted subsequent full-scale test results accurately. The augmenter tube data summarized in the following pages are applicable to full aircraft enclosures or engine test cell enclosures.

A. COMPONENTS

The augmenter tube is composed of five primary components. Figure 2-1 shows the augmenter tube attached to a full aircraft enclosure.

Bellmouth. The function of the bellmouth is to smooth the air flow (augmented air) from the aircraft/engine enclosure into the augmenter tube. This provides more efficient cooling of the engine exhaust gases.

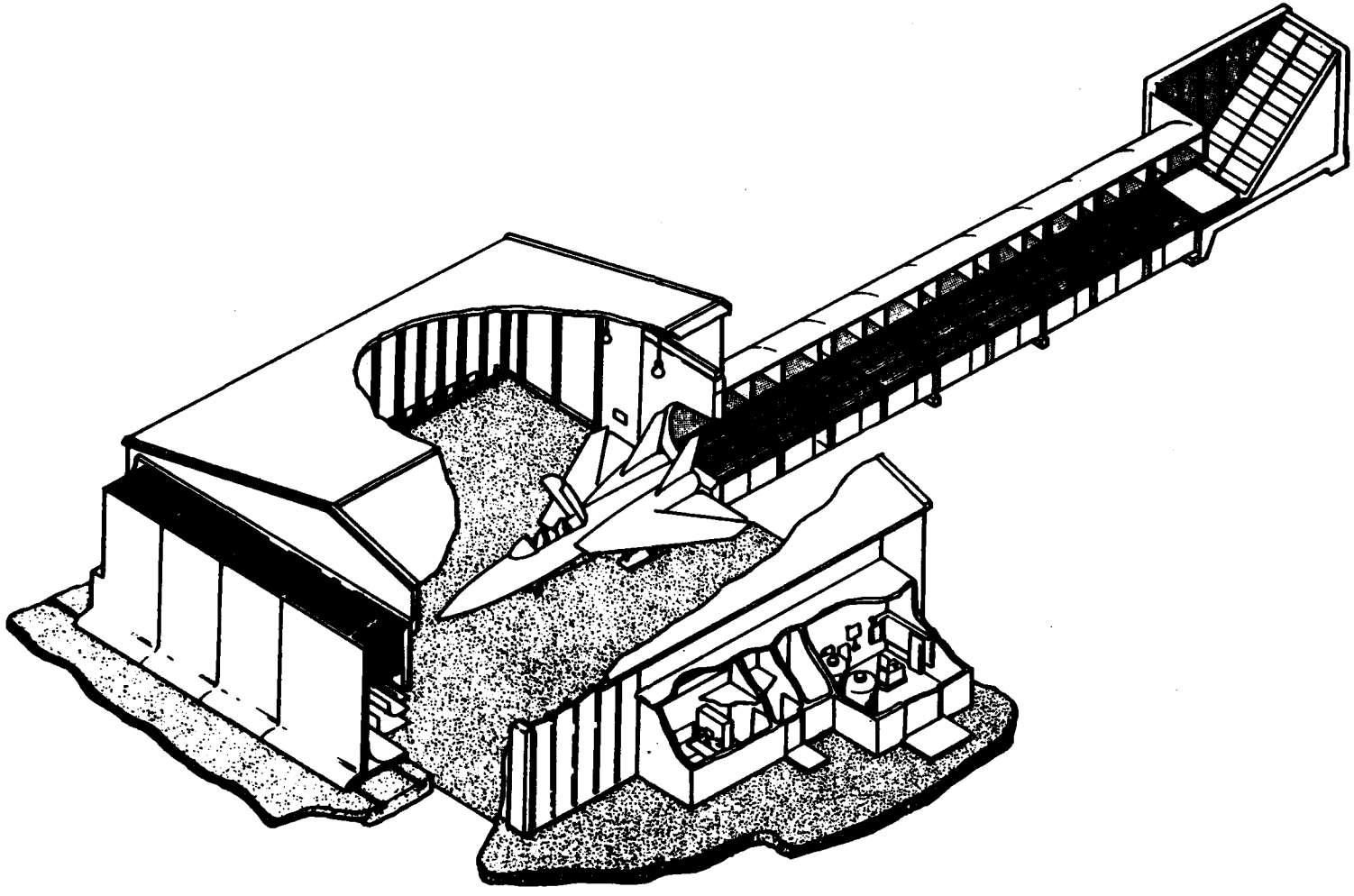

Figure 2-1. Cutaway -- acoustical enclosure with augmenter tube.

Augmenter Tube Shell. The augmenter tube shell provides the frame which directs the hot exhaust flow and which houses the acoustic treatment which attenuates the noise mixed in the exhaust flow. The tube is horizontal.

Acoustic Treatment Pillows. The acoustic treatment pillows are located on the inside of the augmenter shell. The acoustic treatment lines the augmenter shell and attenuates the noise in the exhaust flow. The acoustic treatment consists of pillows of fibrous materials wrapped with stainless steel mesh and fiberglass cloth and covered with corrugated, perforated metal sheets.

45-Degree Ramp. The 45-degree ramp located at the exit end of the augmenter tube is used to redirect the engine exhaust. The ramp also reduces regeneration of noise.

5. Forward Enclosure. The acoustical enclosure forward of the augmenter tube must be designed to be compatible with the aerothermal/acoustic requirements of the augmenter tube. The movable doors forward of the enclosure are designed to house a large turning vane input area for induction of augmented air. The reinforced concrete wall of the enclosure is lined with an acoustic absorbing material.

B. SUPPRESSOR DYNAMICS

The turbulent hot engine exhaust flow is cooled by mixing with the induced augmented air while propagating down a 90-foot length of augmenter tube. The acoustic energy in the flow propagates at 90 degrees to the exhaust flow and impinges on the acoustic absorbing treatment lining the tube.

C. DESIGN CONSIDERATIONS

1. Overview. Three principal design areas have direct applicability to the augmenter tube air-cooled dry sound suppressor. First, augmenter pumping (augmentation ratio) affects induction of air into the engine and secondary air for augmenter tube cooling. Second, augmenter wall temperatures are

related to augmenter pumping and jet impingement on the walls of the tubes. Lastly, augmenter noise reduction design must consider the aerothermal performance of the air-cooled suppressor. Based on aerodynamic, thermodynamic, and acoustic scale-model test data (ref 1-4) and full-scale test data (ref 5, 6), the following design-related conclusions are reached:

a. By using the aircraft jet exhaust momentum flux directed into an augmenter tube, sufficient secondary air can be pumped to cool the exhaust of an afterburning engine even without a subsonic diffuser on the augmenter exit provided that the augmenter cross section is adequately large and the flow leaving the augmenter is not restricted.

b. At afterburning jet temperature conditions, the augmenter pumping performance (augmentation ratio) varied little over the range of augmenter length-diameter ratios tested, indicating that the augmenter length can be chosen entirely on the basis of the required noise reduction.

c. The augmenter pumping performance did not vary significantly with jet nozzle pressure ratio, the axial position of the nozzle exit, or augmenter entrance (bellmouth) configuration.

---

[1] Fluidyne Engineering Report, Aerodynamic and Acoustic Tests of a 1/15 Scale Model Dry Cooled Jet Aircraft Runup Noise Suppression System, October 1975

[2] Fluidyne Engineering Report, Reducing the Acoustic Treatment Exposure Temperature in a Dry Cooled Augmenter During F-14A Operation, December 1976 - reproduced as NOSC TN 125, April 1977

[3] Western Electro-Acoustic Laboratory Report, 1/15 Scale Model Testing of Dry Cooled Jet Engine Noise Suppressor Using a Hot Jet Simulating the TF-30-P-412 Fan Jet Engine, August 1980

[4] Fluidyne Engineering Report, 1/15 Scale Cold Flow Model Tests of the Patuxent River Hush House Configuration, December 1977

[5] Naval Air Engineering Center, report number NAEC-65ED-96, Experimental Evaluation of NAS Miramar Hush House (Project P-114), February 1976

[6] Fluidyne Engineering Report, Aero-Thermo and Acoustical Data from the Post-Construction Checkout of the Miramar #2 and El Toro Hush Houses, April 1979

d. At afterburning jet temperature conditions a hardwalled round non-absorptive augmenter pumps 10% less than an absorptive obround augmenter with the same cross-sectional area.

e. With the obround augmenter, moving the jet nozzle centerline laterally off the augmenter center or deflecting it toward the wall results in decreased pumping and elevated wall temperatures.

f. The addition of a 45 degree exit ramp causes a small reduction in pumping performance.

g. As long as a reasonable distance is maintained between the aircraft exhaust nozzle exit and the augmenter entrance ($X_N/D_{AM} = 0.33$), there will be no excess pumpdown of the nozzle base pressure inside the Hush House.

h. The acoustically absorptive augmenter configurations provided greater noise reduction than the none absorptive augmenter using a vertical stack with parallel baffles.

i. Hush House interior noise levels due to jet exhaust increase significantly if the distance between the jet nozzle exit and augmenter inlet is increased above $X_N/D_{NT} = 2.0$, while the exterior exhaust noise levels decrease as this distance increases.

j. Because of the large relocating temperature gradients in the exhaust flow, the sound in the flow is diffracted toward the lined augmenter wall, thereby resulting in much higher insertion loss than one would predict from simple duct theory.

k. The exit flow, characterized by its speed and velocity, generates aerodynamic noise (self-noise) which places an upper limit on the actual insertion loss achievable by the exhaust system.

l. The presence of an acoustical lining in the upstream end of the augmenter results in a significant reduction in acoustical enclosure interior noise due to jet exhaust.

m. The 45 degree ramp provides significant noise reduction.

n. A screen diffuser can provide measurable noise control.

o. Throttling devices do not aid noise control.

p. A pressure/temperature rake located in the high velocity flow acts as a noise generator.

q. There are optimal locations for exterior noise reduction due to the placement of absorptively lined sections in the augmenter tube; positions from the center of the augmenter tube to the 45 degree ramp were most effective.

r. An ineffectively designed exhaust turning vane system could result in the generation of higher self-noise levels than the 45 degree ramp system. A more effectively designed turning vane configuration used in another model test indicated that turning vane generated noise can be reduced to the same level as ramp generated noise.

s. Exhaust stack extensions used with the 45 degree ramp are ineffective.

t. Exhaust stack extensions used with turning vanes are very effective.

u. The exhaust stack flow distribution for the turning vane system is more uniform than that for the 45 degree ramp. The packing effect is minimized.

2. Initial Design Approach. The primary aim of this report section is to provide information extracted from the model test data and full-scale evaluation data in a form which makes it useful for the design of a future Hush House or makes it possible to predict the performance of an existing Hush House with different aircraft installed. The following parts of this section present an approach for suppressor design. The results are applied (as an

example) to predict the performance of the NAS Miramar Hush House with the F-14A aircraft.

The application of empirically derived data to the design of a typical sound-absorbing dry (air-cooled) augmenter for one or more aircraft types is a trial and error procedure. One must predict augmenter cross-sectional sizes, shapes, and lengths in terms of augmenter pumping, wall temperature, and acoustic goals. A block diagram summarizing the augmenter design procedure is presented in figure 2-2.

a. Augmenter Sizing for Flow Noise. The first step in the design procedure is to find the augmenter cross-sectional shape of smallest area which will (a) provide a low enough augmenter exit flow velocity so that the noise created by the flow leaving the augmenter tube is not excessive, and (b) avoid excessive wall temperatures (T_{wall} = 900°F is acceptable).

To keep the noise generated by the augmenter exit flow within acceptable limits, the ratio of augmenter cross-sectional area to maximum jet nozzle throat area must satisfy the criteria listed in table 2-1.

After determining the minimum augmenter cross-sectional area which will satisfy the flow noise requirement, an augmenter cross-sectional shape which best suits the various engine placements should be selected and various cross-sectional sizes having areas equal to or greater than the noise related minimum should be assumed. Using data for augmenter pumping ratio, nozzle offset, nozzle pressure ratio, and wall temperatures, one must determine the maximum augmenter wall temperature for each augmenter cross-sectional size with the aircraft configuration and engine power setting identified as most critical from an augmenter wall temperature standpoint. (If one aircraft type to be accommodated had offset afterburning engines, such as the F-14, it would be the likely aircraft to assume in calculating the augmenter wall temperature.) From the results of these considerations, it will be possible to select the augmenter cross section of smallest area which meets both flow noise and wall temperature limitations.

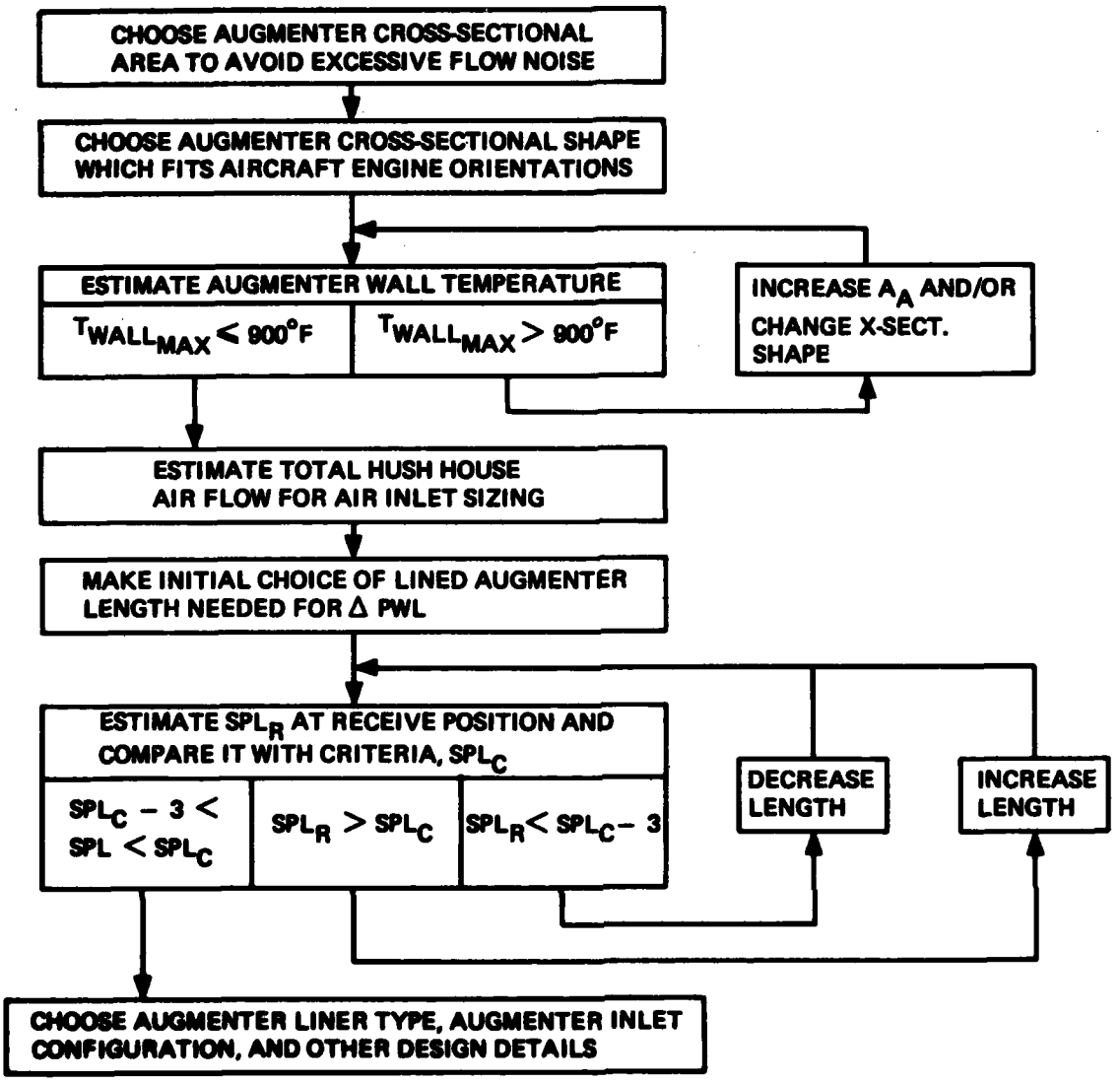

Figure 2-2. Block diagram of augmenter design procedure.

Noise Criterion at 250 ft	One Engine at Max RPM A_A/A_{NT}	Two Engines at Max RPM A_A/A_{NT}
95 dBA	18	16
85	24	21
75 dBA	30	26

where: A_A is the augmenter cross-sectional area
A_{NT} is the jet nozzle throat area neglecting the throat area of idling engines

Table 2-1. Ratio of augmenter cross-sectional area to maximum jet nozzle throat area required to avoid excessive augmenter exit flow noise.

b. Augmenter Pumping Ratio. Adequate augmenter pumping is essential in full-scale dry cooled suppressor operation. Early analytical tests indicated that mass flow ratios of six or more are feasible for a properly sized augmenter.

The scale-model studies by Fluidyne Engineering Corporation (ref 1) provide the primary basis for the following augmenter pumping results.

(1) Summary of Test Results. Reference 1 test data were reduced to an augmentation ratio parameter, ARP, defined as follows:

$$ARP = \frac{W_{pumped}}{W_N} \times \sqrt{\frac{T_{amb}}{T_{T_N}}} \times \frac{mw_N}{mw_{air}}$$

to facilitate correlation of augmenter pumping data.

APR ratios the equivalent pumped and primary flow momentum fluxes. It has the advantage of being primarily configuration oriented, having only a weak sensitivity to the temperature ratio, T_{T_N}/T_{amb}.

Figure 2-3 contains a summary of augmenter pumping performance wherein the augmentation ratio parameter, ARP, is plotted versus jet nozzle to ambient temperature ratio, T_{T_N}/T_{amb}, for a number of selected test configurations at an augmenter length-diameter ratio of 6.0. It is apparent that a subsonic diffuser on the downstream end of the augmenter increases pumping, whereas changing from round to an A/R = 1.7 abround cross section reduces pumping. Pumping performance does not appear to be sensitive to jet nozzle pressure ratio λ_N.

The consistent drop in augmentation ratio parameter with increasing jet nozzle to ambient temperature ratio, T_{T_N}/T_{amb}, shown in figure 2-3, is of particular interest. While it is a secondary effect, it is nevertheless larger than might have been expected on the basis of typical ejector performance data and is probably related to the low loss, high augmentation ratio

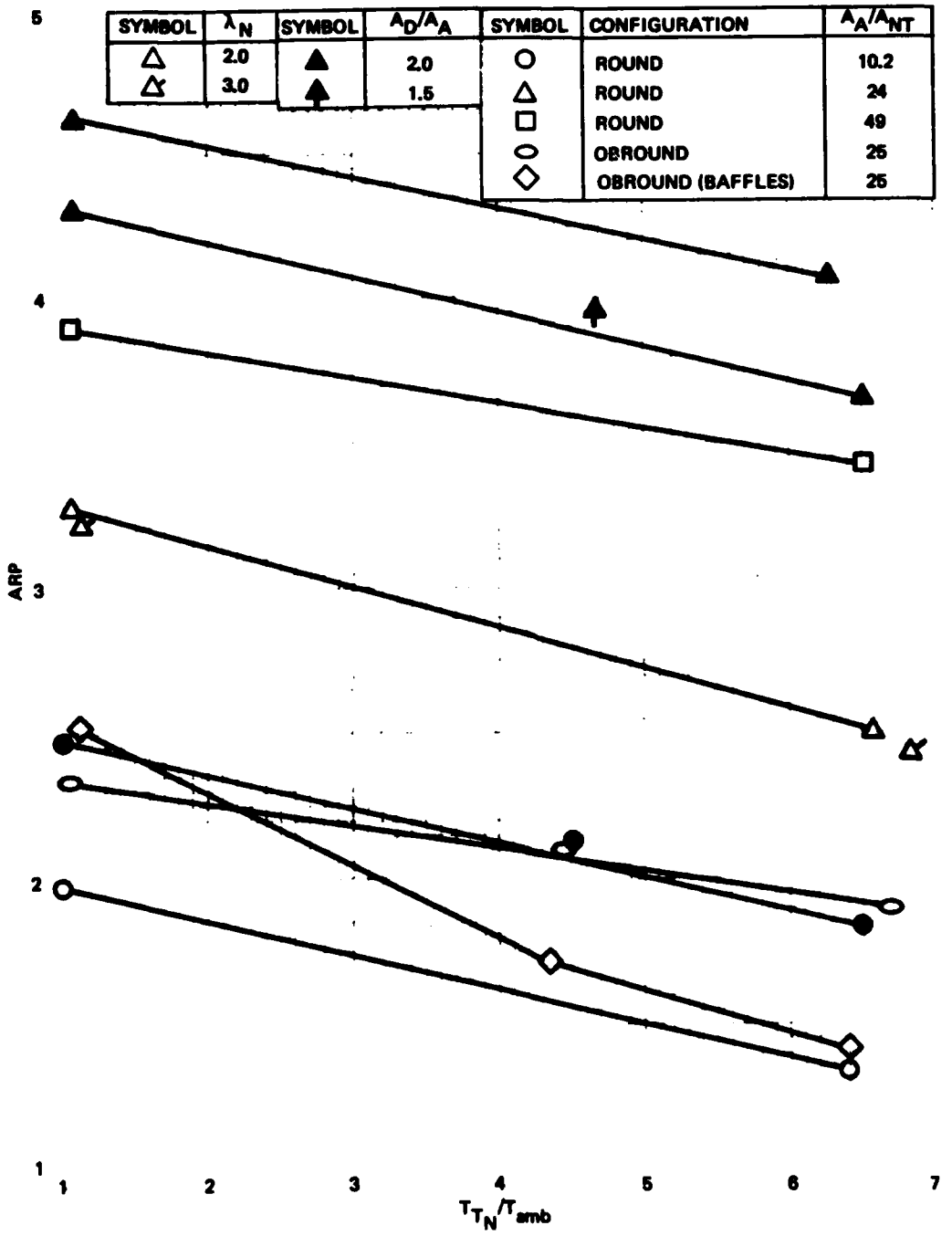

Figure 2-3. Summary of augmenter pumping performance.

situation which is characteristic of dry cooled augmenter installations. At high jet nozzle to ambient temperature ratios, there is a significant exchange of heat from the jet flow to the pumped flow in the mixing region. This increase in the volume flow of the pumped flow requires that it accelerate, producing an additional pressure drop, which must be overcome by the jet momentum, and a resulting drop in pumping performance. When the ejector situation corresponds to a lower augmentation ratio and a higher pumped flow pressure rise (higher loss), this additional pressure drop due to heat exchange is smaller relative to the overall pressure rise required, and the drop in pumping performance is correspondingly less. Although the augmentation ratio parameter decreases with increasing jet temperature to pumped flow temperature ratio, the augmentation ratio actually increases.

Augmenter length - diameter ratio is one of the geometric variables influencing pumping performance. Figure 2-4 (for cases without subsonic diffuser) and figure 2-5 (for cases with subsonic diffuser) present the pumping performance as a function of augmenter length-diameter ratio, L_A/D_A, over the range tested. Both figures show little change in pumping performance above $L_A/D_A = 6$, but some decrease in performance as L_A/D_A is reduced below 6. Although the $T_{T_N}/T_{amb} = 1.0$ ($T_{T_N} = 5000°R$), test results show better pumping performance than at higher T_{T_N}; they also exhibit a greater decrease in pumping as augmenter length-diameter ratio is reduced. This probably arises because mixing progresses more rapidly with the higher gas viscosity associated with high jet temperature and so is closer to completion at any given distance from the nozzle exit. At $T_{T_N}/T_{amb} = 6.6$, the variation in pumping performance is no greater than 10% over the range of L_A/D_A values tested.

A comparison of the data in figure 2-5 for an augmenter having an exit subsonic diffuser with the data taken without diffuser (fig 2-4) shows an increase of roughly 50% in ARP due to the diffuser at $T_{T_N}/T_{amb} = 6.6$. A subsonic diffuser area ratio of 2.0 gave about 7% better pumping performance than one with $A_D/A_A = 1.5$.

SYMBOL	AUGMENTER CONFIGURATION	A_A/A_{NT}
○	ROUND	10.2
△	ROUND	24
□	ROUND	49
⬭	OBROUND WITH RAMP (Y_p = 0.45)	25

SYMBOL	T_{T_N}/T_{amb}
○	1.0
●	6.6
SYMBOL	**λ_N**
▲	2.0
◢	3.0

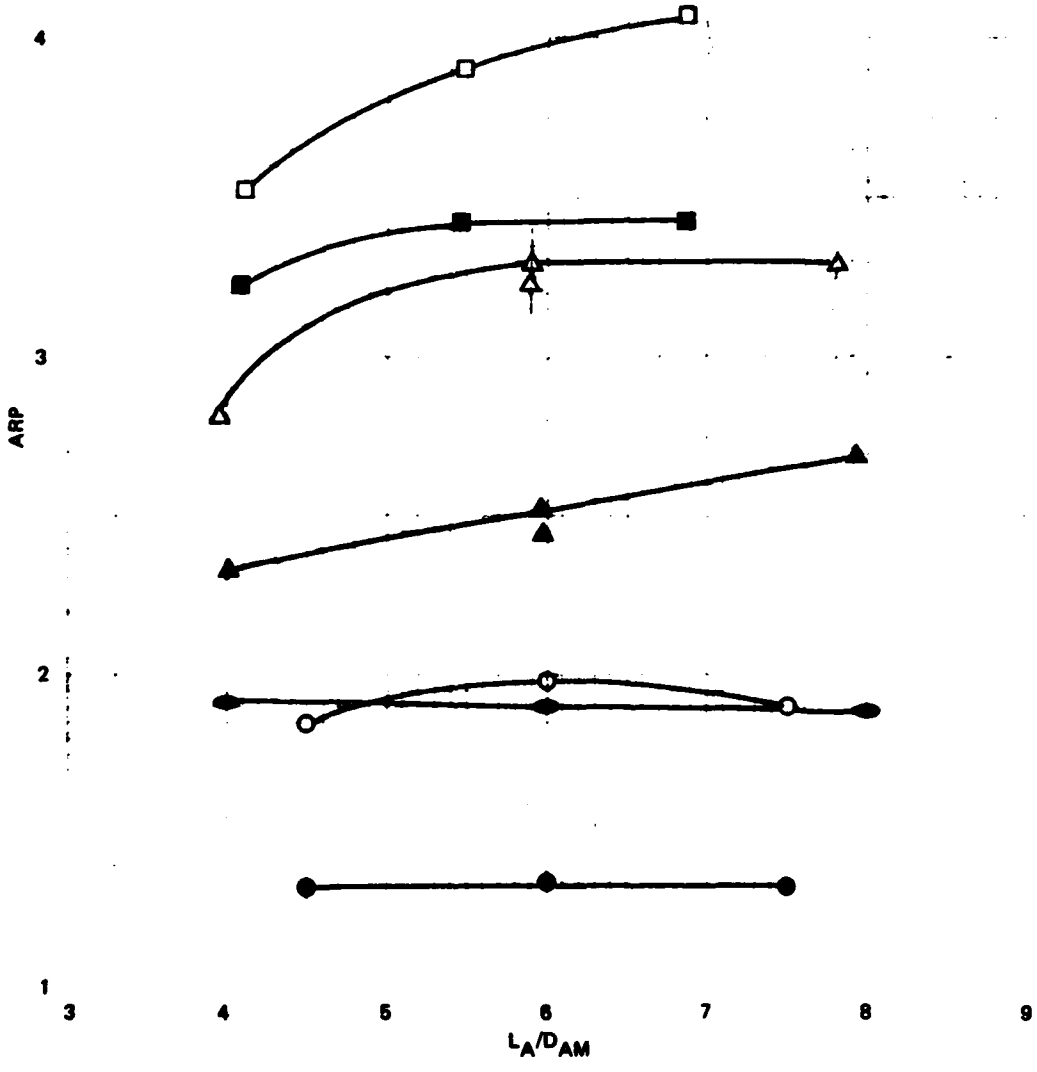

Figure 2-4. Augmenter pumping performance vs augmenter length-diameter ratio-without exit subsonic diffuser.

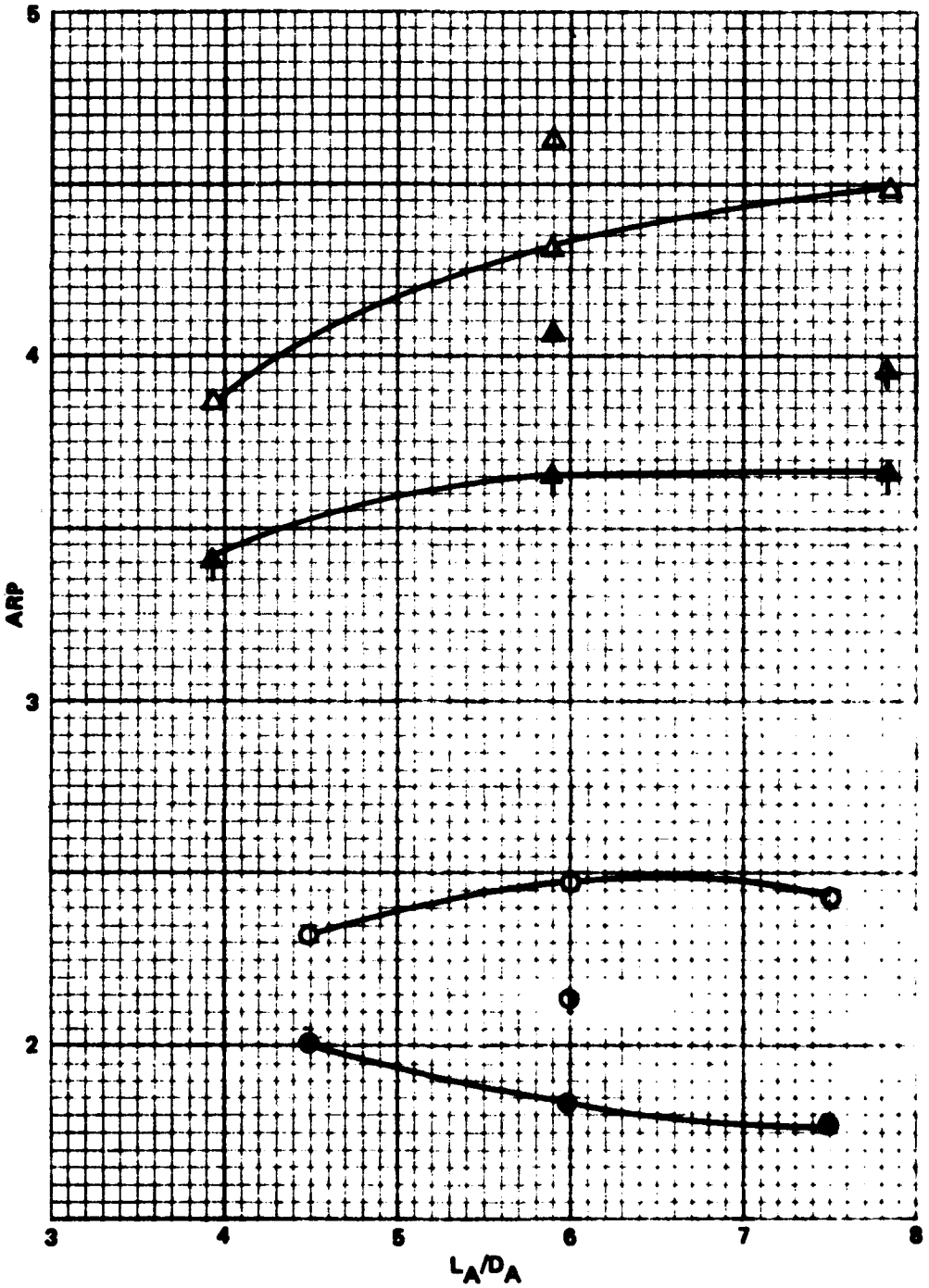

SYMBOL	CONFIGURATION	A_A/A_{NT}	SYMBOL	A_D/A_A	SYMBOL	T_{TN}/T_{amb}
○	ROUND	10.2	△	2.0	○	1.0
△	ROUND	24	⇧	1.5	◐	4.8
					●	6.8

Figure 2-5. Augmenter pumping performance vs augmenter length-diameter ratio-with exit subsonic diffuser.

Movement of the jet nozzle exit axially relative to the augmenter entrance showed no appreciable variation in pumping performance primarily because the augmenter entrance area is 24 times larger than the jet nozzle throat area. Movement of the jet nozzle away from the augmenter entrance did have an appreciable influence (increase) on forward aircraft enclosure interior noise.

The changes to pumping performance for different augmenter entrance geometrics are tabulated below:

Inlet Configuration	APR @ $T_{T_N}/T_{amb} = 1$	APR @ $T_{T_N}/T_{amb} = 6.6$
conical	3.30	2.51
rounded	3.43	2.50
sharp-edged	3.02	2.34
conical plus throttle	3.05	2.41

As shown, these changes had a relatively small influence on pumping performance.

During the aerothermal testing with the obround augmenter, the jet centerline was moved laterally and vertically and also deflected relative to the augmenter centerline. The jet nozzle orientations and the obround cross section both had a significant effect on pumping performance, as is shown in figure 2-6. Changing from a round to an aspect ratio 1.7 obround cross section resulted in a 10% decrease in pumping ratio parameter at T_{T_N}/T_{amb} = 4.6, A_A/A_{NT} = 25. Perhaps as much as half of this decrease is due to the porous, sound-absorbing liner, which limits the rate of pressure rise. As the jet centerline was moved off the centerline of the augmenter or deflected, a reduction in pumping performance occurred. The data point at Y_p = 0.45 and α_s = 1° corresponds to the F-14A configuration. Most of the data shown in figure 2-6 were with no augmenter exit ramp. One point from full-scale

acoustic testing is included to show the influence of the ramp on pumping performance.

Figure 2-7 shows the variation in pumping performance with jet nozzle pressure ratio, λ_N. The apparent drop in performance with λ_N occurs because no attempt was made to keep the inlet loss constant; as a result, the inlet loss and corresponding augmenter pressure rise are higher at $\lambda_N = 3$ than at 2 or 1.2. The low pressure ratio, $\lambda_N = 1.2$, was run specifically to show that adequate pumping occurred at low jet nozzle pressure ratios so as to prevent recirculation of exhaust gases within the Hush House.

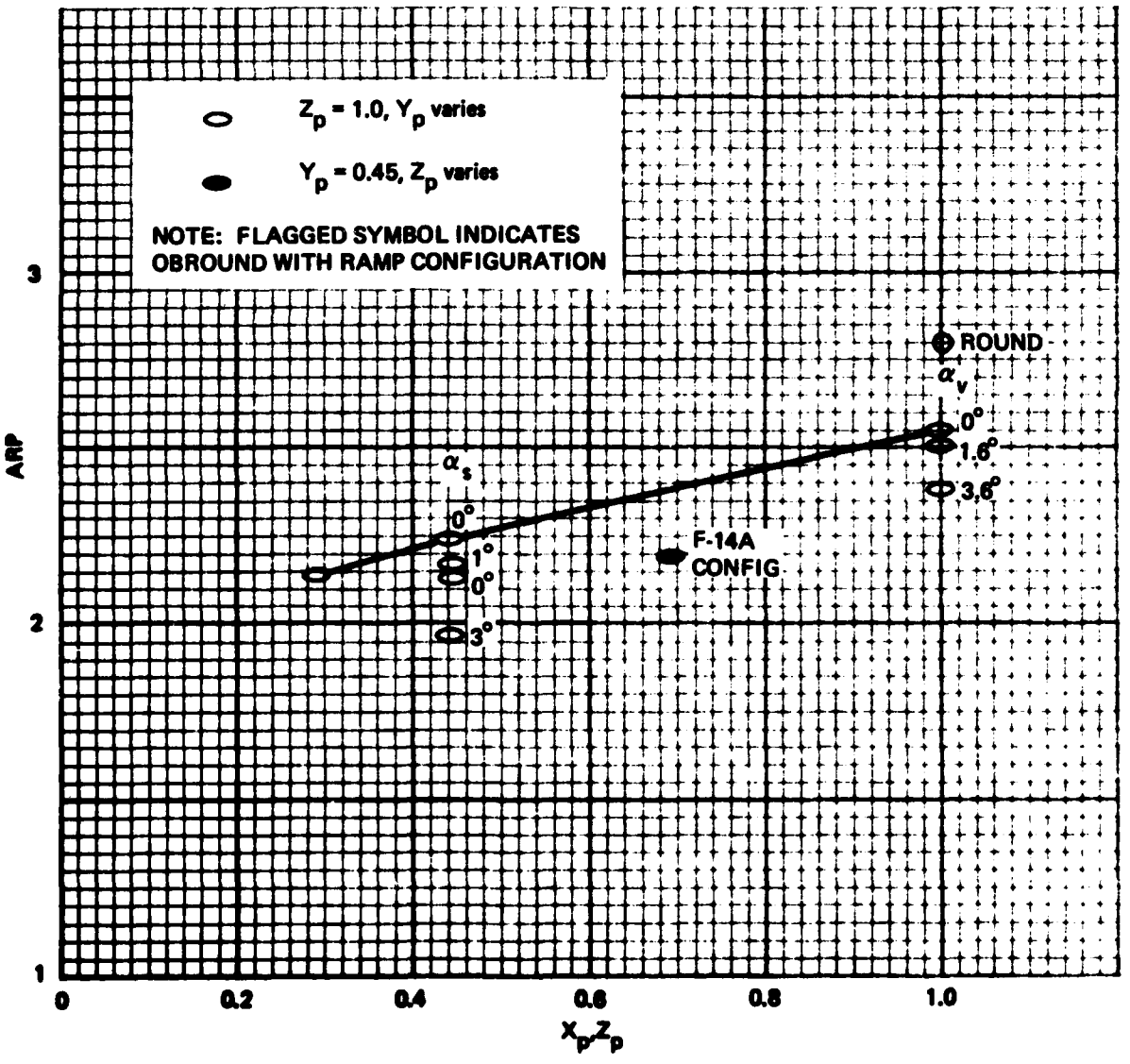

Figure 2-6. Obround augmenter pumping performance with different nozzle positions and inclinations.

The scale-model and full-scale test results presented in this section are based on a nominal augmenter pressure ratio, P_{Tsec}/P_{Texit}, of 0.995 (2" H_2O loss in total pressure through the forward enclosure inlet). Figure 2-8 shows the essentially linear variation in augmentation ratio parameter with P_{Tsec}/P_{Texit}. The slope of the linear variation is not a strong function of either configuration, jet nozzle temperature ratio, or jet nozzle pressure ratio.

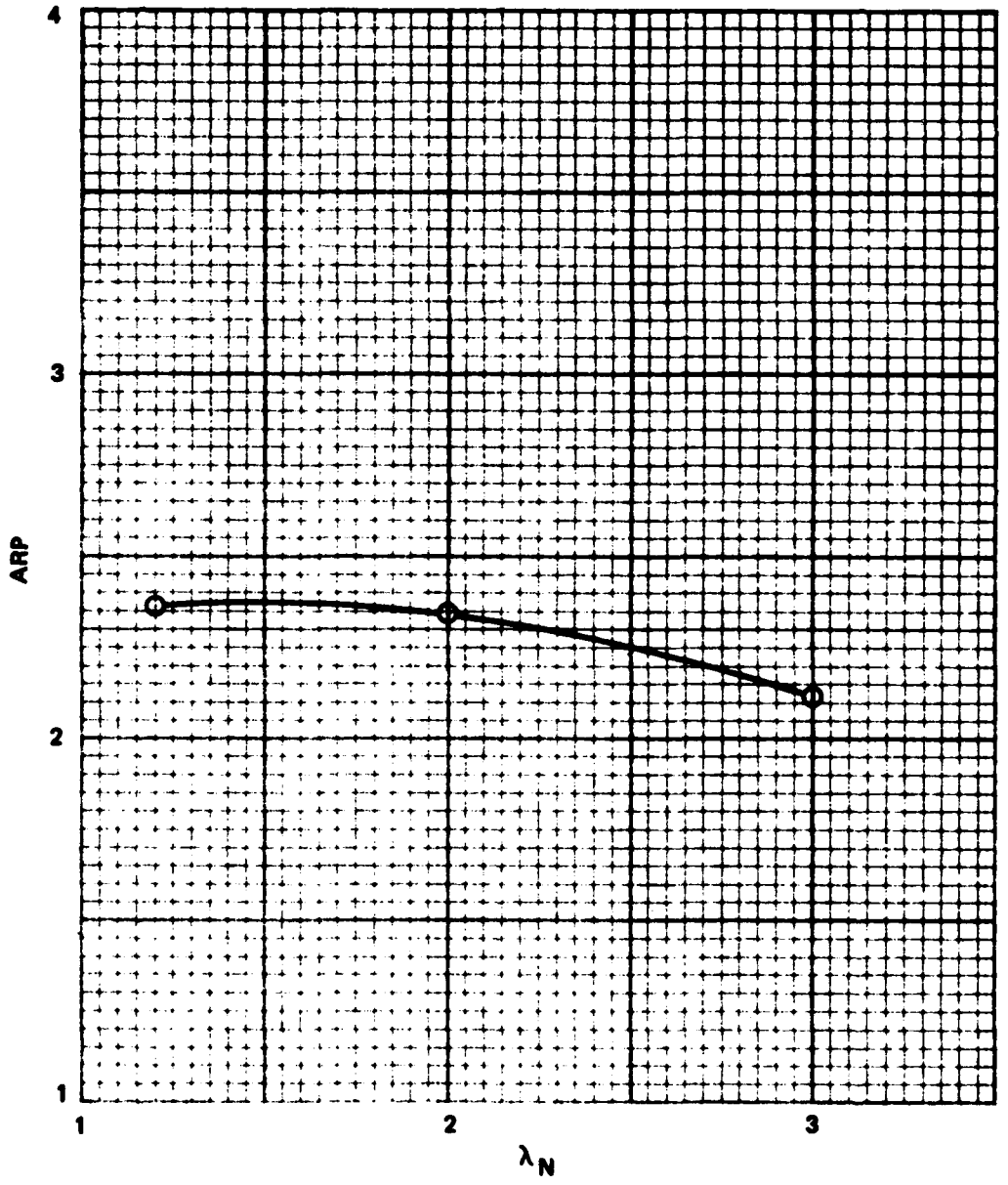

Figure 2-7. Augmenter pumping performance vs jet nozzle pressure ratio for obround augmenter with ramp.

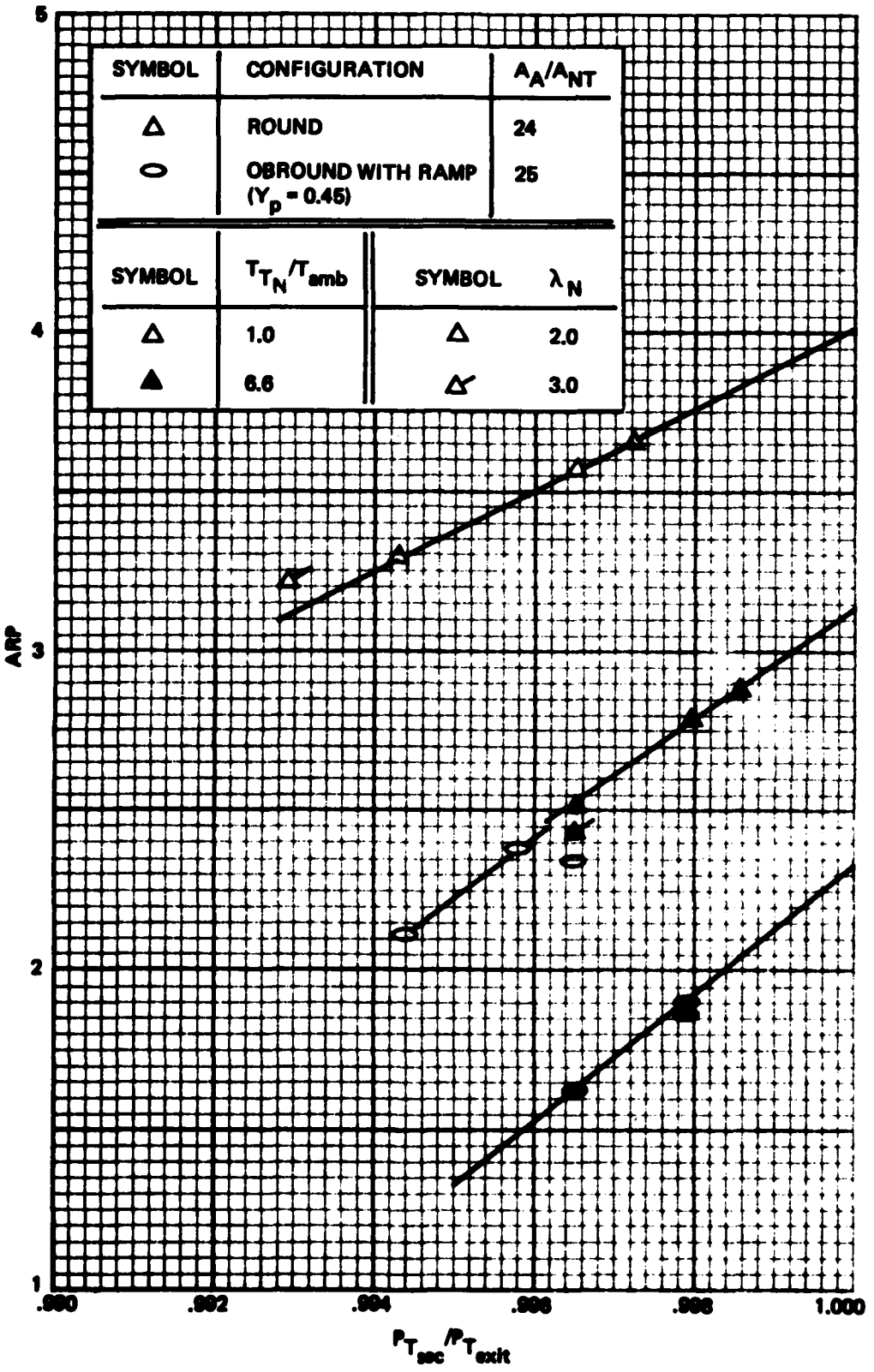

Figure 2-8. Augmenter pumping performance vs augmenter pressure ratio.

A secondary inlet impact on augmenter pumping is calculated just as the single primary inlet case is calculated except the total pumped air is the sum of the primary intake and the secondary intake air. Reference 4 provides details for design with a secondary air source.

(2) Pumping Performance. Using the data from model studies presented in the previous section, this section summarizes the Fluidyne Engineering Corporation (ref 1) calculation of augmenter pumping performance. The augmenter pumping performance is of prime interest in two related areas: predicting maximum augmenter wall temperature with a given combination of aircraft engine and augmenter cross section and determining forward enclosure inlet air flow for sizing the air inlet. Starting with the pumping performance presented in the form of the augmentation ratio parameter, ARP

$$ARP = \frac{W_{pumped}}{W_N} \times \sqrt{\frac{T_{amb.}}{T_{T_N}}} \times \frac{mw_N}{mw_{air}}$$

W_N being the jet nozzle flow rate which corresponds, in full scale, to the aircraft exhaust flow rate ($W_{aircraft}$), and T_{T_N} and mw_N being the jet exhaust total temperature and molecular weight. This parameter was chosen because the pressure rise sustainable by an ejector is related to the relative momentum fluxes (mv) of the driving and secondary flows at the entrance to the mixing section (augmenter). For given expansion ratios, the momentum flux of each flow is proportional to wa_o. Since the speed of sound, a_o, is proportional to mw, the augmentation ratio parameter is proportional to the ratio of pumped flow momentum flux to jet nozzle flow momentum flux. Calculation of pumped air flow is simple, once this parameter is known for a particular case. Accordingly, figures 2-9 - 2-12 have been constructed from the available test data to make possible predictions of pumped air flow and, subsequently, augmenter wall temperature.

Figure 2-9 presents augmentation ratio parameter versus augmenter cross-sectional area to jet nozzle throat area for a variety of configurations without a subsonic diffuser. It is limited to cases in which the nozzle is centered in the augmenter and undeflected and the jet nozzle total temperature

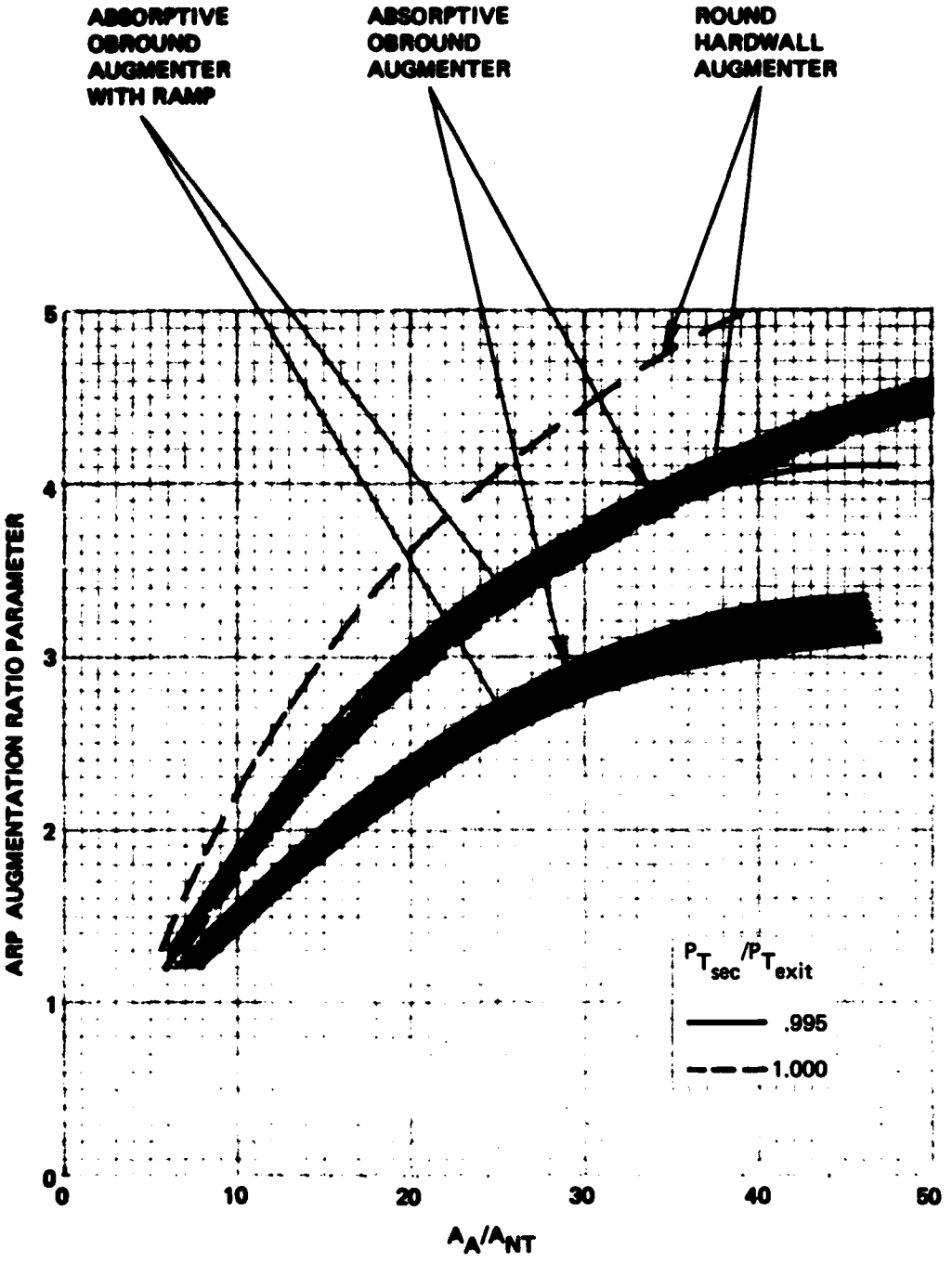

Figure 2-9. Augmenter pumping performance vs augmenter to jet nozzle throat area ratio for cases with no exit subsonic diffuser.

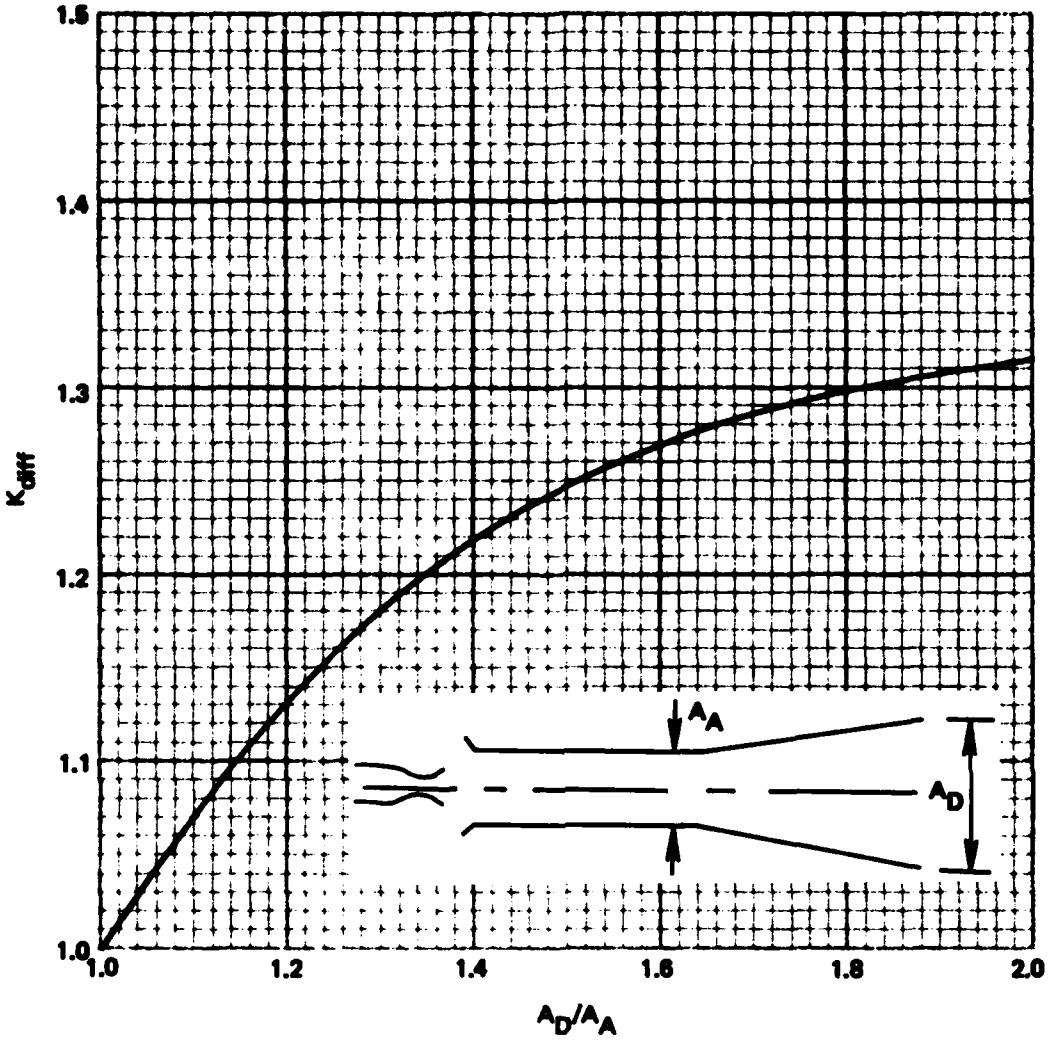

(SUBSONIC DIFFUSER EXIT AREA/AUGMENTER CROSS SECTION AREA)

$$K_{diff} = \frac{ARP_{with\ diffuser}}{ARP_{w/o\ diffuser\ @\ T_{T_N}/T_{amb} = 1.0}}$$

Figure 2-10. Influence of augmenter exit subsonic diffuser area ratio on augmenter pumping performance.

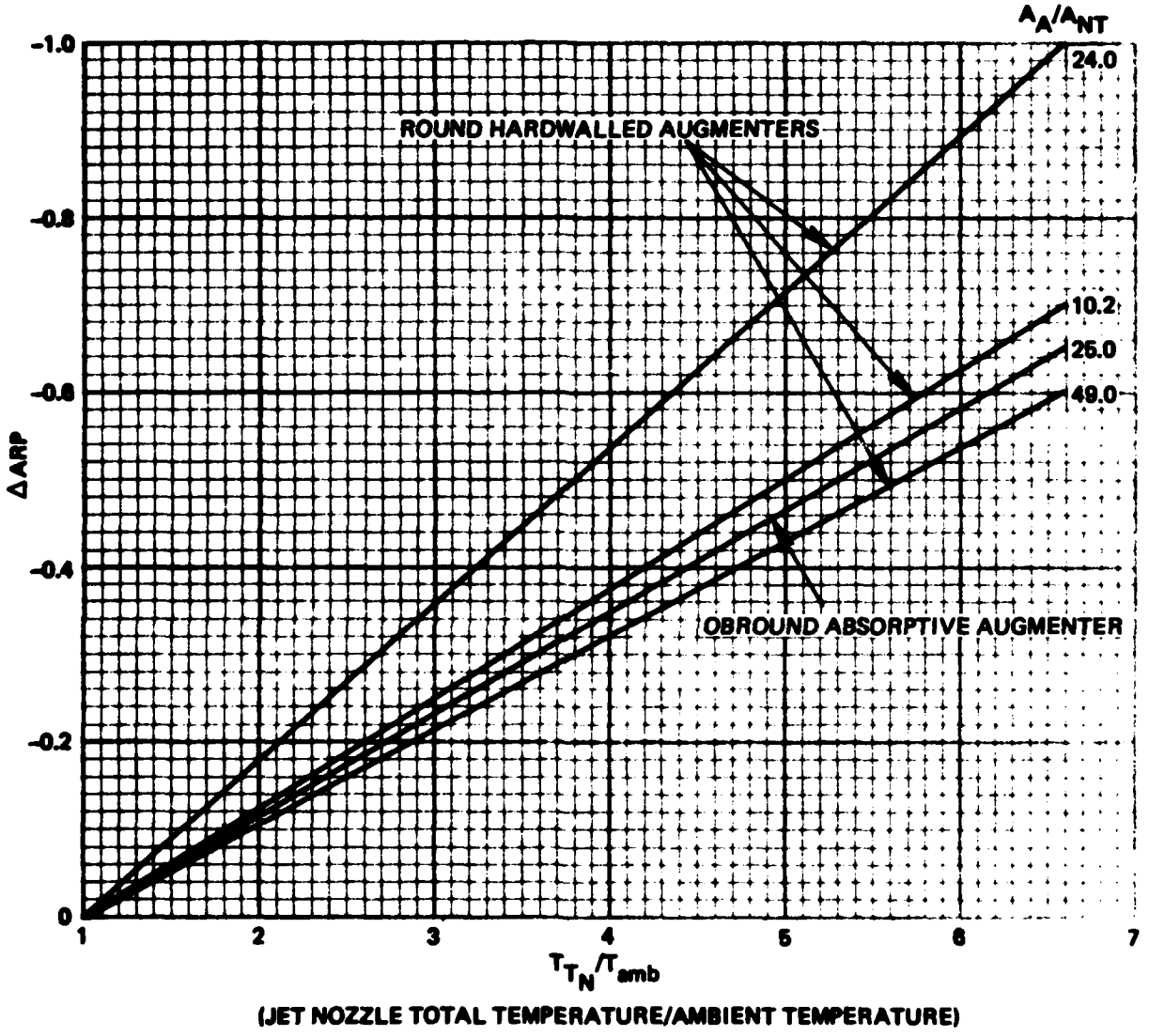

Figure 2-11. Influence of jet nozzle to ambient temperature ratio on augmenter pumping performance.

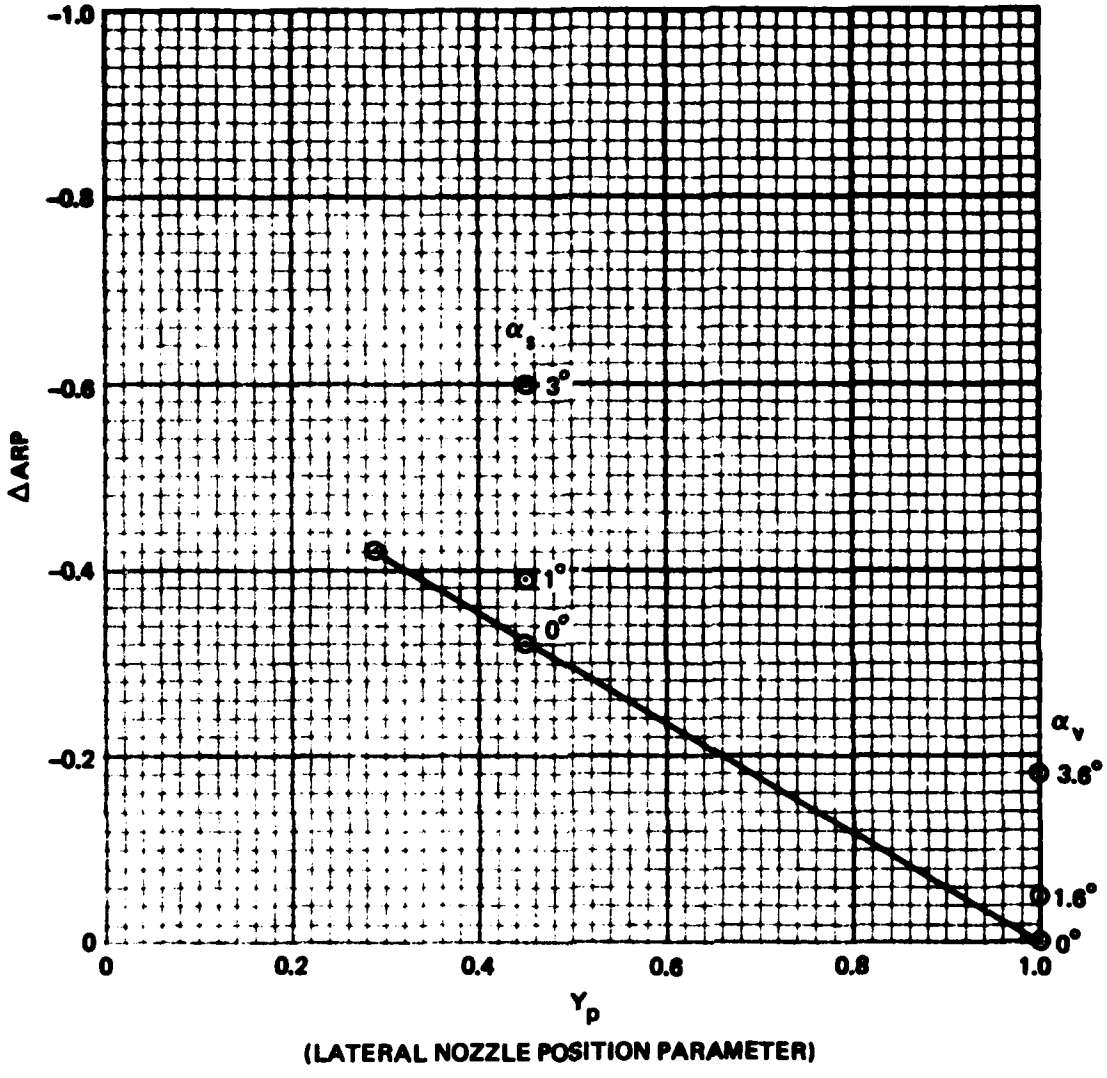

Figure 2-12. Influence of jet nozzle offset and deflection on augmenter pumping performance.

and pumped air (ambient) temperature are equal. Since model test data show no appreciable influence of jet nozzle pressure ratio on augmentation ratio parameter, it can be assumed that these curves are valid for most engines, without regard to nozzle pressure ratio. In figure 2-9, curves are presented for augmenter pressure ratios of both 1.000 and 0.995 (1.000 corresponds to zero Hush House pressure depression, while 0.995 would correspond to roughly 2" H_2O total pressure loss). This figure also shows a small reduction in augmentation ratio parameter due to the addition of the 45 degree deflector ramp. Such a ramp has been a feature of Hush House designs because it deflects both the flow and the noise upward without unduly penalizing augmenter pumping performance. Any major alterations to this basic configuration would have to be studied carefully to make sure that they did not increase the augmenter exit backpressure and cause a large reduction in cooling air pumping.

Although Hush House augmenters do not typically require an exit subsonic diffuser for adequate pumping performance, the influence of a subsonic diffuser is presented for information. This is shown in figure 2-10 as the ratio of $ARP_{\text{with diffuser}}/ARP_{\text{w/odiffuser}} = K_{\text{diff}}$. This information would be useful in case a vertical stack with baffles were to be added to an absorptive augmenter to increase noise reduction. Such an addition would tend to increase the augmenter backpressure ($P_{T_{exit}}$, P_{amb}) and reduce pumping. A subsonic diffuser might be required to restore adequate cooling air pumping. To properly estimate the augmentation ratio parameter for a configuration having a diffuser, the correction to figure 2-9 values for the diffuser must be applied before adding the succeeding corrections discussed in the following two paragraphs.

Figure 2-11 concerns the same configurations as figures 2-9 and 2-10, and provides a correction to the augmentation ratio parameter for jet nozzle total temperature, T_{T_N}, higher than the pumped air temperature, T_{amb}. This is observed in every full-scale instance. Figure 2-12 provides an additional correction usable when the jet nozzle is off center in the augmenter or deflected. It was developed from the obround augmenter test results. Figure 2-11 shows a decrease in augmentation ratio parameter with increasing jet

nozzle to ambient temperature ratio. By virtue of the definition of the augmentation ratio parameter, however, the actual augmentation ratio will increase with increasing jet temperature, as illustrated in figure 2-13 for the case of an obround absorptive augmenter with ramp, $A_A/A_{NT} = 24$, having a centered jet and with $P_{T_{sec}}/P_{T_{exit}} = 0.9975$.

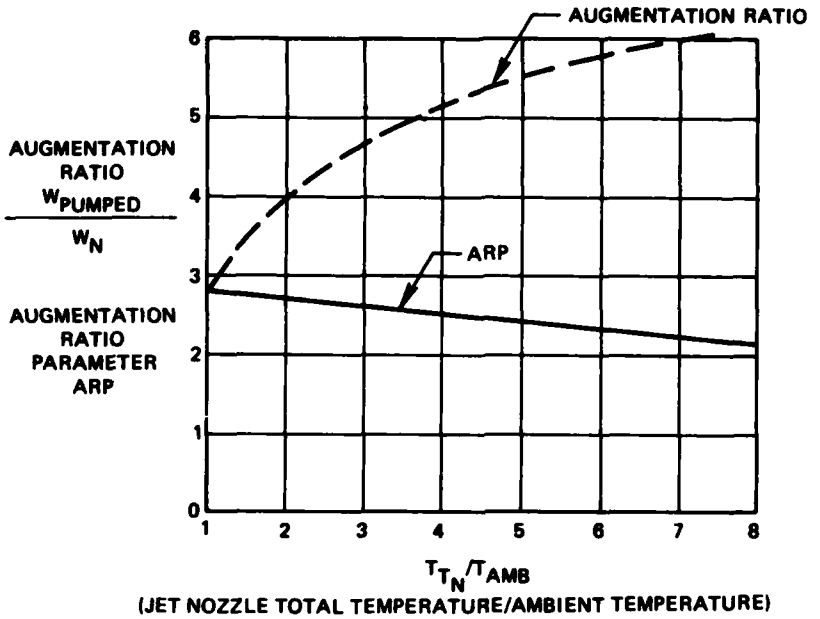

Figure 2-13. Augmentation ratio and augmentation ratio parameter vs jet nozzle stagnation temperature to ambient temperature ratio.

To estimate the augmentation ratio parameter for an arbitrary engine configuration, the augmentation ratio parameter from figure 2-9 is corrected as follows, using figures 2-10, 2-11, and 2-12.

$$APR = \left(APR_{\text{fig 2-9}} \times K_{diff_{\text{fig 2-10}}}\right) + \Delta ARP_{\text{fig 2-11}} + \Delta ARP_{\text{fig 2-12}}$$

Using the chosen range of pressure ratios (P_{Tsec}/P_{Texit}), one can obtain APR values as a function of nozzle temperature ratios (T_{T_N}/T_{amb}). The pumped air flow rate and total inlet air flow rate can be calculated for each augmenter pressure ratio case.

$$W_{pumped} = W_N \times APR \times \sqrt{\frac{TT_N}{T_{amb}} \times \frac{mw_{amb}}{mw_N}}$$

$$= W_N \times \sqrt{\frac{T_{T_N}}{T_{amb}} \times \frac{mw_{amb}}{mw_N}} \times APR$$

then $W_{inlet} = W_{pumped} + W_N$

Since most applications of dry augmenter design have an inlet ratio equal to the augmenter pressure ratio, one can plot inlet characteristic and augmenter pumping performance on the same curve. The crossing point for the two curves is the operating point for the assumed configuration.

c. Wall Temperature Distributions. Augmenter wall temperatures are a function of augmenter geometry, pumping ratio, and jet flow impingement angle. The scale-model studies by Fluidyne Engineering Corporation (ref 1, 2) provide the primary basis for the following wall temperature results. This report only summarizes the scale-model and full-scale (ref 5, 6) measured data.

(1) Summary of Test Results. The augmenter cross section survey results presented in reference 1 indicate that, with lateral translation or deflection of the jet nozzle centerline relative to the obround augmenter centerline, the jet tended to be carried to the augmenter sidewall.

The results of this tendency are graphically illustrated in figure 2-14, which shows the longitudinal distribution of augmenter wall temperature parameter, T_{wall_p}, for a number of different lateral nozzle centerline locations and deflections. The data in the figure indicate unexpectedly high augmenter sidewall temperatures for a lateral offset and deflection representative of the F-14A aircraft configuration ($Y_p = 0.45$, $\alpha_s = 1°$). Similar top and bottom wall data show appreciable jet impingement effects when the jet is deflected vertically. Figure 2-14 shows, for example, that the orientation corresponding to the F-14A ($Y_p = 0.45$, $\alpha_s = 1°$) results in over 100% greater maximum wall temperature parameter than for the centered, undeflected jet.

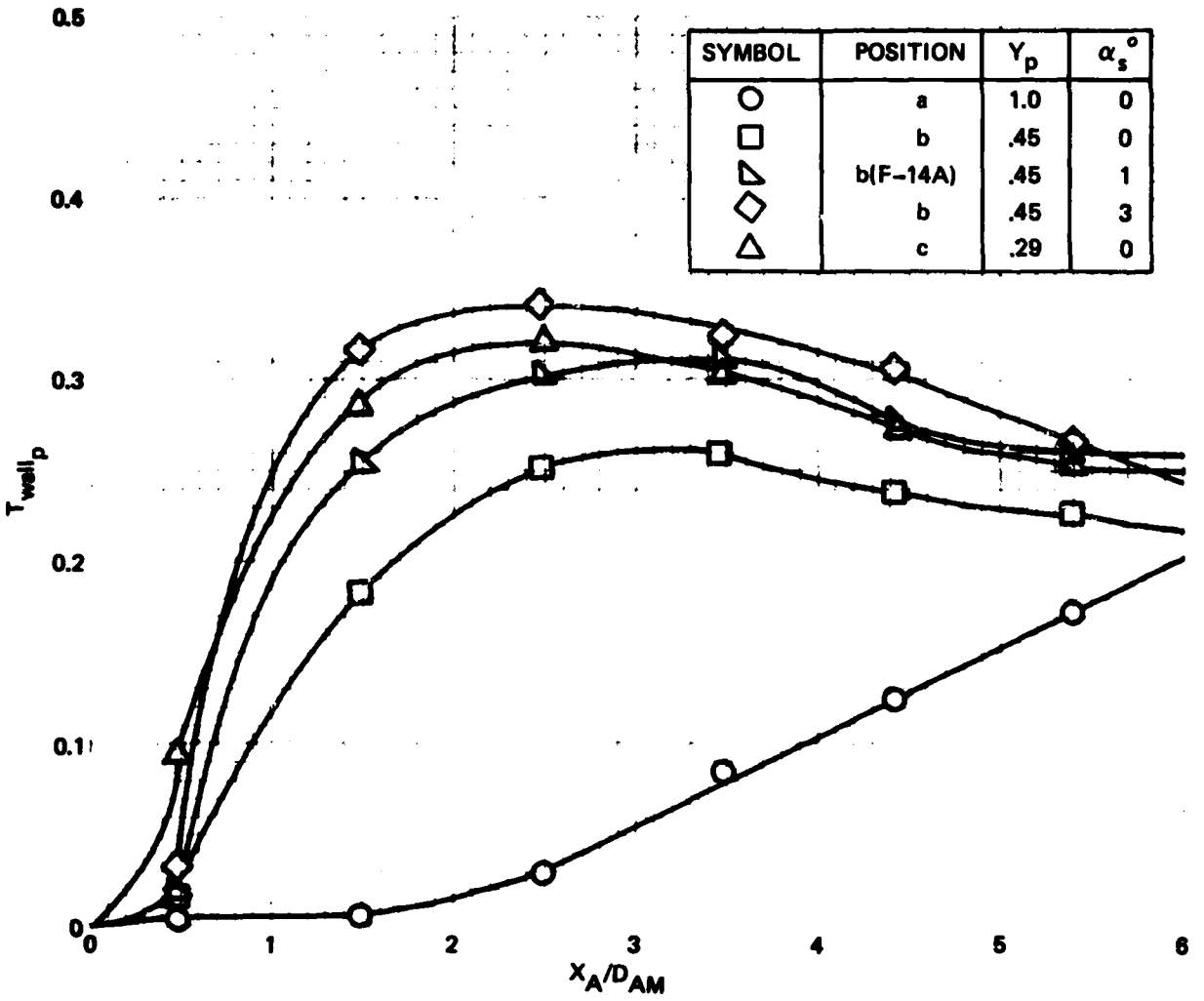

Figure 2-14. Longitudinal sidewall temperature distribution vs jet nozzle lateral position and deflection for obround augmenters.

Additional obround augmenter sidewall temperature data were obtained to determine the influence of the augmenter exit ramp and the influence of jet nozzle total temperature and pressure ratio on wall temperature. Figure 2-15 shows the distribution of sidewall temperature parameter at λ_N = 2.0 with and without ramp for nozzle total temperatures of 2300°R and 3300°R (T_{T_N}/T_{amb} = 4.6 and 6.6). The data show a slightly lower maximum wall temperature parameter at T_{T_N} = 3300°R than at 2300°R (which is due to a slightly mixed temperature parameter, and a slight increase in maximum wall temperature when the ramp is added because of the reduction in pumped air).

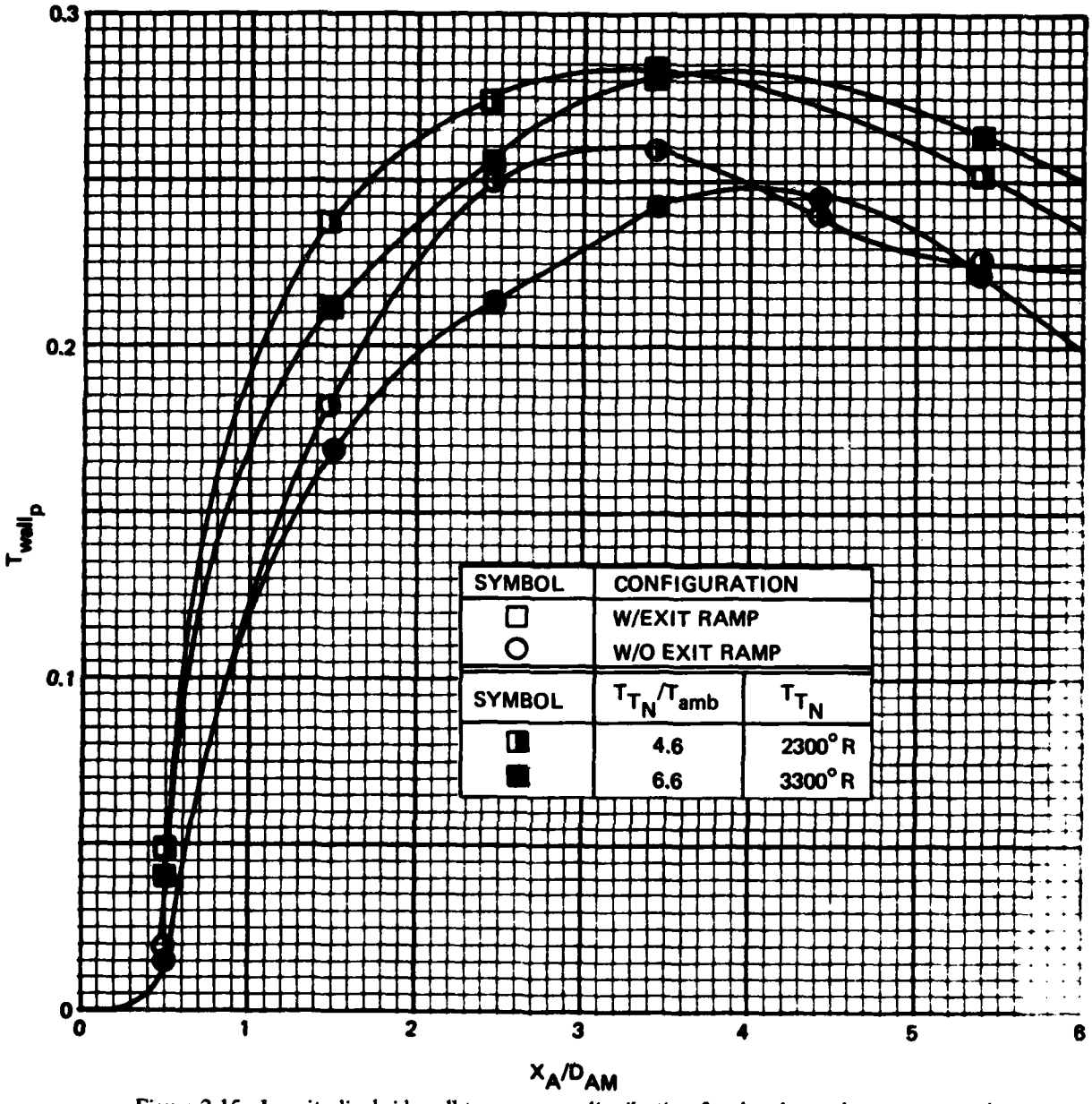

Figure 2-15. Longitudinal sidewall temperature distribution for the obround augmenter with and without the exit ramp and at different jet nozzle to ambient temperature ratios.

The effects of jet nozzle pressure ratio on the sidewall temperature parameter with the offset jet (Y_p = 0.45, αs = 0°) appear in figure 2-16. Operation at λ_N = 3.0 rather than 2.0 greatly reduces the extent of jet impingement on the augmenter sidewall. This is to be expected on the basis of the augmenter cross section results wherein the higher pressure ratio offset jet was not carried closer to the sidewall.

Figure 2-17 contains wall temperature parameter data for different augmenter length-diameter ratios. These data indicate that, within the accuracy

obtainable, augmenter length-diameter ratio has little effect on the longitudinal wall temperature distribution.

(2) Maximum Augmenter Wall Temperature. When the jet is centered in the augmenter and aligned, the high temperature core of the mixing jet is insulated from the augmenter walls by the colder pumped flow. On the other hand, if the jet centerline is moved closer to one wall or is angled

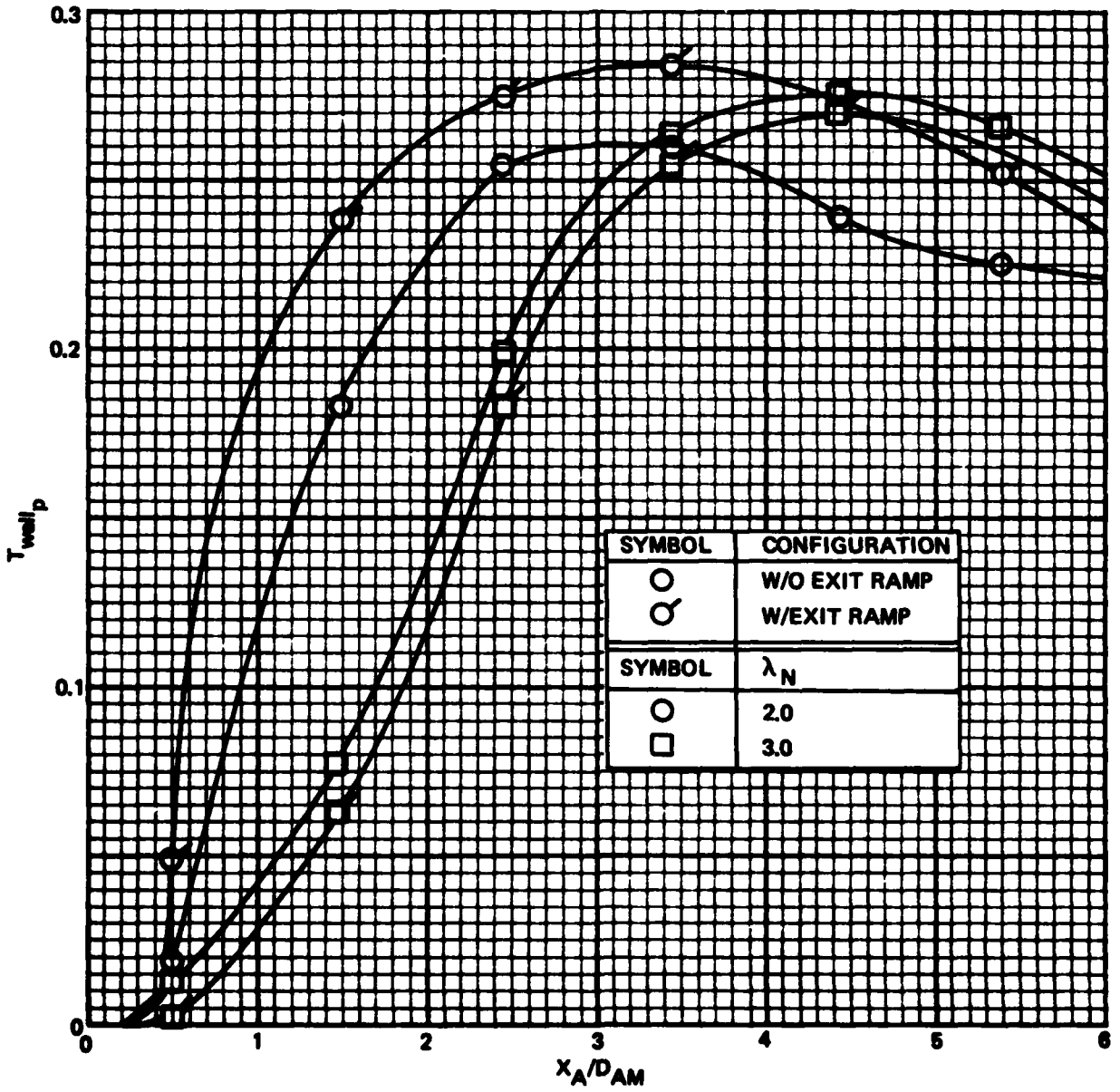

Figure 2-16. Longitudinal sidewall temperature distribution for the obround augmenter with and without the exit ramp for jet nozzle pressure ratios of 2.0 and 3.0.

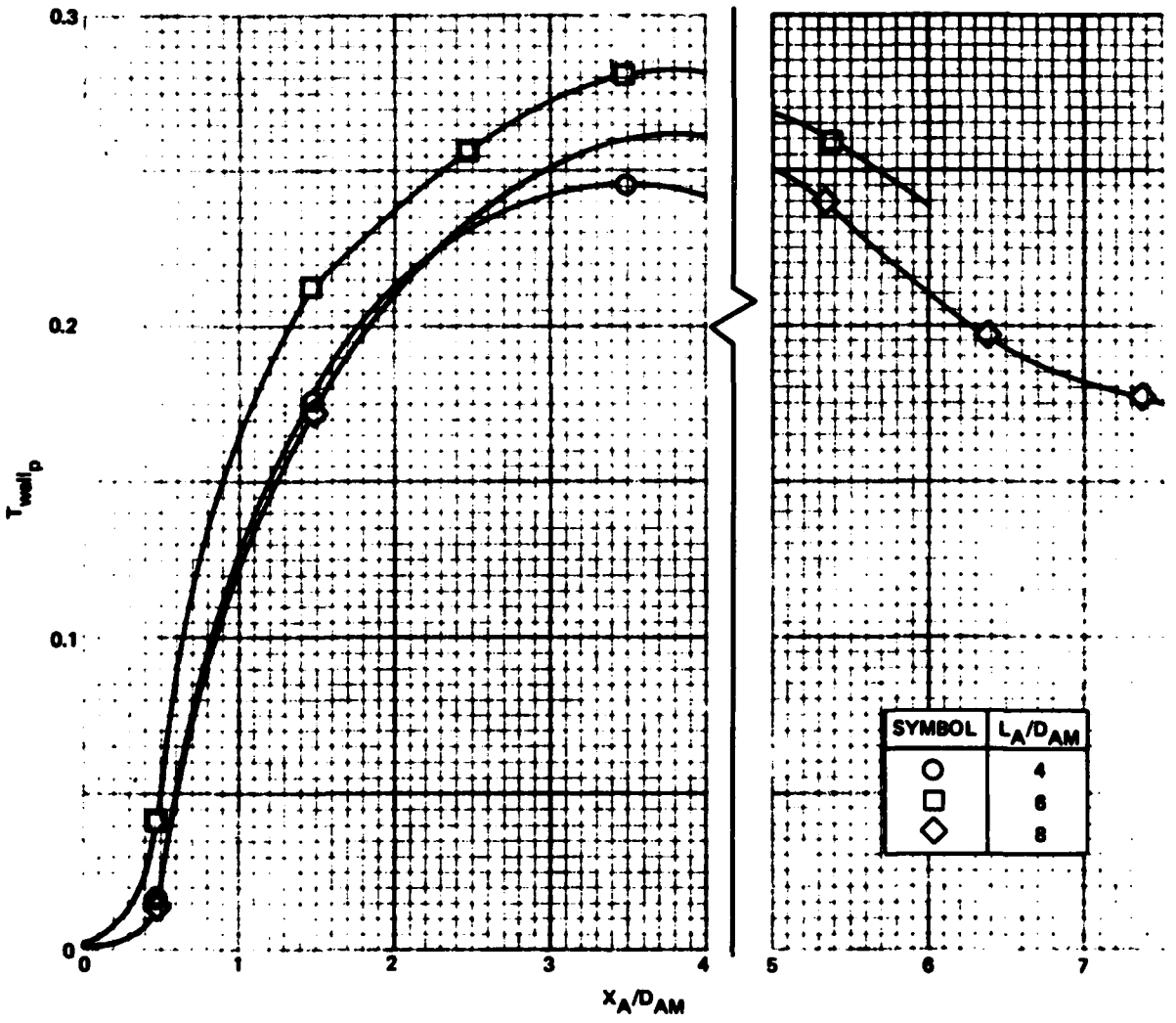

Figure 2-17. Longitudinal sidewall temperature distribution for the obround augmenter and exit ramp for varying augmenter length – diameter ratios.

toward the wall, there is a tendency for the hot mixing regions to impinge on the augmenter wall. This is illustrated in figure 2-18, which shows the relationship between the hot jet centerline temperature and the wall temperature for two nozzle position cases.

Basically, two things determine the maximum wall temperature: (1) the relative amount of ambient air pumped through the augmenter (which determines the mixed average temperature of the jet flow and pumped flow), and (2) the degree of jet exhaust flow impingement on the augmenter wall. Figures 2-19, 2-20, and 2-21 have, therefore, been provided to make possible either the prediction of maximum augmenter wall temperatures for an arbitrary combination of aircraft and augmenter or the design of an augmenter to avoid overheating with a given aircraft. Figure 2-19 presents the mixed average temperature parameter as a function of T_{T_N}/T_{amb} and augmentation ratio parameter.

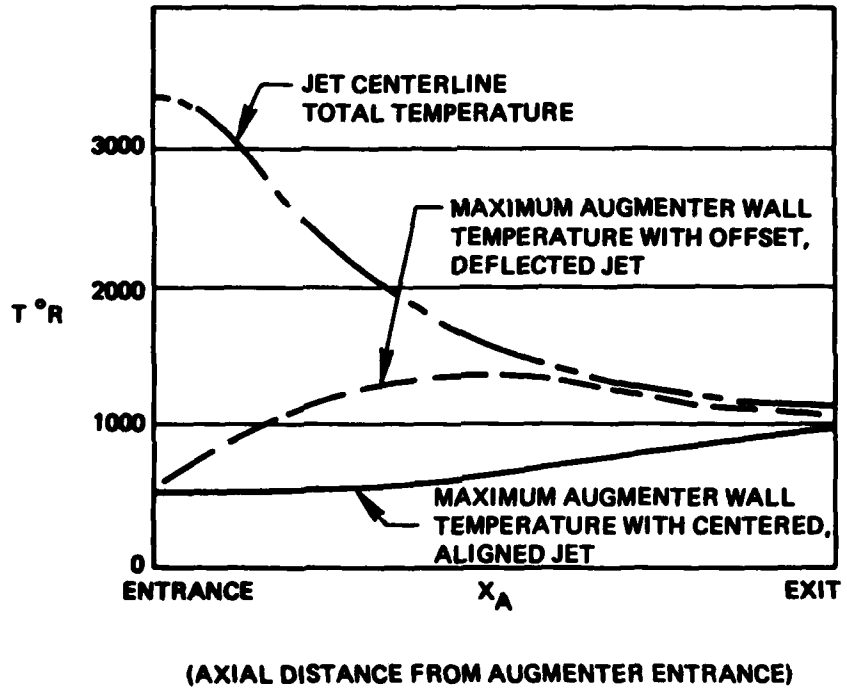

Figure 2-18. Relationship between the jet temperature and the augmenter wall temperature.

Figures 2-20 and 2-21 give the maximum wall temperature parameter as a function of jet nozzle orientation in relation to the mixed average temperature parameter. To simplify the use of these curves, the mixed temperature and corresponding augmentation ratio parameter are to be determined for the

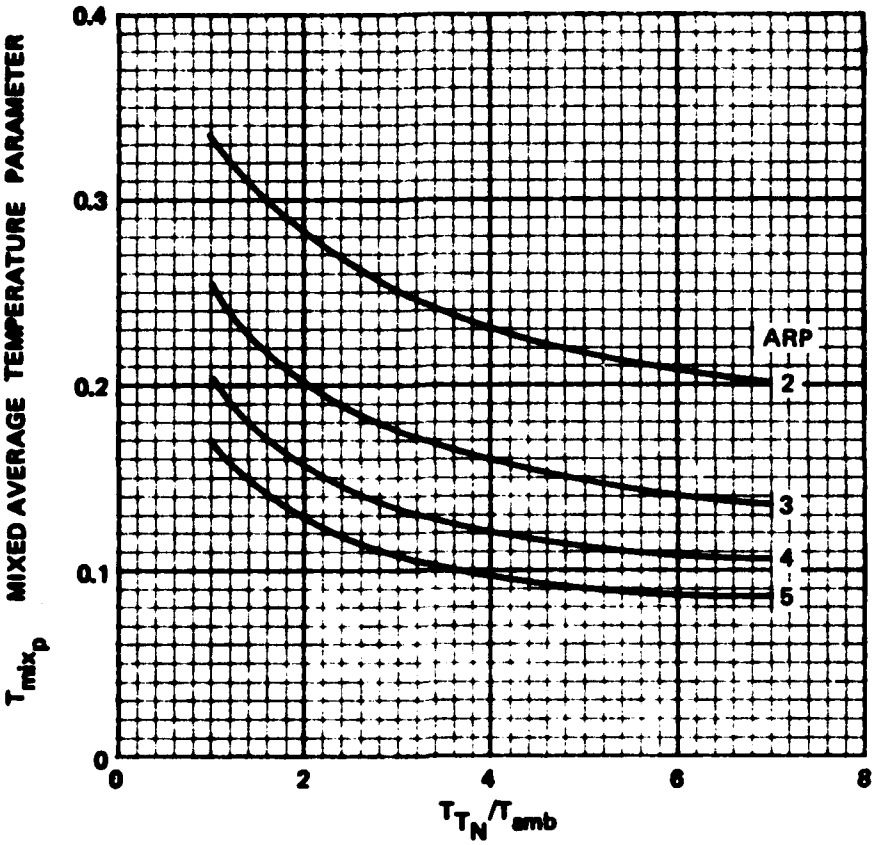

$$T_{mix_p} = \frac{T_{mix} - T_{amb}}{T_{T_N} - T_{amb}}$$

Figure 2-19. Calculated variation of mixed average temperature parameter with jet nozzle to ambient temperature ratio parameter.

case with the engine exhaust centered in the augmenter and undeflected, giving the resulting form of the presentation

$$\frac{T_{wall\ max_p}}{T_{mix_{p_{jet\ =\ centered}}}}$$

$$\text{where } T_{wall\ max_p} = \frac{T_{wall\ max} - T_{amb}}{T_{T_N} - T_{amb}}$$

$$T_{mix_{p_{jet\ centers}}} = \frac{T_{mix} - T_{amb}}{T_{T_N} - T_{amb}} \quad \text{(exhaust jet centered and undeflected)}$$

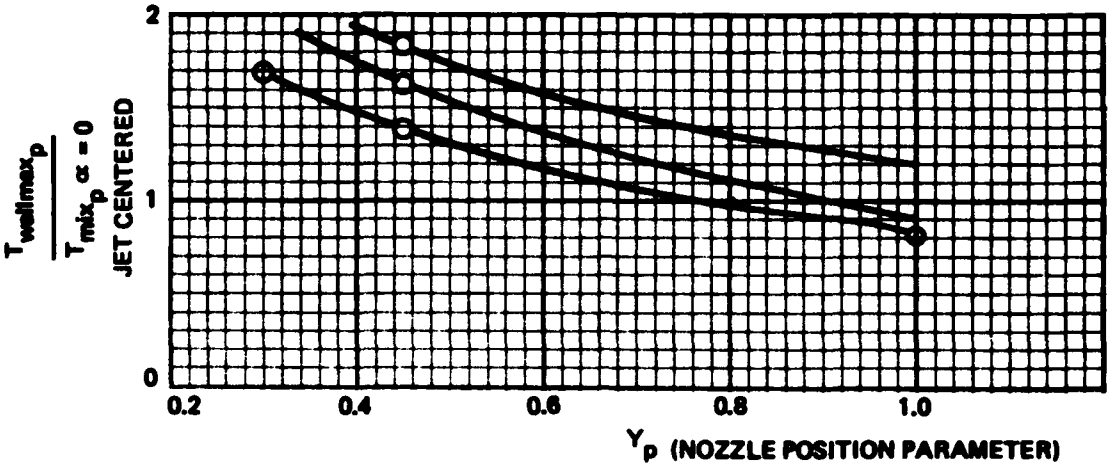

MAXIMUM SIDEWALL TEMPERATURE VARIATION

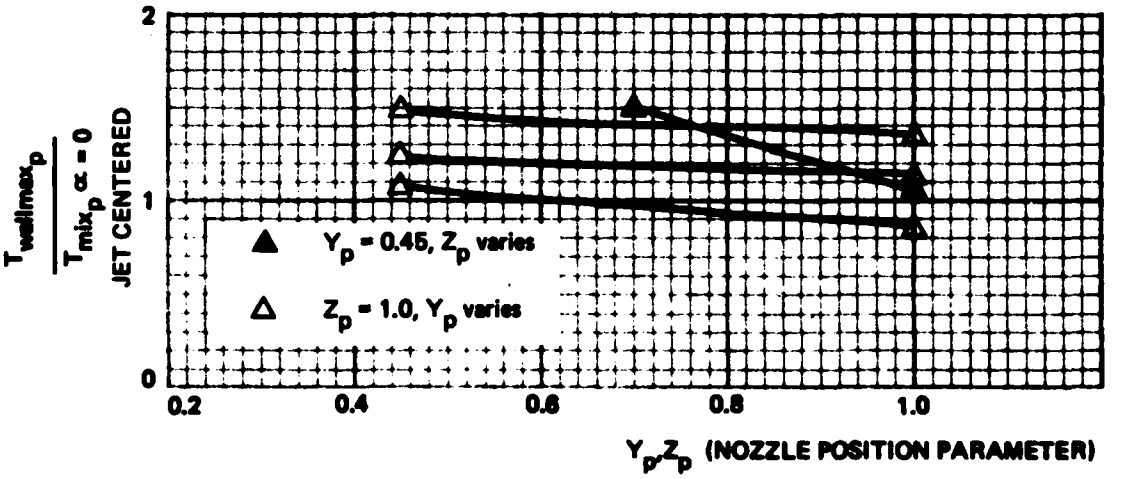

MAXIMUM TOP AND BOTTOM WALL TEMPERATURE VARIATION

NOTE: VERTICAL SCALES DEFINED ON FIGURE 2-21

Figure 2-20. Variation of maximum wall temperature with jet nozzle lateral and vertical position for the obround augmenter.

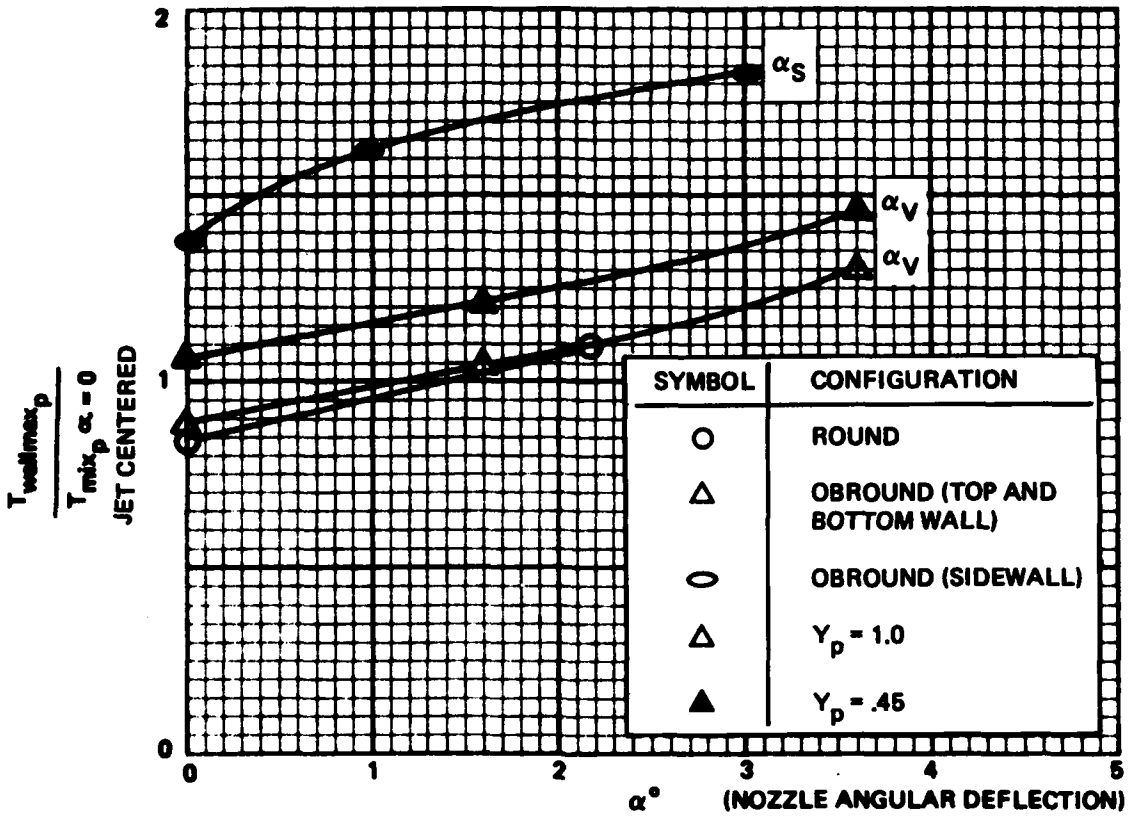

$$\frac{T_{wallmax_p}}{T_{mix_p\ \alpha=0\ \text{JET CTR'D}}} = \frac{\text{maximum wall temperature parameter}}{\text{mixed average temperature parameter for a centered, undeflected jet}}$$

Figure 2-21. Variation of maximum wall temperature with lateral and vertical jet nozzle deflection.

To apply these curves, the applicable curves in figures 2-9, 2-10, and 2-11 are used to get the augmentation ratio parameter for the centered, undeflected exhaust. In design calculations, one will probably assume an augmenter pressure ratio of

$$\frac{P_{T_{sec}}}{P_{T_{exit}}} = 0.9975$$

which typically corresponds to a Hush House static pressure depression of 2" H_2O. Next, figure 2-19 is applied to find the mixed temperature parameters T_{mix}. The curves in figure 2-19 were calculated from conversion of energy

relationships assuming values of exhaust specific heat which were reasonable at each T_{T_N}/T_{amb} level. Finally, figure 2-20 or 2-21 are used to determine the ratio

$$\frac{T_{\text{wall max}_p}}{T_{\text{mix}_{p_{\alpha=0}}}}$$
(jet centered)

from which $T_{\text{wall max}_p}$ and $T_{\text{wall max}}$ can be calculated.

d. Jet Nozzle Base Pressure. Scale-model test measurements (ref 1) were made to determine how the base pressure is affected by the total suppressor environment. Because of the nozzle "boattail" configuration, the base pressure was significantly below ambient pressure.

$$\frac{P_{NB}}{P_{amb}} = .996 \text{ for all } \lambda_N \text{ and } T_{T_N} \text{ conditions.}$$

A base pressure parameter, P_{NB_p}, is defined to show how the base pressure pump-down with the jet inside a Hush House would compare to the pump-down during out-of-doors (free-field) operation.

$$P_{NB_p} = \frac{(P_{NB} - P_{interior}) - (P_{NB} - P_{amb})}{P_{amb}}$$

$$= \frac{(P_{NB} - P_{EE})_{\text{with augmenter}} - (P_{NB} - P_{EE})_{\text{jet survey}}}{P_{EE}}$$

When an aircraft is placed in a Hush House, the Hush House interior pressure becomes, in effect, a different reference ambient pressure. A base pressure parameter of -0.0005, for example, would imply that the nozzle base pressure in the Hush House environment is 2" H_2O lower, relative to this new reference ambient pressure, than the free-field base pressure relative to barometric pressure. Figure 2-22 presents the base pressure parameter plotted

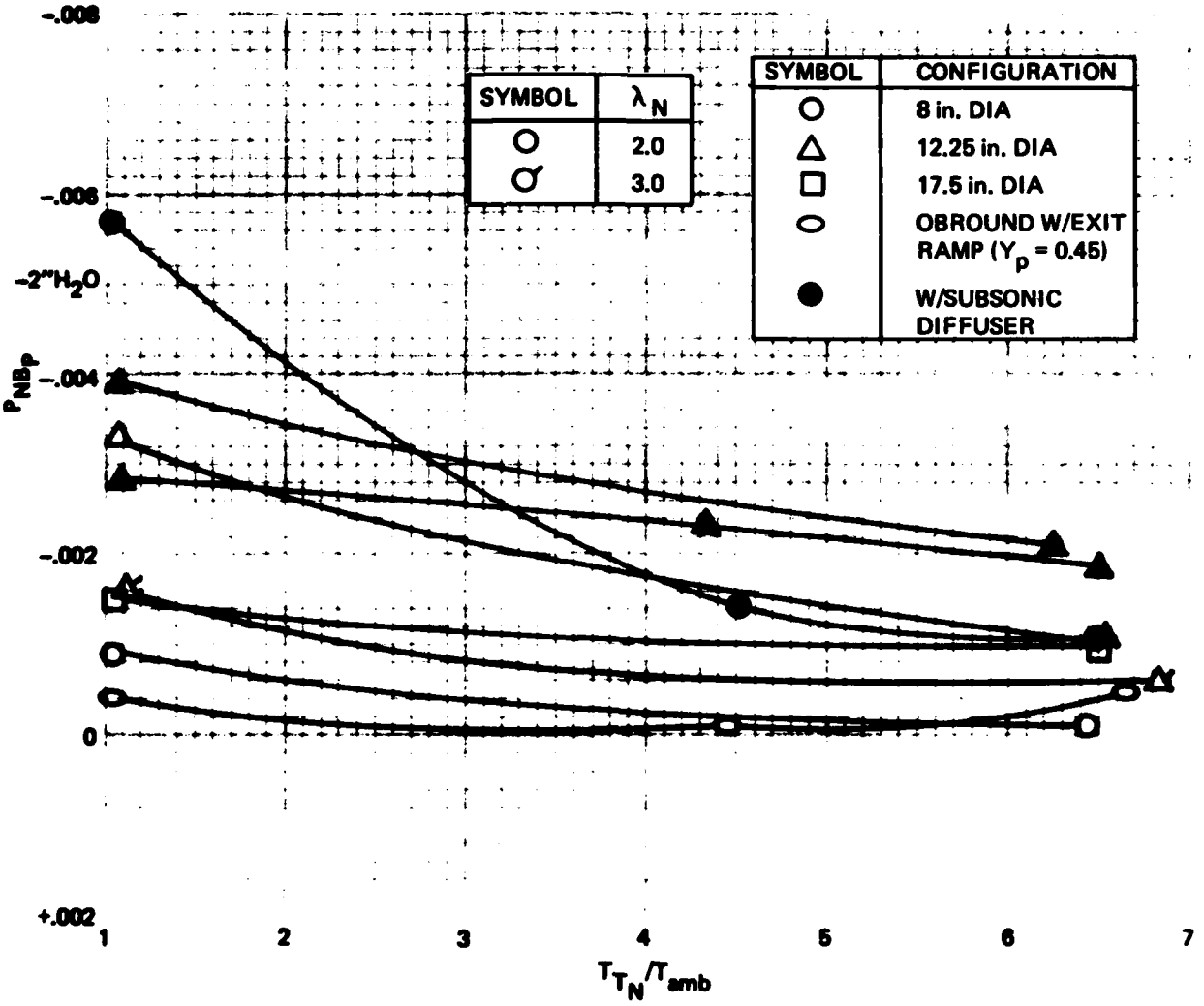

Figure 2-22. Nozzle base pressure parameter vs jet nozzle to ambient temperature ratio for various augmenter configurations.

versus jet nozzle to ambient temperature ratio for a variety of test configurations with a typical military engine nozzle exit to augmenter entrance spacing configuration. The data show little excess nozzle base pump-down for most configurations when the jet nozzle to ambient temperature ratio, T_{T_N}/T, corresponds to military or afterburning power. The pump-down increases with the increased pumped flow associated with the addition of a subsonic diffuser. A very small pump-down is apparent with the obround augmenter, which implies that the nozzle base pressure with Hush House operation will bear the same relationship to the Hush House interior pressure as the free-field operation base pressure does to barometric pressure.

Figure 2-23 shows the influence of nozzle exit to augmenter spacing on base pressure parameter. As the jet nozzle exit is moved very close to the augmenter entrance, the base pressure is influenced more and more by reduced static pressures in the pumped flow entering the augmenter, and the base pressure parameter becomes more and more negative. At large spacings between the nozzle exit and augmenter entrance, on the other hand, the situation at the nozzle base approaches the free field situation and $P_{NB_p} = 0$ within the measurement accuracy.

The base pressure parameter shows little excess pump-down for configurations typical of Hush House installation with normal engine operating conditions.

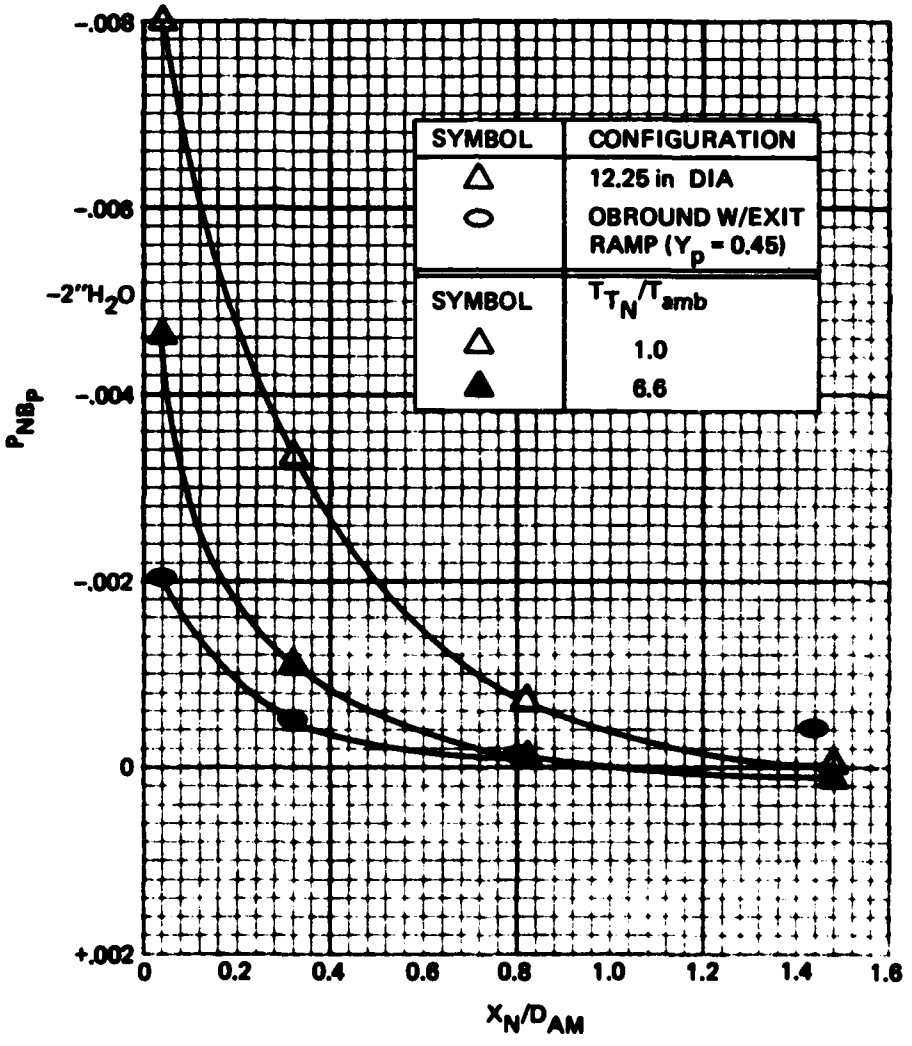

Figure 2-23. Nozzle base pressure parameter vs jet nozzle exit to augmenter entrance spacing parameter.

e. Acoustical Design. This section presents a method for predicting the sound power level (PWL) of exhaust noise (in octave bands) radiated from the augmenter exit of any prospective "Hush House" design. This prediction procedure, which is based on measurements made during scale-model experiments (ref 1), enables one to estimate:

- The octave-band sound power level spectra of jets of various diameters, pressure ratios, and temperatures.
- The differences in radiated sound power level as a function of frequency among lined augmenter tubes of different lengths, diameters, and lining depths (thicknesses).
- The octave-band sound pressure level (SPL) of the exhaust noise at various distances from the exit.
- The octave-band sound power level of interior noise attributable to the exhaust.

The lining consists of a thin porous layer with partitioned airspace behind. This configuration must be designed to optimize the low frequency attenuation of the augmenter for a chosen geometry. The considerations of lining material are discussed more fully in the Final Design Considerations section further along in this text. Careful consideration must be given to choice of specific flow resistances of lining material.

The basic design concept of a lined augmenter tube, to attenuate jet exhaust noise to meet typical community noise criteria, is considered to be generally applicable to modern-day military jet engines with afterburner. However, if the noise output or the community noise criteria strongly differ from these typical values, then a redesign of the liner yielding more effective use of space and materials may be called for.

(1) Prediction of Jet Sound Power Level Spectra. The PWL spectra of various aircraft are usually available either from the manufacturer or from the environmental noise groups. If unavailable, the PWL spectrum of an engine is estimated by using the procedure outlined below. It is recommended that estimates based on the following procedure be compared to measured levels. To be conservative, use the higher of these two levels as a design guide.

- Calculate from equation below the upward shift (PWL_s) of the sound power level spectrum shown in figure 2-24.

- Shift the "normalized PWL" curve in figure 2-24 vertically by the dB amount calculated.

- Establish full-scale frequencies by shifting to the right the model-scale by the factor 0.36 D_N, where D_N is the full-scale nozzle diameter in inches.

$$PWL_s = 20 \log (D_N) + 20 \log (T_T) + 30_N \log (\lambda_N) - 63$$

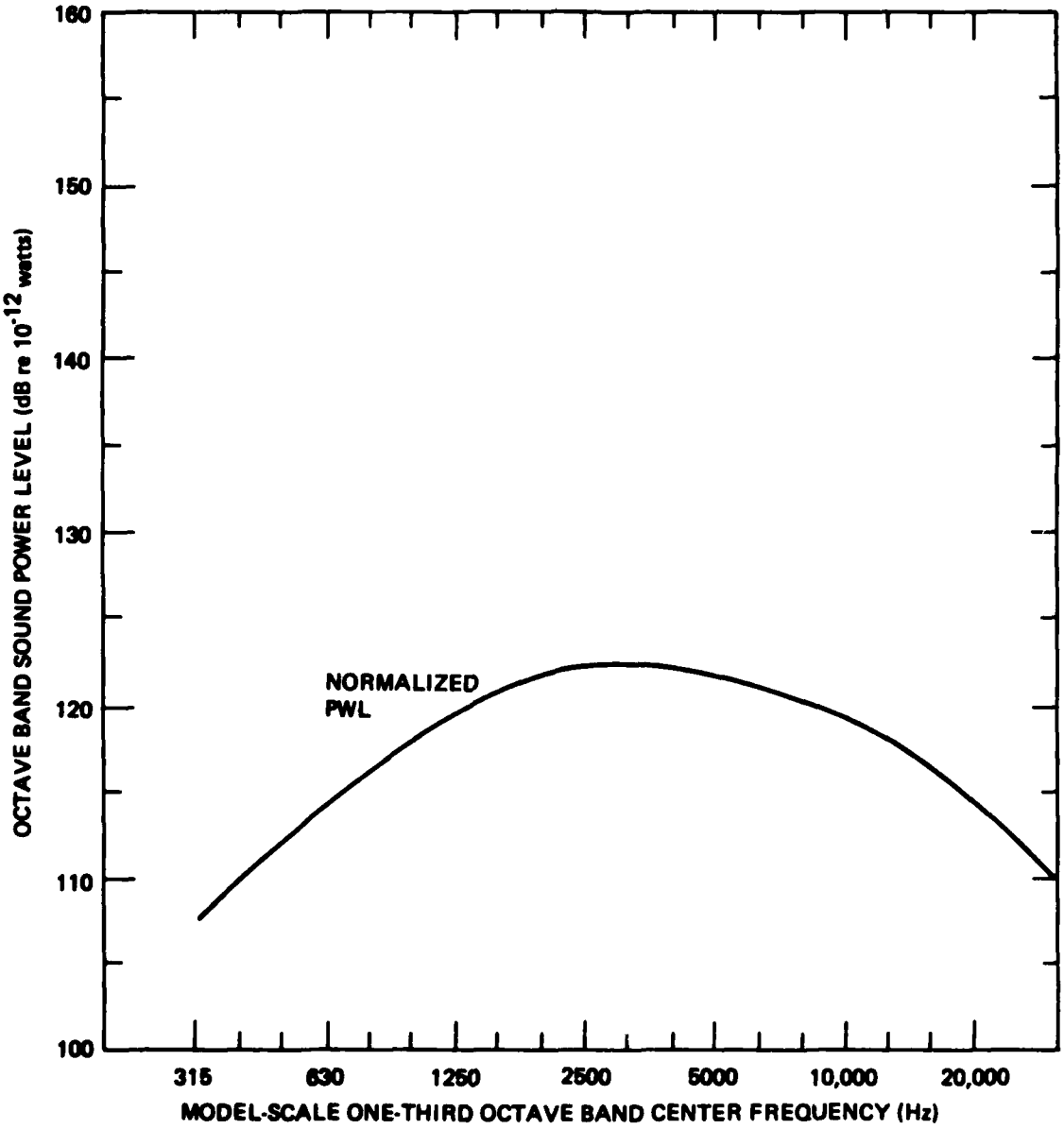

Figure 2-24. Normalized octave band PWL spectrum.

where T_{T_N} is the jet nozzle total temperature in degrees (°) Rankin and λ_N is the jet nozzle pressure ratio.

(2) Augmenter Attenuation. Before considering the attenuation characteristics of the lined augmenter, one must first check that the open cross section is of sufficient area that the exit velocity of the exhaust flow is minimized to the point at which self-noise levels are low enough to meet the noise criteria. We recommend that, until more accurate design information becomes available, the initial cross section be chosen so that the exit velocities listed in table 2-2 are not exceeded. The average exit velocity can be calculated from the total facility mass flow, the mixed average exhaust temperature, and the augmenter cross-sectional area. In listing the maximum velocities, we further assumed that the ratio of maximum to average velocity is 2.4. The attenuation provided by the augmenter (ΔPWL), depends in a complex manner on a variety of parameters. Baseline data (ΔPWL_o) are provided in figures 2-25 and 2-26 for a range of pressure ratios (λ_N) and total temperatures (T_{T_N}). These data were obtained during 1/15 scale-model tests with a single augmenter effective duct diameter of 12.5 inches, a duct length

Criteria At 140 ft	Maximum Permissible Velocity (fps)	
(dBA)	$V_{mix\ max}$	V_{AV}
75	360	150
80	440	180
85	530	220
90	640	265
95	775	320

Table 2-2. Maximum exit flow velocity to meet noise criteria at 140 ft from the exhaust box.

of 72 inches, a ramp of 45 degrees, and an axial distance (X_N) of 4 inches between the jet nozzle exit and the augmenter entrance. The obround augmenter was used with the nozzle in the offset position (Y_p = 0.45). To the ΔPWL_0 obtained from figure 2-25 or 2-26, one must add incremental attenuations that account for changes in lined augmenter length (ΔPWL_1), augmenter diameter (ΔPWL_2), axial and radial positions of the engine within the augmenter inlet (ΔPWL_3 and ΔPWL_4), and angular alignment (ΔPWL_ζ). Methods for estimating these corrections are given below. The final estimate of augmenter attenuation is the sum of the components:

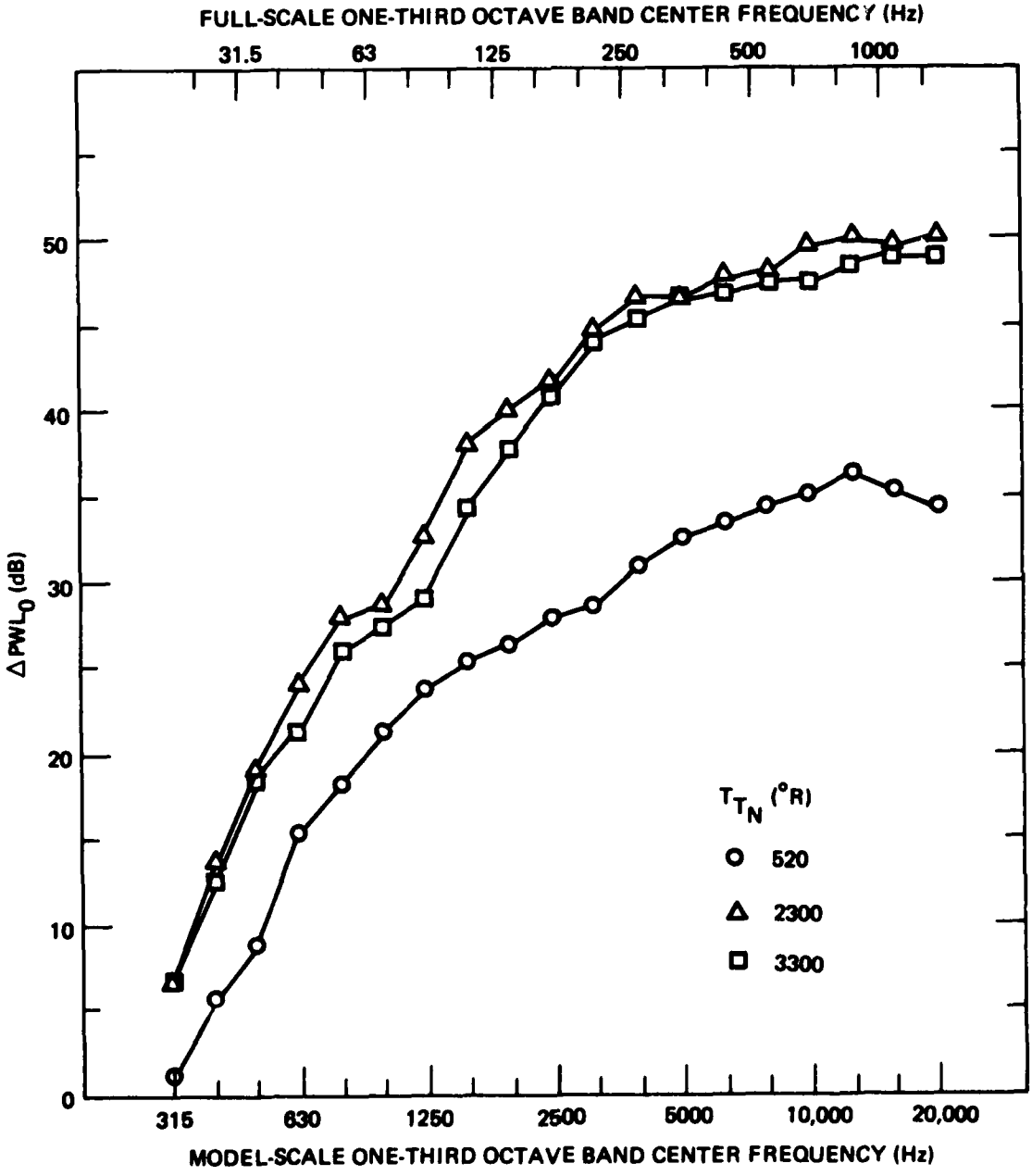

Figure 2-25. PWL_0 for 72-inch-long BBN model augmenter for λ_N = 2.

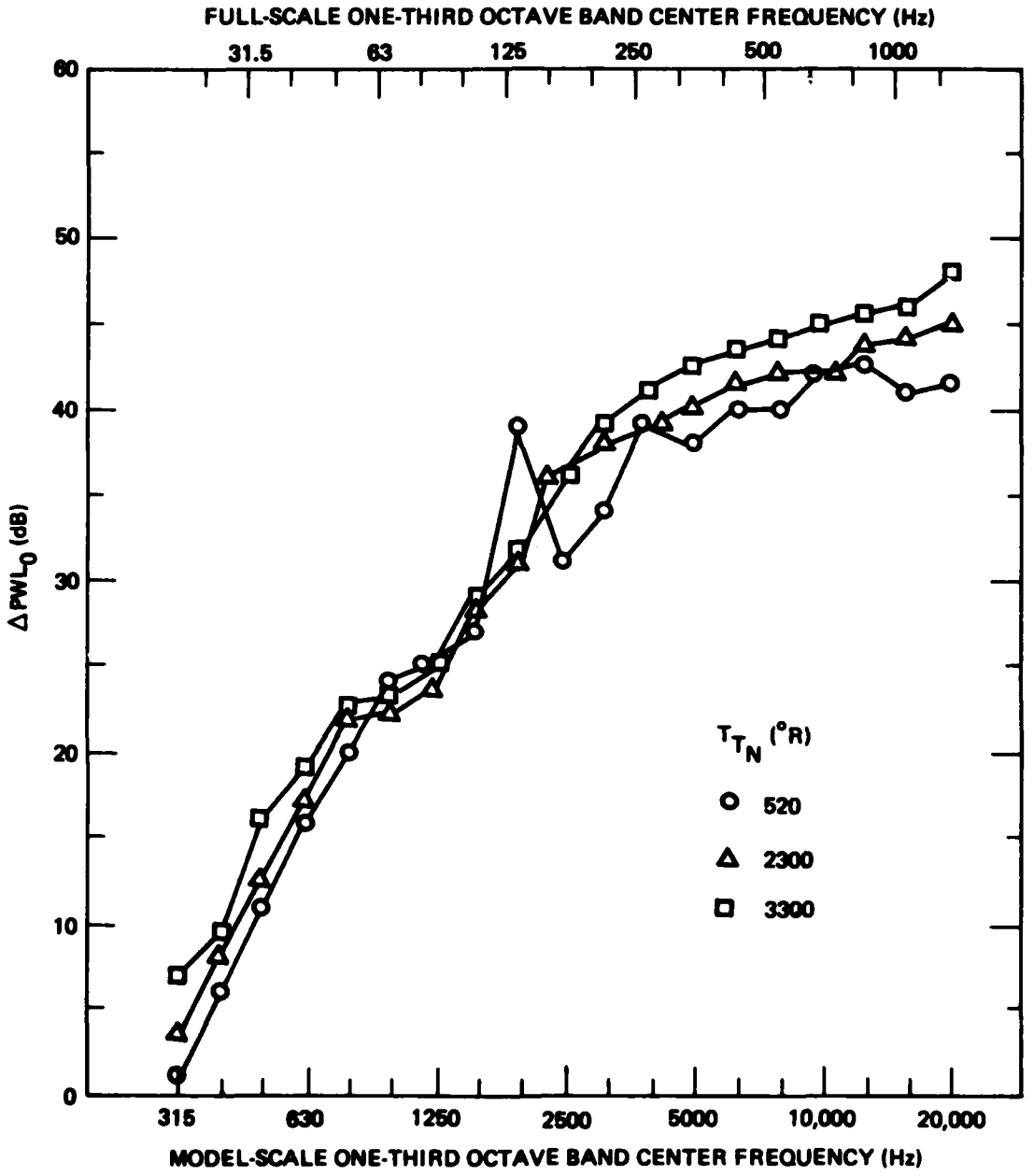

Figure 2-26. PWL_o for 72-inch-long BBN model augmenter for $\lambda_N = 3$.

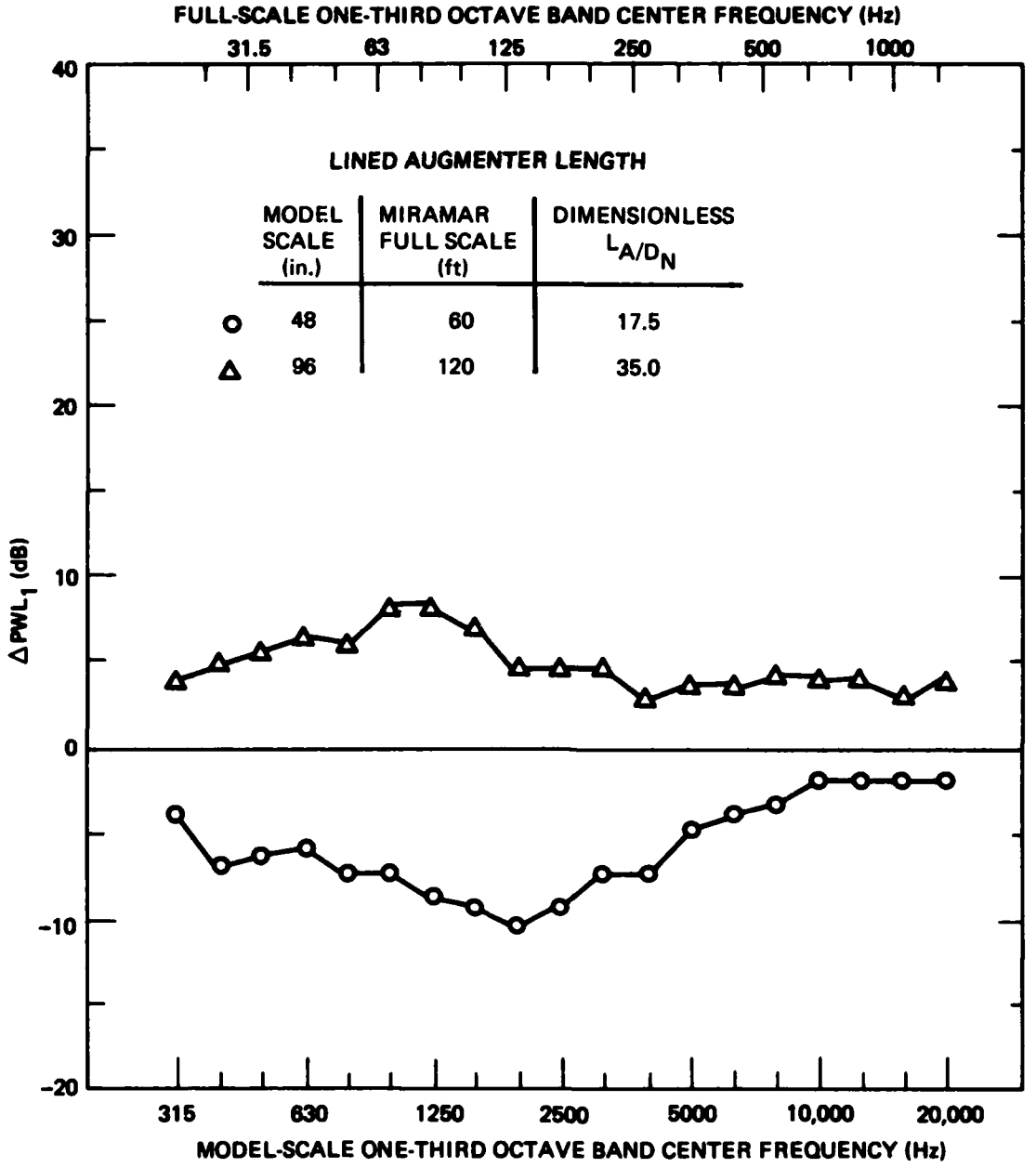

Figure 2-27. Correction to Δ PWL for different augmenter lengths.

$$\Delta PWL = \Delta PWL_0 + \Delta PWL_1 + \Delta PWL_2 + \Delta PWL_3 + \Delta PWL_4 + \Delta PWL_5.$$

(3) Augmenter Length. The baseline data (ΔPWL_0) are presented for a model augmenter tube length of 72 inches. In figure 2-27 is shown a correction, ΔPWL_1, to the attenuation provided by the baseline augmenter for dimensionless augmenter lengths of 17.5 and 35.0 - ie, ratios of augmenter length to nozzle diameter (L_A/D_N). ΔPWL_1 for intermediate lengths can be determined by interpolation.

(4) Augmenter Diameter. All lined augmenter configurations tested had the same cross-sectional dimensions, corresponding in model scale to the Miramar Hush House augmenter. The dimensionless ratio of the equivalent diameter of the augmenter cross section (D_A) and the nozzle diameter (D_N) for all the test runs was 4.54. No other augmenter diameters were tested, so the corrections (ΔPWL_2) for augmenter diameter suggested here are based on theoretical considerations. The analytical models from which they were derived ignored the effects of velocity and temperature gradients and so should be used to account for small variations in the dimensionless effective augmenter length.

At low frequencies, frequencies at which the wavelength of sound in the augmenter tube is large compared to the transverse dimensions of the augmenter tube, the correction ΔPWL_2 for a change in the effective diameter of the augmenter is

$$\Delta PWL_2 = \Delta PWL_0 \left(\frac{nD_{AM}}{D_A} - 1 \right)$$

where D_{AM} is the effective diameter of the augmenter tube in the model (12 inches) and n is the linear scale factor for the augmenter being designed.

At high frequencies, frequencies at which the wavelength is smaller than the transverse dimensions of the duct, the correction for the effective diameter of the augmenter tube is

$$\Delta PWL_2 = -10 \log_{10} \left(\frac{D_A}{nD_{AM}} \right)$$

A rough estimate of the change in augmenter attenuation with diameter can be synthesized from these two relations by using the first of the above equations for full-scale frequencies that are less than c/D_A and the second for full-scale frequencies that are greater than $10c/D_A$. The correction at intermediate frequencies should be faired to provide a smooth progression between the two extreme values.

(5) Nozzle Position. The correction (ΔPWL_3) for three variations in the axial position of the nozzle is presented in figure 2-28; a correction (ΔPWL_4) for centering the nozzle on the longitudinal axis of the augmenter is provided in figure 2-29. The corrections for 1 and 3-degree angular misalignments are given in table 2-3.

	Octave-Band Center Frequency (Hz)								
	31	63	125	250	500	1000	2000	4000	8000
PWL_5 for 1°	0	0	0	-1	-2	-2	-2	-2	0
PWL_5 for 3°	0	0	0	-4	-4	-4	-4	-4	0

Table 2-3. Corrections for angular alignments.

(6) Augmenter Lining. The open cross-sectional area of the augmenter tube must be chosen to satisfy pumping requirements along with wall temperature and self-noise limitations. The capability of the augmenter to attenuate the noise of the engine under test is determined by the type of dissipative lining used and by the length of the lined augmenter. Practically all linings that provide a high degree of sound absorption in the entire frequency range of interest will yield high sound attenuation. This high absorption coefficient can be achieved either by filling the entire lining depth with a porous sound absorbing material or by concentrating near the augmenter wall a relatively thin layer of porous material backed by an airspace.

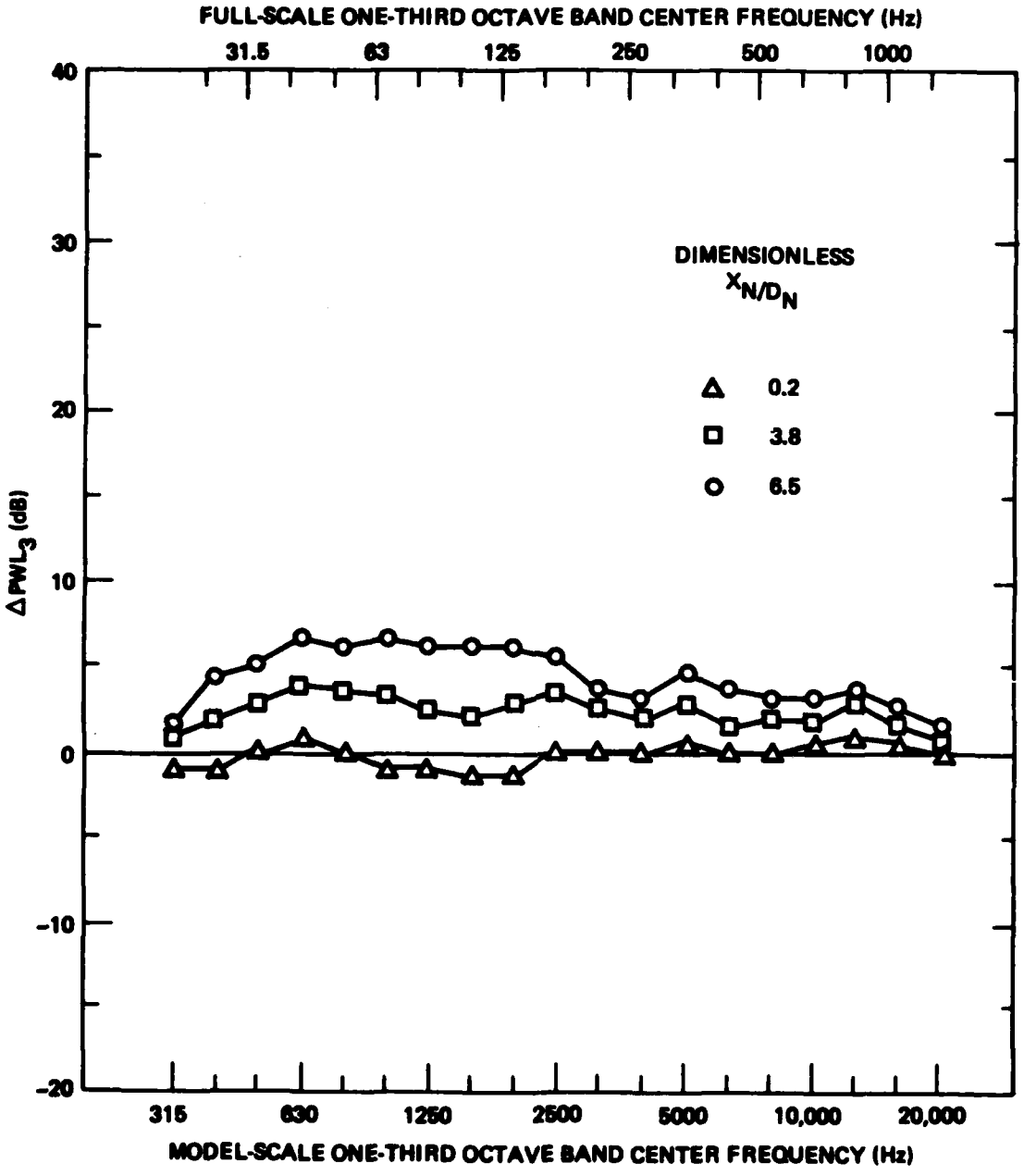

Figure 2-28. Correction to Δ PWL for different jet nozzle axial positions.

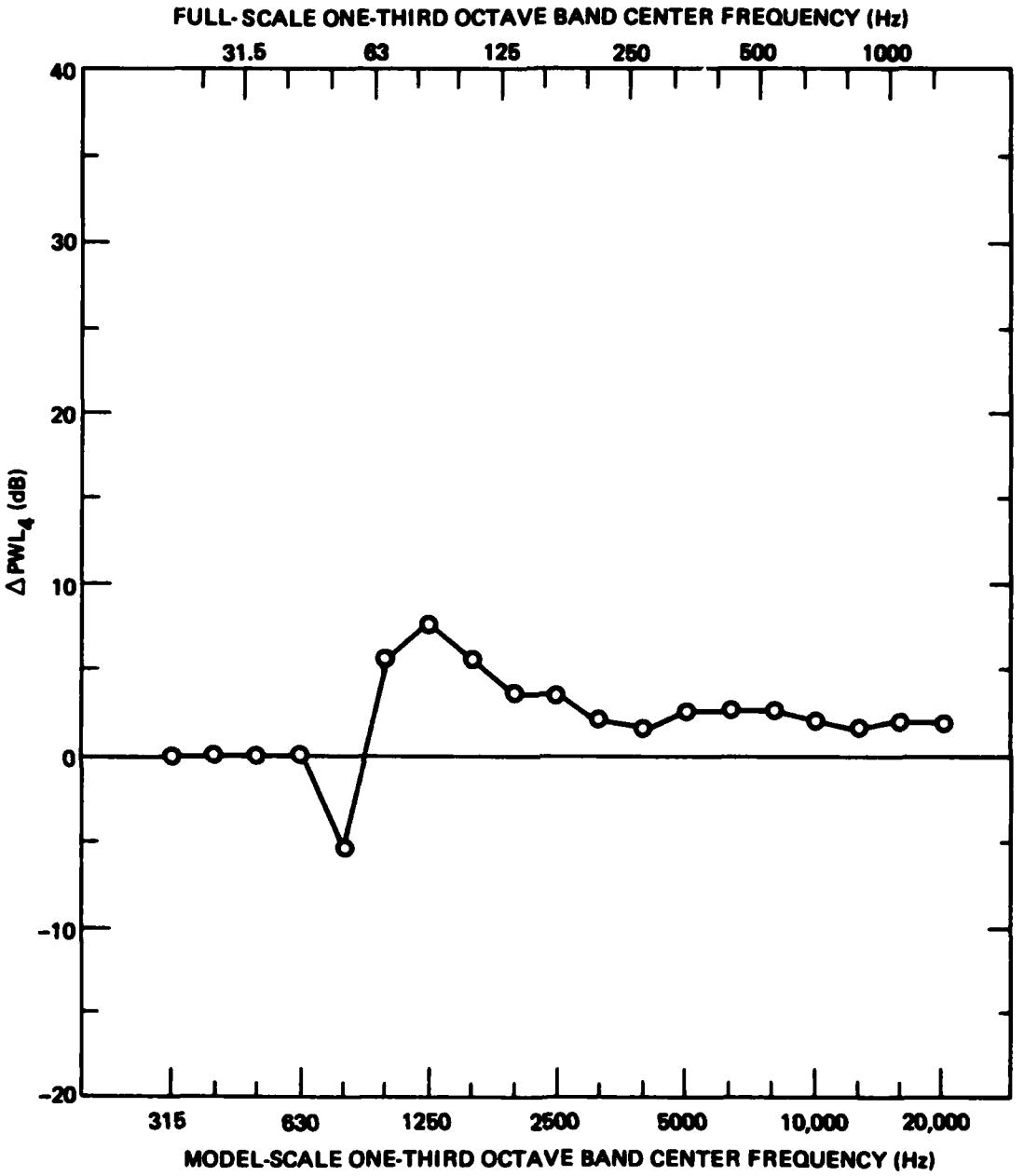

Figure 2-29. Correction to Δ PWL for center position of jet nozzle.

The lowest frequency at which substantial attenuation is achievable is determined by the total thickness of the lining (including the porous layer and the airspace behind). A reasonable choice is to have the average thickness of the lining correspond to 1/6 wavelength at room temperature for the lowest frequency of interest.

The thin porous lining backed by an airspace provides better low frequency attenuation than the "fully packed" lining. As a practical rule, the lining thickness should be between 4 and 12 inches and the total flow resistance should be in the range of 1600 and 5000 rayls [a unit of flow resistance - ie, $\frac{\text{dyne-s}}{\text{cm}^3}$] at room temperature.

The specific choice of lining materials is dictated by temperature and mechanical stability considerations and by availability. Accordingly, each material which fulfills these requirements and has the above-listed or up to 50% lower specific flow resistance can be used. The lining must maintain characteristics under adverse (high noise, temperature, and airflow) conditions. Present trend in the construction of lining material is a tightly wrapped pillow.

(7) Estimation of Sound Pressure Level Spectra. The exhaust PWL radiated by the augmenter outlet is estimated by subtracting the attenuation (PWL) calculated in accordance with section (b) from the free-field sound power level of the jet obtained from experimental data or scaled up from model data by the method of section (a):

$$PWL_{outlet} = PWL_{free} - \Delta PWL.$$

The octave-band SPL at a distance R from the augmenter outlet is then given by

$$SPL = PWL_{outlet} - 20 \log R + 3 + DI\ (\phi),$$

where R is the distance (ft) from the center of the exhaust stack and DI is the directivity correction in (dB) for sound propagation parallel to the ground. The directivity correction as a function of frequency and directivity

angle (ϕ) was determined experimentally for the full-scale Miramar exhaust with a 45 degree exhaust ramp. The angle is defined as being 0° in the downstream direction along with the centerline of exhaust stack, and increasing in the direction of the engine. For example, 90 degrees is perpendicular to the augmenter tube and is to the right (looking upstream) if the starboard engine is running and to the left if the port engine is running. Table 2-4 presents a typical measured directivity.

	Octave-Band Center Frequency (Hz)								
Direction	31.5	63	125	250	500	1000	2000	4000	8000
0°	0	1	2	2	3	2	3	2	3
45°	1	1	2	3	4	3	4	3	4
90°	-1	-1	-1	-1	1	1	2	1	1
270°	-1	-4	-3	-3	-3	-3	-3	-3	-2
315°	-1	-1	-1	-1	-0	-1	-1	-2	-2

Table 2-4. Directivity of the Miramar exhaust for F-14A with one engine in maximum afterburner.

(8) Prediction of Exterior Noise Level. Using the calculated PWL value, and the calculated/measured, nozzle/aircraft, engine PWL value, we can then correct for angular alignment (ΔPWL_5) and distance from the exhaust stack to the point of concern (-20 log (distance to point) + 3 dB). It is easiest to work in A-weighted level and octave frequency bands.

(9) Prediction of Interior Noise Level. In addition to the exhaust, other noise sources affect interior noise levels (eg, engine inlet and casing noise). Thus, we cannot present here a quantitative design of Hush House interior acoustic treatment.

Parameters that affect exhaust SPLs in the interior of a Hush House are:

- Jet sound power level

- Jet nozzle position, especially axial distance from the augmenter inlet

- Augmenter lining

- Acoustical absorbing material on walls and ceiling (it is assumed that the floor will be hard)

- Position in the Hush House (ie, distance and direction from the jet nozzle).

General guidelines for minimizing exhaust noise in the Hush House interior are:

(a) Place the jet nozzle as close as possible to the augmenter inlet. (Remember, however, that exterior exhaust noise decreases with increasing X_N.)

(b) Acoustically treat the bellmouth of the augmenter and the augmenter retaining wall. This will provide absorption for the acoustic energy radiated by the jet at angles greater than 20 degrees from the jet exhaust axis.

(c) Line the augmenter from the inlet to a minimum of 9 jet diameters downstream of the inlet.

(d) Make sure that the lined augmenter has sufficient attenuation that, at all frequencies, the sound returning to the Hush House through reflections from the end of the augmenter tube is low compared to the noise of the free jet propagating forward. This condition can usually be met if the attenuation of the augmenter tube exceeds 10 dB.

(e) If SPLs in the Hush House are not to exceed the levels measured at corresponding locations in free field about the aircraft by more than 2 or 3 dB, acoustically treat all interior surfaces (except the floor) with sound absorbing material.

3. Design Considerations - Life Cycle

The aim of this section is to provide information extracted from investigations of acoustically related problem areas associated with suppressor operation and alternative considerations for noise reduction. Problem areas (primarily maintenance cost) were identified during early full-scale fleet operation of the first acoustical enclosure. Structural and acoustical material investigations were performed. Alternative noise reduction techniques and augmenter tube material selections and techniques for reduction of wall temperature were investigated for use in future acoustical enclosure design. The subsequent designs based on material selection and noise reduction techniques presented must still be evaluated for cost benefit relative to the initial augmenter tube designs.

a. Background. During initial design the basic augmenter tube configuration is determined by the type of aircraft to be tested and suppressor utilization. This configuration is based on augmenter sizing for flow/jet noise reduction, augmenter pumping, wall temperature limits, and life cycle requirements. A noise suppression study by Gustav Getter Associates (ref 7) provided the basic structural design and material choice for acoustical enclosures using an air-cooled augmenter tube. Completion of the first full-scale acoustical enclosure and Fleet operation provided valuable data for future design. Using identified materials, problem areas, and potential requirements for further reducing noise levels, both model and full-scale evaluations were performed.

b. Materials. Full-scale and analytical analyses were made of the structural integrity of the forward enclosure; ie, the augmenter acoustic liner material and the perforated metal liner. The objective was to develop the least cost (life cycle) design alternative.

---

[7] Gustav Getter Associates Engineers Report, Aircraft Noise Suppression Study, July 1973.

(1) Forward Enclosure. The forward enclosure that houses the jet aircraft is of a modular Butler-type construction. The frame is fabricated from 4.8 mm A-36 plate bent to form a channel. The concrete panels are precast on to light gage metal forms between the channels. The channels are then bolted together with the metal forms facing the enclosure interior. Acoustic treatment is integral to the panels on the interior surface between frame bases.

A potential problem was identified during early operation of the acoustical enclosure. Cracks developed along the concrete panel walls. A full-scale test program was performed in the acoustical enclosure to determine whether the high steady jet noise state and/or high impulse sound levels during compressor stall would degrade the structural integrity of the the forward enclosure. Reference 8 provides details of the test program. Tests of the structure's response during actual aircraft operation, which included peak pressure levels of 149 dBA during afterburner ignition, showed stresses reaching plus or minus .5 kPA (.07 psi); maximum accelerations were found to be plus or minus 7 g in the steel frame of the roof; acceleration in the concrete panels found to be plus or minus 3.5 g. Mathematical analysis of the structure shows that instability of the design occurs in the frame supports at 10 kPA (1.5 psi) and in the concrete panels at 3.5 kPA (0.5 psi). These levels are well above the operational acoustic/vibration levels measured in the forward enclosure. The full-scale evaluation indicated that acoustic induced levels within the acoustic enclosure were not sufficient to damage the structure. The concrete cracks were considered cosmetic rather than structurally damaging.

(2) Augmenter Tube. The augmenter tube is constructed of obround metal sections fastened at the channels. The obround section's interior consists of numerous frame bays. The original design (ref 7) used mineral wool to fill the bays. A facing of corrugated metal liner supports the mineral wool. During operation two types of problems developed with augmenter

---

[8] Civil Engineering Laboratory; G Warren, Ambient Excitation of Hush House Acoustical Enclosure during F-8 Tests, TM-51-78-19, August 1978

tube. The hot jet velocity exhaust flow shifted/decinerated the mineral wool and caused the metal liner to crack/break off.

Programs were initiated to evaluate cost effective approaches to these problems. The programs had two thrusts: (1) to develop an acoustic liner material or resonator concept, and (2) to develop the technology to provide a least-cost metal liner which would function in the jet exhaust environment in conjunction with the acoustic liner material.

(a) Acoustic Absorption. The augmenter tube jet exhaust presents a destructive environment for most acoustical lining materials. Since the acoustic liner material (bulk absorber) in combination with the metal liner provides the necessary absorption, two approaches were pursued in order to provide a cost effective treatment. The first involved the concept of a multituned resonator. The second involved the selection of a bulk absorber lining material with flow resistance and absorption coefficients sufficient to insure a reduction in jet noise exhaust to 85 dBA when measured at a 250-foot radius from the engine exhaust plane.

(i) Multituned Resonator. An investigation (ref 9) devised an approach to achieve acoustic absorption in an obround augmenter tube without the use of acoustic bulk absorber material. The concept is referred to as a multituned resonator. The concept has not been tested. Figure 2-30 predicts the attenuation from the multituned resonator concept. Figures 2-31 and 2-32 provide the design of the obround augmenter tube sections for a 1/15 scale-model acoustic evaluation. This approach may offer the most cost effective design with respect to material cost and mean time between failures. The actual full-scale construction costs have not been determined.

---

9 Rohr Industries Report, An Analytical Study on Acoustical Performance of Perforated Plate Liner for the Augmenter of a Stationary Jet Noise Suppressor, reproduced as NOSC TN 125, April 1977

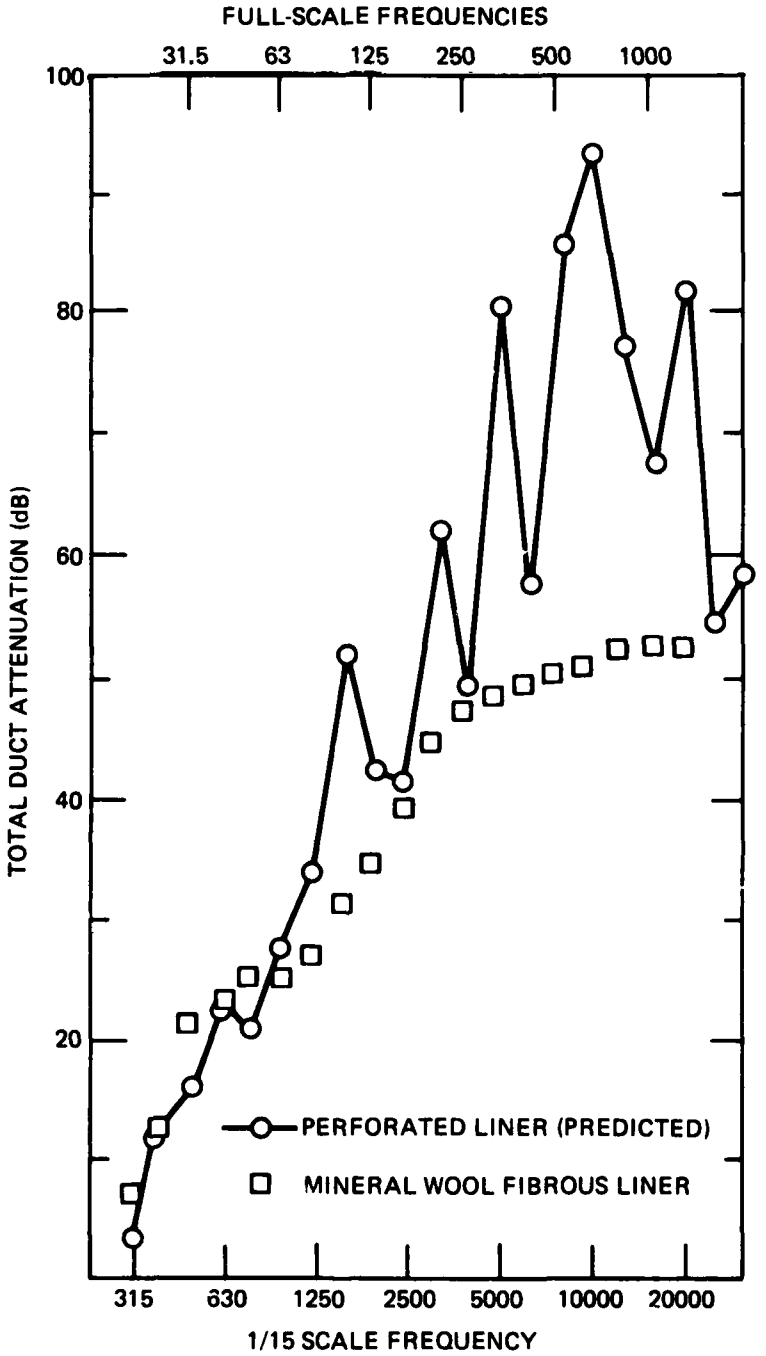

Figure 2-30. Noise attenuation of liners in augmenter.

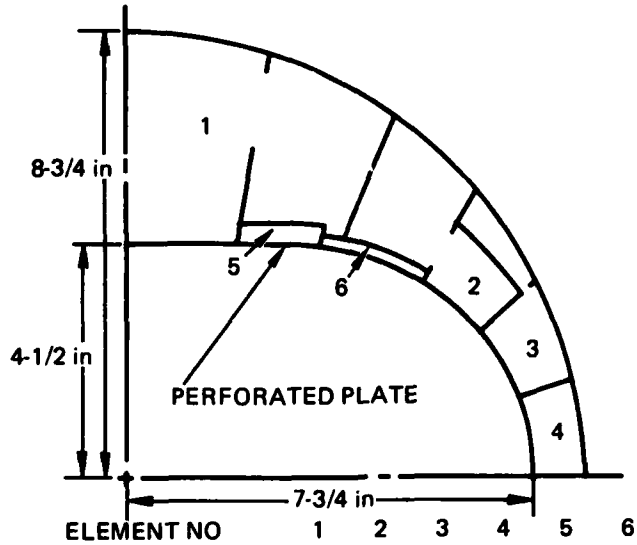

ELEMENT NO	1	2	3	4	5	6
% AREA	20	14.5	14.5	14.5	16	20
CAVITY LENGTH AVAILABLE (in)	7.2	3.6	1.8	1.1	0.45	0.23

Figure 2-31. Perforated liner (multituned resonator) – design of the 1/15-scale obround augmenter (0-48 in = 0-60 ft).

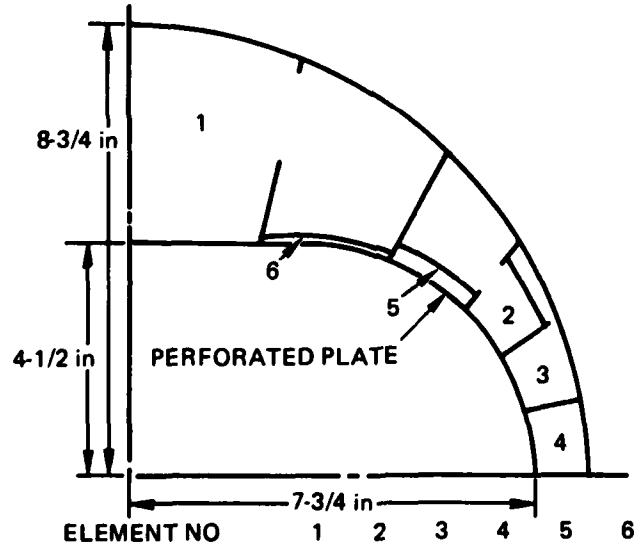

ELEMENT NO	1	2	3	4	5	6
% AREA	25	11.3	11.3	11.3	16	25
CAVITY LENGTH	6.8	3.2	1.6	1.0	0.4	0.2

Figure 2-32. Perforated liner (multituned resonator) – design of the 1/15-scale obround augmenter (49-72 in = 61-90 ft).

(ii) Bulk Absorbers. Numerous materials were evaluated for use in the augmenter tube environment. The first full-scale augmenter tube used batts of mineral wool between the outer cylindrical shell of the tube and the tube interior perforated metal liner. The temperature and acoustic environment burned/decinerated the acoustic absorber (mineral wool). The primary problem areas were along the sides of the obround tube where impingement of the jet exhaust was most pronounced.

Rohr Industries, Fluidyne Engineering Corporation, and Naval Ocean Systems Center used flow facilities, impedance tubes, and some full-scale testing to evaluate candidate material configurations. The following materials were identified as candidates for use in the augmenter tube environment: (1) basalt wool, (2) quartz fibers, (3) mineral wool, (4) stainless steel wool, (5) ceramic blankets, (6) and fiberglass fabric. At least one style of each material above was found acoustically acceptable for the augmenter tube. Temperature constraints and cost (both initial and life cycle) resulted in three approaches in addition to the initial mineral wool batts. The replacement material chosen by Fluidyne for the first full scale-acoustical enclosure exhaust was TIW fiberglass pillows. After installation in the suppressor, the material burned out mainly in the high temperature areas of the augmenter tube. Pillows of basalt wool were used in the design of the second full-scale acoustical enclosure. The basalt wool was found to be an acceptable acoustic liner material. Due to the high cost of basalt wool pillows, a composite pillow consisting of basalt wool and TIW fiberglass was installed and tested in the full-scale augmenter tube. The composite pillow with the basalt wool side facing the jet flow withstood the hot exhaust environment for at least one year. No significant damage was observed. Figures 2-32 and 2-33 show the acceptable range of absorption coefficients for use in the augmenter tube.

We recommend that the design of the composite pillow shown in figure 2-34 be used to line the sides in new augmenter tube design. This composite pillow is the most cost effective (initial cost/life cycle) acoustic absorber tested to date. We further recommend that TIW pillows be installed in the top and bottom sections of the augmenter tube.

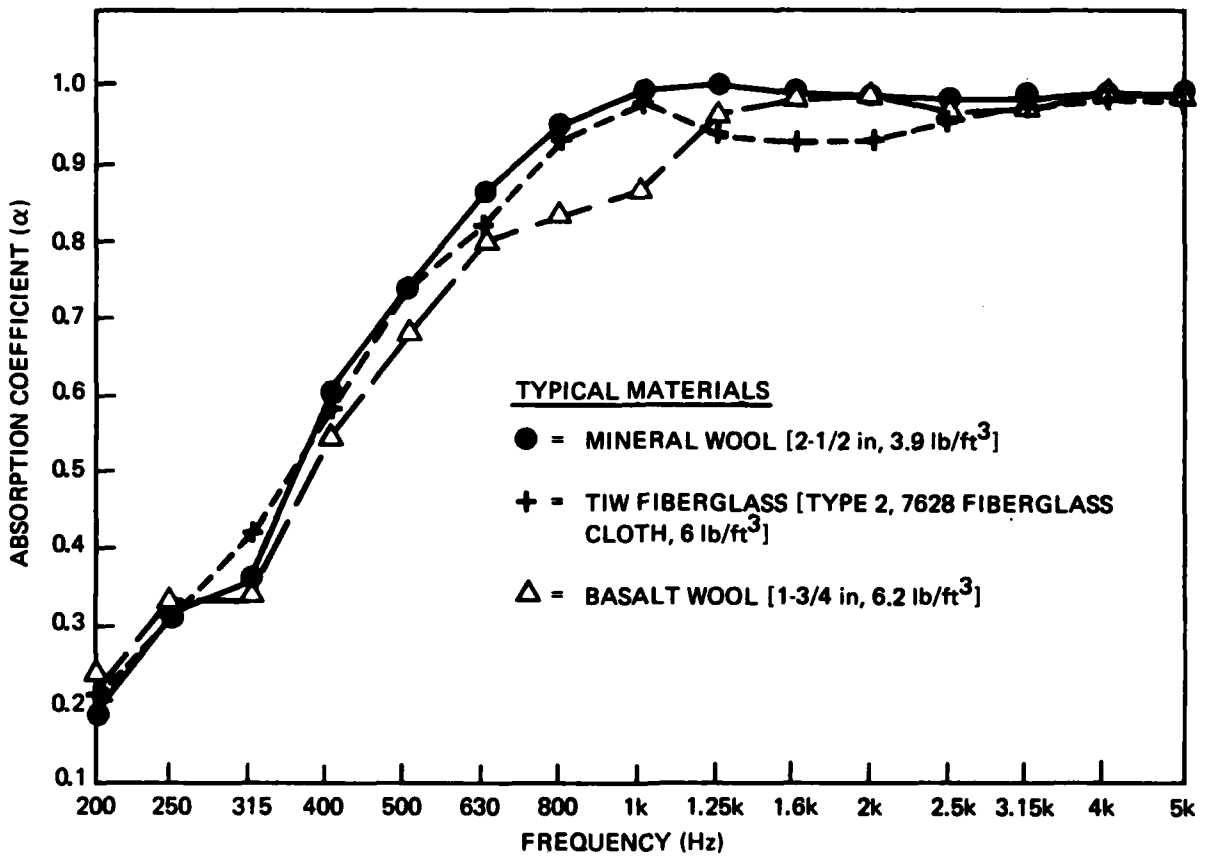

Figure 2-33. Acceptable range of absorption coefficients.

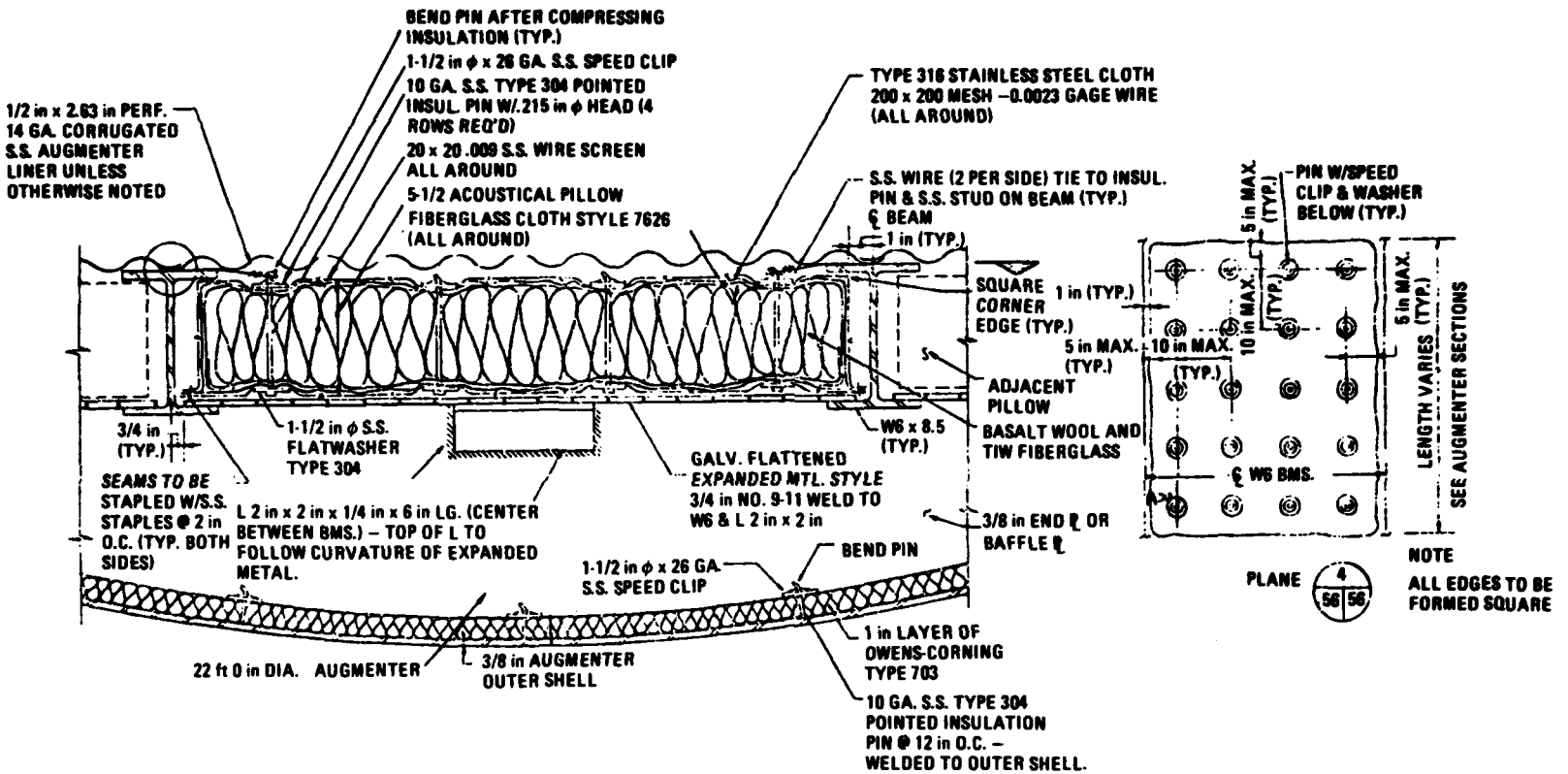

Figure 2-34. Typical composite (basalt wool/fiberglass) acoustical pillow detail.

(b) Metal Liner. The metal liner material for the first full-scale acoustical enclosure is perforated to allow acoustic energy to flow through the bulk absorber acoustical lining material of the augmenter tube. The first full-scale acoustical enclosure used perforated, corrugated panels of stainless steel (type 321) in 3' x 10' sheets. During the first six months of Fleet operation, cracks began to appear in the perforated metal liner. Some sections of panels were eventually blown out by the exhaust flow. Three investigations were performed to establish design changes necessary to increase the metal liner life cycle. Sonic fatigue analytical studies including laboratory test of materials and tests in the augmenter tube of the full-scale acoustical enclosure were performed.

(i) Temperature Exposure Indicators. An investigation (ref 10) was performed to illustrate the changes in color of stainless steel (type 321) as a function of temperature and time. The figure (2-35) provides an inexpensive first indicator of augmenter tube metal liner (stainless steel 321) temperature exposure. The closest color match between the actual metal liner and the grid of heat tint colors gives an indication of the temperature of the metal surface.

(ii) Metal Liner Selection. The selection, sizing, and shape of the material for the design of jet enclosures must be concerned with the static strength of the material as well as with problems of structural, mechanical, acoustical, and thermal fatigue which the enclosure is expected to experience during its operational lifetime. Of most importance in this selection is cost, and it is to cost that optimizations of the various engineering parameters will have to be made in the final analysis. This section deals with the problems of mechanical fatigue, thermal fatigue, source fatigue, and their application to jet enclosures, to decision making processes, and relation to cost factors.

---

[10] Civil Engineering Laboratory; JF Jenkins, Heat Tint Colors on Stainless Steel, TM-52-77-12, February 1977

Mechanical Fatigue. A basic problem in the design of acoustical enclosures will be material fatigue caused by cyclical stresses (ie, stress reversals over a long time period) combined with temperature fatigue.

It has long been known that stresses far below the ultimate strength of a material, as determined by a single load application, will cause rupture if repeated a sufficient number of times. This reduced value of stress is called the endurance limit. This type of mechanical fatigue failure is usually caused by the progressive growth across the section of a minute crack formed in the material at some point of highly localized stress. The point of localized stress may be at a small flaw in the material or at some scratch or discontinuity of the surface. It is vital for this reason that proper selection of a structure material failure strength be considered, as well as the contributing factors to material failure such as (1) surface finish of the material, (2) discontinuities as represented by abrupt changes in cross section, and (3) holes located near or at the edges of the material. For example, in the acoustical enclosure at the Naval Air Station Facility (NAS) at Miramar, it was found that some structural failures had occurred. A contributing factor to these structural failures was found to be the corrugated sheets, which were perforated over 100% of the sheet without leaving unperforated edge margins as called for on the drawing. This resulted in ragged slotted holes under the bolts and welds through perforations at the fixed end of the panel. The jagged edge and welded holes resulted in higher stress concentrations, especially in the welded regions, and consequently resulted in failure initiation points.

Thermal Fatigue. The term "thermal fatigue" is used to describe the failure of reasonably ductile metals by a repetition of thermally-induced stresses. Brittle materials (those with an elongation less than 4 - 5%) usually exhibit such poor behavior in temperature fatigue as to preclude their extensive use. The total stresses include any residual stress from fabrication and heat treatment plus that from temperature gradients plus that from any constraint of free expansion, as well as the applied stress which, if cyclic, will further induce fatigue failure. The choice of material for optimum fatigue performance at elevated temperatures is determined

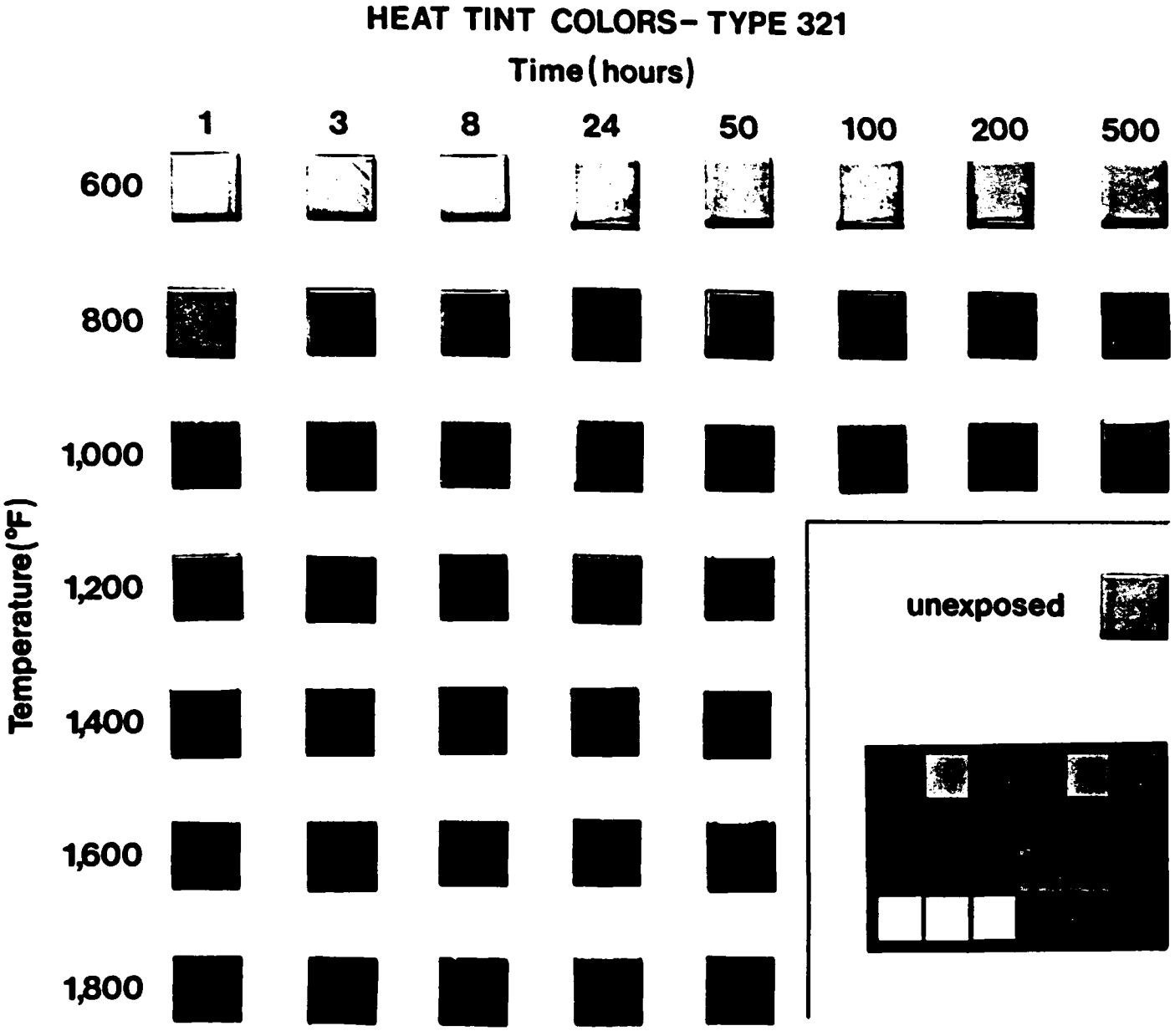

Figure 2-35. Heat tint colors on type 321 stainless steel.

essentially by inherent strength, metallurgical stability, and resistance to corrosion. Changes in the metallurgical structure as a function of temperature are especially important as they may lead to loss of strength, localized strain, and gross distortion.

In designing for thermal fatigue, several factors for the reduction of thermal stresses are:

1. Reduction of constraint on deformation.
2. Minimization of nonuniform expansion.
3. Introduction of compressive residual stress.
4. Reduction of stress concentration factors.
5. Protection of the surface.

Acoustic Fatigue. A purely analytical approach can give only a rough estimate of a structure's life under acoustic excitation, and for this reason it is seldom used except in the most simple of configurations. Most design calculations will combine theory with experiment on the actual structure involved. The experiments, serving to bypass the theoretical difficulties, usually involve the measurement of response, stress, or fatigue life under excitation by noise. These experiments have to be made on a full-scale structure and lead to the development of a sound field in which a given structure would be satisfactory, or this can lead to determination of the stress or strain that can be compared with the known fatigue properties of the materials. To carry out this comparison it is necessary to derive a random fatigue curve using standard, reverse cycle stress and number of cycles data. A most direct approach to the design of a structure such as a jet enclosure involves a chart or nomograph for the particular geometry of fabrication. It further requires only the overall sound pressure level (SPL), duration of the exposure or number of cycles, and the material's random fatigue curve. Of these three parameters, only the last may not be available, but the conversion of the standard S-N data is readily, if approximately, accomplished if the following parameters are known:

$$\bar{s}_r^2 = \frac{\pi}{4\delta(f_n s_o^2 p_r^2)}$$

δ = the damping ratio

f_n = the natural frequency

S_o = the response to the unit static load

P_r = the spectral density

(iii) Augmenter Tube Liner Material. In the design of previous jet enclosures, 321 stainless steel has been used primarily because it is easy to work with and also because it is one of the least expensive of materials suitable for such applications. If one considers cost, then 321 stainless steel proves to be cost effective for most acoustical enclosures. It is, however, a marginal material for structural applications above 1000 degrees F. Almost all tests in a jet enclosure can be so arranged, and the enclosure built large enough, that the test item does not impose extremely high temperatures on the surrounding structure for long time durations. If, however, expected temperature ranges much in excess of 1000 degrees F, then other materials need to be considered.

For example, A286 and 410 have advantages over 321. A286 is a high strength alloy and would lend itself to use in a simple design allowing fairly large unsupported panel sizes. 410 is a low strength material, but is also cheaper and has a low coefficient of thermal expansion. Its marginal strength properties above 1000 degrees F would require more frame supports, tending to off set the material cost savings. Before making definite selections, cost tradeoffs would have to be made depending on sizing, availability of material, costs at that particular time, and factors relating to construction.

Mechanical Properties. Static and fatigue tests have been conducted by Rohr Industries, Inc (ref 11, 12), on several test specimens. These tests included measuring ultimate and yield strengths, elongation, and fatigue lives at room temperature, at 600 degrees F, and at 1200 degrees F. The specimens were "soaked" at these temperatures (ie, temperatures held for a long period of time). This may not be the case in most jet engine testing, as temperatures will not be constantly impinging on the structure at these high values, and, in many instances, the temperature can be considered to be transient. The values obtained in static tests are summarized in tables 2-5, 2-6, and 2-7. They can be considered to be on the conservative side. The four candidate materials tested — CRES 321, A286, Ph15-7, and Inconel 625 — are considered at the present time to be the best choices. From the results of the static tests as shown by the tables, it can be seen that degradation due to temperature effects varies from material to material. A286 shows the least degradation (90% of room temperature yield and 80% of ultimate strength at 1200 degrees F). Ph15-7 shows unacceptable degradation, down to 24% of room temperature values. CRES 321 degraded to approximately 60% of room temperature values and Inconel 625 degraded to 70%. These results show A286 to be the best high strength alloy choice. CRES 321 and Inconel 625 are acceptable and comparable. However, since Inconel 625 is considerably more expensive, it can be eliminated from serious consideration. Thus, based on static test results, A286 and CRES 321 are the best choices. Based on fatigue tests and considering cost, ease of fabrication, and availability, the choice would be CRES 321.

It should be noted that elevated temperatures not only reduce the strength of the material, but also cause gradual deformation or creep that accompanies stress at high temperatures. The rate of creep varies with the stress, temperature, and time. The rapid initial deformation

---

[11] Rohr Industries Report, Investigation and Testing of High Temperature Fatigue-Resistant Materials for Ground Noise Suppression, November 1978

[12] Civil Engineering Laboratory; T Roe Jr, Investigation of High Temperature-Resistant Materials for Acoustical Insulation in Jet Engine Test Facilities, TM-52-77-12, July 1977

Description Sheet Material	Non-Perforated Sheet — Mechanical Properties — Room Temperature								
	Yield Strength			Ultimate Strength			Elongation		
	Longitudinal	Transverse	MIL HDBK 5B	Longitudinal	Transverse	MIL HDBK 5B	Longitudinal	Transverse	MIL HDBK 5B
	ksi	ksi	ksi	ksi	ksi	ksi	%	%	%
(A) Cres 321 (t = .063)	36.0	36.8	30	86.8	86.2	75	45.5	50.3	40
(B) Cres 321 (t = .080)	31.2	31.2	30	81.1	81.0	75	55.6	59.1	40
(C) A286 (t = .063)	107.5	109.2	95	160.5	159.6	140	4.3	1.9	15
(D) Ph 15-7* (t = .063)	193.1	199.8	170	197.8	205.3	190	2.4	1.8	--
(E) Inc. 625 (t = .063)	60.9	60.6	55	123.0	123.8	120	54.0	52.3	30

*Heat treated by User (Rohr) per RPS 12.01.

Table 2-5. Mechanical properties — static tests - nonperforated - room temperature.

Perforated Sheet Material	Perforated Sheet Yield Strength			
	Room Temperature		600°F	1200°F
	Longitudinal	Transverse	Transverse	Transverse
	ksi	ksi	ksi	ksi
(A) Cres 321 (t = .063)	23.2	23.3	18.5	15.4
(B) Cres 321 (t = .080)	22.6	22.6	18.4	13.3
(C) A286 (t = .063)	56.0	56.3	52.1	50.5
(D) Ph 15-7* (t = .063)	83.8	86.5	75.1	20.5
(E) Inc. 625 (t = .063)	32.7	33.4	26.0	23.6

Table 2-6. Mechanical properties — yield strength

Perforated Sheet Material	Perforated Sheet Ultimate Strength			
	Room Temperature		600°F	1200°F
	Longitudinal	Transverse	Transverse	Transverse
	ksi	ksi	ksi	ksi
(A) Cres 321 (t = .063)	39.6	39.2	26.4	21.8
(B) Cres 321 (t = .080)	39.0	38.6	25.6	20.7
(C) A286 (t = .063)	67.6	67.4	62.2	57.8
(D) Ph 15-7* (t = .063)	90.1	93.1	77.9	22.7
(E) Cres. 625 (t = .063)	51.5	50.8	42.1	35.6

Table 2-7. Mechanical properties — ultimate strength.

produces a strain hardening of the material that tends to decrease the creep rate. The effect of continued high temperature on the structure of the metal is to temper it and increase its ductility and thus the creep rate. When the temperature effect predominates, a transition point is reached, beyond which the creep increases very rapidly. Therefore, any extrapolation beyond the time limit of a test must be carried out with extreme caution and the designer must select design stresses that will keep the creep or deformation within prescribed limits during the expected time of tests in the jet enclosures as well as for the expected life of the enclosure.

To decrease the potential of creep/deformation of the CRES 321 as witnessed at NA_S Miramar Hush House 1 one can select a heavier thickness of CRES 321 sheet material using t = 0.080 inch rather than 0.063 inch, and in even worse conditions, it will be far cheaper to replace some of the CRES 321 sheet material that shows fatigue failures than to go to the enormous expense of using exotic materials.

Fatigue Testing. Fatigue tests were conducted at Rohr Industries. The fatigue tests consisted of measuring fatigue lives corresponding to a range of stress levels for each of the test materials at room temperature, 600 degrees F, and 1200 degrees F. Figures 2-36 - 2-39 are typical fatigue (S-N) curves for CRES 321 taken at room temperature, 600 degrees F, and 1200 degrees F, respectively. None of the elevated temperature fatigue curves showed any degradation in fatigue life due to elevated temperature. This fact again indicates that CRES 321 is a material that can be used in the building of an acoustical enclosure and that it is not necessary to consider expensive, exotic materials.

Estimating Endurance Limit. Fatigue data may not be available for a particular material in a particular shape. In the absence of such data, the endurance limit can be determined graphically by the use of

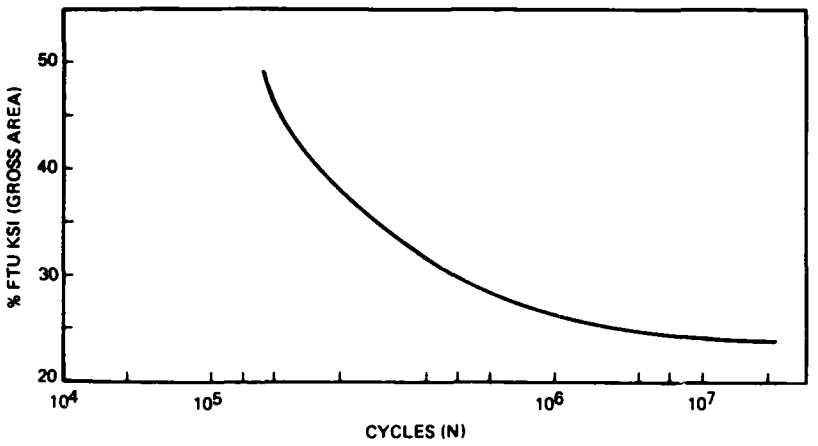

Figure 2-36. Tension-tension fatigue-type 321 .062 gage room temperature.

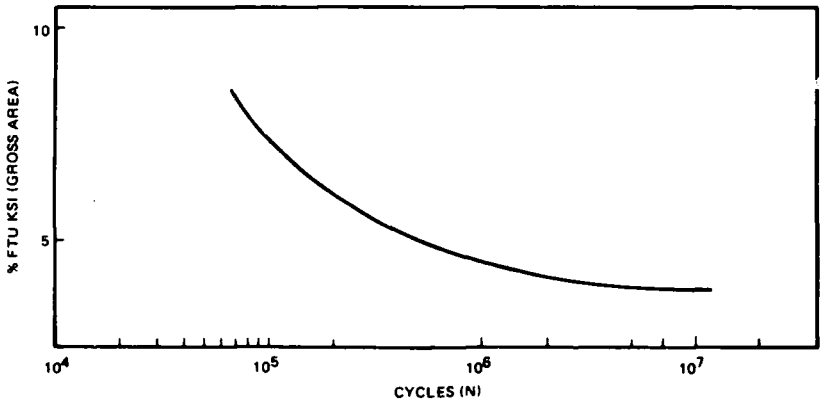

Figure 2-37. Fully reversed random fatigue-type 321 .062 gage room temperature.

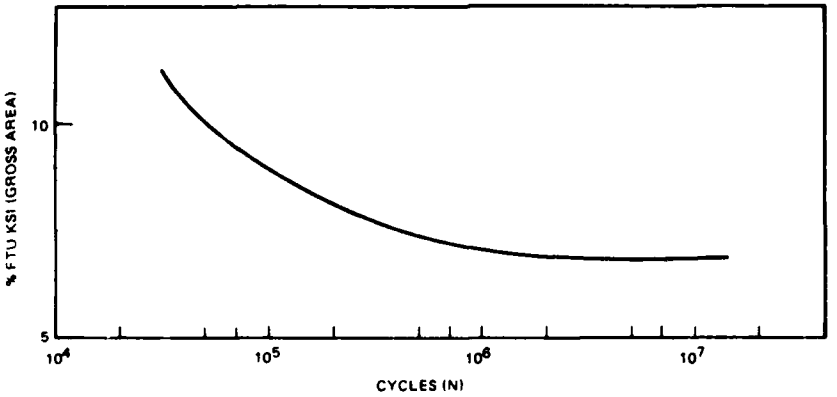

Figure 2-38. Fully reversed random fatigue-type 321 .078 gage, 600 deg F.

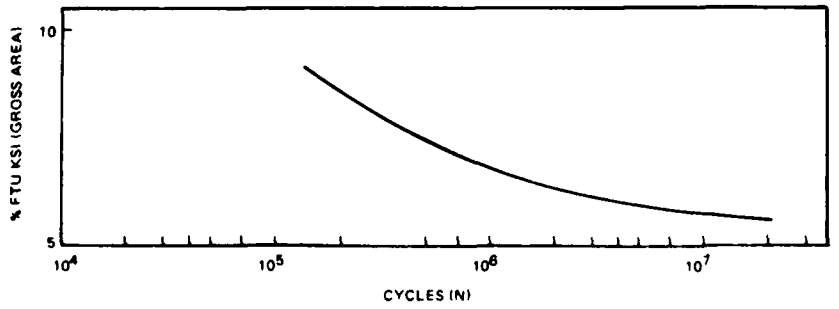

Figure 2-39. Fully reversed random fatigue-type 321 .078 gage, 1200 deg F.

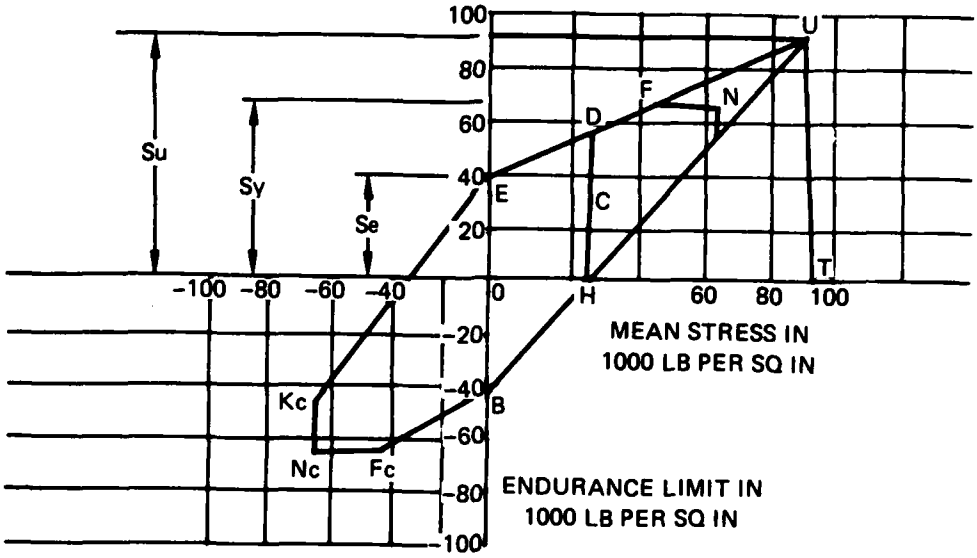

Typical Endurance Diagram for Mild Steel

a diagram such as a Goodman diagram which is based on the straight-line relationship where

S_a = alternating stress
S_m = mean stress
S_u = ultimate stress
S_e = endurance limit stress

It is often convenient to use a diagram for analytical purposes. This endurance diagram can be constructed when the ultimate strength, yield stress, and alternating stress are known. Analysis and experimental work indicate that, if a variable stress is superimposed upon a steady stress, the plotted results will determine a maximum and a minimum stress line between which safe operation can be maintained. These lines are

EV and BU in the diagram shown. The lines should be slightly curved. There is no appreciable error in assuming the line is straight as an approximation in the design of a structure such as an acoustical enclosure.

The stress corresponding to point U is the ultimate strength, and the points E and B correspond to the endurance limit for complete stress reversals. Any point on OU, as point C, will represent a steady stress and CD and CH represent variable stress. The lines EU, BU, and OU indicate stress combinations that will ultimately cause rupture, but in no case should the maximum stress exceed the yield stress. Hence, the endurance diagram above the limits described by EFNKB outlines the possible stress combinations. This figure then forms the endurance diagram for flexural stresses.

Design Techniques. The reason for making such "Goodman" diagrams is to assist in the decision-making process. Materials, surface finish, corrosion, and other stress concentration factors that influence mechanical fatigue are very important considerations. As noted previously, fatigue failure usually starts by the progressive growth across the section of a minute crack formed in the material at some point of highly localized stress. Therefore, sharp corners, severe notches of small radius, very poor surface finish, improper oiling, holes near the edges, fillets, grooves, coarse threads, and the many other factors previously noted either must be avoided for proper designing against fatigue failure or their stress concentration factors must be accounted for in the design calculations. It should be noted, for example, that energy absorption requires a longer length bolt rather than a short bolt of larger cross-sectional area. A finer threaded bolt has much less of a stress concentration factor than a coarse threaded bolt. Bonding instead of riveting decreases stress concentrations. Good design practice requires the use of all applicable techniques.

What has been learned from the failures in the jet enclosure at Miramar is the fact that, in the building of the structure, careful attention must be paid to the details of design during the fabrication and the inspection process. There were large stress concentration factors at

the edges which were perforated contrary to the drawings. The most important factor in improving fatigue life is the following: Careful attention must be paid to detail design, especially in the joints, and proper inspection must be made to ensure that these details are incorporated during fabrication and construction.

(iv) Metal Liner Design Recommendations. These recommendations are divided into two groups. The first addresses the present augmenter design (ref 7). The second addresses possible design changes based on laboratory tests and some full-scale evaluations which have not been tested in Fleet use.

(aa) Present Augmenter Design Recommendations.

- Stainless steel (type 321) is a good economic choice for the liner material.
- The panels should not be perforated to the edges but a 3-inch catstrip should be maintained along edges where bolt holes are placed.
- Bolts should be carefully tightened to required torque levels.
- Welds should not be used to restrain panel edges.
- The liner perforations should be performed so that burrs are limited to less than .004 inch in raised height above the sheet and should be uniform in configuration.
- Bolts in different rows should be located in tandem (ie, along the load line, not staggered). Bolts should be of the same size and each row should contain an equal number of bolts.

(bb) Possible Design Recommendations.

- Stainless steel (type 321) and the A286 alloy tested could be used without corrugations if smaller panels with adequate support are provided.
- Optimum cost benefit (initial cost and life cycle cost) may be achieved using one liner for a majority of the augmenter tube and a more costly but longer life cycle liner for hot sections. This is

especially pertinent if designs for new engine augmenter tube facilities indicate temperatures above 1000 degrees F.

- Cost benefit may show that use of stainless steel (type 321) with panel replacement when required is less expensive than replacement with high cost alloys.

(cc) Noise Reduction Alternatives. Scale-model studies were used for investigating techniques to reduce augmenter noise and wall temperatures. Successful prediction by earlier 1/15 scale models of acoustical and aerothermal parameters measured in full-scale operational augmenter tube suppressors forms the basis for the noise reduction alternative modeling efforts.

Western Electro-Acoustics Laboratory performed the alternative evaluation 1/15 scale-model tests (ref 3). The tests evaluated the acoustical properties of various obround and round augmenter tubes, both with and without 45-degree exit ramps. Tests involved cold flow (500 degrees R = 40 degrees F) and two hot flow conditions (2300 degrees R = 1840 degrees F and 3300 degrees R = 2840 degrees F) of the simulated jet nozzle.

The baseline condition for comparison of all alternatives is the obround suppressor with a length (72" = 90'), a 45-degree exit ramp, nozzle temperature of 2300 degrees R, and nozzle pressure ratio of 2.0. This condition is nearly identical to the original modeling efforts and the resultant full-scale evaluations.

Figure 2-40 shows the difference of noise level with hot flow and cold flow nozzle conditions. Figure 2-41 shows the impact of the 45-degree exit ramp, a screen diffuser (a method of smoothing flow), and reduced augmenter tube length. Figure 2-42 provides an indication for maximum benefit for acoustic absorbing materials in the augmenter tube.

Figures 2-43, 2-44, and 2-45 show the impact of exhaust stack extensions with a 45-degree exit ramp or turning vanes at the exhaust end of the augmenter tube. Figure 2-43 indicates that little benefit is gained from exhaust stack extensions with a 45 degree exit ramp. Figure 2-44 indicates

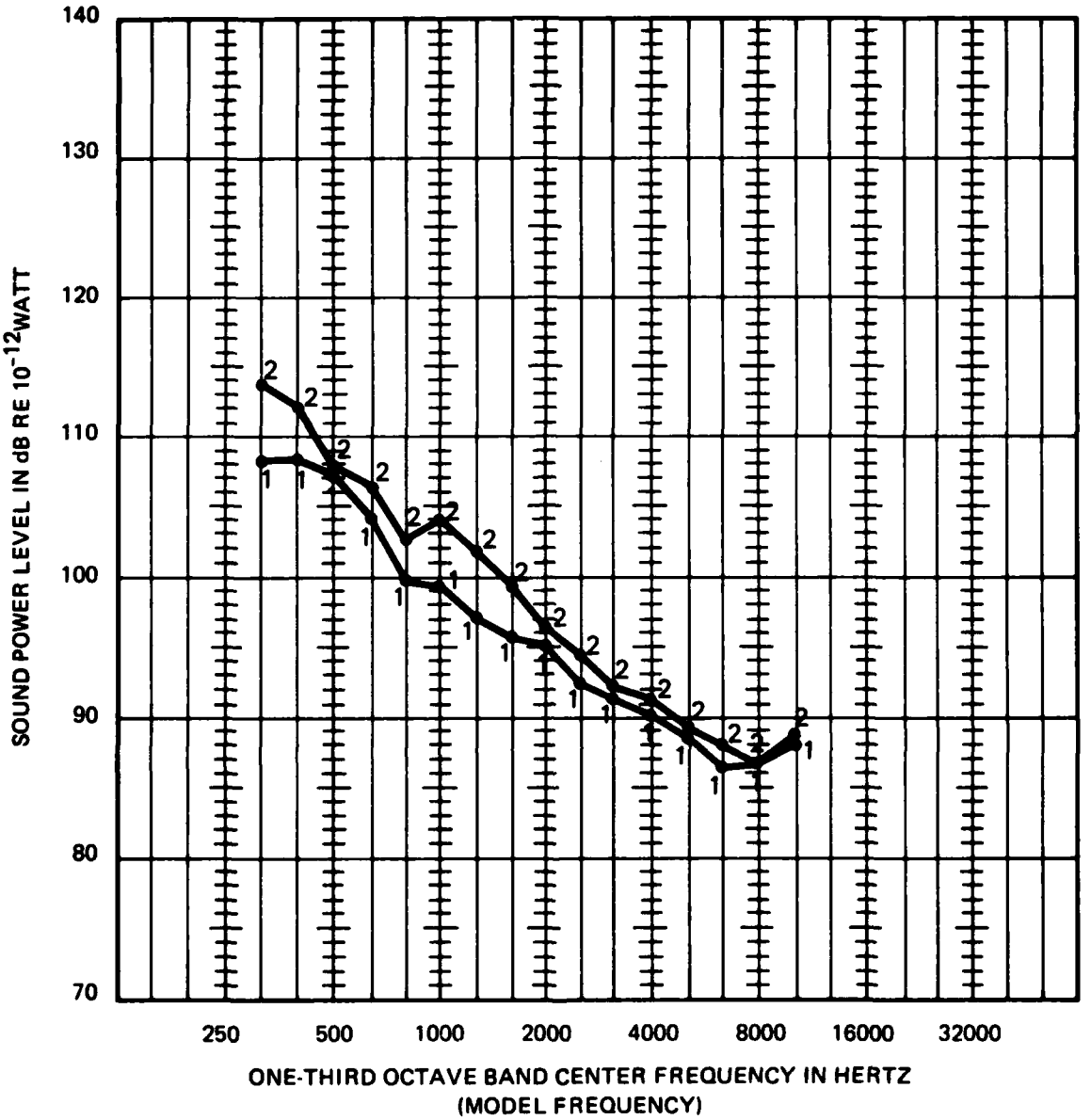

1-1 T_N = 500 deg R
2-2 T_N = 2300 deg R

Figure 2-40. Sound power levels – obround noise suppressor – (72 in = 90 ft), 45-degree ramp, λ_N = 2.0.

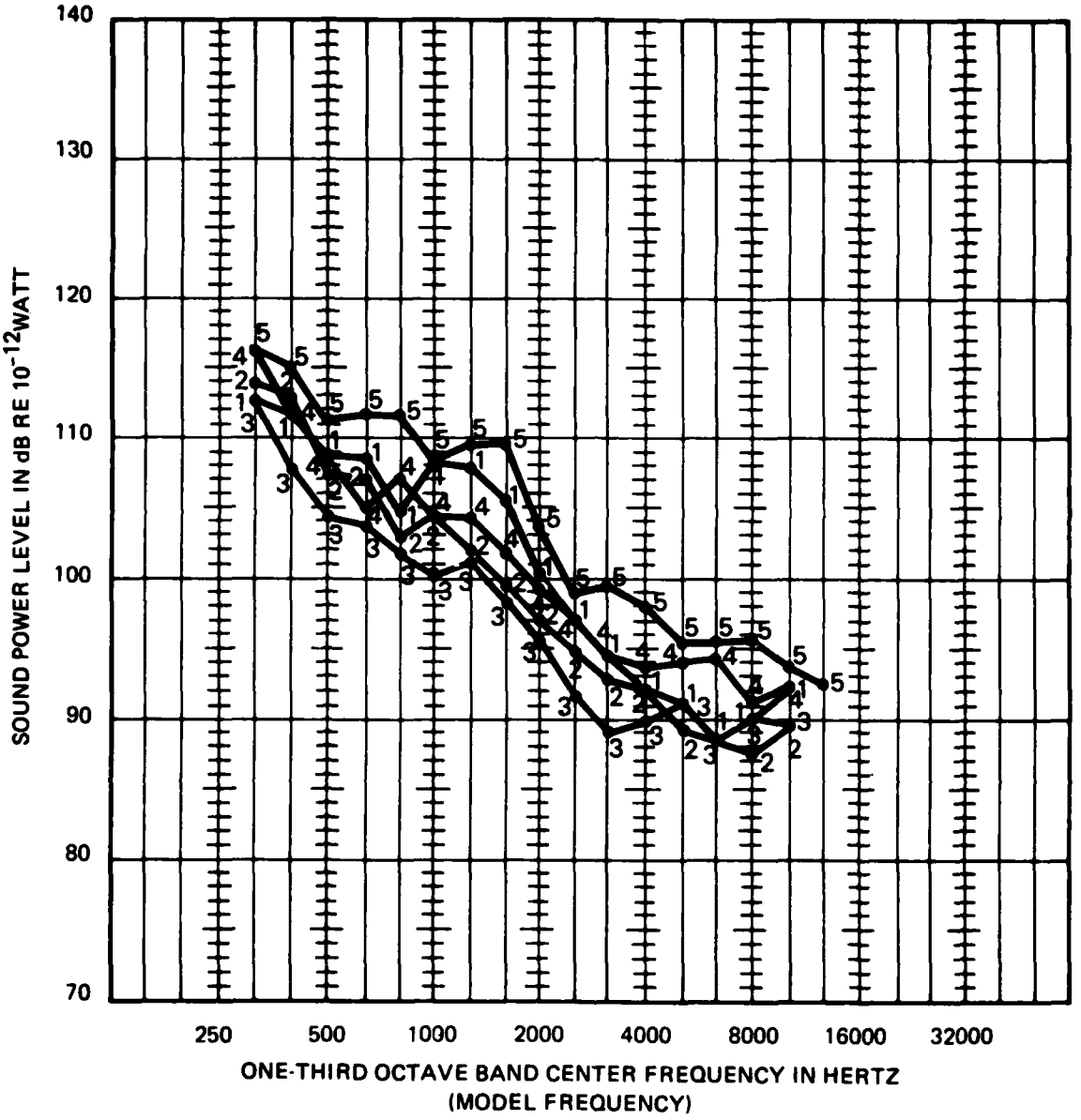

1-1 Suppressor (72 in = 90 ft) No ramp
2-2 Suppressor (72 in = 90 ft) 45 deg ramp (existing configuration)
3-3 Suppressor (72 in = 90 ft) 45 deg ramp* – screen diffuser at (48 in = 60 ft) position
4-4 Suppressor (60 in = 75 ft) 45 deg ramp – screen diffuser at (48 in = 60 ft) position
5-5 Suppressor (60 in = 75 ft) No ramp – screen diffuser at (48 in = 60 ft) position

*Note: Nearly identical without ramp

Figure 2-41. Sound power levels – obround noise suppressor – T_N = 2300 deg R, λ_N = 2.0.

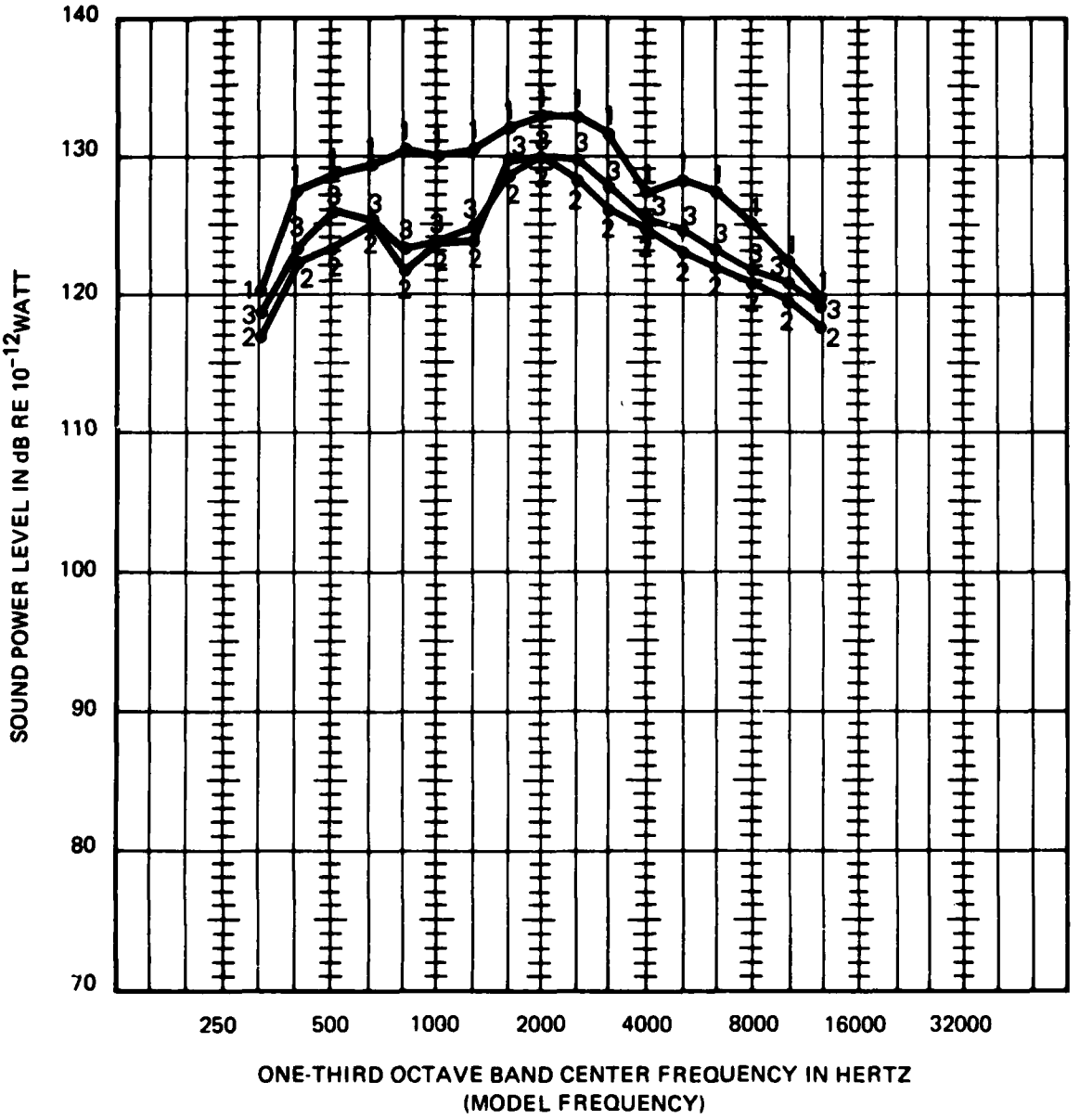

1-1 (12 in = 15 ft) section at inlet (0 in – 12 in; 0 ft – 15 ft)
2-2 (12 in = 15 ft) section at exit (60 in – 72 in; 75 ft – 90 ft)
3-3 (12 in = 15 ft) section at middle (36 in – 48 in; 45 ft – 60 ft)

Figure 2-42. Sound power levels – obround noise suppressor – (72 in = 90 ft) no ramp, liner location testing.

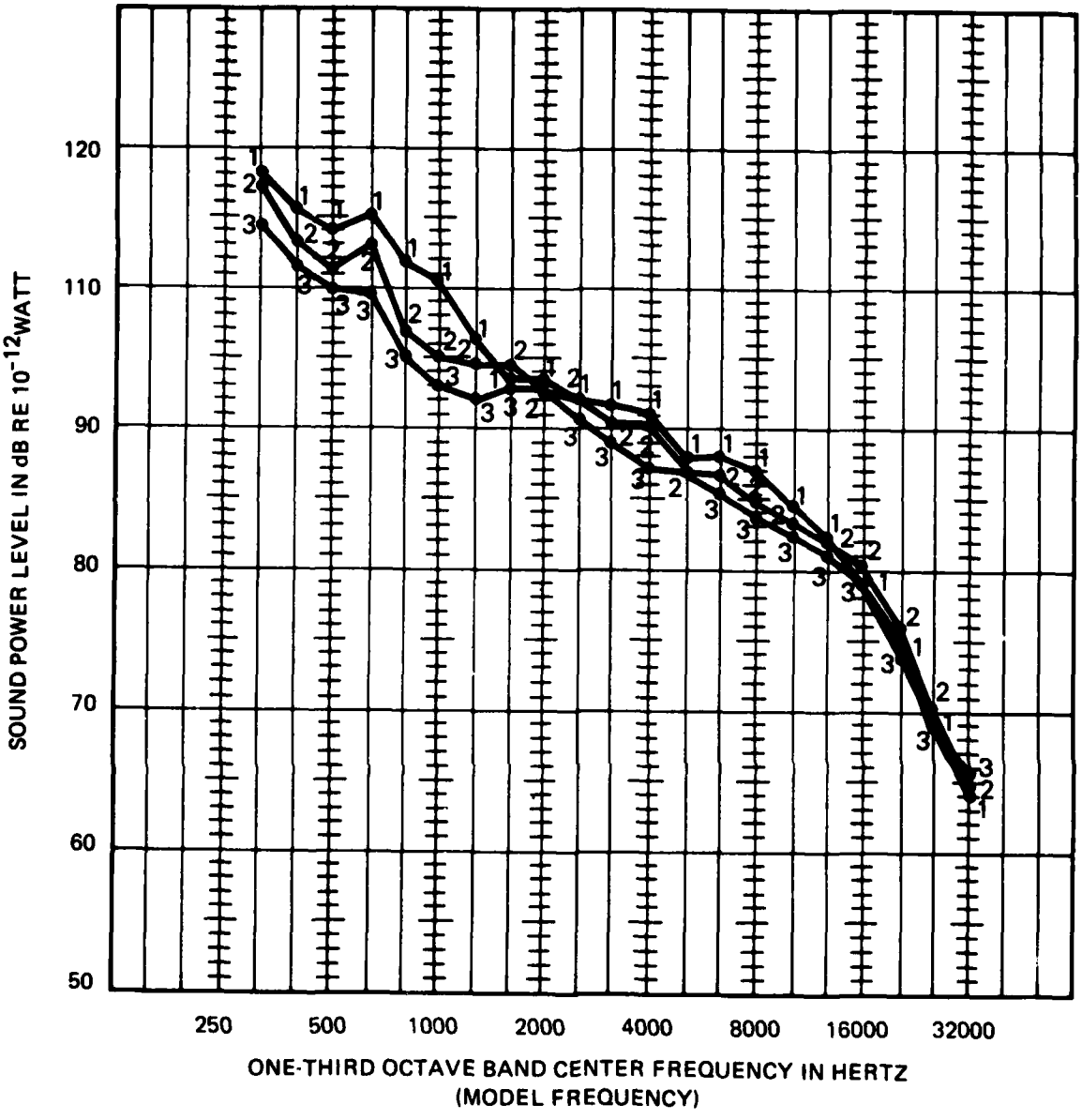

1-1 45 deg exhaust ramp
2-2 45 deg exhaust ramp, plus one stack extension (12 in = 15 ft)
3-3 45 deg exhause ramp, plus two stack extensions (24 in = 30 ft)

Figure 2-43. Sound power levels – obround noise suppressor – (72 in = 90 ft) 45 deg ramp, T_N = 2300 deg R, λ_N = 2.0, exhaust stack extensions.

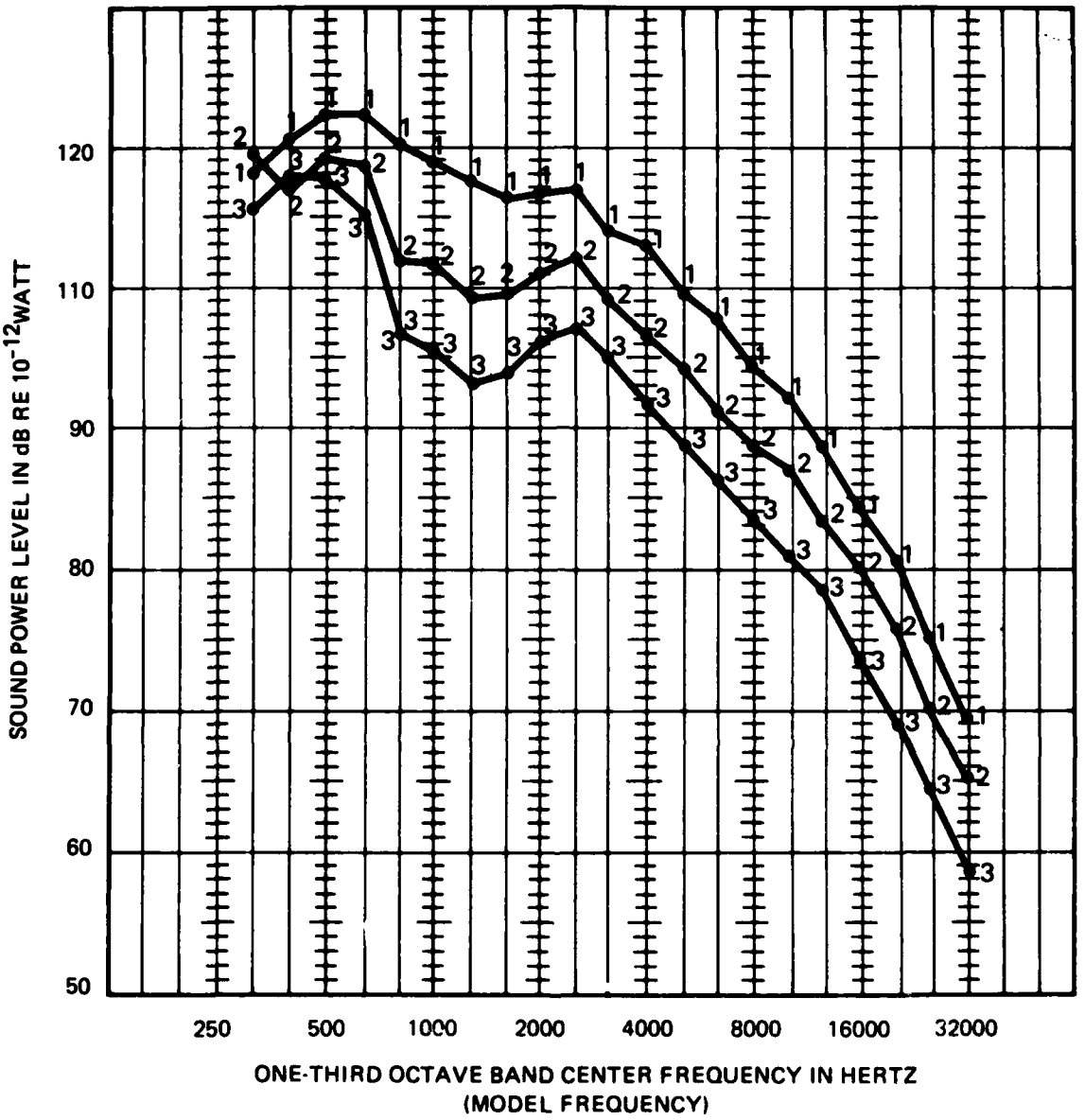

2-44 1-1 Turning vanes in exhaust plenum
2-2 Turning vanes, plus one stack extension (12 in = 15 ft)
3-3 Turning vanes, plus two stack extensions (24 in = 30 ft)

Figure 2-44. Sound power levels – obround noise suppressor – (72 in = 90 ft) turning vanes, T_N = 2300 deg R, λ_N = 2.0 – 45 deg ramp plus extensions and turning vanes plus extensions.

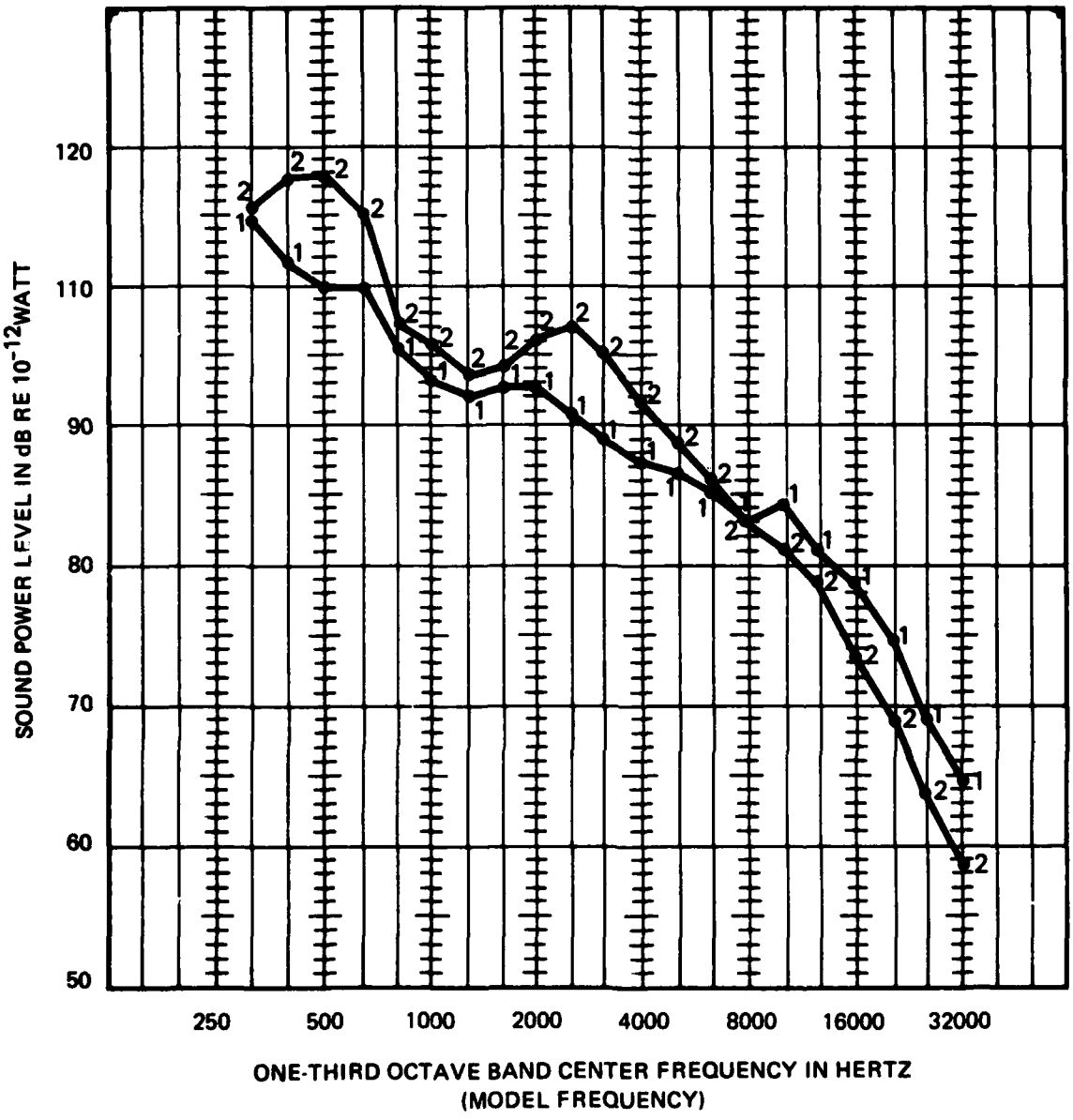

1-1 45 deg ramp, plus two stack extensions (24 in = 30 ft)
2-2 Turning vanes, plus two stack extensions (24 in = 30 ft)

Figure 2-45. Sound power levels – obround noise suppressor – (72 in = 90 ft) T_N = 2300 deg R, λ_N = 2.0 – 45 deg ramp plus extensions and turning vanes plus extensions.

that substantial benefit is gained from exhaust stack extensions with turning vanes. Figure 2-45 indicates overall that the extensions with 45-degree ramp provide a slightly lower noise output than the extensions with turning vanes. The turning vane data, however, based on temperature/pressure data in reference 3, indicate that the turning vane system tested produces smoother, more uniform exhaust flow but also created flow-generated noise. Better design of the turning vane system (less area between individual turning vanes) would reduce the flow-generated noise. This was achieved in contractor tests outside the scope of the Navy project. The resultant overall noise with acoustically treated exhaust stack is then projected to be lower than the 45-degree exit ramp condition with acoustically treated exhaust stack extensions.

Figures 2-46 - 2-49 show the noise characteristics of round augmenter tube designs using inlet throats (two augmenter diameters) relative to the obround augmenter design. Basically round augmenter tube designs using inlet throats produce higher noise levels than the obround augmenter tube designs. There is a characteristic high noise output between 1000 and 2000 Hz model frequency (66 to 125 Hz full scale) which is probably a function of the discontinuity and tube diamter.

Figures 2-50 and 2-52 show the noise characteristics of round augmenter tube designs with cooling slots. The untreated noise slots although small provide up to 14 dB increased for field noise level. Additionally, figures 2-51 and 2-53 indicated that no augmenter wall cooling is accomplished with the cooling slots tested. The cooling slots evaluated, however, are felt to be poorly designed thus not delivering a sufficient quantity of cooling air.

D. Demisters

There are two commercially available demister devices capable of operating under the impacts of Hush House temperature and strength requirements. Their purpose is the reduction of rain, ice/snow and foreign objects through the Hush House inlets. The two demister devices ("Euroform-D-Mist-R" by the Munters Corp and "Heilex-EB" by the Heil Process Equipment Corp.) were

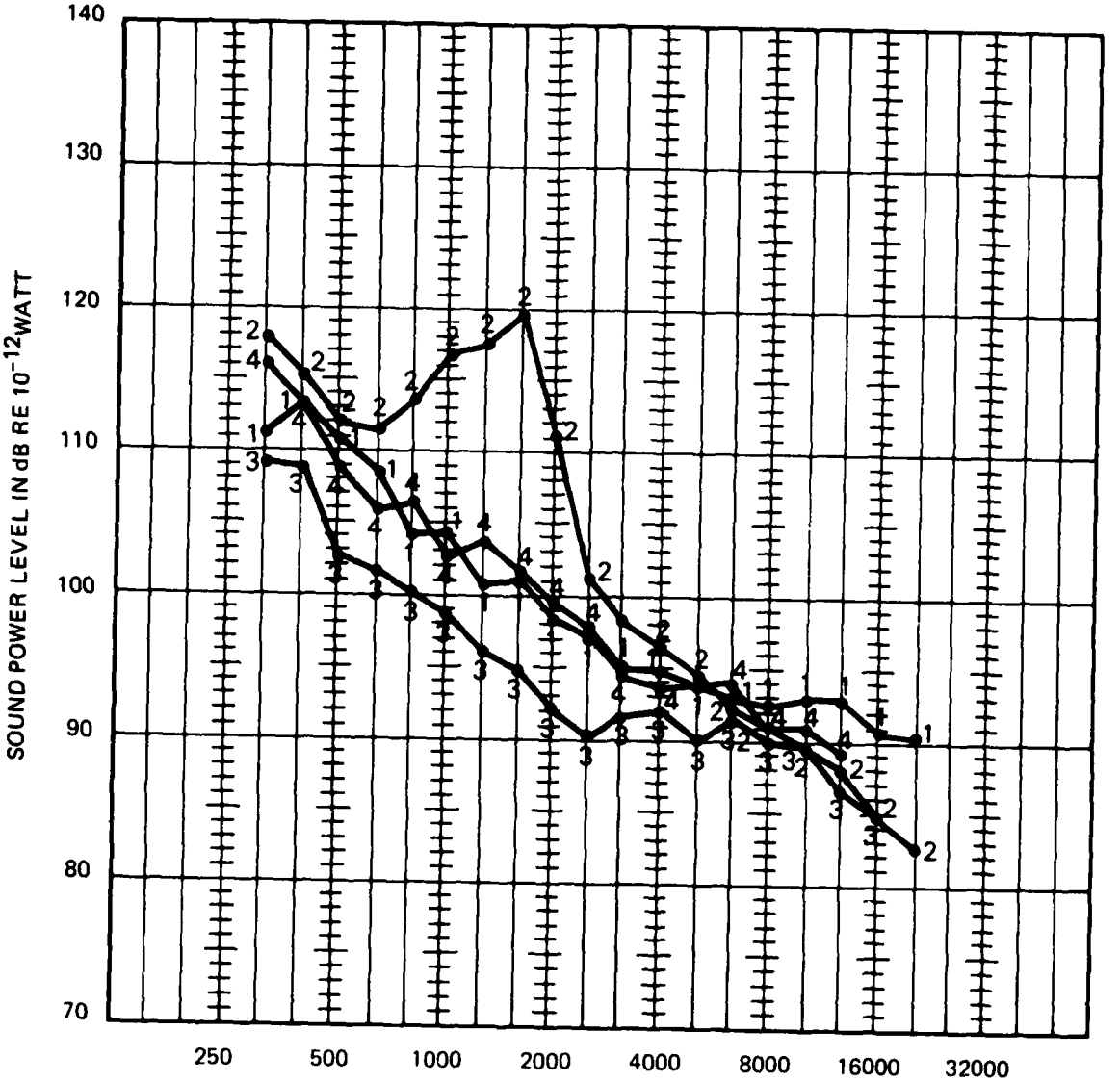

1-1 Round suppressor, throat* length (12 in = 15 ft), T_N = 500 deg R
2-2 Round suppressor, throat* length (12 in = 15 ft), T_N = 2300 deg R
3-3 Obround suppressor, screen diffuser (48 in = 60 ft), T_N = 500 deg R
4-4 Obround suppressor, screen diffuser (48 in = 60 ft), T_N = 2300 deg R

*Note: The throat reduces diameter by 20% for the length of the throat.

Figure 2-46. Sound power levels -- (60 in = 75 ft), 45 deg ramp, λ_N = 2.0 round/obround comparisons.

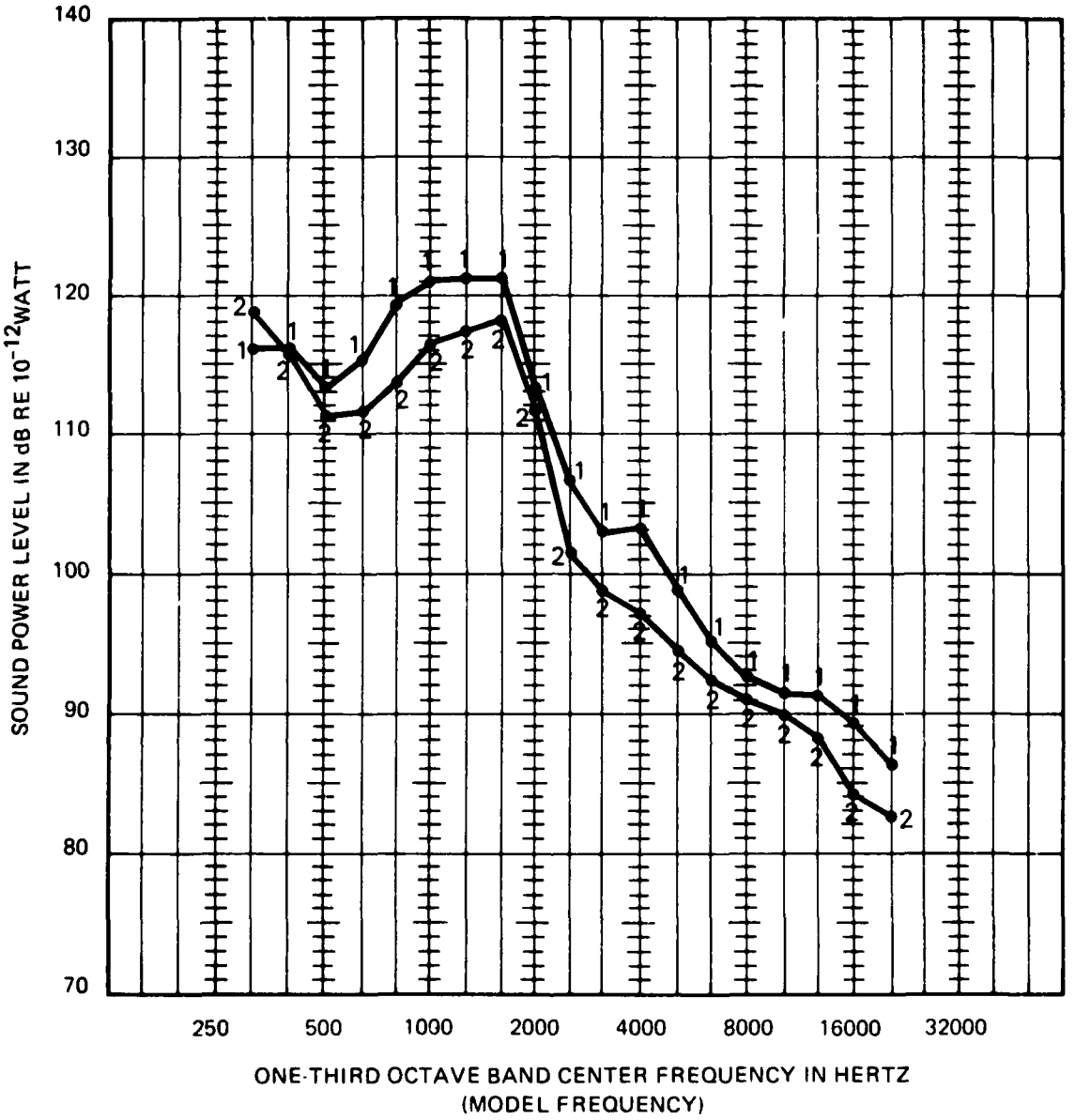

Figure 2-47. Sound power levels - round noise suppressors - (60 in = 75 ft) T_N = 2300 deg R, λ_N = 2.0, throat length (12 in = 15 ft), ramp vs. no ramp.

AD-A122 025 GROUND RUNUP NOISE SUPPRESSION PROGRAM PART 3 DRY SUPPRESSOR TECHNOLOGY BASE(U) NAVAL OCEAN SYSTEMS CENTER SAN DIEGO CA R GLASS ET AL. 20 JUN 82 2/3

UNCLASSIFIED NOSC/TR-674 F/G 20/1 NL

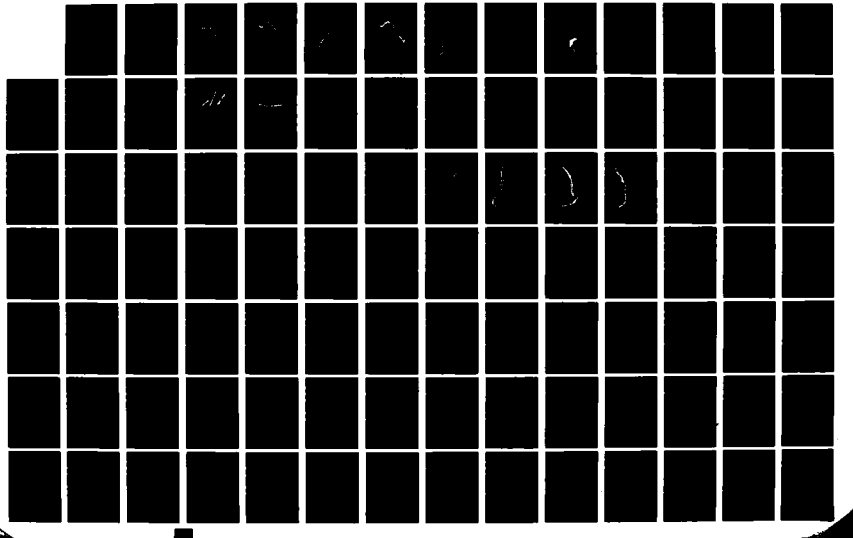

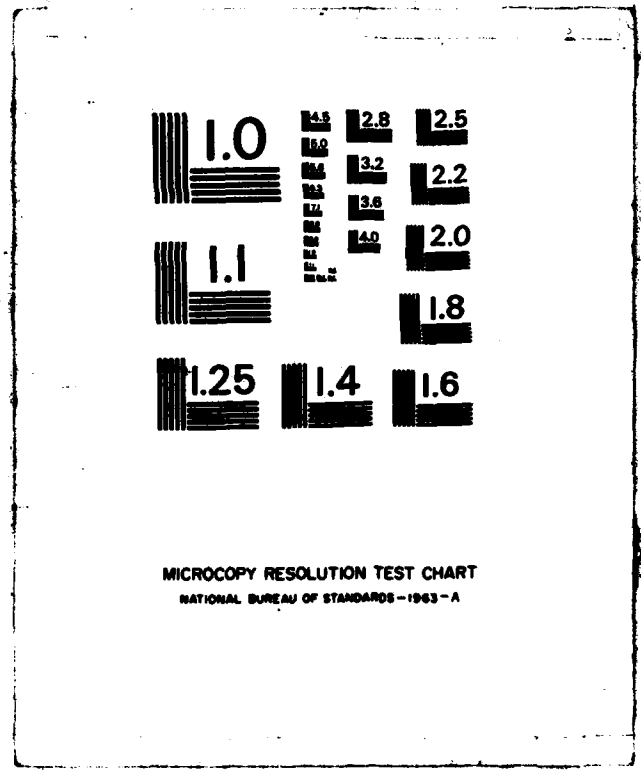
1.0
1.1
1.25
1.4
1.6
1.8
2.0
2.2
2.5
2.8
3.2
3.6
4.0
4.5
5.0
MICROCOPY RESOLUTION TEST CHART
NATIONAL BUREAU OF STANDARDS-1963-A

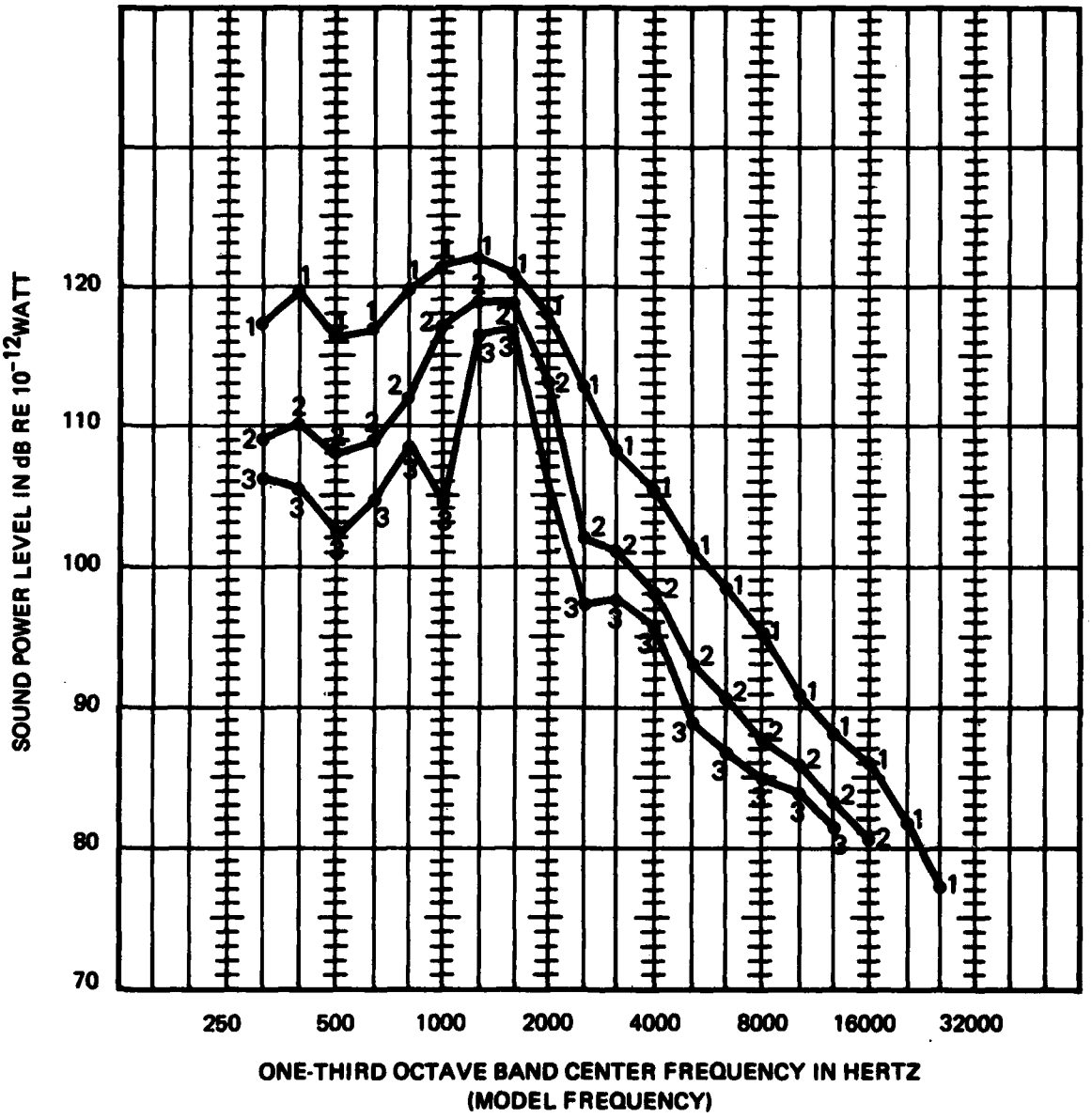

1-1 Suppressor length (48 in = 60 ft)
2-2 Suppressor length (60 in = 75 ft)
3-3 Suppressor length (72 in = 90 ft)

Figure 2-48. Sound power levels – round noise suppressors – throat length (12 in = 15 ft), no ramp, T_N = 2300 deg R, λ_N = 2.0, suppressor length comparison.

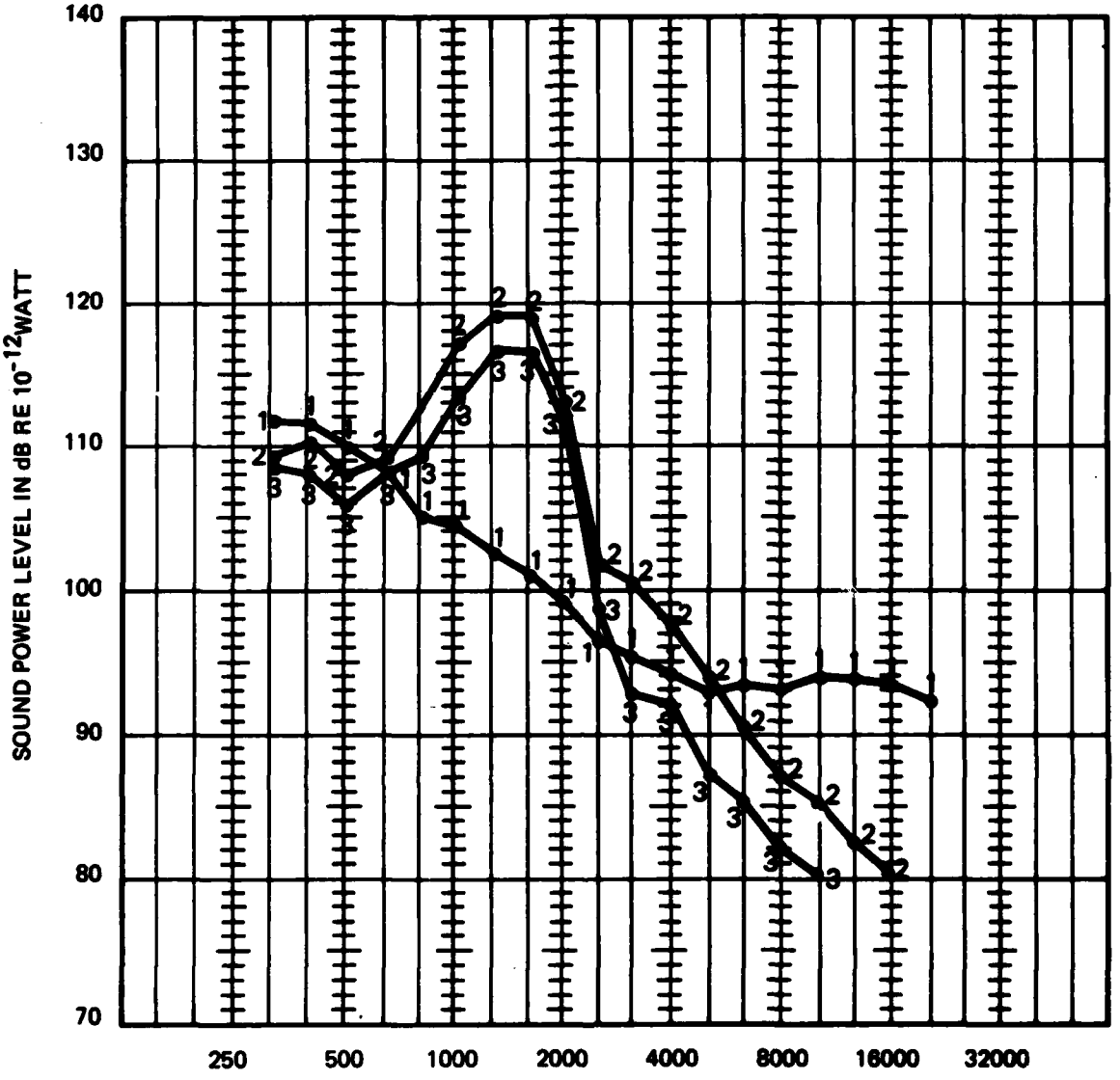

1-1 T_N = 500 deg R, λ_N = 2.0
2-2 T_N = 2300 deg R, λ_N = 2.0
3-3 T_N = 3300 deg R, λ_N = 2.0

Figure 2-49. Sound power levels – round noise suppressors – (60 in = 75 ft), no ramp, throat length (12 in = 15 ft), source temperature comparison.

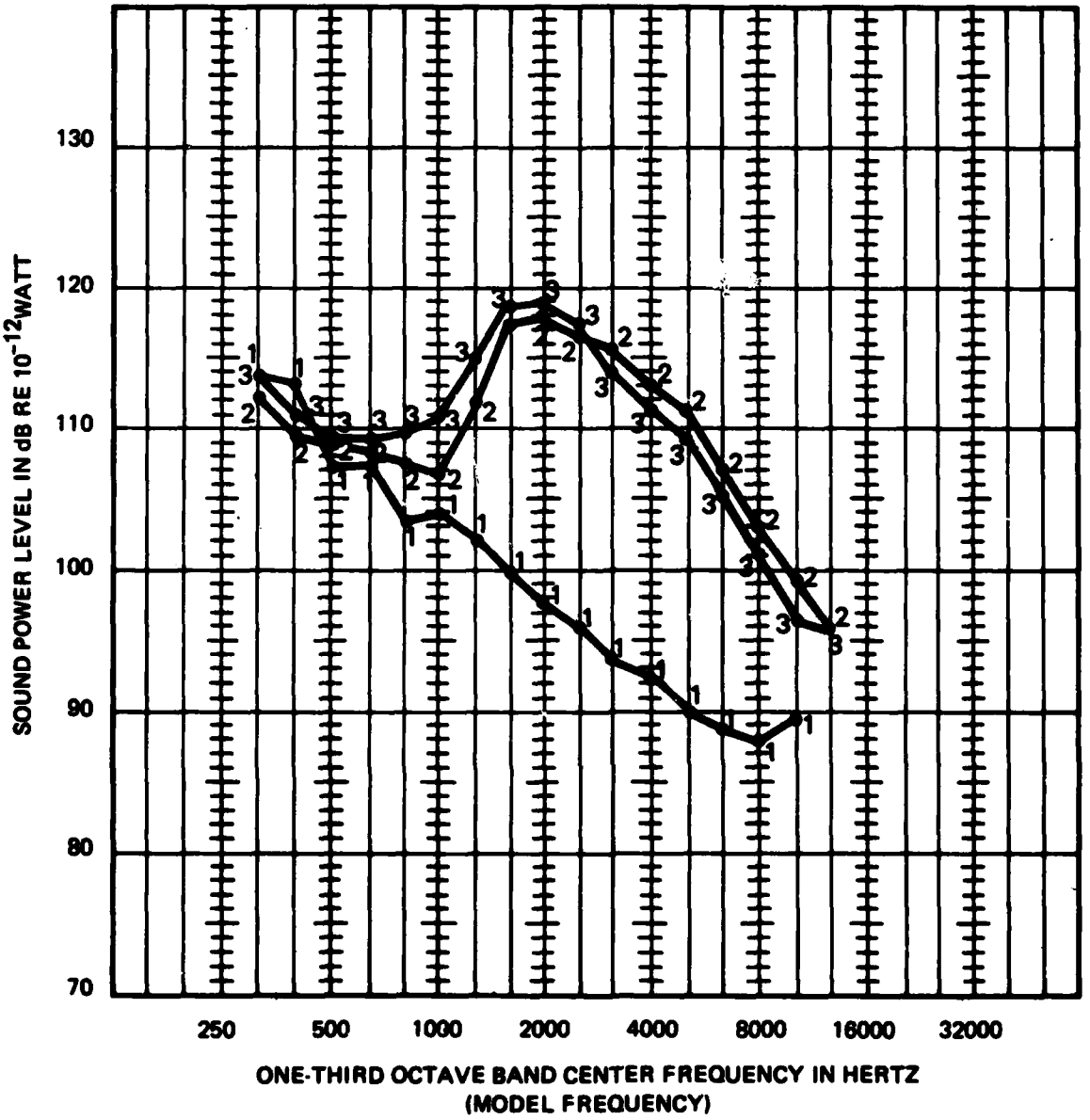

1-1 Suppressor (72 in = 90 ft), 45 deg ramp, (existing configuration)
2-2 Suppressor (72 in = 90 ft), 45 deg ramp, (two .2 in gap cooling slots)*
3-3 Suppressor (72 in = 90 ft), 45 deg ramp, (one .4 in gap cooling slots)*

*Note: Use of input throttle causes a minor (typically 1 dB) reduction in the 1000 Hz to 8000 Hz range.

Figure 2-50. Sound power levels – obround noise suppressors – no ramp, T_N = 2300 R, λ_N = 2.0 – cooling slots.

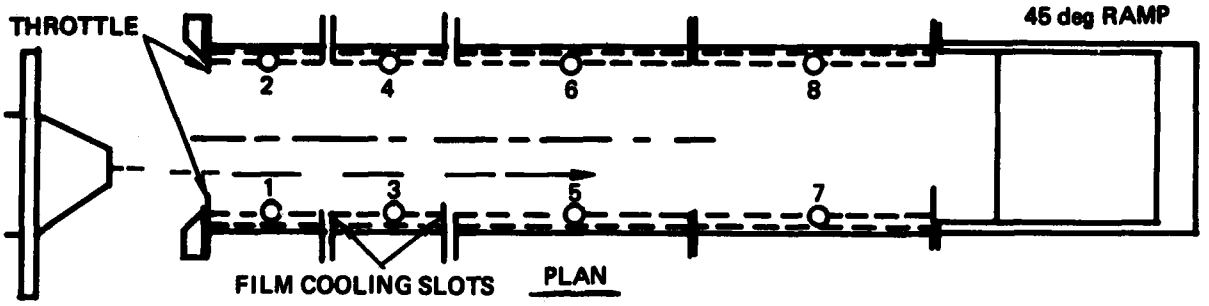

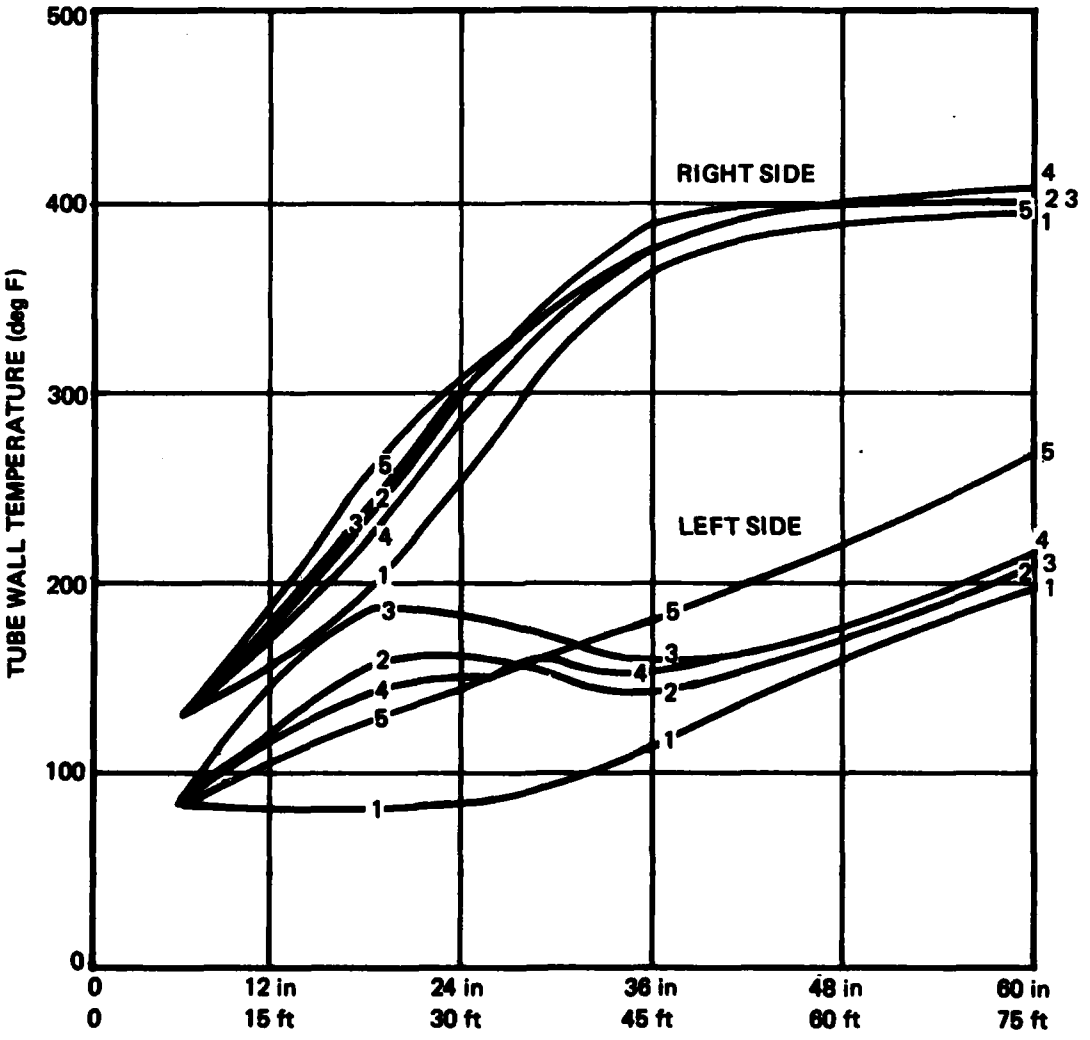

1-1 NO SLOTS
2-2 ONE SLOT: 0.2 in
3-3 ONE SLOT: 0.4 in
4-4 TWO SLOTS: 0.2 AND 0.2 in
5-5 TWO SLOTS: 0.2 AND 0.2 in, plus throttle

Figure 2-51. Tube wall temperatures – obround suppressor – engine offset right – offset right – cooling slots.

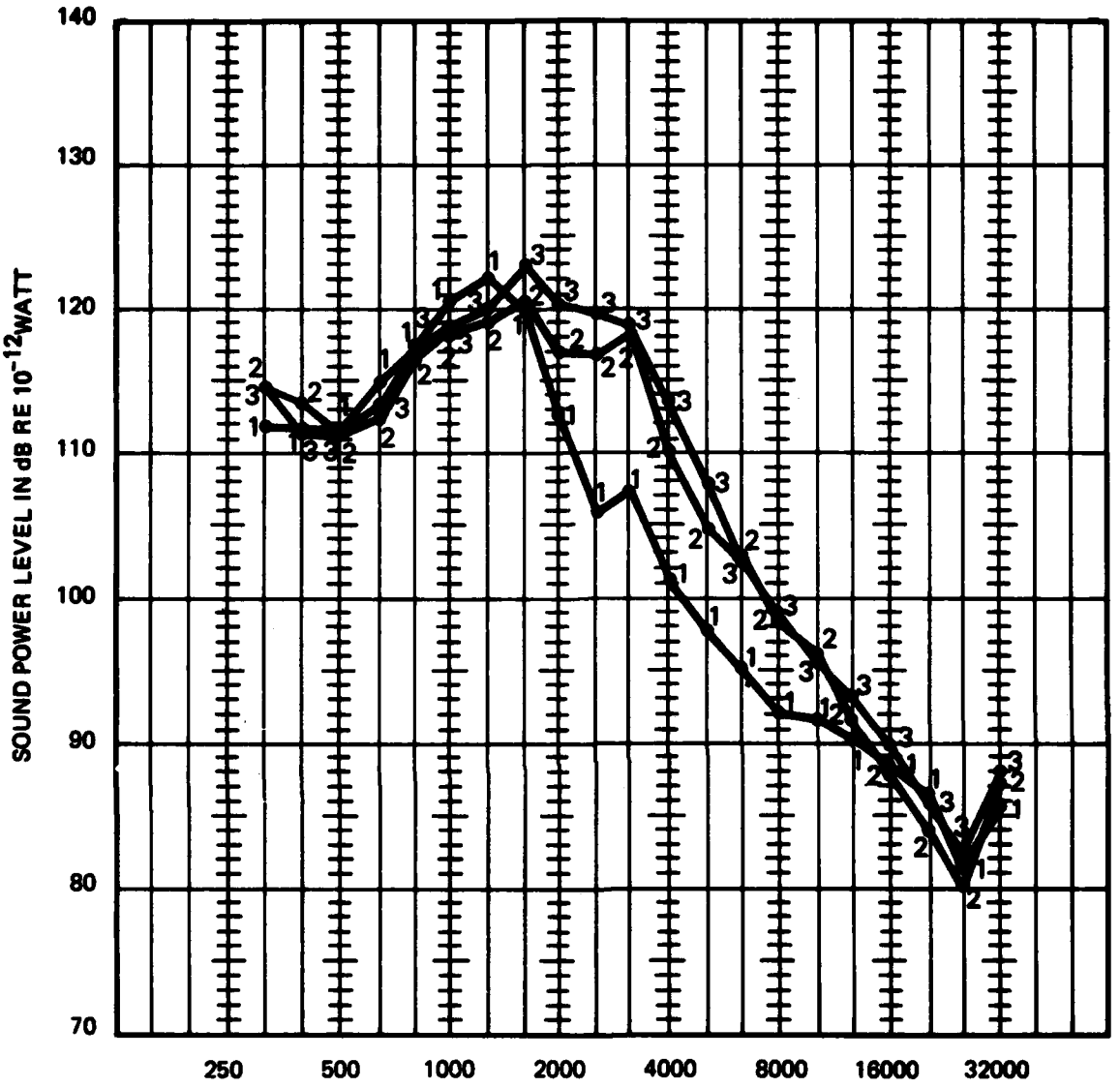

Figure 2-52. Sound power levels – round noise suppressors – (60 in = 75 ft) – no ramp – T_N = 2300 deg R, λ_N = 2.0.

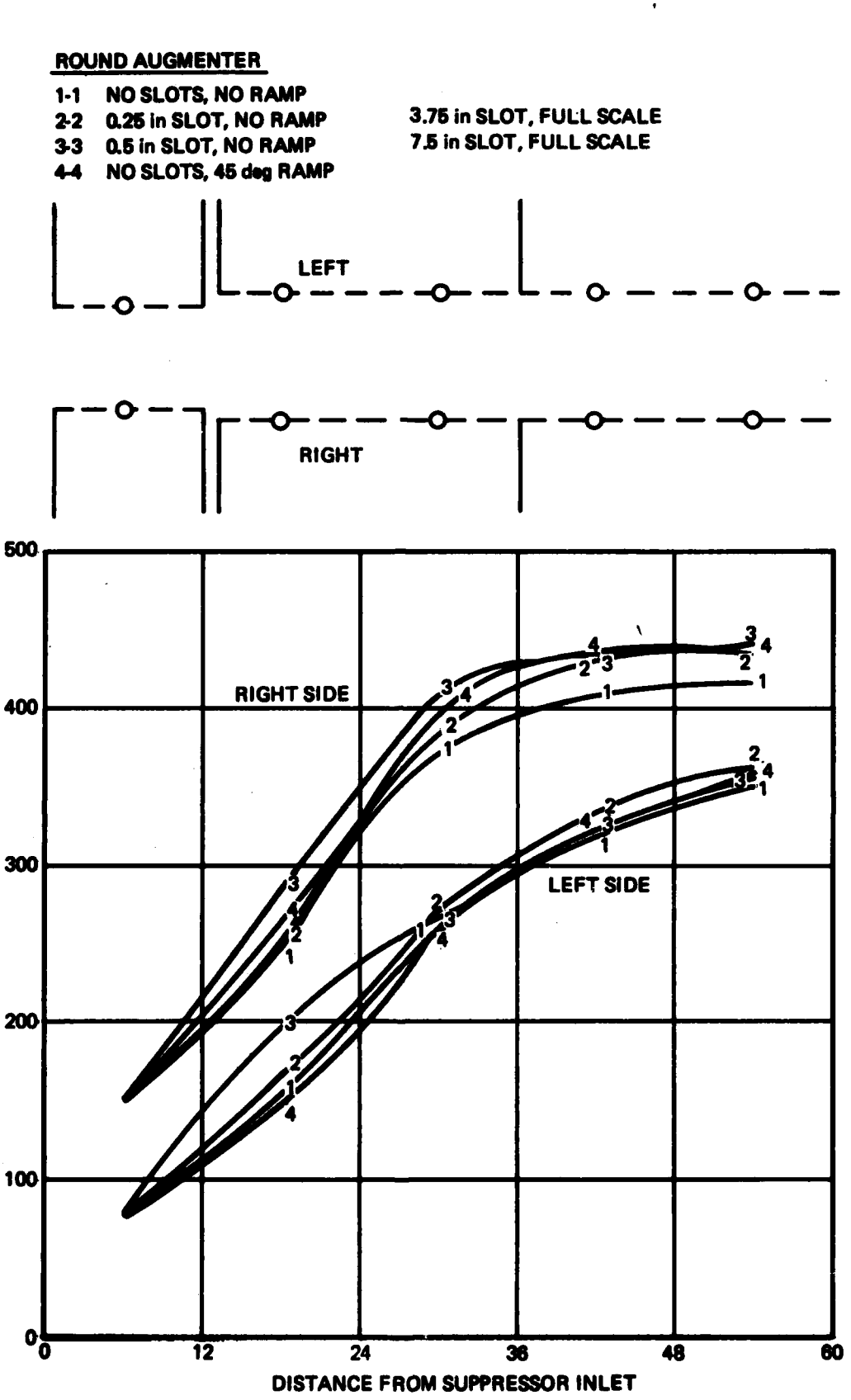

Figure 2-53. Tube wall temperatures – round suppressor - cooling slots.

tested in an environment chamber (ref 13). Both units meet the Navy's operational requirements of effectively removing mist/rain from airstreams flowing about 1800 ft/sec. and creating less than 2 inches of water pressure drop. Figure 2-54 shows the pressure drop characteristics.

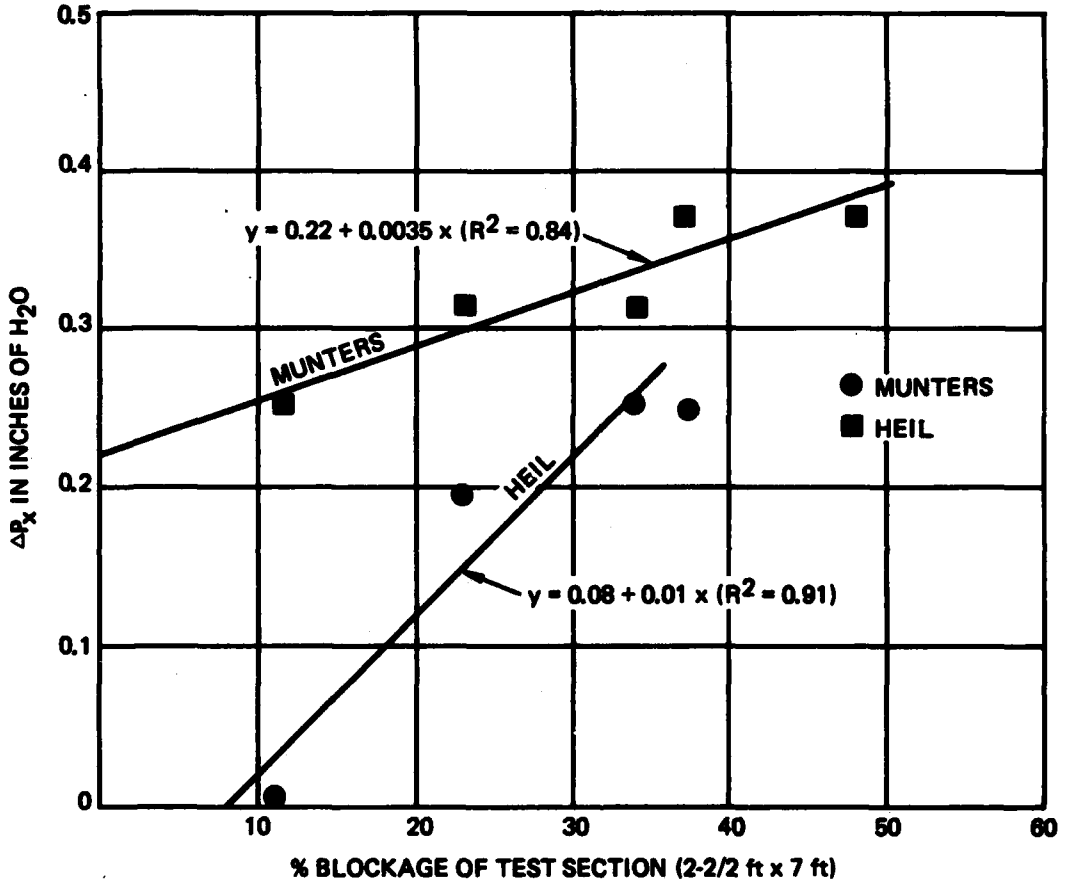

Figure 2-54. Demister pressure drop characteristics.

---

13 Civil Engineering Laboratory; Edward Skillman, Test and Evaluation of Candidate Demister Hush House Assemblies, TM-54-77-5, September 1977

III. COANDA/REFRACTION TECHNOLOGY

The Coanda/refraction air-cooled dry exhaust technology was developed as part of the Navy's Coanda/Refraction Noise Suppression Concept Advanced Development Program. The effort included analytical, scale-model (1/6 scale), and full-scale evaluation of aerothermal/acoustical properties. The 1/6 scale-model tests predicted values near those measured for a full-scale demonstration unit. The Coanda technology has not been used in the Fleet as of September 1981. The Coanda/Refraction program has produced a design manual based on scale-model tests and analytical predictions.

A. COMPONENTS

The Coanda/refraction air-cooled exhaust system is composed of five primary components. Figure 3-1 shows the typical suppressor configuration. Outlined below is a brief explanation of each component.

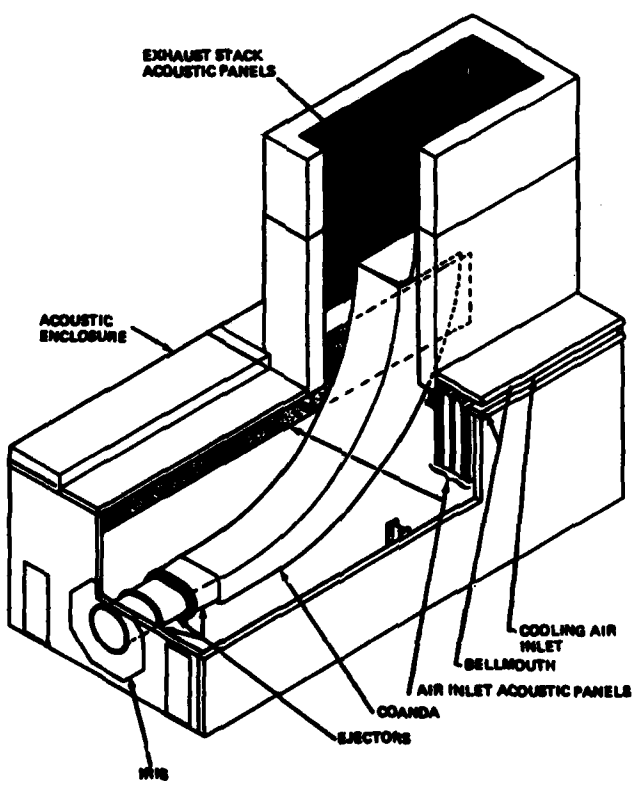

Figure 3-1. Cutaway of Coanada/refraction noise suppression.

Ejectors. The functions of the three-stage ejector set are to shape the flow from the circular exhaust jet to a rectangular sheet for introduction onto the Coanda surface, to provide mixing of ambient air with the primary exhaust, and to provide a layer of cooling air next to the Coanda surface. The cooling air enters through a controlled gap between the top of the third-stage ejector exit and the entrance to the Coanda surface and provides a supplementary film of ambient cooling air to protect the Coanda surface from the hot exhaust stream.

Coanda Surface. The Coanda surface is a curved channel which turns the jet exhaust flow through 90 degrees without the use of turning vanes or deflectors in the jet exhaust stream. The surface curvature is extremely critical for flow attachment.

Enclosure. An acoustic enclosure surrounds the ejectors and Coanda surface. The enclosure is double-walled to limit noise within the interior from being transmitted to the surrounding environment. Special acoustic panels are installed on the enclosure wall to absorb the refracted noise from the deflected exhaust. Ejector and Coanda cooling air intakes are integral to the enclosure.

Cooling Air Intakes. Inlets for the cooling air are horizontal, acoustically-treated passages located immediately under the roof of the enclosure and running the length of both sides. After entering the passages, the cooling air branches into three streams and flows downward through three acoustically-treated channels. These inlet passageways limit propagation of airborne noise from within the enclosure to the environment. They are sized to provide the required cooling air without reducing pressures within the enclosure to unacceptable levels.

Exhaust Stack. An acoustically-lined exhaust stack is located on the top of the Coanda enclosure. The acoustic treatment within the stack further absorbs noise from the exhaust stream before it is discharged into the atmosphere.

B. SUPPRESSOR GAS DYNAMICS

The flow transitioning and turning elements of the Coanda system are illustrated in figure 3-2. The hot high velocity primary flow is received by a three-stage ejector system, which shapes the flow into a rectangular sheet for introduction onto the Coanda surface and provides mixing of ambient air with the primary exhaust. The gap between the last ejector exit and the Coanda surface is provided to supply supplemental cooling air which forms an insulating film between the hot exhaust gas and the Coanda surface. The Coanda surface is a curved channel (open on the lower side) which turns the flow through approximately 90 degrees without reliance on turning vanes or deflectors in the severe environment of the jet exhaust. Flow turning is accomplished by creation of a pressure gradient across the exhaust stream existing from the ejectors. The proximity of the high velocity stream to the underside of the Coanda surface causes a reduction in surface static pressure because of unreplenished fluid entrainment near the surface. The higher pressure (ie, local ambient) on the opposite side of the flow (open side of the channel) forces the fluid sheet to attach to the Coanda surface and turn through 90 degrees.

The jet velocity existing from the Coanda surface is reduced to levels which produce low residual jet noise because of turbulent entrainment of large quantities of secondary cooling air.

C. DESIGN CONSIDERATIONS

1. Overview.

Two principal design considerations form the basis for development of the Coanda/refraction air-cooled dry sound suppressor operation. First, flow attachment/turning is the basis of the technology application. Factors such as temperature, pressure, and air flow must be considered in conjunction with the engine operating parameters. Second, the acoustic environment due to the engine noise must be reduced to the desired near-field and far-field levels.

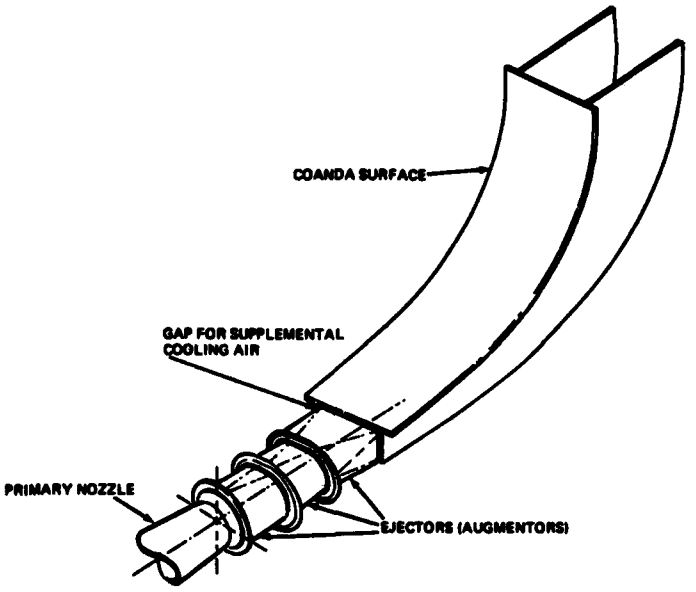

Figure 3-2. Coanda surface and ejectors.

Analytical studies, 1/6 scale-model tests, and full demonstration unit measurements (ref 14-16) formed the basis of a design handbook (ref 17). The final design-related conclusions based on Naval Air Engineering Center (NAEC) Coanda research efforts are presented; however, they have NOT been tested under fleet operating conditions:

- Within reasonable limits, misalignment of engine nozzle to ejector centerlines, typical of improper aircraft initial positioning or in-airframe movement of the engine nozzle, does not affect exhaust flow attachment to the Coanda surface.

---

14 Naval Air Engineering Center, Final Technical Report-Feasibility/Initial Model Studies Coanda/Refraction Noise Suppression Concept Exploratory Development, NAEC-GSED-80, May 1974

15 Naval Air Engineering Center, Final Technical Report Configuration Scale-Model Studies Coanda/Refraction Noise Suppression Concept Exploratory Development, NAEC-GSED-81, May 1974

16 Naval Air Engineering Center, Final Technical Report - Test Cell Experimental Program-Coanda/Refraction Noise Suppression Concept Advanced Development, NAEC-GSED-97, March 1976

17 Naval Air Engineering Center, Design Configuration Handbook Test Cell System Coanda/Refraction Noise Suppression Concept, NAEC Design Data 92-136, 30 March 1979

- The Coanda concept functions equally well with coannular or axial flow engine exhaust.

- With proper design, the dual Coanda system can operate with two side-by-side exhaust flows at dissimilar power settings (eg, two engine aircraft).

- With proper ejector configurations, the Coanda system can accommodate reasonable variations in distances between the engine nozzle and ejector inlet without affecting flow attachment or cooling.

- With an appropriately-designed ejector transition section, the dual Coanda system can accommodate reasonable angular and offset misalignment of twin engine exhaust flow while maintaining good flow attachment and acceptable surface temperature.

- Adequate Coanda surface cooling can be maintained by providing the proper gap between the top of the final-stage ejector exit and the Coanda surface.

2. Initial Design Approach.

The initial design approach for the Coanda/refraction technology requires the range of engine temperature, velocity, and noise parameters to be determined, then an analysis of each suppressor component configuration to be completed in the following order:

a. Ejector Design. The ejector usually uses a three stage system (found optimum in ref 15 and 16) to shape and cool the exhaust flow. Figure 3-3 shows this configuration along with the pertinent parameters which form the basis of suppressor design. Figures 3-4 - 3-7 present the range of temperatures experienced in the ejector area.

---

15 Naval Air Engineering Center, Final Technical Report Configuration Scale-Model Studies Coanda/Refraction Noise Suppression Concept Exploratory Development, NAEC-GSED-81, May 1974

16 Naval Air Engineering Center, Final Technical Report - Test Cell Experimental Program-Coanda/Refraction Noise Suppression Concept Advanced Development, NAEC-GSED-97, March 1976

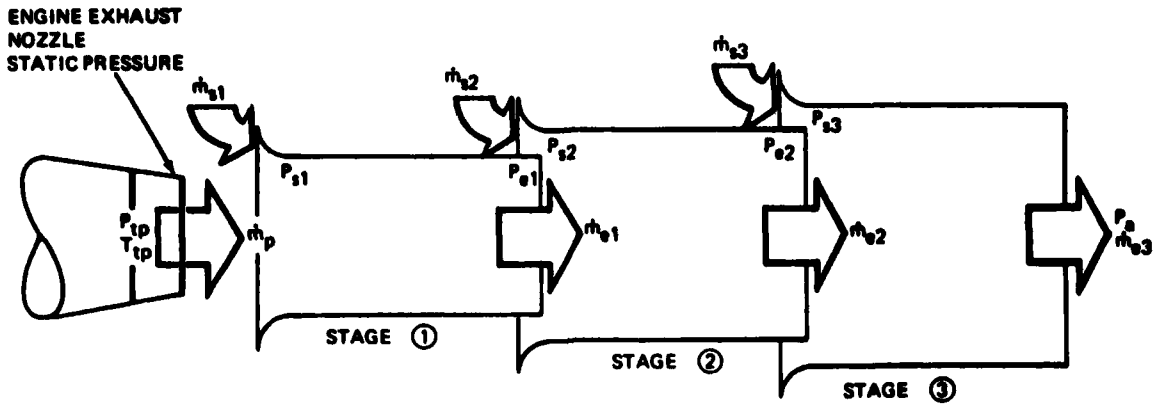

Figure 3-3. Multistage ejector.

The basic function of the ejector set is to transition the flow from a circular to a rectangular cross section, and to provide enough cooling flow to each stage to maintain ejector surface temperature below 1000 degrees. It has been shown in reference 16 that in order for the ejector set to function properly, the geometrical design must be fixed within vary narrow limits. This means that, for any given application, the ejector set is fixed and it is not possible or necessary to generate parametric curves for a variety of engine-ejector combinations. This situation will be explained more fully in the detailed design procedure which follows.

(1) Single Stage Design Approach. As stated previously, the design will use a three-stage ejector. Unfortunately, the calculation of staged ejector performance is very complicated and involves a time consuming iteration process best suited to a computer. However, NAEC research efforts have shown that a single-stage design procedure produces results in excellent agreement with experimental data. This approach allows for a closed-form, mathematical solution for the ejector pumping ratio which greatly simplifies the design.

The basic single-stage ejector geometry is shown in figure 3-8. This geometry is determined from the requirement to transition from a round entrance to a rectangular exit.

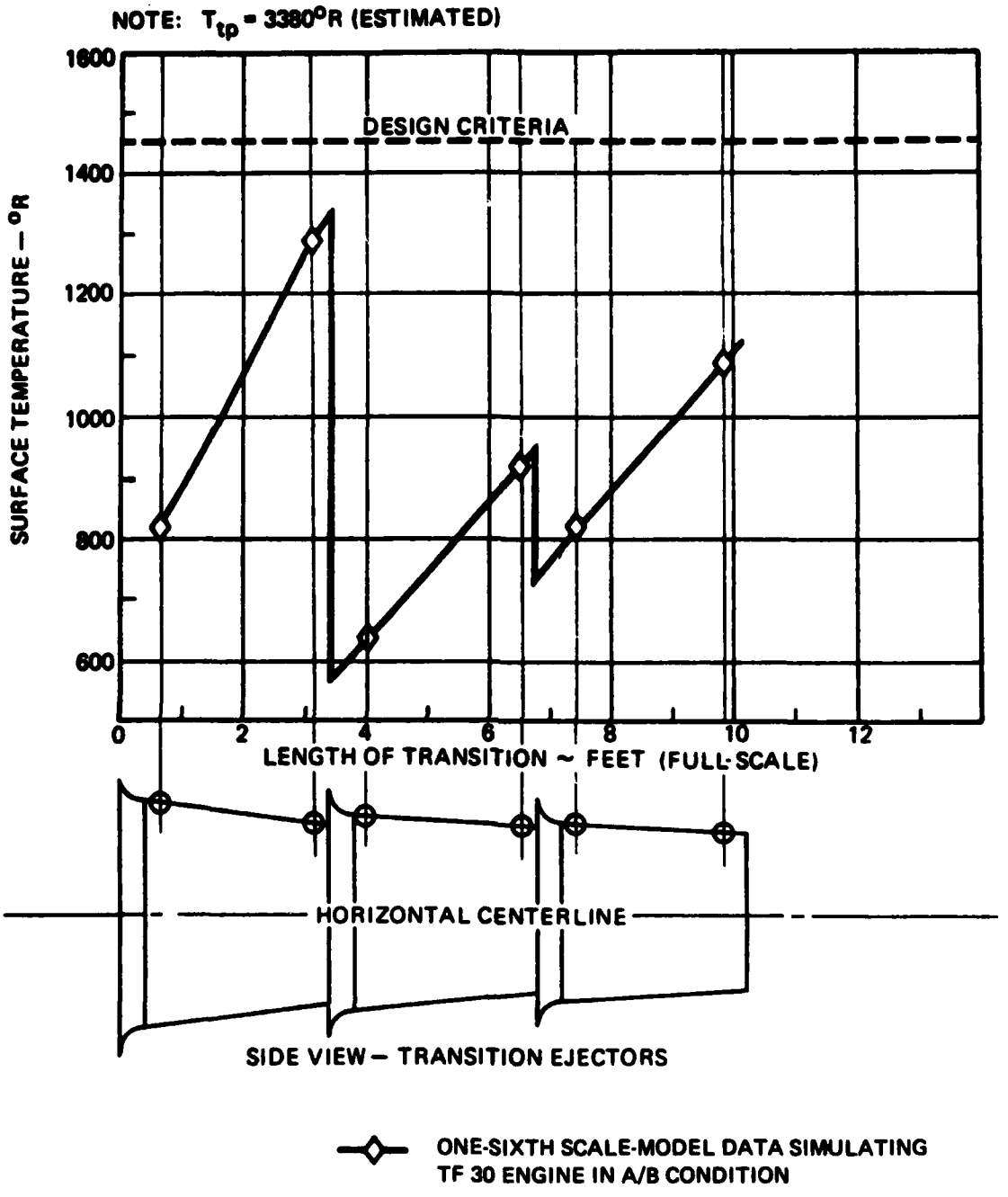

Figure 3-4. Ejector upper surface temperature.

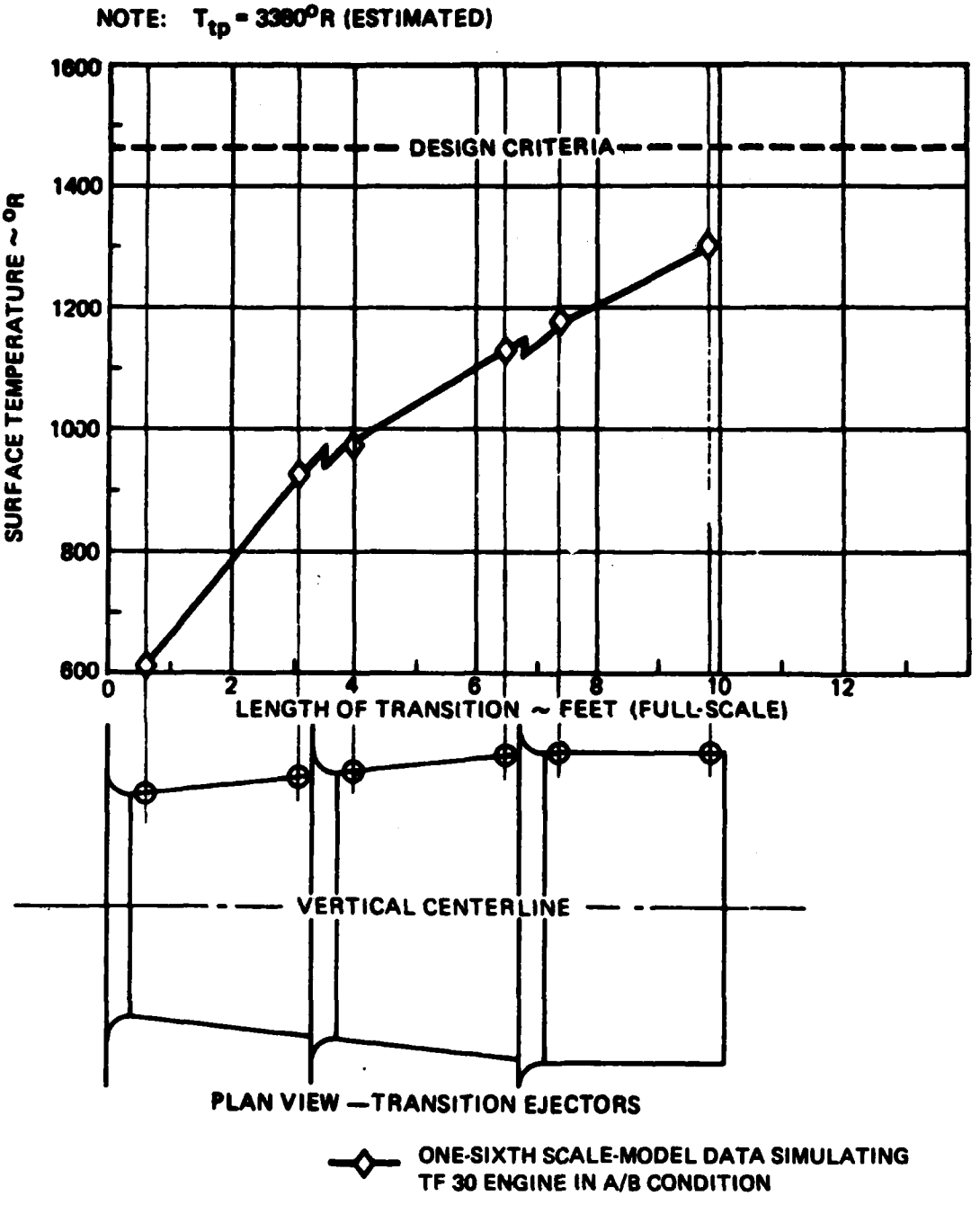

Figure 3-5. Ejector side surface temperature.

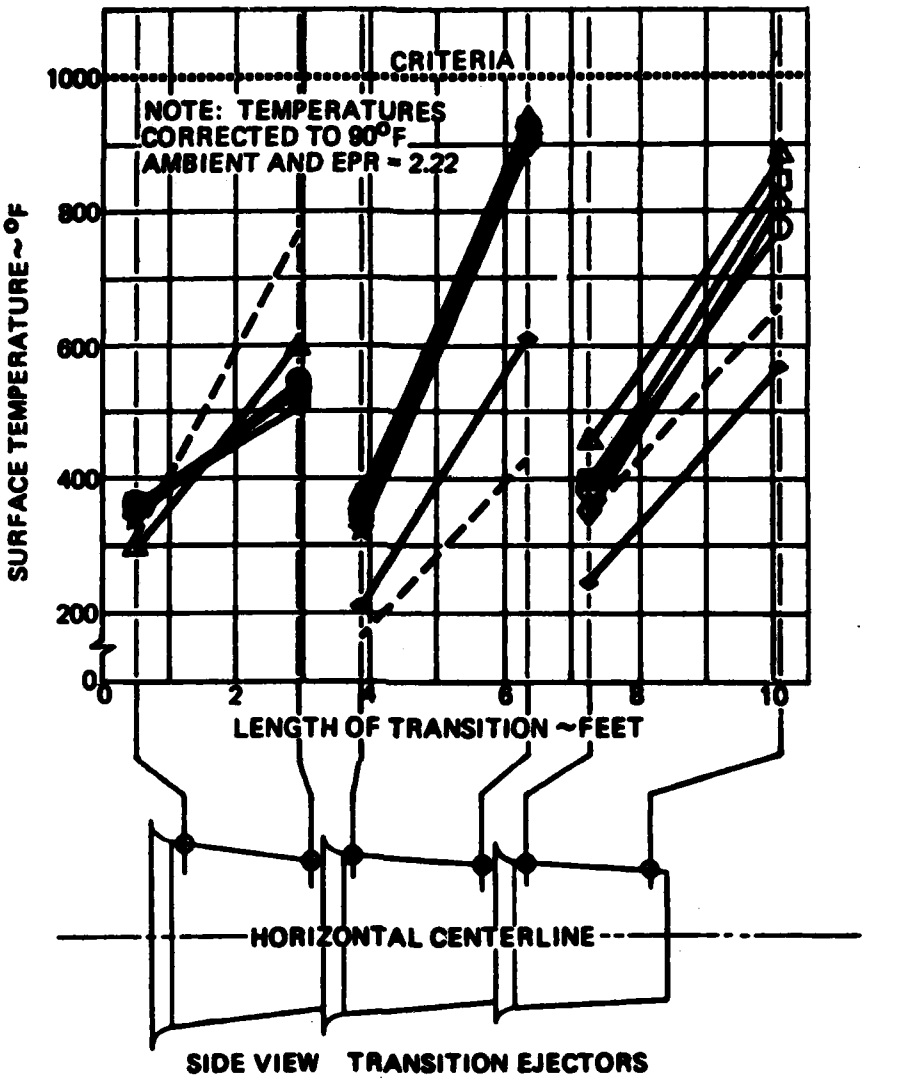

Figure 3-6. Ejector upper surface temperatures – J57A/B condition.

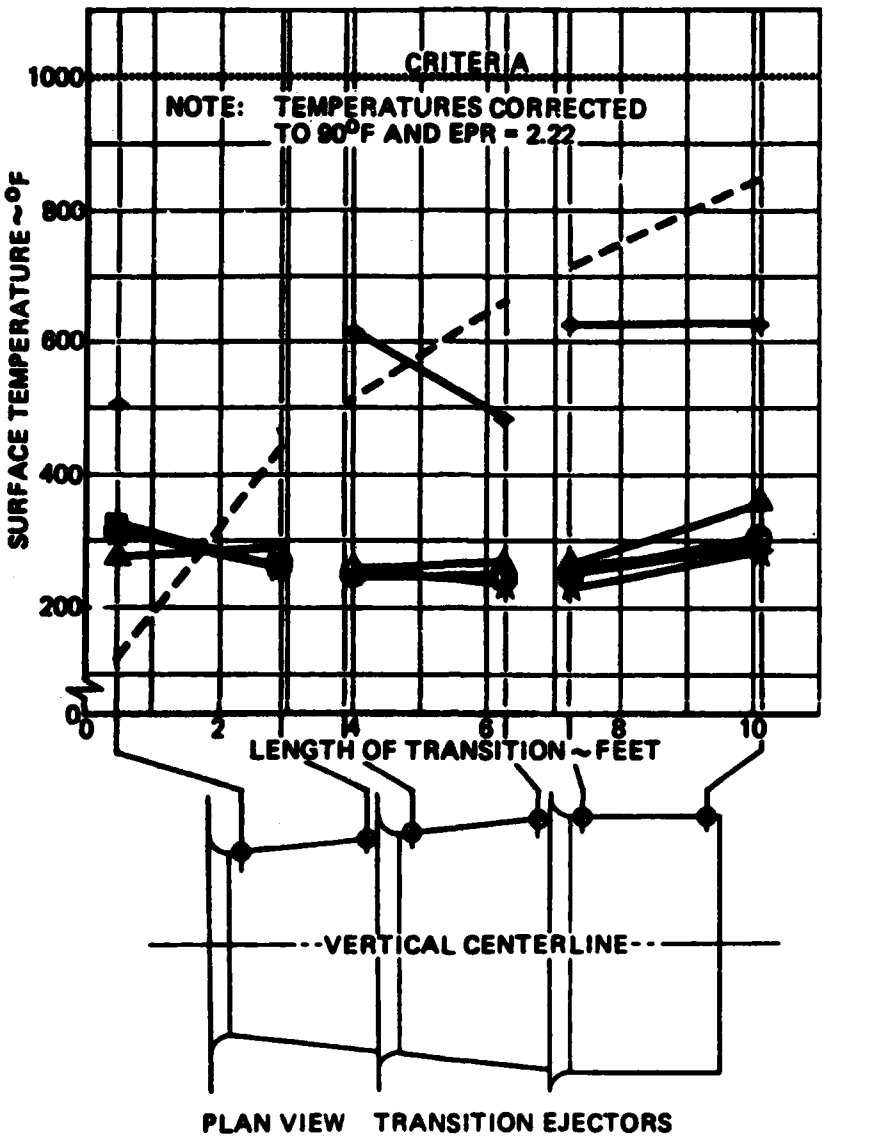

Figure 3-7. Ejector side surface temperatures – J57A/B condition.

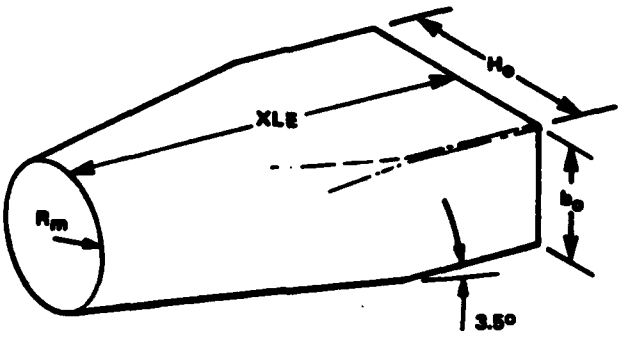

Figure 3-8. Single-stage ejector geometry.

By referring to figure 3-8, the following relations can be derived.

$$AR = \frac{H_o}{b_o} \tag{1}$$

The maximum side wall divergence angle as defined from experiment is 3.5 degrees. Therefore:

$$XLE = \frac{\frac{H_o}{2} - R_m}{\text{Tan } 3.5^\circ} = 16.35 \left(\frac{H_o}{2} - R_m\right) \tag{2}$$

Since the ejector is constant area,

finally:

$$\pi R_m^2 = b_o H_o = AR \times b_o^2 = \frac{H_o^2}{AR} \tag{3}$$

$$XLE = 16.35 \ (.886 \sqrt{AR} - 1) \ R_m \tag{4}$$

Empirical data have set the optimum aspect ratio at 2.13. Therefore, from equation (4) all ejectors will have a length - diameter ratio of 2.4. In addition, it has been shown that 1.87 is the required value for the ratio of ejector area to engine exit area. This means that, for a given engine, the ejector geometry is fixed.

The next step is to develop the equations needed to calculate the ejector pumping ratio (ratio of entrained flow to primary flow) of the equivalent single-stage ejector. After this is done, it is then possible to determine the geometry and operation of the three-stage ejector set that would be used in the final Coanda system.

Figure 3-9 displays the parameters and relationships for the ejector pumping ratio.

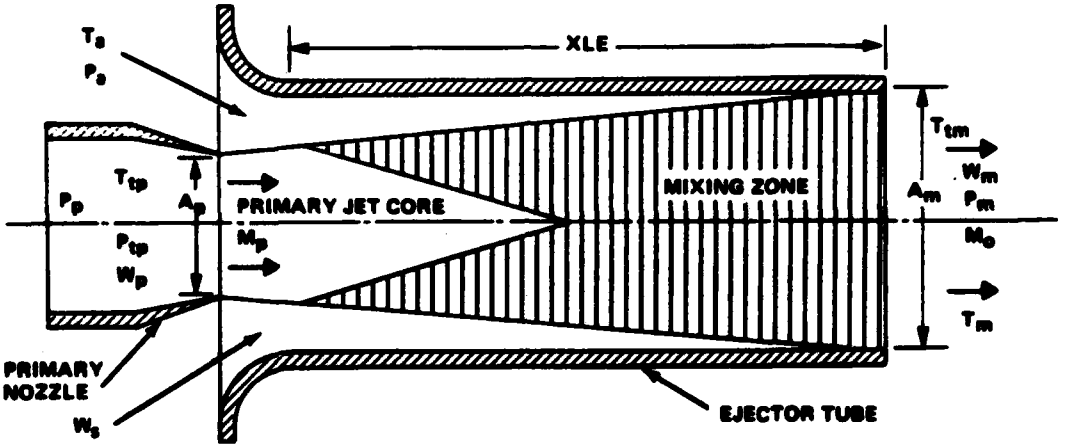

Figure 3-9. Equivalent single-stage ejector flow schematic.

$$(1 + R)^2 = \frac{1.405}{M_p^2} \frac{T_{tp}}{T_{tm}} \frac{P_m}{P_p} \left(\frac{A_m}{A_p}\right)^2 \left[\frac{A_p}{A_m}^{\eta} \left(\frac{P_{tp} - P_a}{P_p}\right) - \left(\frac{P_m - P_a}{P_p}\right)\right] \qquad (5)$$

where the pumping ratio R is defined as:

$$R = \frac{W_s}{W_p} \qquad (6)$$

and: η = ejector pumping efficiency.

The normal assumption is that the engine exhaust static pressure and the ejector exhaust static pressure are both equal to ambient pressure: $P_m = P_a = P_p$.

Therefore, equation (5) reduces to:

$$(1 + R)^2 = \frac{1.405}{M_p^2} \frac{T_{tp}}{T_{tm}} \frac{A_m}{A_p} \eta \left(\frac{P_{tp} - P_a}{P_a} \right) \tag{7}$$

Reference 6 gives the equation for T_{tm} as follows:

$$T_{tm} = \frac{RT_a + 1.2T_{tp}}{R + 1.2} \tag{8}$$

A is defined as:

$$A = \frac{1.405}{M_p^2} \frac{A_m}{A_p} \eta \left(\frac{P_{tp} - P_a}{P_a} \right) \tag{9}$$

where from reference 19:

$$M_p^2 = \frac{2}{\gamma - 1} \left[\left(\frac{P_{tp}}{P_p} \right)^{\frac{\gamma - 1}{\gamma}} - 1 \right] \tag{10}$$

Substituting equation (8) and equation (9) into equation (7) gives the cubic for R.

$$R^3 + \frac{2T_a + 1.2T_{tp}}{T_a} R^2 + \frac{T_a + T_{tp}(2.4 - A)}{T_a} R + \frac{1.2T_{tp}(1 - A)}{T_a} = 0 \tag{11}$$

This equation has a standard solution; however, for completeness it will be repeated here. Defining the following quantities:

$$p = \frac{2T_a + 1.2T_{tp}}{T_a} \tag{12}$$

$$q = \frac{T_a + T_{tp}(2.4-A)}{T_a} \tag{13}$$

$$r = \frac{1.2T_{tp}(1-A)}{T_a} \tag{14}$$

equation (11) reduces to:

$$R^3 + pR^2 + qR + r = 0 \tag{15}$$

substituting:

$$R = x - \frac{p}{3} \tag{16}$$

gives:

$$x^3 + ax + b = 0 \tag{17}$$

where:

$$a = \frac{1}{3}(3q - p^2) \tag{18}$$

and:

$$b = \frac{1}{27}(2p^3 - 9pq + 27r) \tag{19}$$

Equation (17) will have three roots; however, only one is meaningful for the ejector solution, which is extracted as follows:

Compute the value of the angle (ϕ) in the expression:

$$\cos\phi = - \frac{\frac{b}{2}}{\sqrt{\left(- \frac{a^3}{27}\right)}} \qquad (20)$$

Then x will have the following value:

$$x = 2 \sqrt{- \frac{a}{3}} \quad \cos \frac{\phi}{3} \qquad (21)$$

Finally, R is obtained from equation (16).

For a given ejector and engine, all the quantities in equations (9), (10), and (11) are known with the exception of η, the pumping efficiency. Values of η must be determined from experiment. By using the results in references 17 and 18, the variation of η with overall ejector area ratio was developed. It is shown in figure 3-10. This figure was drawn for an ejector length - diameter ratio of 2.4 since this will be fixed for all ejector sets as explained earlier. Also, it should be remembered that figure 3-10 is based on data from the three-stage Coanda ejector set and its use cannot be extended beyond that application.

By using the theory developed above for the equivalent single-stage ejector and the emperical curve for pumping efficiency, it is possible to calculate the total secondary flow entrained by the three-stage ejector set.

---

17 Naval Air Engineering Center, Design Configuration Handbook Test Cell System Coanda/Refraction Noise Suppression Concept, NAEC Design Data 92-136, 30 March 1979

18 Naval Air Engineering Center, Jet Engine Demountable Test Cell Exhaust System Phase - Coanda/Refractor Noise Suppression Concept Advanced Development, NAEC-92-112, April 1979

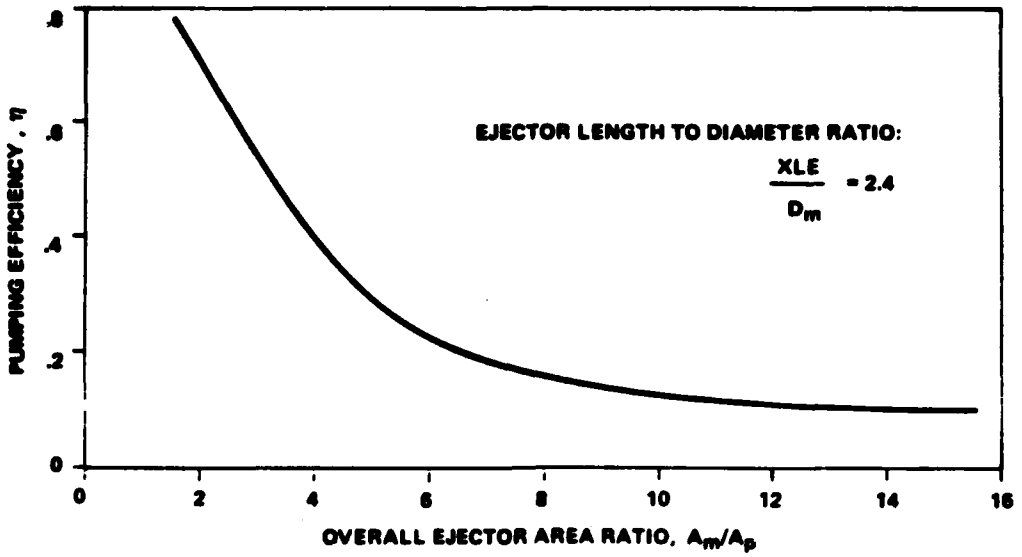

Figure 3-10. Variation of pumping efficiency vs overall ejector area ratio.

After the value of pumping ratio, R, is obtained from equation (16), the total entrained secondary flow is given by:

$$W_s = RW_p \tag{22}$$

and the mixed total temperature is given by equation (8).

(2) Ejector Set Exit Mach Number Calculation. The ejector set exit Mach number is needed to calculate the amount of secondary air that will be entrained by the Coanda surface flow. The ejector exit flow is the flow incident to the Coanda surface.

In addition, the exit Mach number must be calculated as a check on the ejector pumping ratio solution. Under certain conditions, the pumping ratio obtained from equation (16) results from trying to force too much air through the given ejector area. This situation arises when the calculation of exit Mach number produces a value which exceeds unity. It would therefore be required to increase the ejector area.

The equation for the ejector set exit Mach number is:

$$m_o = .0204 \frac{W_m R_a \sqrt{T_m}}{gP_a A_m} \tag{23}$$

where:

W_m = ejector weight flow (lb/s)

T_m = ejector static temp (°R)

g = gravitational constant = 32.2 ft/s^2

P_a = ambient pressure (lb/ft^2)

A_m = ejector area (ft^2)

R_a = gas constant for air = 1716 ft^2/s^2 °R

This equation uses the static temperature of the gas whereas equation (8) gives the ejector exit total temperature. The static temperature is a function of the total temperature and the exit Mach number so a short iteration is required.

The recommended procedure is to assume that the static temperature is 90% of the total temperature and calculate M_o. This value of M_o is used with the flow tables in appendix A to obtain a value for T_m/T_{tm} which gives a new T_m to use in equation (23). This process is repeated until the Mach number becomes constant. Usually four or five iterations are needed.

(3) Three-Stage Ejector Set Design. The final step in the ejector set design procedure is to calculate the three-stage ejector geometry on the basis of the operation and geometry of the single-stage approximation. The following equation is used to determine the equivalent radius for each ejector stage.

$$R_n^2 = \frac{W_{ns}}{W_s}(R_m^2 - R_p^2) + R_n^2 - 1 \qquad (24)$$

where: n varies from 1 to 3 and $R_o = R_p$.

Experimental test results indicate that for proper ejector operation the first stage should entrain 60% of the total entrained flow, the second stage 19%, and the third stage 21%.

Therefore:

$$W_{1s} = 0.60\ W_s$$

$$W_{2s} = 0.19\ W_s$$

$$W_{3s} = 0.21\ W_s$$

And equation (24) yields for the equivalent radii of each stage:

$$R_1^2 = 0.60\ (R_m^2 - R_p^2) + R_p^2 \tag{25}$$

$$R_2^2 = 0.19\ (R_m^2 - R_p^2) + R_1^2 \tag{26}$$

$$R_3^2 = 0.21\ (R_m^2 - R_p^2) + R_2^2 \tag{27}$$

The ejector stage lengths should be calculated from the following experimentally-derived relationships:

$$L_1 = 0.50\ XLE \tag{28}$$

$$L_2 = 0.25\ XLE \tag{29}$$

$$L_3 = 0.25\ XLE \tag{30}$$

The values R_1, R_2, and R_3 are called equivalent radii because only the first-stage ejector inlet is circular. The primary function of the ejector set is to transition the flow from a circular cross section to a rectangular cross section. The details of the transition will be outlined later.

(4) Standard Coanda Ejector Set. The procedure outlined previously can be used to design an ejector set for any specific engine. However, a standard ejector set has been developed that is capable of handling

most existing Navy engines, and this design is shown in figure 3-11. As can be seen, the first-stage transitions from circular to elliptical, the second stage from elliptical to elliptical, and the third stage from elliptical to rectangular. If a different size ejector is designed, it should be based on figure 3-11 with the exact dimensions determined from figure 3-11. The ratio of inlet radii is used to establish the new cross-sectional dimensions and then the new XLE is based on the results of the ejector set design procedure. (See table 3-6.)

(5) Ejector Set Design Results. The ejector design technique outlined above was used to design ejector sets for Navy turbojet and turbofan engines. In addition, the operation of each engine in the standard Coanda ejector set was determined. Table 3-1 shows the engine exhaust parameters used for the calculations. Tables 3-2 through 3-6 present the results for standard atmospheric conditions. As changes in atmospheric conditions have a minor effect on ejector performance, the tabulated values can be used for Coanda system design without recalculation for variations in ambient temperature and pressure. However, if it is desired to determine performance for nonstandard conditions, it is a simple matter to follow the procedure outlined.

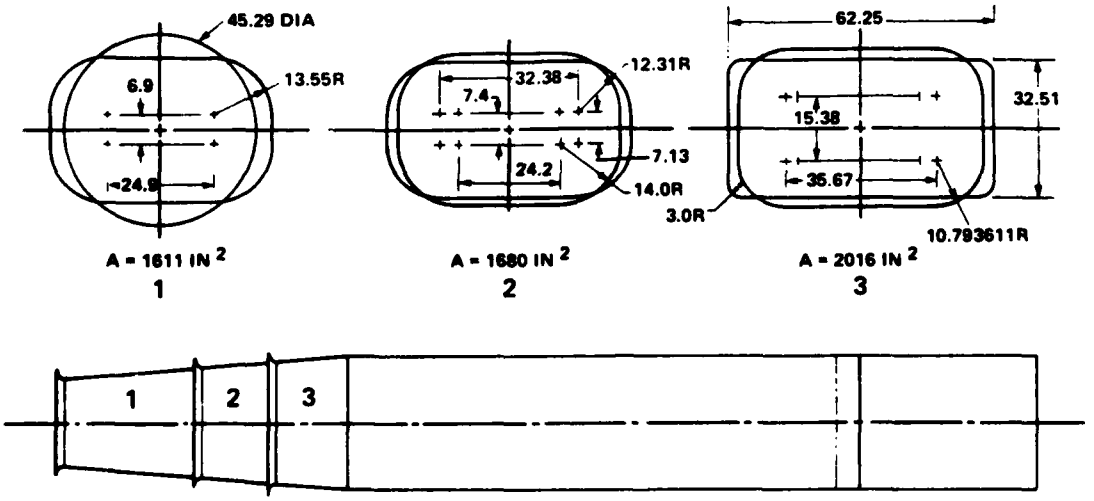

Figure 3-11. Standard ejector set design.

Calculation of the ejector set exit Mach number for the J-52 engine produced a value greater than unity. Therefore, tabulated values for the J-52 are for operation in the J-79 ejector set.

Table 3-1. Engine Exhaust Parameters, Standard Day Conditions

ENGINE	EXHAUST TOTAL PRESSURE psia	EXHAUST TOTAL TEMP °R	EXHAUST EXIT AREA $in.^2$	AIRFLOW lb/sec
J52-P-408	46.9	1800	257.9	146.0
J57-P-420 (MIL)	37.1	1660	398.4	186.0
J57-P-420 (A/B)	36.0	3360	666.8	186.0
J60-P-3A	30.6	1560	133.0	49.5
J79-GE-10 (MIL)	43.52	1547	327.0	167.0
J79-GE-10 (A/B)	42.12	3520	520.0	170.0
J85-GE-4A	30.80	1750	106.0	43.6
TF30-P-408	32.60	1797	526.6	257.0
TF30-P-412A (MIL)	30.56	1360	612.0	242.0
TF30-P-412A (A/B)	28.30	3100	1084.0	243.0
TF41-A-2	37.30	1524	486.9	263.0

Table 3-2. Ejector Pumping Ratio Results, Engine Specific Ejector Set T_a = 519°R P_a = 14.696 psia

ENGINE	EJECTOR AREA RATIO A_m/A_p	PUMPING EFFICIENCY η	PUMPING RATIO R
J52-P-408	3.77	.42	0.888
J57-P-420(MIL)	3.12	.53	0.798
J57-P-420(A/B)	1.87	.73	0.644
J60-P-3A	1.87	.73	0.484
J79-GE-10(MIL)	2.97	.54	0.826
J79-GE-10(A/B)	1.87	.73	0.737
J85-GE-4A	1.87	.73	0.496
TF30-P-408	1.87	.73	0.578
TF30-P-412A(MIL)	3.96	.40	0.611
TF30-P-412A(A/B)	1.87	.73	0.518
TF41-A-2	1.87	.73	0.566

Table 3-3. Pumping Ratio Results for Engines Operating in Standard Ejector Set T_a = 519°R P_a = 14.696 psia

ENGINE	EJECTOR AREA RATIO A_m/A_p	PUMPING EFFICIENCY η	PUMPING RATIO R
J52-P-408	7.82	0.18	0.746
J57-P-420(MIL)	5.04	0.29	0.668
J57-P-420(A/B)	3.02	0.54	0.805
J60-P-3A	15.16	0.10	0.598
J79-GE-10(MIL)	6.17	0.22	0.640
J79-GE-10(A/B)	3.88	0.41	0.681
J85-GE-4A	19.02	0.10	0.594
TF-30-P-408	3.84	0.41	0.693
TF30-P412A(MIL)	3.94	0.40	0.615
TF30-P-412A(A/B)	1.87	0.73	0.518
TF41-A-2	4.18	0.39	0.706

ENGINE	FIRST STAGE ENTRAINED FLOW W_{1s} lb/s	SECOND STAGE ENTRAINED FLOW W_{2s} lb/s	THIRD STAGE ENTRAINED FLOW W_{3s} lb/s	TOTAL ENTRAINED FLOW W_s lb/s	EJECTOR EXIT TEMP. T_{tm} °R	TOTAL EXIT FLOW W_m lb/s	EXIT MACH NUMBER M_e
J52-P408	77.53	24.55	27.13	129.21	1256.3	276.21	.704
J57-P-420 (MIL)	88.24	27.94	30.88	147.07	1206.3	332.07	.649
J57-P-420 (A/B)	71.86	22.75	25.15	119.78	2367.8	305.76	.838
J60-P-3A	14.38	4.55	5.03	23.96	1260.8	73.46	.736
J79-GE-10 (MIL)	82.76	26.21	28.97	137.94	1127.9	304.94	.739
J79-GE-10 (A/B)	75.17	23.81	26.31	125.29	2378.2	295.29	1.000
J85-GE-4A	12.98	4.11	4.54	21.63	1390.0	95.23	.860
TF30-P-408	81.41	25.78	28.49	135.69	1406.5	392.70	1.000
TF30-P-412A (MIL)	88.72	28.09	31.05	147.86	1076.3	389.86	.443
TF30-P-412A (A/B)	75.52	23.92	26.43	125.87	2363.7	368.87	.621
TF41-A-2	89.28	28.27	31.25	148.80	1201.9	411.80	1.000

Table 3-4. Three-stage ejector performance results – engine specific.

ENGINE	FIRST STAGE ENTRAINED FLOW W_{1s} lb/s	SECOND STAGE ENTRAINED FLOW W_{2s} lb/s	THIRD STAGE ENTRAINED FLOW W_{3s} lb/s	TOTAL ENTRAINED FLOW W_s lb/s	EJECTOR EXIT TEMP. T_{tm} °R	TOTAL EXIT FLOW W_m lb/s	EXIT MACH NUMBER M_e
J52-P-408	65.26	20.67	22.84	108.77	1309.3	264.77	.333
J57-P-420 (MIL)	73.04	23.13	25.56	121.73	1256.0	306.73	.393
J57-P-420 (A/B)	99.88	31.63	34.96	166.47	2146.7	352.47	.590
J60-P-3A	17.76	5.62	6.22	29.60	1213.8	79.10	.099
J79-GE-10 (MIL)	64.13	20.31	22.44	106.88	1189.4	273.88	.341
J79-GE-10 (A/B)	98.02	31.04	34.31	163.37	2185.5	333.37	.563
J85-GE-4A	23.12	7.32	8.09	38.54	1228.0	82.14	.104
TF30-P-408	106.86	33.84	37.40	178.10	1329.1	435.10	.573
TF30-P-412A (MIL)	89.29	28.28	31.26	148.83	1075.0	390.83	.463
TF30-P-412A (A/B)	75.52	23.92	26.43	125.87	2363.7	368.87	.621
TF34-GE-2	101.19	32.05	35.42	168.66	808.6	506.66	.520
TF41-A-2	119.61	37.88	41.86	199.35	1135.0	462.35	.563

Table 3-5. Three-stage ejector performance results – standard ejector set.

ENGINE	EJECTOR LENGTH XLE in	FIRST STAGE EQUIVALENT RADIUS R_1 in	FIRST STAGE LENGTH L_1 in	SECOND STAGE EQUIVALENT RADIUS R_2 in	SECOND STAGE LENGTH L_2 in	THIRD STAGE EQUIVALENT RADIUS R_3 in	THIRD STAGE LENGTH L_3 in
J57-P-420	95.45	17.97	47.72	18.92	23.86	19.92	23.86
J60-P-3A	42.60	8.03	21.30	8.45	10.65	8.90	10.65
J79-GE-10	84.30	15.87	42.15	16.71	21.07	17.59	21.07
J85-GE-4A	38.0	7.16	19.00	7.54	9.50	7.94	9.50
TF30-P-408	84.80	15.96	42.40	16.80	21.20	17.69	21.20
TF30-P-412A	121.70	22.91	60.85	24.12	30.42	25.40	30.42
TF41-A-2	81.50	15.35	40.75	16.16	20.37	17.02	20.37

Table 3-6. Three-stage ejector geometry results, engine specific.

With the tabulated values in tables 3-2 through 3-6, it is possible to select an ejector set for any engine or combination of engines without further calculation. Also, all necessary performance parameters to design the other components of the test system can be obtained from the tables for any rational engine-ejector set combination. It is now possible to proceed with the Coanda surface design.

b. Coanda Surface Design. The performance of the Coanda turning surface is a function of exit Mach number, surface pressure, pumping ratio and surface temperature. Figures 3-12, - 3-21 present the results of scale-model/full-scale demonstration unit measurements.

After the ejector set exit geometry and exit flow properties have been determined, it is a relatively simple matter to calculate the Coanda radius and the amount of secondary air entrained by the Coanda surface flow. With this information it is possible to calculate the exhaust stack flow and the secondary air inlet flow. The exhaust flow is a combination of the ejector exit flow and Coanda entrained air, while the secondary inlet flow is a combination of Coanda entrained air and the entrained air of the second and third ejector stages.

NAEC research has determined, based on water table and other experimental results, that the critical ratio for Coanda surface attachment is the ratio of ejector exit height (b_o) to Coanda surface radius (R_o). More precisely, it has been shown that the value 0.16 is optimum for Coanda surface design.

Therefore:

$$\frac{b_o}{R_o} = 0.16 \tag{31}$$

where from equation (3):

$$b_o = \sqrt{\frac{A_m}{AR}} \tag{32}$$

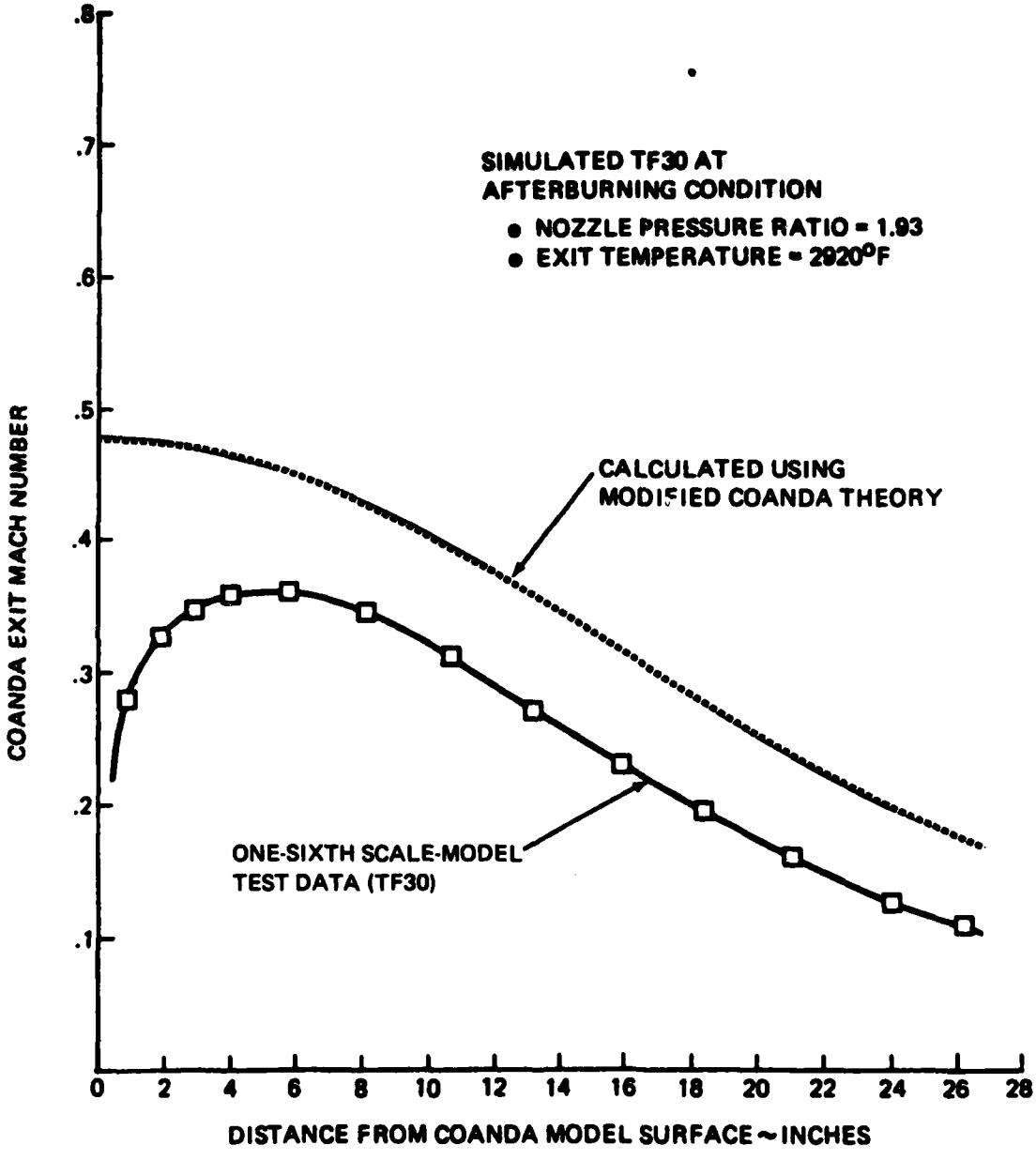

Figure 3-12. Comparison of Coanda exit Mach number profile at afterburning condition.

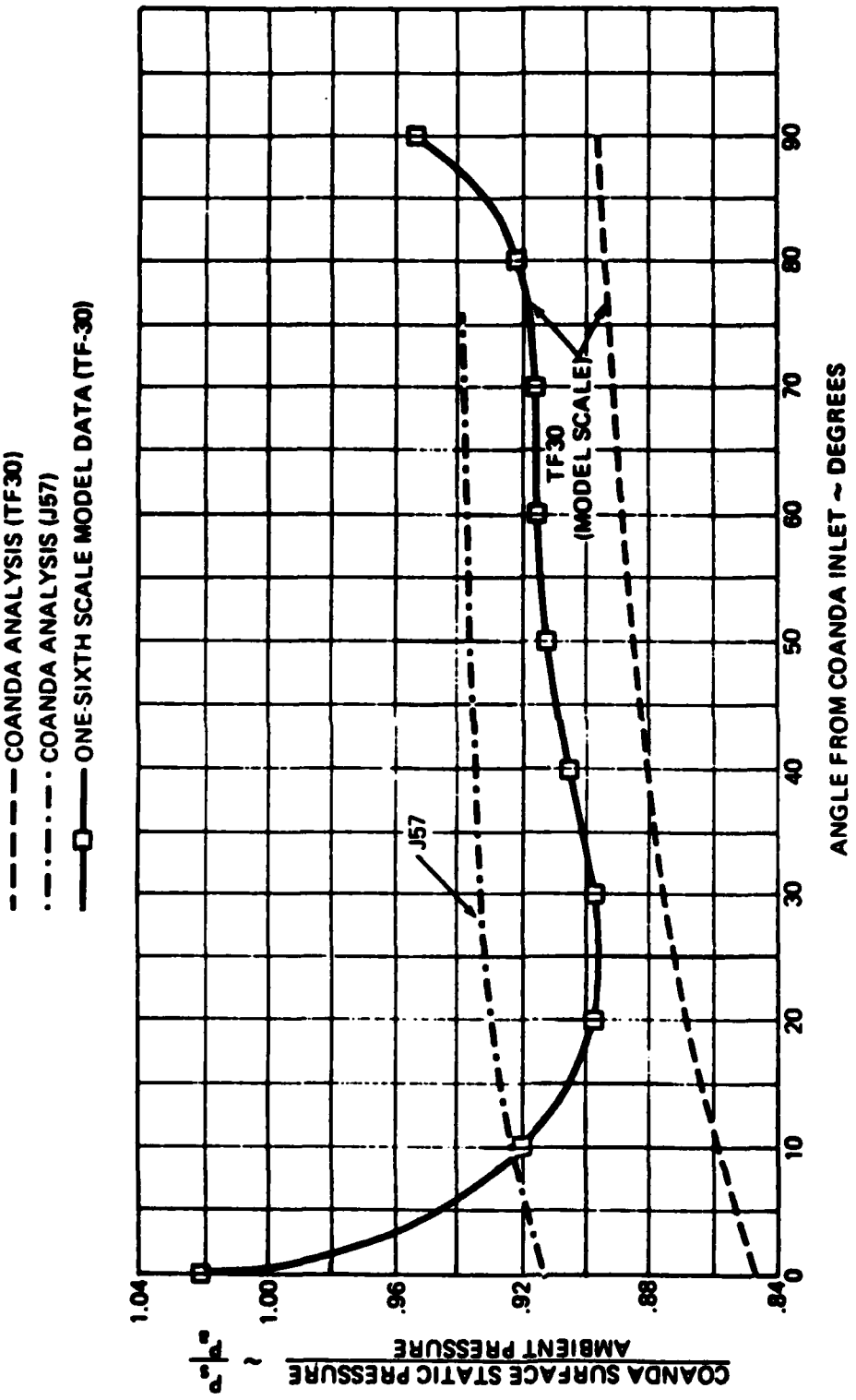

Figure 3-13. Comparison of Coanda surface pressure distribution at afterburning power.

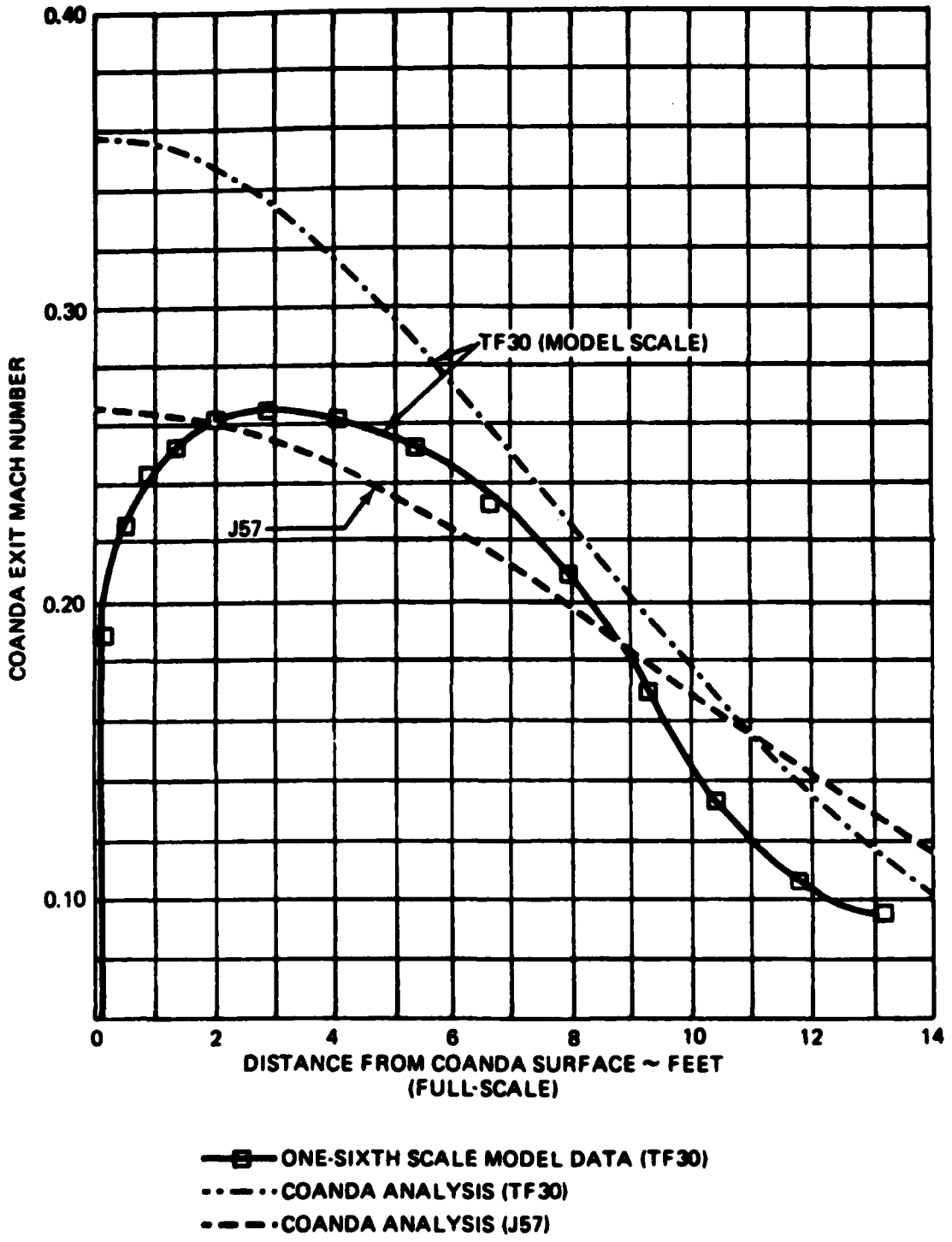

Figure 3-14. Comparison of Coanda exit Mach number profiles at military power.

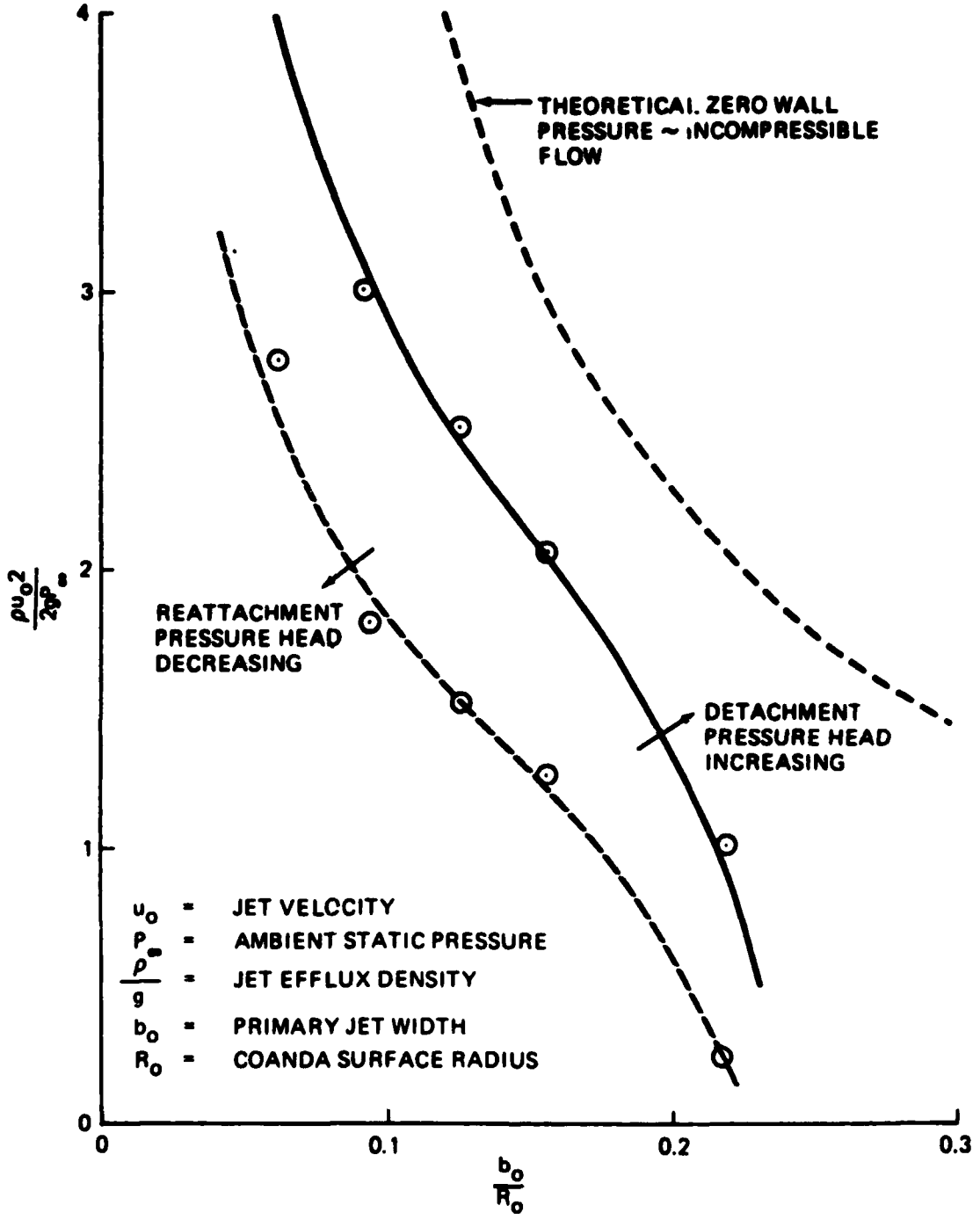

Figure 3-15. Water table model data – Coanda jet attachment limits.

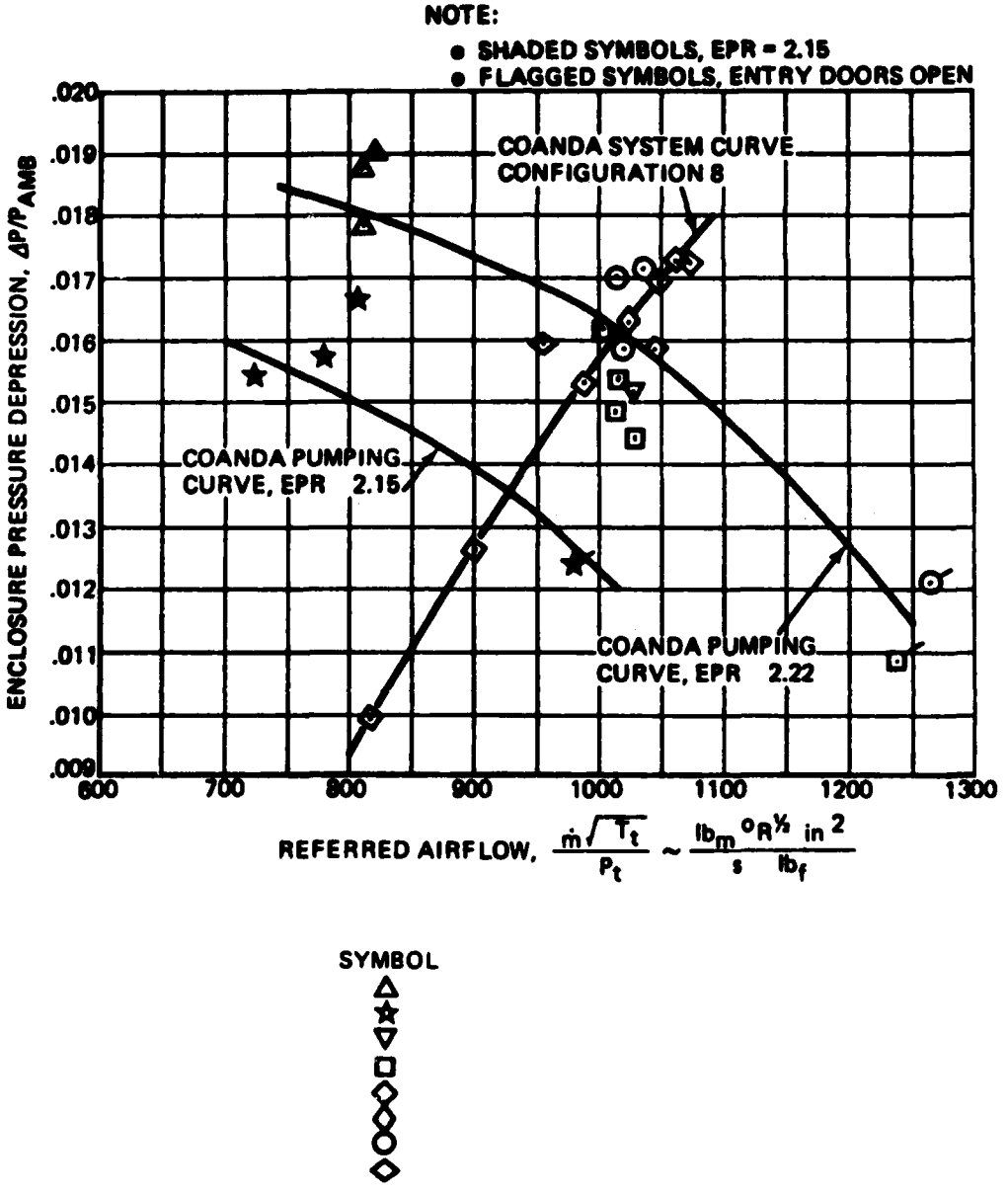

Figure 3-16. Coanda system and pumping curves – A/B condition.

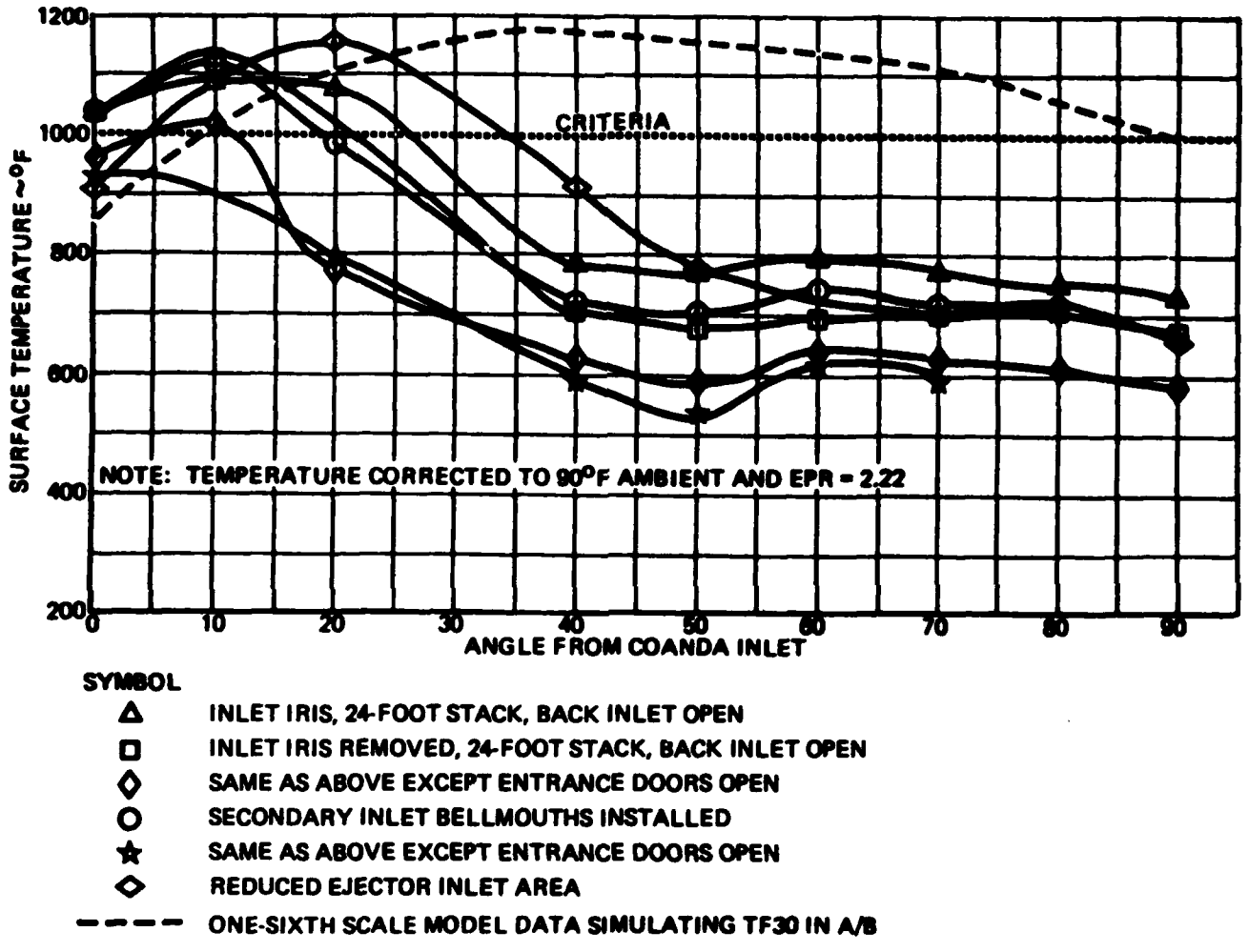

Figure 3-17. Coanda surface temperatures – J57 afterburning condition.

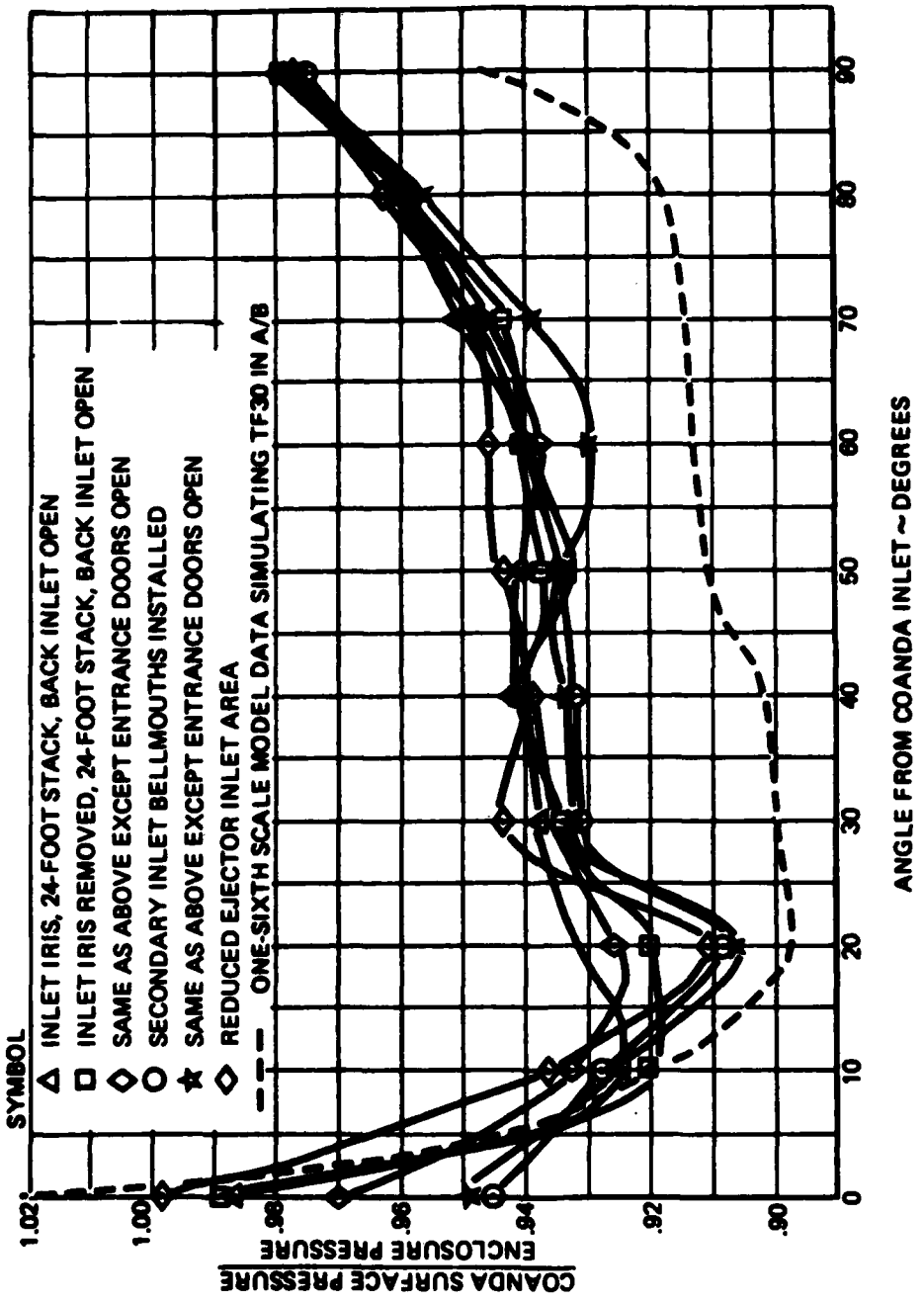

Figure 3-18. Coanda surface pressure – J57 afterburning condition.

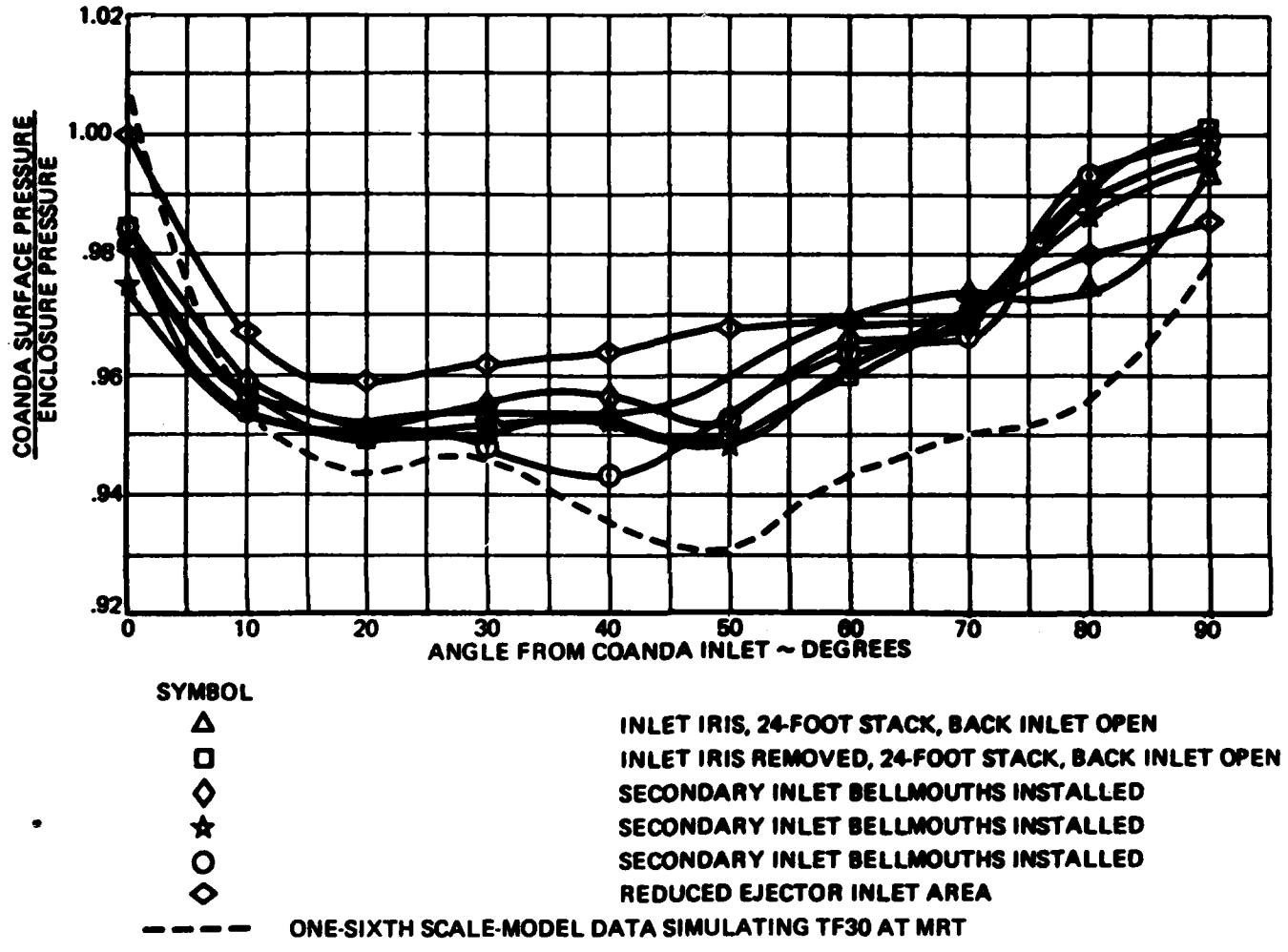

Figure 3-19. Coanda surface pressure -- J57 military rated condition.

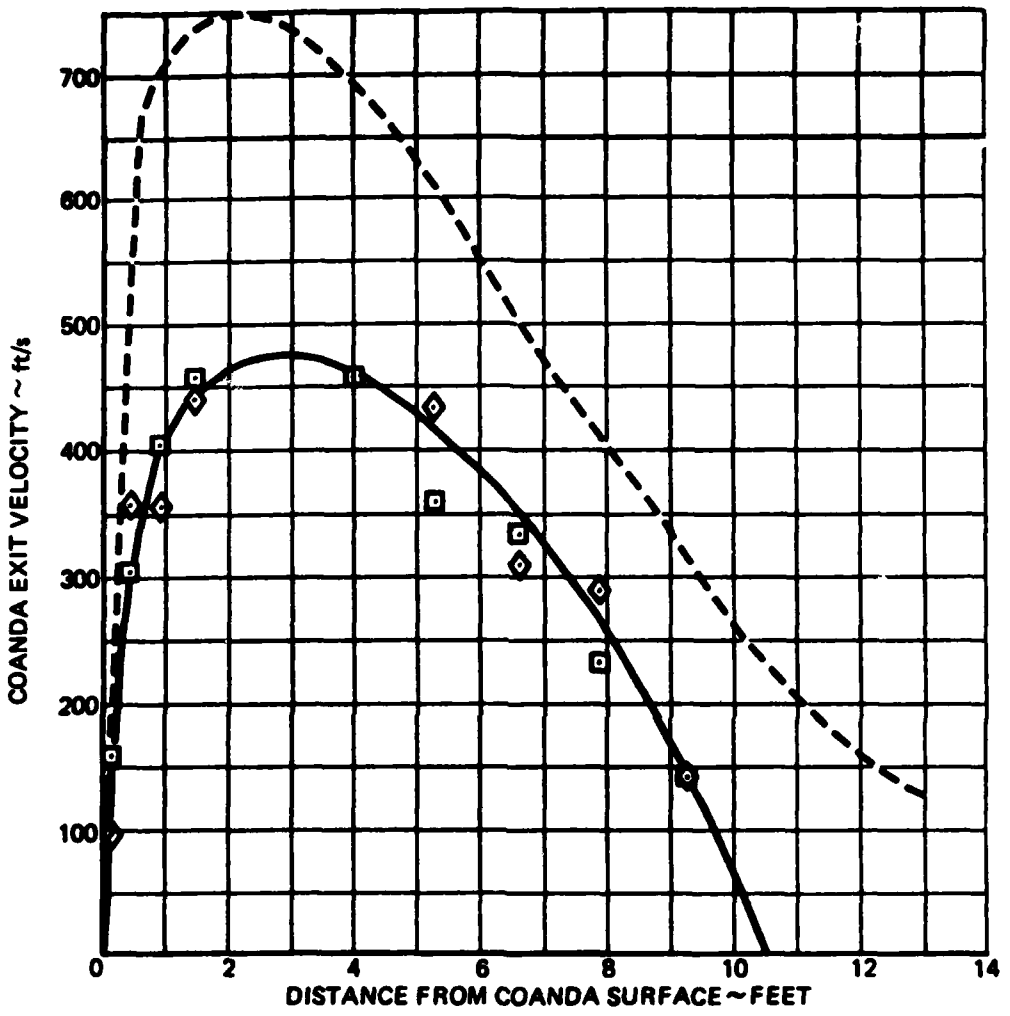

SYMBOL

□ INLET IRIS REMOVED, 24-FOOT STACK, BACK INLET OPEN

◇ SAME AS ABOVE EXCEPT ENTRANCE DOORS OPEN

– – – – ONE-SIXTH SCALE-MODEL DATA SIMULATING TF30

Figure 3-20. Coanda exit velocity – J57 afterburning condition.

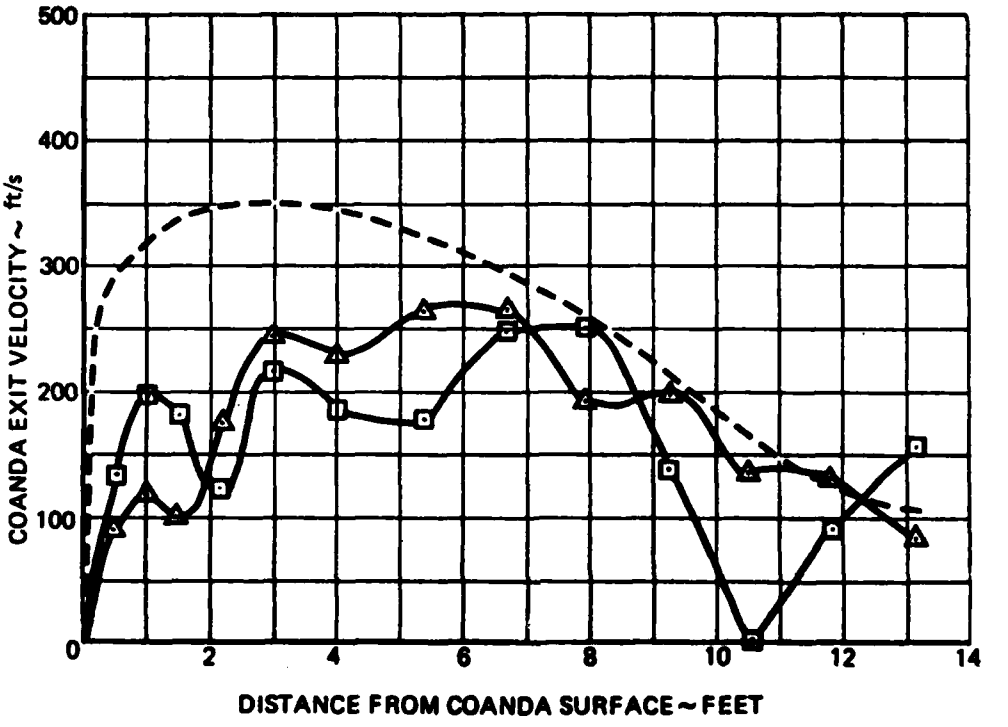

Figure 3-21. Coanda exit velocity – J57 military rated condition.

and from equation (1):

$$H_o = AR \times b_o$$

Equations (31 and (32) can be used to obtain the required Coanda radius, and since the Coanda surface width is equal to the last-stage ejector width, equation (1) defines this value. In equation (32), the area for the equivalent single-stage ejector (A_m) is used since this is equal to the third-stage ejector exit area.

The amount of secondary cooling air entrained by the Coanda surface flow is obtained with the use of figure 3-22, remembering that the Coanda surface incident flow is the third-stage ejector exit flow. If the value of b_o/R_o is defined as 0.16, then from figure 3-22 the entrainment function is:

$$\epsilon \frac{\left(\frac{T_{tm} - T_a}{T_a}\right)^{.03}}{M_o^{.05}} \left(\frac{(90)}{\theta_o}\right)^{.78} = 1.988 \qquad (33)$$

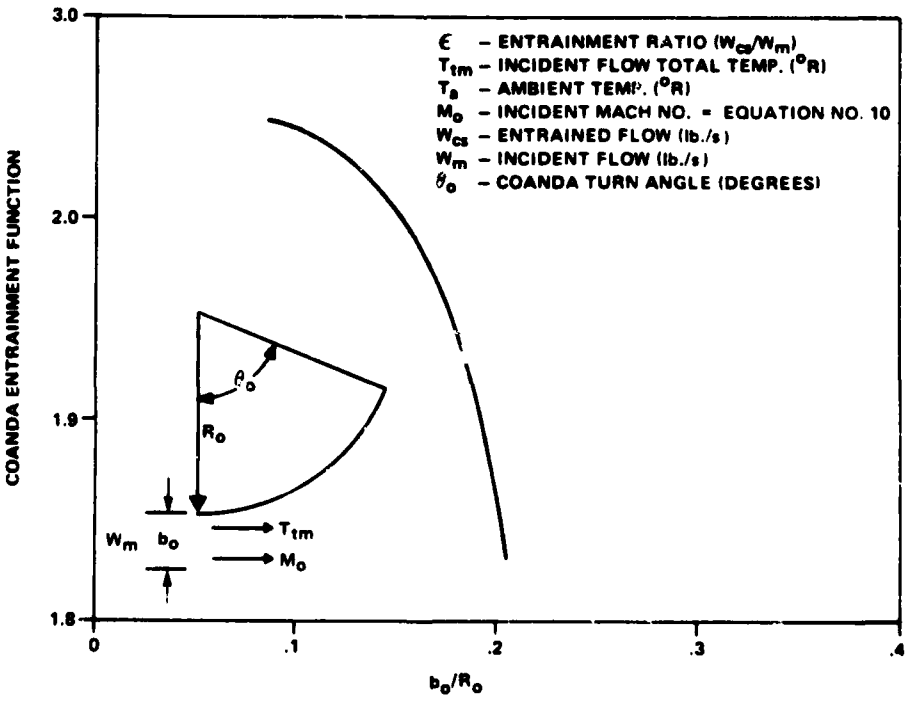

Figure 3-22. Coanada entrainment function vs b_o/R_o.

If the turning angle is given as 90°, the equation for Coanda entrainment becomes:

$$E = \frac{1.98M_o^{.05}}{\left(\frac{T_{tm} - T_a}{T_a}\right)^{.03}} \tag{34}$$

The Coanda entrained flow is then:

$$W_{cs} = \epsilon W_m \tag{35}$$

and the total exhaust flow becomes:

$$W_{se} = W_m + W_{cs} \tag{36}$$

Equation (8) is used to calculate the exhaust flow total temperature. Noting that T_{tm} replaces T_{tp} and ϵ replaces R:

$$T_{te} = \frac{\epsilon T_a + 1.2T_{tm}}{\epsilon + 1.2} \tag{37}$$

The Coanda design procedure can be used to match a Coanda surface to any of the ejector sets designed previously. In addition, a standard Coanda surface has been designed to complement the standard ejector set. The details of this design are shown in figure 3-23.

As before, calculations were made for a matching Coanda surface for each ejector set previously designed as well as for the performance of each engine in the universal Coanda system. The results are presented in tables 3-7 and 3-8 for standard atmospheric conditions. The Coanda entrainment ratio, ϵ, is little affected by ambient conditions so these values can be used for further design calculations which involve changes from standard conditions. This is not the case with the mixed gas temperature and inlet and exit velocities, which must be calculated for the worst combination of ambient conditions.

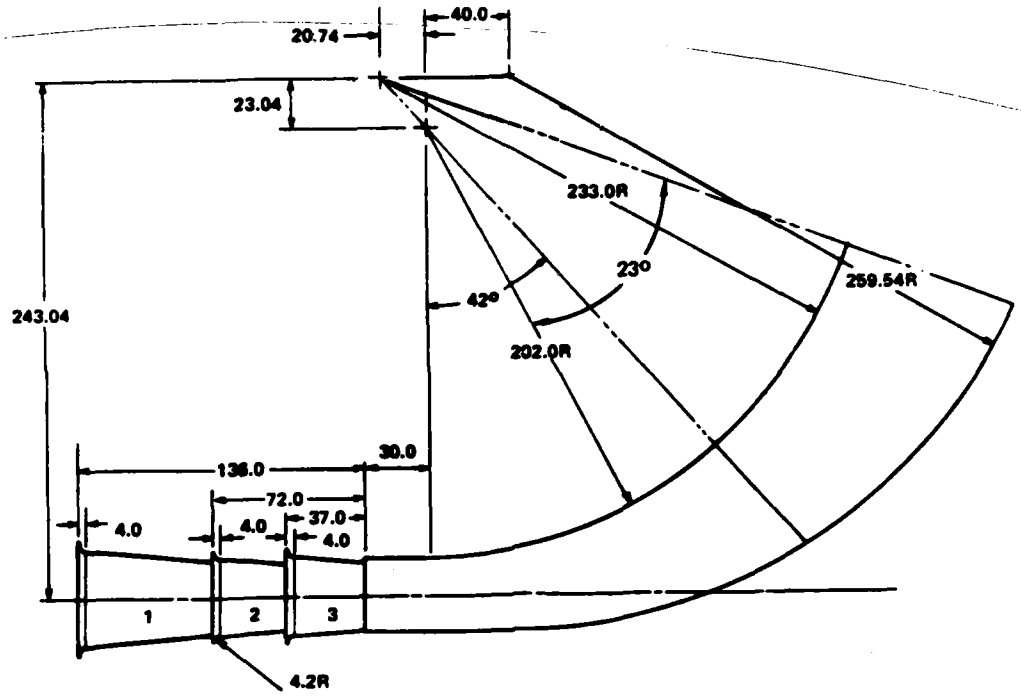

Figure 3-23. Standard Coanda surface design.

Table 3-7. Coanda surface geometry and performance – engine specific.

T_a = 519°R P_a = 14.696 psia

ENGINE	EJECTOR EXIT HEIGHT b_o in	COANDA RADIUS R_o in	COANDA SURFACE ENTRAINMENT ϵ	COANDA SURFACE ENTRAINED FLOW W_{cs} lb/s	TOTAL EXIT FLOW W_{se} lb/s	STACK EXIT TEMP. T_{te} °R	COANDA SURFACE WIDTH H_o in
J52-P-408	21.37	133.54	1.93	531.16	806.37	801.67	45.52
J57-P-420(MIL)	24.19	151.20	1.93	640.90	972.97	782.12	51.50
J57-P-420(A/B)	24.19	151.20	1.90	580.94	868.70	1234.66	51.50
J60-P-3A	10.80	67.50	1.94	142.51	215.97	802.49	23.00
J79-GE-10(MIL)	21.37	133.54	1.95	594.63	899.57	750.96	45.52
J79-GE-10(A/B)	21.37	133.54	1.91	564.00	859.29	1236.38	45.52
J85-GE-4A	9.65	60.29	1.94	126.55	191.78	851.87	20.60
TF30-P-408	21.48	134.26	1.96	769.70	1162.40	856.03	45.80
TF30-P-412A(MIL)	30.85	192.80	1.90	740.73	1130.59	734.73	65.70
TF30-P-412A(A/B)	30.85	192.80	1.87	689.79	1058.66	1240.06	65.70
TF41-A-2	20.67	129.18	1.97	811.25	1223.05	777.51	44.00

b_o/R_o = 0.16 AR = 2.13

Table 3-8. Standard Coanda surface performance.

$T_s = 518.6°R$ $P_s = 14.696$ psia – for Coanda Entrainment
$T_s = 580°R$ $P_s = 13.0$ psia – for Stack Exit Temperature

ENGINE	COANDA SURFACE ENTRAINMENT ϵ	COANDA SURFACE ENTRAINED FLOW W_{ss} lb/s	TOTAL EXIT FLOW W_{se} lb/s	STACK EXIT TEMP. T_{te} °R
J52-P-408	1.86	473.87	728.64	828.92
J57-P-420(MIL)	1.88	576.65	883.38	806.14
J57-P-420(A/B)	1.87	659.12	1011.89	1155.08
J60-P-3A	1.76	139.22	218.32	800.88
J79-GE-10(MIL)	1.87	512.16	786.04	781.05
J79-GE-10(A/B)	1.87	623.40	956.77	1170.40
J85-GE-4A	1.76	144.57	226.71	806.43
TF30-P-408	1.91	831.04	1266.14	831.58
TF30-P-412A(MIL)	1.91	746.49	1137.32	733.53
TF30-P-412A(A/B)	1.87	689.79	1058.66	1240.06
TF34-GE-2	1.96	993.05	1499.71	628.97
TF41-A-2	1.92	887.71	1350.06	755.92

c. Exhaust Stack Design. The exhaust stack calculations involve only two simple equations, both derived from the basic continuity equation.

If the exit area is chosen and the resulting exhaust velocity is to be determined, the following equation is used.

$$V_{se} = \frac{W_{se} R_a T_{te}}{P_a A_{se} g} \tag{38}$$

If the maximum exit velocity is set and the resultant exit area is to be calculated, the following equation is used.

$$A_{se} = \frac{W_{se} R_a T_{te}}{P_a V_{se} g} \tag{39}$$

The units used in these two equations are:

W_{se} (lb/s)
$R_a = 1716\ ft^2/s^2 \cdot R$

P_a (lb/ft^2)

$g = 32.2\ ft/s^2$

V_{se} (ft/s)

T_{te} (°R)

As stated previously, exhaust stack calculations should be made by assuming ambient conditions that would produce either the highest velocity or area. By designing for the worst case, all other operating conditions will remain within limits. The worst case results with high ambient temperature and low ambient pressure. Therefore, it will be assumed that:

$$T_a = 120°F = 580°R$$

$$P_a = 13.00\ psia$$

With these assumptions it is first necessary to recalculate the exit temperature, T_{te}, by using equations (8) and (37) and the worst case ambient temperature. As mentioned above, the values of ϵ and R already calculated can still be used because of the slight effect ambient conditions have on these quantities. Then either the velocity or area can be calculated from equation (38) or (39) respectively.

The final step using the above assumptions is to determine the length and width of the exhaust stack flow area. The exhaust stack should allow for 6 inches of clearance on either side of the Coanda surface.

Therefore the exit width is given by:

$$S_{ew} = H_o + 12 \tag{40}$$

and the resulting length is:

$$L_e = \frac{A_{se}(144)}{S_{ew}} \tag{41}$$

Equations (38) through (41) can now be used for the necessary exhaust stack calculations. These calculations have been done for common Navy engines and the results are given in tables 3-9 and 3-10. The required exhaust areas for the individual designs in table 3-9 were obtained by using a maximum exhaust velocity of 255 ft/s. Only the results for the afterburning case are given as they represent the design condition producing the largest required area.

Table 3-9. Exhaust stack performance results – engine specific.

$T_a = 580°R$ $P_a = 13.0$ psia $V_{se} = 255$ ft/s

ENGINE	EJECTOR EXIT TEMP T_{tm} °R	EXHAUST STACK EXIT TEMP T_{te} °R	EXHAUST STACK AREA A_{se} ft²	EXHAUST STACK WIDTH S_{sw} in	EXHAUST STACK LENGTH L_s in
J52-P-408	1282.16	849.20	76.45	57.5	191.46
J57-P-420(MIL)	1229.62	829.05	–	–	–
J57-P-420(A/B)	2389.11	1280.30	126.76	63.5	287.45
J60-P-3A	1278.34	846.88	20.43	36.0	84.05
J79-GE-10(MIL)	1152.75	798.19	–	–	–
J79-GE-10(A/B)	2401.37	1282.78	123.08	57.5	308.23
J85-GE-4A	1407.83	896.37	19.22	32.6	84.90
TF30-P-408	1426.14	900.94	116.93	57.8	291.31
TF30-P-412A(MIL)	1096.84	780.07	–	–	–
TF30-P-412A(A/B)	2382.09	1284.40	151.82	77.8	281.00
TF41-A-2	1221.45	822.82	112.36	56.0	288.82

Table 3-10. Exhaust stack performance results – standard Coanda system.

$T_a = 580°R$ $P_a = 13.0$ psia $A_{se} = 150$ ft²

ENGINE	EJECTOR EXIT TEMP T_{tm} °R	EXHAUST STACK EXIT TEMP T_{te} °R	EXHAUST STACK EXIT VEL V_{se} ft/s
J52-P-408	1332.70	875.18	121.04
J57-P-420(MIL)	1277.52	851.76	142.82
J57-P-420(A/B)	2172.36	1202.42	230.87
J60-P-3A	1234.06	845.16	35.02
J79-GE-10(MIL)	1210.65	826.51	123.31
J79-GE-(A/B)	2212.53	1218.14	221.20
J85-GE-4A	1253.70	863.12	36.72
TF30-P-408	1351.47	877.67	210.92
TF30-P-412A(MIL)	1095.70	778.98	168.16
TF30-P-412A(A/B)	2382.09	1284.40	258.08
TF34-GE-2	826.50	673.60	191.75
TF41-A-2	1168.55	802.52	205.64

d. Secondary Air Inlet Design. The secondary air inlet acoustic panels use a perforated plate with 50% open area ratio and 5/64-inch-diameter holes. If this design is adhered to, the empirical curve on figure 3-24 can be used to calculate the total pressure loss through the acoustic panels. In the recommended design the channel height, H, is 4.875 inches; therefore, from figure 3-24,

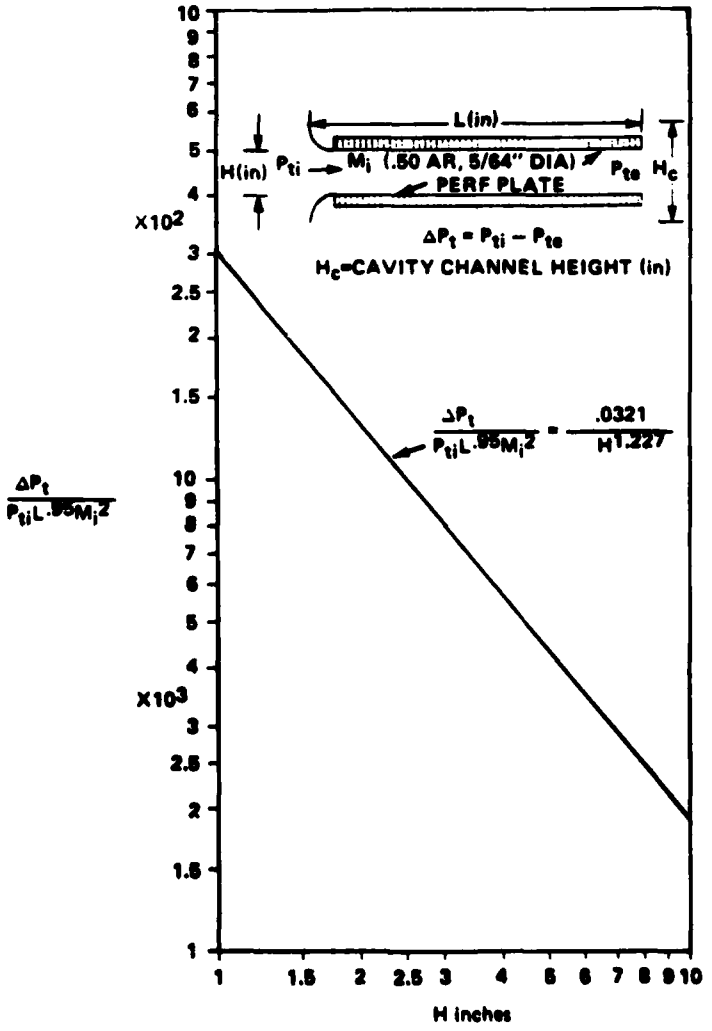

Figure 3-24. Normalized total pressure loss function vs channel height.

$$\frac{\Delta P_{ti}}{P_{ti} L^{.95} M_i^2} = .00475 \qquad (42)$$

where:

$L = 144$ in (based upon tests)

$P_{ti} = P_a$ (psia)

and M_i is given by the following equation:

$$M_i = \frac{W_{si} R_a \sqrt{T_a}}{P_a A_{si} g} \quad (.0204) \tag{43}$$

where:

P_a (lb/ft^2)

P_{xi} ($ft.^2$)

T_a (°R)

W_{si} (lb/s)

$R_a = 1716$ $ft^2/s^2 \cdot R$

The secondary inlet flow is a combination of the Coanda entrained flow and the second- and third-stage ejector entrained flow. Therefore:

$$W_{si} = W_{cs} + W_{2s} + W_{3s} \tag{44}$$

Equation (43) is used when the inlet area has been specified. If the maximum inlet velocity is specified (140 ft/s for the panel design), then the inlet Mach number is:

$$M_i = \frac{V_{si}}{\sqrt{49\ T_a}} \tag{45}$$

and the required inlet area becomes:

$$A_{si} = \frac{W_{si} R_a T_a}{P_a V_{si} g} \tag{46}$$

Equation (42) gives the decrease in total pressure from the beginning of the inlet to the acoustic panel exit.

Therefore:

$$P_{te} = P_{ti} - \Delta P_{ti} \tag{47}$$

Since, $P_{ti} = P_a$

Then:

$$P_{te} = P_a - \Delta P_{ti} \tag{48}$$

The pressure loss into the Coanda enclosure is the combination of the pressure loss through the panels (given above) and the pressure loss due to the sudden expansion in flow area at the exit of the panels. The sudden expansion loss is given by:

$$P_{te} - P_{tc} = 0.7\, P_e M_e^2 K_t \tag{49}$$

where K_t is the sudden expansion loss coefficient and is defined as:

$$K_t = \left(1 - \frac{H}{H_c}\right)^2 \tag{50}$$

Since H equals 4.875 inches and with 12-inch panels H_c = 16.875, then:

$K_t = 0.506$

Calculation of the panel exit Mach number, M_e, and the panel exit static pressure, P_e, proceeds as follows:

First calculate the exit weight flow function defined as:

$$W_t = \frac{W_{si}\sqrt{T_a}}{A_{si} \times 144 \times P_{te}} \quad (51)$$

where:

T_a = ambient temp (°R)
W_{si} = inlet air flow (lb/s)
A_{si} = inlet area (ft.^{2})
P_{te} = panel exit total pressure (psia)

By using the value of W_t obtained from equation (51) and the tables to appendix A, it is possible to determine M_c and P_e/P_{te}. (In the tables these values would be M and P/P_t.)

Then, using the value for the ratio P_e/P_{te} and the value of P_{te} from equation (48):

$$P_{te} = \frac{P_e}{P_{te}} P_a \quad (52)$$

with the value of P_e, and the value of M_e from the tables in appendix A, P_{te} is calculated from equation (49).

Finally, the cell depression in inches of water is given by:

$$\text{Negative pressure} = 28.10\ (P_a - P_{tc}) \quad (53)$$

where P_a and P_{tc} are in psia.

The procedure outlined above was used to calculate the cell depression in the plenum chamber of the Coanda enclosure both for the individual designs and for each engine operating in the Standard Coanda. For the individual designs, the inlet velocity was set at 140 ft/s and the resulting cell depression and required areas were calculated. As the inlet velocities were the same, the cell depressions were all the same. Calculations were made for the worst case

(ie, T_a = 580°R and P_a = 13.0 psia). The Standard Coanda design has a fixed inlet area of 96.7 ft^2 and therefore, calculations were made for inlet velocity and resulting cell depression. The results are shown in tables 3-11 and 3-12. It is apparent that the larger turbofan engines (TF30, TF41, and TF34) exceed both the inlet velocity limit and the cell depression limit (6 inches of water). This indicates that these engines require a larger Coanda exhaust system. This system is considered in detail in a later section.

Table 3-11. Secondary air inlet results - engine specific
T_a=580°R P_a=13.0 psia
V_{si}=140 ft/s

ENGINE	SECONDARY AIR INLET FLOW W_{si} lb/s	SECONDARY AIR INLET AREA A_{si} ft^2
J52-P-408	582.84	68.74
J57-P-420-(MIL)	699.72	82.52
J57-P-420(A/B)	628.84	74.16
J60-P-3A	152.09	17.93
J79-GE-10(MIL)	649.81	76.64
J79-GE-10(A/B)	614.12	72.43
J85-GE-4A	135.20	15.94
TF30-P-408	823.97	97.18
TF30-P-412A(MIL)	799.87	94.33
TF30-P-412A(A/B)	740.14	87.29
TF41-A-2	870.77	102.69

Table 3-12. Secondary air inlet results, standard Coanda T_a=580°R P_a=13.0 psia A_{si}=96.7 $ft.^2$

ENGINE	SECONDARY AIR INLET FLOW W_{si} lb/s	SECONDARY AIR INLET VELOCITY V_{si} ft/s	COANDA ENCLOSURE CELL DEPRESSION in H_2O
J52-P-408	517.38	88.34	1.85
J57-P-420(MIL)	625.34	106.77	2.74
J57-P-420(A/B)	725.71	123.91	3.68
J60-P-3A	151.06	25.79	0.343
J79-GE-10(MIL)	554.91	94.75	2.25
J79-GE-10(A/B)	688.75	117.60	3.27
J85-GE-4A	159.98	27.32	0.343
TF30-P-408	905.28	154.06	5.58
TF30-P-412A(MIL)	890.00	137.62	4.61
TF30-P-412A(A/B)	740.14	126.38	3.76
TF34-GE-2	1060.52	181.08	7.63
TF41-A-2	967.45	165.19	6.51

NOTE: Negative pressure for each case = 4.67 inches H_2O

e. Primary Air Inlet Design. The primary air inlet calculations for cell depression and required inlet area follow the same procedure as that outlined for the secondary air inlet. There are only a few changes in some of the parameters involved.

Since the first stage of the ejector set is the only one that communicates with the cell room, the primary inlet flow is the sum of the engine airflow and the air entrained by the first ejector stage.

Therefore:

$$W_{pi} = W_p + W_{ls} \tag{54}$$

Then W_{pi} is simply substituted for W_{si} in the equations of the previous section for secondary inlet design.

The recommended inlet design uses the same perforated plate and 12 inch panels used in the secondary inlet with several changes. The channel height, H, is 7.25 inches, which gives a sudden expansion cavity height, H_c, equal to 19.25 inches. The recommended length is 96 inches.

Using these values:

$$\frac{\Delta P_{ti}}{P_{ti} L^{.95} M_i^2} = .003 \tag{55}$$

and:

$$K_t = (1 - \frac{H}{H_c})^2 = .3886 \tag{56}$$

By using these changes and the fact that the maximum inlet velocity is 90 ft/s, calculations can be made for required inlet area and resulting cell depression. As before, these calculations have been made for the worst case (T_a = 580°R, P_a = 13.0 psia) and the results tabulated in tables 3-13 and 3-14. Since the areas were calculated to maintain the inlet velocity at 90 ft/s, the cell depression is the same for all cases. For the afterburning engines, the larger of the areas between A/B and military power should be selected for the design.

It was stated earlier that a larger turbofan Coanda would be recommended for the nonafterburning turbofan engines because certain operational limits in

the Standard Coanda are exceeded. The logical approach would be to use table 3-14 to select the largest required inlet area (minus the TF34, TF41, and TF30 non-A/B). This then becomes the design area and the operation of the other engines with this inlet can be calculated. From table 3-14, the inlet area is selected as 61 square feet. The resulting inlet velocity and cell depression were calculated and are shown in table 3-15.

Table 3-13. Primary air inlet results - engine specific T_s=580°R P_a=13.0 psia=90 ft/s.

ENGINE	PRIMARY AIR INLET FLOW W_{pi} lb/s	PRIMARY AIR INLET AREA A_{pi} ft^2
J52-P-408	223.53	40.82
J57-P-420(MIL)	273.24	50.13
J57-P-420(A/B)	257.86	47.31
J60-P-3A	63.88	11.72
J79-GE-10(MIL)	249.76	45.82
J79-GE-10(A/B)	245.17	44.98
J85-GE-4A	56.58	10.38
TF30-P-408	338.41	62.08
TF30-P-412A(MIL)	330.72	60.67
TF30-P-412A(A/B)	318.52	58.43
TF41-A-2	352.26	64.65

NOTE: Negative Pressure = 1.09 in. H_2O

Table 3-14. Primary air inlet results - standard Coanda T_a=580°R P_a=13.0 psia V_{pi}=90 ft/s.

ENGINE	PRIMARY AIR INLET FLOW W_{pi} lb/s	PRIMARY AIR INLET AREA A_{pi} ft^2
J52-P-408	211.26	38.76
J57-P-420(MIL)	258.04	47.34
J57-P-420(A/B)	285.88	52.45
J60-P-3A	67.26	12.39
J79-GE-10(MIL)	231.13	42.40
J79-GE-10(A/B)	268.02	49.17
J85-GE-4A	66.72	12.24
TF30-P-408	363.86	66.75
TF30-P-412A(MIL)	331.29	60.78
TF30-P-412A(A/B)	318.52	58.43
TF34-GE-2	439.19	80.57
TF41-A-2	382.61	70.19

NOTE: Negative Pressure = 1.09 in. H_2O

Table 3-15. Fixed geometry primary air inlet results - standard Coanda exhaust design. Inlet Area = 70 ft^2, T_a = 580°R, P_a = 13.0 psia

ENGINE	PRIMARY AIR INLET FLOW W_{pi} lb/s	PRIMARY AIR INLET VELOCITY V_{pi} ft/s	CELL DEPRESSION in H_2O
J52-P-408	211.26	56.64	0.510
J57-P-420(MIL)	258.04	96.62	0.626
J57-P-420(A/B)	285.88	76.70	0.791
J60-P-3A	67.26	17.70	0.303
J79-GE-10(MIL)	231.13	62.54	0.531
J79-GE-10(A/B)	268.02	71.98	0.683
J85-GE-4A	66.72	17.70	0.304
TF30-P-412A(MIL)	331.29	89.68	1.090
TF30-P-412A(A/B)	318.52	86.14	0.976

f. Engine Enclosure Design. The total cellroom flow is the sum of the engine primary airflow and the first-stage ejector entrained flow. This total flow exists only up to the face of the engine. Beyond the engine face, only the first-stage ejector entrained flow is left. Therefore, the maximum cellroom velocity with respect to the walls would be between the inlet and the engine face. This velocity is calculated very easily from the following equation.

$$V_{cell} = \frac{W_{pi} R_a T_a}{g P_a A_{cell}} \tag{57}$$

where:

V_{cell} = cellroom velocity ft/s
A_{cell} = cellroom area ft^2
T_a = ambient temp °R
P_a = ambient pressure lb/ft^2
R_a = 1716 ft^2/s^2
W_{pi} = primary inlet flow lb/s
g = 32.2 ft/s^2

To be precise, the pressure used in equation (57) should be ambient pressure minus the cell depression. However, the error in the velocity calculated by using ambient pressure is insignificant.

Calculations of maximum cellroom velocity were made using the cross sectional area of the demountable test cell, which is 225 square feet. Again the worst case was used (T_a = 580°R, P_a = 13.0 psia). The results are shown in table 3-16. As can be seen, all velocities are well below the maximum allowable of 50 ft/s.

In general when an engine operates in a test cell enclosure its performance will be different from runup pad operation. One way to minimize this effect is to decrease the static pressure difference between the engine inlet and exit. This is the external static pressure due to the flow over the

engine. In the coanda system, the only airflow over the engine is that due to the first-stage ejector flow. This flow is very small compared to alternate designs which use augmenter tubes. The static pressure difference is correspondingly low. However, for completeness, the following technique has been developed to calculate this difference.

Table 3-16. Maximum cellroom velocity. T_a = 580°R
P_a = 13.0 psia A_{cell} = 225 ft^2

ENGINE	MAXIMUM CELLROOM VELOCITY FOR INDIVIDUAL COANDA SYSTEMS Vcell ft/s	MAXIMUM CELLROOM VELOCITY FOR UNIVERSAL COANDA SYSTEM Vcell ft/s
J52-P-408	16.45	15.50
J57-P-420(MIL)	20.11	18.93
J57-P-420(A/B)	18.98	20.98
J60-P-3A	4.70	4.93
J79-GE-[illegible]3(MIL)	18.38	16.96
J79-GE-10(A/B)	18.04	19.67
J85-GE-4A	4.16	4.90
TF30-P-408	24.91	26.70
TF30-P-412A(MIL)	24.34	24.31
TF30-P-412A(A/B)	23.44	23.37
TF34-GE-2	-	32.23
TF41-A-2	25.93	28.08

The basic approach is to determine the Mach number at both the cellroom inlet and the first-stage ejector from which the ratio of static to total pressure can be obtained from appendix A. Since the total pressure is known (ambient pressure minus the cell depression), it is a simple matter to calculate the static pressure at both places.

Since the secondary flow will usually not occupy the total available area, it is necessary to determine the actual area the flow will use. Experimental evidence has shown that at the inlet plane, the flow will occupy 90% of the total cell cross-sectional area regardless of engine size. At the exit plane, the flow will occupy 15% of the available area (cell cross-sectional area minus the engine exhaust nozzle area). With this information, the following equations can be used to calculate the respective Mach numbers.

From the engine inlet plane:

$$M_x = .0204 \frac{W_{1s} R_a \sqrt{T_a}}{P_{tc} A_x g} \tag{58}$$

and for the engine exit plane:

$$M_y = .0204 \frac{W_{1s} R_a T_a}{P_{tc} A_y g} \tag{59}$$

Using the Mach numbers calculated above and the tables in appendix A:

$$P_x = \frac{P_x}{P_{tc}} P_{tc} \tag{60}$$

and:

$$P_y = \frac{P_y}{P_{tc}} P_{tc} \tag{61}$$

Since P_x and P_y are the static pressure in psia, the pressure difference in inches of water is given by:

$$\Delta P = 28.10 (P_x - P_y) \tag{62}$$

This procedure was used to calculate static pressure differences for engines operating in the individual Coanda designs as well as operating with the Standard Coanda exhaust system. All calculations used a total cellroom area of 225 square feet and assumed worst day conditions (T_a = 580°R, P_a = 13.0 psia).

The results are shown in tables 3-17 and 3-18. As can be seen, the differences are all extremely small because of the very small airflow over the engine using the Coanda exhaust system.

Table 3-17. External engine static pressure difference between inlet and exhaust-engine specific.
T_a = 580°R P_a = 13.0 psia A_{cell} = 225 ft^2

ENGINE	FIRST STAGE EJECTOR ENTRAINED FLOW W_{1s} lb/s	CELL MACH NO. ENGINE INLET PLANE M_x	CELL MACH NO ENGINE EXIT PLANE M_y	STATIC PRESSURE DIFFERENCE ΔP in H_2O
J52-P-408	77.53	0.00536	0.0324	0.232
J57-P-420(MIL)	86.24	0.00610	0.0370	0.321
J57-P-420(A/B)	71.80	0.00496	0.0300	0.223
J60-P-3A	14.38	0.00100	0.0060	0.008
J79-GE-10(MIL)	82.76	0.00572	0.0350	0.256
J79-GE-10(A/B)	75.17	0.00519	0.0320	0.255
J85-GE-4A	12.98	0.00100	0.0050	0.006
TF30-P-408	81.41	0.00562	0.0340	0.289
TF30-P-412A(MIL)	88.72	0.00613	0.0370	0.344
TF30-P-412A(A/B)	75.52	0.00522	0.0320	0.255
TF41-A-2	89.28	0.00617	0.0380	0.362

Table 3-18. External engine static pressure difference between inlet and exhaust planes - standard Coanda exhaust system.
T_a = 580°R P_a = 13.0 psia A_{cell} = 225 ft^2

ENGINE	FIRST STAGE EJECTOR ENTRAINED FLOW W_{1s} lb/s	CELL MACH NO. ENGINE INLET PLANE M_x	CELL MACH NO. ENGINE EXIT PLANE M_y	STATIC PRESSURE DIFFERENCE ΔP in H_2O
J52-P-408	66.26	0.0045	0.0272	0.182
J57-P-420(MIL)	73.04	0.0050	0.0307	0.239
J57-P-420(A/B)	99.88	0.0069	0.423	0.437
J60-P-3A	17.76	0.0012	0.0074	0.012
J79-GE-10(MIL)	64.13	0.0044	0.0268	0.182
J79-GE-10(A/B)	98.02	0.0068	0.0413	0.417
J85-GE-4A	23.12	0.0016	0.0096	0.024
TF30-P-408	106.86	0.0074	0.0450	0.504
TF30-P-412A(MIL)	89.29	0.0062	0.0376	0.359
TF30-P-412A(A/B)	75.52	0.0052	0.0314	0.239
TF34-GE-2	101.19	0.0070	0.0423	0.438
TF41-A-2	119.61	0.0083	0.0500	0.622

3. Acoustic Considerations.

As discussed in the previous sections, the dimensions and configuration of a Coanda/refraction type exhaust noise suppression system are derived primarily from the aerodynamic and thermodynamic characteristics of the engines to be tested. Engine exhaust nozzle diameter, temperature, mass air flow, and pressure ratio are the basis for calculating the ejectors and deflection surface parameters and for sizing the acoustic enclosure, including cooling air inlet and exhaust stack.

The acoustic performance of the overall suppressor system is determined by the acoustically lined elements comprising the cooling air inlet and exhaust stack with acoustic enclosure. Noise reduction requirements for each of the suppressor elements were determined analytically and experimentally. The noise spectrum generated inside the suppressor enclosure is determined by the effects of the ejectors and Coanda burning surface on the jet mixing process, the confinement of the noise source in the enclosure, and the effect of the enclosure average room absorption coefficient on the total sound power produced by the engine.

a. Standard Coanda System Acoustic Development. The actual acoustic performance characteristics of the Standard Coanda/refraction system were developed to reduce the bare engine noise levels of the TF-30-P-412 engine in afterburner power to acceptable near (less than 100 feet) and far-field (greater than 100 feet) levels. The iterative design and test procedure is described below.

Full-scale experimental model tests achieved a far-field noise level of 90 dBA (measured along a circle of 250 foot radius centered at the exhaust stack) and a near-field noise level of 97dBA (measured along the "Air Force 20 feet rectangle") with a J-57-P-20 engine at afterburner power.

The success in reducing the near-field noise, directly outside the enclosure walls, to 97dBA (the experimental acoustic goal was 125 dBA) is attributed to the design approach for the enclosure walls. The double-wall design features tuned hollow panels with interior acoustic treatment and vibration

isolators. This approach was especially effective in reducing low frequency noise. This same configuration is used in the Standard enclosure design.

The success in reducing the far-field noise to 90 dBA is attributed to optimum selection of acoustic elements. A significant design technology outcome was discerned:

- The lined exhaust stack and internal acoustic elements are sufficient to achieve 90 dBA in the far field without inclusion of acoustic lining material in the exhaust stack.

- Improved acoustic performance of 85 dBA and 80 dBA is feasible by utilizing a combination of the various acoustic elements (stack extensions, additional exhaust stack lining material, use of acoustic treatment of plenum floor area, and use of acoustic wedges in plenum) which were evaluated during the scale-model tests.

b. Standard Coanda System Acoustic Properties. The estimated far-field acoustic performance of the Standard Coanda/refraction system with the TF-30-P-412 engine at afterburner power is approximately 88 dBA. This calculated value is based upon:

- Projected acoustic properties of the suppressor elements.

- One-sixth scale-model tests using a scaled TF-30 engine nozzle to determine comparative effects of several types of exhaust stack acoustic linings and various configurations of internal acoustic absorptive baffles and panels.

- Extrapolation of actual full-scale acoustic performance with the J-57-P-20 engine at afterburner power to the distinct acoustic spectrum SPL of the TF-30-P-412 engine at afterburner power.

- Shortening of the Coanda surface from 90° to 65° turning angle, but maintaining a 40-foot stack height, thereby allowing the exhaust gas path to traverse a greater length of lined duct in the exhaust stack after leaving the top of the Coanda surface; ie, 23 feet of lined duct length versus 14 feet.

c. Improved Acoustic Performance. The following design techniques may be implemented in order to achieve improved performance from the Standard

system. These alternatives were tested and analyzed during the full-scale model program (ref 15) and the final one-sixth scale-model program (ref 19). It is at the discretion of the designer of a particular test cell installation to employ one or a combination of several of these techniques.

- With the same exhaust stack design and material selection as the Standard system, an additional 8-foot length of stack is estimated to have the following effect on far-field noise reduction (taking into account atmospheric absorption and directivity):

(i) Estimated TF-30-P-412 engine at afterburner power SPL at 250 feet from Standard Coanda (40-foot stack height) exhaust stack in octave bands 63 through 8000 Hz

63	125	250	500	1k	2k	4k	8k
94	92	82	84	86	83	77	75

which is equivalent to 88 dBA.

(ii) Acoustic effect of an additional eight-foot section is experimentally and analytically determined to be

-5 -6 -8 -10 -11 -9 -5 -3

(iii) Improved SPL

89 86 74 74 75 72 72 72

(iv) Apply "A" scale weighting factors

-26 -16 -9 -3 0 +1 +1 -1

---

19 Naval Air Engineering Center, Jet Engine Class "C" Test Cell Exhaust System Phase - Coanda/Refraction Noise Suppression Concept Advanced Development, NAEC-92-113, May 1979

(v) Combine the following levels acoustically

63 70 65 71 75 73 73 71

which is equivalent to 82 dBA. The improved acoustic performance with the additional stack height is 6 dB.

- The deck-mounted acoustic absorptive panels, which were evaluated during the full-scale model tests and described in reference 16, produced a far-field noise reduction effect of approximately 2 dBA. Caution needs to be taken to prevent a build-up of jet fuel by the floor elements located below the ejectors and deflection surface.

- The 1/6 scale-model unit hollow enclosure walls were lined acoustically during the test program. While this neither hampered nor enhanced the low frequency noise reduction capability of the hollow-wall design, it was effective in providing an additional 1.5-dBA far-field noise reduction. The lining is described in reference 16.

- The Standard system acoustic performance is based upon an exhaust stack lining thickness of 16.5 inches. Based upon comparative analysis from the final one-sixth scale-model tests, an estimated 3 dB per octave band (approximately 1.4 dBA overall) of additional far-field noise reduction was achieved with the exhaust stack lined with 24 inches of the same material. The exhaust stack open area must remain constant in both cases — this means that the exhaust stack overall cross-sectional dimensions will be different by approximately 15 inches.

- During the final one-sixth scale model tests, dual wedge-shaped acoustic absorptive elements were located at the bottom of the exhaust stack. These two wedges in full scale are equivalent to 8 feet in depth with a base width that is half the width of the back wall. The face sheet is 50% open perforated plate and the backing material is Johns-Manville Glas-Mat 1200 (ref 17). These elements provided a significant reduction of overall far-field noise levels (especially low frequency components). Since model tests indicate disturbances in the aerodynamic and thermodynamic characteristics in the exhaust flow, this design technique shall be considered only with trade offs involving an increased Coanda surface turning angle of 73 degrees and an increased stack height.

d. Useful Coanda Data

Reference 20 presents a computer program set for basic Coanda system design. Reference 21 provides a reliability analysis of the Coanda design. The reliability analysis is a projection and not based on full-scale operational data.

---

[20] Naval Air Engineering Center, Coanda Design/Performance Program Set, NAEC Design Data 92-194, November 1979

[21] Naval Air Engineering Center, Reliability Analysis for the Coanda/Refraction Noise Suppression Test Cell System, NAEC Design Data 92-211, 23 May 1980

IV. COST ANALYSIS

A. INTRODUCTION

The purpose of this section is to acquaint designers with the basic tools and methods for incorporating cost analysis as a part of the dry suppressor design process. This section summarizes previous work accomplished in cost/benefit analysis of air-cooled Hush Houses (ref 22 and 23). The following documents should be consulted for further background and discussion of related topics since the treatment here is brief. Additional references that provide greater depth in the cost analysis process are:

- o DoD Instruction 7041.3 "Economic Analysis of Proposed Department of Defense Investment."
- o Life Cycle Costing Procurement Guide: LCC-1 Department of Defense, July 1970.
- o Casebook Life Cycle Costing in Equipment: LCC-2, Department of Defense, July 1970.
- o Life Cycle Costing Guide for System Acquisitions: LCC-3, January 1973.
- o Economic Analysis Handbook, NAVFAC P-422, Department of the Navy, Naval Facilities Engineering Command, June 1975.

This section attempts to acquaint the designer with (1) design and program parameters applicable to dry suppressors, (2) cost calculations, (3) identifying a cost effective suppressor design, (4) assessing cost risks, and (5) evaluating costs of new technology.

---

[22] Science Applications, Inc, Report, Benefit/Cost Analysis of U.S. Navy Jet Engine Test Facilities, Stephen Kornish, November 1976 - reproduced as NOSC TN 126, April 1977

[23] Science Applications, Inc, Report, Study of Noise Suppression Systems: A Cost/Benefit Analysis, Stephen Kornish and David Jordan, October 1978

The results of the cost/benefit comparison will provide the decision-maker a ranking of alternatives using one of the following criteria:

- o Least-cost alternative (equal-benefit case).
- o Maximum benefit (at a given level of cost).
- o Unequal benefits and unequal costs. (This case requires judgment. The critical question is to determine whether the extra effectiveness of a given alternative is worth the additional cost it requires.)

The remainder of this section illustrates the above methods by summarizing previous work accomplished for the case of the NAS Miramar air-cooled augmenter tube acoustical enclosure (ref 22 and 23).

B. OBJECTIVES

The primary objective of the dry suppression system is the cost effective reduction of maintenance runup jet noise. The noise control criterion established by the Navy for aircraft ground runup of engines is 85 dBA at 250 feet from the engine exhaust plane. A system that meets that condition and has a life cycle cost less than competing technical alternatives would be the preferred system. In addition to the primary noise criterion objective many secondary benefit objectives exist in operational and programmatic areas.

C. ALTERNATIVES FOR ABATING AIRCRAFT GROUND RUNUP NOISE

The Navy is continuing its efforts to provide fleet support for jet engine maintenance testing while reducing the overall testing costs. The two air-cooled noise suppression technologies are alternatives to the existing water-cooled test cell techniques. The air-cooled technologies have capabilities for in-airframe testing and/or conventional out-of-airframe testing.

There are six terminologies used to describe methods of abating aircraft/engine runup noise. Some of the terminology refers to the same general device.

Test Stand. A metal device which cradles the jet engine. The device has the capability to be tied down to restrict movement. This device can be located in the open air (test pad) or inside test cells Hush Houses.

Test Cell. A concrete or metal building which consists of a forward enclosure to house the bare engine and an augmenter tube (wet technology before the 1980s) to cool and direct the exhaust flow. The purpose is to decrease bare engine maintenance runup noise. New test cells may use the new air-cooled exhaust technology.

Acoustical Enclosure (also called Hush House). A full aircraft enclosure for maintenance runup testing. It consists of a forward enclosure to totally enclose the aircraft and air-cooled exhaust section. The forward enclosure can accommodate a variety of aircraft types.

Noise Suppressor. A device, usually metal, used to reduce maintenance runup noise for aircraft. The aircraft is backed to an exhaust section and acoustic devices are moved around the engine inlet area. The aircraft is not fully enclosed. The device can only accommodate one aircraft type.

Demountable Suppressor. A modularly constructed suppressor. Usually it is metal. Some test cells (small engine/metal constructed) and most noise suppressors (see previous description) are commonly referred to as demountable. This implies the device can be disassembled and moved to a new location. For most test cells or noise suppressors called demountable, this may be possible but not practical.

Hybrid Suppressor. A new term emanating from the air-cooled acoustical enclosure. It defines the capability to perform in-airframe, fully enclosed aircraft maintenance runup or test cell-like bare engine (on a test stand) maintenance runups in the same facility. This allows full use of a facility at small/low use activities in preference to constructing two devices (ie, test cell and acoustical enclosure).

1. In-frame Testing. Several facility types offer alternatives for jet engine in airframe testing. These are acoustical enclosure (Hush House) with

an air-cooled augmenter tube, acoustical enclosure with the air-cooled Coanda, and noise suppressors (usually water-cooled).

Air-cooled augmenter tube acoustical enclosures have been designed and implemented at fleet activities (Naval Air Station, Miramar and MCAS, El Toro). Air-cooled Coanda suppressors have been tested at full scale as a possible alternative to the augmenter tube technology although no hardware has been used at fleet activities or tested for multiple-engine aircraft application. Originally, eight sizes of air-cooled acoustical enclosures underwent preliminary design to accommodate a variety of aircraft types, with larger designs accommodating a greater variety of aircraft.

Noise suppressors have had limited employment in the past both by the Navy and the Air Force since these suppressors are unique to a particular aircraft and cannot accommodate a mix of aircraft types. The A-7 noise suppressor is an example of one that has been built and is still operational at NAS, Alameda. An F-4 noise suppressor, formerly used at MCAS, El Toro, has not proved effective and is not used today. The Air Force has used a variety of noise suppressors in recent years.

2. Out-of-Frame Testing. Several facility types are current alternatives for jet engine out-of-frame testing. These include retrofit of current test cells with the air-cooled augmenter tube or the air-cooled Coanda system, and the current technology which uses A and C type cells with wet exhaust.

Existing methods of cooling exhaust employed at Navy jet engine test cells use water spray immediately downstream from the aircraft engine. Water spray application as a coolant results in higher energy and water costs, waste water treatment costs, and loss of water due to evaporation. Repair and replacement rates are also increased by water-enhanced corrosion and repetitive cycles of soaking and drying rapidly as water is converted into steam. The Navy is considering the application of air-cooled Coanda or augmenter tube modifications to existing C cells to improve this situation.

3. Facilities for Both In- and Out-of-Frame Testing. Since jet engine in-airframe test requirements at some Naval and Marine Corps air stations are

at a sufficiently low use level, it is practical to design a hybrid facility. This facility uses the flexibility of the air-cooled technology which accommodates a large range of aircraft types while still providing some engine testing. Both full aircraft hold-downs and a mobile engine test stand are provided in the facility.

D. DEVELOPING THE COST ESTIMATE

Life cycle cost (LCC), used as the framework for developing the cost estimate, includes the following phases:

- Design and development
- Investment
- Operations and support (annually for the equipment life)

The method to be followed in developing the estimate includes:

- Developing a comprehensive work breakdown structure (WBS).
- Developing the estimate for each element of the WBS. For consistency, use constant dollars; viz, 1978.
- Time phase the estimate.
- Calculate total LCC.
- Develop discounted net present value and uniform annual cost data to account for the time value of money.

Since the acoustical enclosure (Hush House using an augmenter tube) cost data base has the best documentation, it is used to illustrate more detailed life cycle cost information and data. Since facilities have a relatively long life, these concepts have significant impact on determining economic worth of alternative investments.

Life cycle costs in this section are for selected program alternatives. A work breakdown structure can be utilized as a guideline for establishing the framework for the life cycle cost analysis. This is shown in table 4-1.

Table 4-1. Nominal life cycle cost work breakdown structure.

Nonrecurring Cost

- Research and Development
- Facility Investment
  - Land acquisition
  - New construction
  - Rehabilitation or modification
  - Collateral equipment
  - Plant rearrangement and tooling
  - Demolition and site restoration
  - Personnel (recruitment, training, etc)
  - Nonrecurring services

Recurring Annual Costs

- Personnel
  - Military
  - Civilian
- Operating Costs
  - Materials, supplies, utilities, and other services
  - Maintenance and repair
  - Overhead

All cost data are normalized to the FY78 dollar level. In addition, all program costs are delineated in terms of annual cash flows to permit the development of discounted and net present value.

Cost data and resource estimates have been primarily obtained from existing studies, NAVFAC, NAVAIR, USAF, NAS, NFEC, etc. The data vary in the level of confidence and detail available. Acoustical enclosure (Hush House) costs and estimated data collected in this study have excellent documentation. Other suppression system (eg, Coanda facility) costs are less well understood. There are various reasons for this, including factors such as the relatively "early" development stage of a particular design. Since there is greater uncertainty in costs for such devices, it is appropriate to conduct sensitivity analyses to explore the impact of changing key assumptions and parameter values on the results of the cost/benefit study. Sensitivity analysis, when used appropriately, can in effect direct attention to key issues.

E. ACOUSTICAL ENCLOSURE (AUGMENTER TUBE) LIFE CYCLE COST

Life cycle costs for the first enclosure located at NAS, Miramar are presented in table 4-2. The costs, which are adjusted to FY78 dollars, are based on both actual costs that have been incurred (design and investment costs) and estimated recurring operations and maintenance cost for a 20-year life of the facility. These costs are essentially updated values that were derived from reference 22. The investment cost or initial construction cost estimate is based on the "Schedule of Prices" obtained from ROICC, San Diego (NFEC). Recurring costs (with the exception of manpower) are based on NAVFAC Southern Division estimates adjusted to FY78 dollars as follows:

Recurring Annual Costs:

Utilities	$ 7392
Routine maintenance (Source: Public Works, NAS Miramar)	10 000

Replace inlet acoustical panels and refill the augmenter in 6th and 16th year 199 630

Replace inlet acoustical panels and reline in addition to refilling and augmenter in 11th year 317 733

Annual manpower costs are based on FY78 pay and allowance rates for nine personnel (two men per shift plus one supervisor for a three-shift operation). The annual cost is $85 574.

Table 4-2. Acoustical enclosure (constant FY78 dollar level - in thousands), NAS, Miramar Facility 1.

Project Year	Nonrecurring Design	Nonrecurring Investment	Recurring Operations	Annual Cost	10% Discount Factor	Discounted Annual Cost
0	140.1	2011.2		2151.3	1.0	2151.3
1			103.0	103.0	.954	98.3
2			103.0	103.0	.867	89.3
3			103.0	103.0	.788	81.2
4			103.0	103.0	.717	73.8
5			103.0	103.0	.652	67.2
6			302.6	302.6	.592	179.1
7			103.0	103.0	.538	55.4
8			103.0	103.0	.489	50.4
9			103.0	103.0	.445	45.8
10			103.0	103.0	.405	41.7
11			420.7	420.7	.368	154.8
12			103.0	103.0	.334	34.4
13			103.0	103.0	.304	31.3
14			103.0	103.0	.276	28.4
15			103.0	103.0	.251	25.8
16			302.6	302.6	.228	69.0
17			103.0	103.0	.208	21.4
18			103.0	103.0	.189	19.5
19			103.0	103.0	.156	16.1
	Total	2151.3 (44%)	2776.9 (56%)	4928.2 (100%)		3351.9 NPV

It is noted that the operating and maintenance costs are subject to some uncertainty and could be subject to change. For instance, manpower levels are dependent on policy of the local air station.

On the technology side, current research and development effort on design changes to the augmenter tube (eg, new linings, materials, multiple tuned resonator, etc) could potentially reduce O&M costs in the future.

Similarly, the possibility of lower O&M cost through the use of Coanda as a replacement for the augmenter tube should be examined in future design tradeoff studies.

Summary life cycle costs for the original series of acoustical enclosures (with augmenter) designed by NAVFAC are shown in table 4-3. Also shown are discounted LCC values and uniform annual costs.

A set of life cycle cost data for demountable (wet) sound suppression equipments is also given in table 4-3. The derivations for these data can be found in reference 22. The values shown span a range of investment costs as well as estimated useful lives of 6 to 10 years. This parametric data set will be used to illustrate the cost/benefit analysis of the acoustical enclosure augmenter tube versus the wet sound suppressor.

F. COANDA SUPRESSOR LIFE CYCLE COST

Life cycle costs for the Coanda suppressor are not available. The only full-scale Coanda system built was a test prototype. The ability of the Coanda suppressor to handle a variety of aircraft/engines was not determined during Fleet operations.

Table 4-3. Summary of life cycle cost comparison acoustical enclosure vs sound suppressors.

Type Acoustical Enclosures	Life Cycle Cost $X10^3	Life Cycle Cost Discounted $X10^3	Uniform Annual Cost-Discounted Values $X10^3
(20 yr life)			
NAS, Miramar	4928	3369	377
Type, 1a	4986	3472	387
1b	4631	3117	348
2	4908	3395	380
3	4428	2914	326
4a	4300	2786	312
4b	4194	2681	300
4c	4062	2548	285
5	3706	2192	245
Sound Suppressors - Wet			
290k Invest 6 yr life 3 cycles	2588	1355	158
465k Invest 6 yr life 3 cycles	3110	1676	195
700k Invest 6 yr life 3 cycles	3806	2103	244
290k Invest 10 yr life 2 cycles	2489	1245	139
465k Invest 10 yr life 2 cycles	2837	1487	166
400k Invest 10 yr life 2 cycles	3301	1805	202

G. DEVELOPING THE BENEFIT ASSESSMENT

The benefit assessment begins by determining the costs to be reduced. For aircraft enclosures, these are:

1. Cost of Implementation

    a. Capital improvements
    b. Staff time
    c. Consultant fees
    d. Operational changes

2. Long-Run Costs

    a. Fuel consumption
    b. Maintenance

3. Costs of Affecting the Natural Environment

    a. Degradation of air quality
    b. Alteration of wildlife habitat

4. Costs of Foregoing the Use of Installation Land

    a. Where abatement in one place shifts noise impact to another place

5. Costs of Restricting Off-Installation Land Use

    a. Foregone taxes
    b. Probable dampening effect on development

6. Costs of Permitting Noise Impact

    a. Litigation
    b. Physiological and psychological costs

c. Reduction in usable land

d. Poor public image

e. Depressed land value

f. Reduced economic activity

These benefits are generically comprehensive. The first two items, cost of implementation and long-run costs, essentially define life cycle cost which we have already quantified. The degrees of life cycle cost benefit between augmenter tube acoustical enclosure and the wet sound suppressor are treated in the cost/benefit evaluation.

A compendium of benefits established through literature searches and interviews conducted during the course of references 22 and 23 is illustrated in table 4-4. Many of these benefits restate, in other ways, those already cited above. The benefits are grouped in the following manner:

1. Benefits of acoustical enclosures
2. Peculiar benefits of demountable suppressor
3. Benefits of dry suppressors
4. General benefits listing

H. BENEFIT/COST EVALUATION OF DRY AUGMENTER TUBE ACOUSTICAL ENCLOSURES VS WET SOUND SUPPRESSORS

The benefit/cost evaluation described here will consider the noise abatement programs the Navy has previously undertaken; namely, the dry augmenter tube acoustical enclosure versus the demountable sound suppressor where Fleet operating information is available.

Although the acoustical enclosure has a noise reduction advantage of 5 dBA over a demountable sound suppressor, for purposes of cost effectiveness exposition, we make the assumption that the sound abatement effectiveness is equivalent in order to find the minimum cost case. A primary benefit of the acoustical enclosure is its ability to accommodate many aircraft types. The sound suppressor, conversely, is unique (one application) for each aircraft

Table 4-4. Dry suppressor compendium of benefits.

Benefits of Acoustical Enclosure

- Meets OSHA acceptable noise levels
- Multiple-aircraft application
- High usage rate
- Increase in operational safety
- Improved acoustical performance
- More efficient siting
- Improved environment for operating personnel
- Can test at nighttime
- Disbenefit from compressor stall (ear/fire hazard and hazard to acoustical enclosure)

Peculiar Benefits of Mobile Suppressors

- Opacity law (no law re moveable devices - just pertains to permanent installations)
- Procurement Aircraft and Missile-Navy funding through NAVAIR
  - "Things move faster"
  - MILCON cycle is on order of five years

Benefits of Dry Vs. Wet Suppressors

- Maintainability
- Availability
- Supportability
- Readiness
- Wet causes mist which causes fog and icing (runway)
  - Fog--occasional runway closing
  - Icing--occasional runway closing
- Eliminate H_2O, scrubbers and utility (energy) costs

General

- Noise abatement
- Complaint abatement
- Potential efficiencies in use of:
  - Manpower
  - Aircraft (availability)
  - Pipeline inventories
  - Land usage
- Spillover effect
  - Local economy
  - Opportunity cost
- Energy Saving - oil for utility
- Emissions
- Safety - compressor stalls

design. Another important benefit of the acoustical enclosure is its relatively long economical life (20 years) when compared to demountable sound suppressors, which have typical economical lives of 6 years. This study combines these two considerations in an exchange rate analysis which is depicted in table 4-5. Uniform annual cost is used as a common comparator. This table assumes that an acoustical enclosure is built which can house any aircraft at the facility. The table then provides the decision point for building individual aircraft demountable noise suppressors or one acoustical enclosure. For example, if the naval facility were to obtain the largest acoustical enclosure (type 1a — which will house any Navy fighter or attack aircraft) to accommodate the aircraft present, the naval facility would incur a uniform annual cost of $387000. Since each aircraft type tested at the facility would require a unique demountable suppressor with a uniform annual cost of $195000, then once we have at least two types of aircraft to be tested, it is cost effective to build the acoustical enclosure.

I. COST SENSITIVITY ANALYSIS

Cost sensitivity analysis can be conducted in either a deterministic or a probabilistic manner. In the deterministic approach one would vary a key variable or cost element and determine the net effect on the outcome. Cost estimating relationships developed from the acoustic enclosure data set are shown in table 4-6. Independent variables include volume, square footage, etc. By varying these or other key cost issues one can parametrically determine cost variations or sensitivities to changes in design assumptions. Another, more involved approach is that of cost/risk or uncertainty analysis. We have illustrated this method by applying it to the acoustical enclosure.

Uncertainty analysis consists of three major tasks: (1) collection of data regarding possible cost variations for system components, (2) combination of the component uncertainties to estimate the uncertainty regarding the total cost variable, and (3) providing management with the increased information and statistical inferences made possible by the analysis. The data collection, of course, is the basis for the entire analysis and its results are crucial. The combination of cost component uncertainties as shown here is analytical in nature. The types of inference made possible by the analysis include the

Table 4-5. Acoustical enclosure vs equivalent suppressors.

AE Type	SS Type / Investment / Uniform Annual Cost	6-Year Life 290 (158)*	6-Year Life 465 (195)	6-Year Life 700 (244)	10-Year Life 290 (139)	10-Year Life 465 (166)	10-Year Life 700 (202)
1a (387)*		2.5	2.0	1.6	2.8	2.3	1.9
1b (348)		2.2	1.8	1.4	2.5	2.1	1.7
2 (380)		2.4	1.9	1.5	2.7	2.3	1.9
3 (326)		2.1	1.7	1.3	2.1	2.0	1.6
4a (312)		2.0	1.6	1.3	2.2	1.9	1.5
4b (300)		1.9	1.5	1.2	2.2	1.8	1.5
4c (285)		1.8	1.5	1.2	2.0	1.7	1.4
5 (245)		1.6	1.26	1.0	1.8	1.5	1.2

AE - Acoustical Enclosure
SS - Sound Suppressor
* (Value) - Uniform Annual Cost in Thousands

$$\text{Equivalent Suppressors} = \frac{\text{AE Uniform Annual Cost}}{\text{SS Uniform Annual Cost}}$$

Key

AE TYPE	AIRCRAFT HANDLING ABILITY
1a	A5,F14,A6,F4,F8,AV8,A7,T2,A4
1b	A5,A6,F4,F8,AV8,A7,T2,A4
2	F14,A6,F4,F8,AV8,A7,T2,A4
3	A6,F4,F8,AV8,A7,T2,A4
4a	F4,F8,AV8,A7,T2,A4
4b	F8,A7,T2,A4
4c	A7,T2,A4
5	A4

Table 4-6. Cost estimating relationships for acoustical enclosure (dry augmenter tube)

Item	CER/Cost Factor (THOUSANDS OF FY 78 $)	SOURCE/RATIONALE
Acoustical Augmenter	COST = 125.1 + .006 * Volume of Augmenter	3,4
Acoustical Intake Door	Cost = 0.0315 * Volume of Door	1,2
Building Panel System	Cost = 0.0371 * Panel Square Footage	1,2
Nose Gear Elevator Platform	Cost = 20. per Item	1,2
Fire Protection	Cost = .005 * Area of Main Building	1,2
Plumbing	Cost = 36.6 per Building	1
Heating	Cost = 8.7 per Building	1,2
Electrical	Cost = 63.0 per Building	1,2
Compressed Air	Cost = .003 * Area of Main Building	1,2
Exhaust Deflector	Cost = .19 * Panel Square Footage	1,2
Sitework	Cost = .012 * Area of Planned Construction	1,2
Concrete Work	Cost = .013 * Area of Planned Construction	1,2
Masonry Work	Cost = 7.0 per Building	1,2
Metals	Cost = 25.0 per Building	1,2
Doors, Windows, Glass	Cost = 18.5 per Building	1,2
Finishes	Cost = 1.3 per Building	1,2
Curved Section in Augmenter	Cost = .0125 * Volume of Section	2
Secondary Air Inlet	Cost = 178 per Item	5

1. Aircraft Acoustical Enclosure (P-182) NAS, Miramar, Bid, Trepte Construction Company, Inc.
2. Aircraft Acoustical Enclosure (P-995) MCAS, El Toro, Bid, Trepte Construction Company, Inc.
3. Aircraft Acoustical Enclosure (P-114) NAS, Miramar, Schedule of Prices, Gene Fuller, Inc.
4. Cost Estimates, Aircraft Noise Suppression Study, Gustav Getter Associates Engineers.
5. NAVFAC Estimate.

probability of final cost being at or below the final estimate, the probability of an overrun, and the slope of the cost curve on either side of the estimated cost.

The analyst develops the work breakdown structure and collects or makes the estimates for the data inputs. A computer program (ref 24) developed by OP96D "sums" the WBS element probability distribution inputs into a total program cost probability distribution. The analyst or program decision-maker interprets the output by making probability statements concerning the total program cost and analyzes these results.

To illustrate the use of this analytical tool, cases were run on the computer program developed in reference 24. The case illustrated is the NAS, Miramar Acoustical Enclosure Life Cycle Cost.

Four data inputs at each of the sub-element level of the facility work breakdown structure are the most likely (mode) cost estimate, the lowest and the highest cost estimates, and the uncertainty coefficient. The uncertainty coefficient takes a value from 0 to 1.0; the higher the value, the higher the uncertainty. The inputs are the analysts' objective probability estimates obtained from discussion with engineers, systems analysts, manufacturers, and program personnel, as well as from examination of related data.

The data inputs for the NAS, Miramar acoustical enclosure life cycle cost are shown in table 4-7. These were obtained by examining the actual schedule of prices for the acoustical enclosure built at NAS, Miramar as well as the estimate for the second facility at Miramar, which was prepared by Naval Facilities Engineering Command, Southern Division personnel, along with architectural and engineering consultants.

---

[24] Chief of Naval Operations, An Application of Subjective Probabilities to the Problem of Uncertainty in Cost Analysis, Resource Analysis Group, System Analysis Division, H.R. Jordan and M.R. Klein

Table 4-7. Cost uncertainty input data for NAS, Miramar acoustical enclosure life cycle cost (single enclosure case).

Work Breakdown Structure Element	Variable Number	FY78 $ 000's Cost Estimate			Uncertainty Coefficient
		Low	Median	High	
Earthwork	1	86	93	135	.3
Concrete Work	2	111	170	176	.6
Masonry	3	7	10	14	.7
Metals	4	17	25	56	.8
Carpentry	5	.5	1	1.5	.1
Moisture Protection	6	.5	2	14	.9
Doors, windows, glass	7	18	25	59	.8
Finishes	8	2	14	16	.9
Bldg panel system	9	380	400	477	.5
Augmenter	10	342	380	386	.4
Ramp deflector	11	49	60	81	.7
Retaining walls, Acoustic panels	12	15	20	27	.7
Acoustic intake door	13	312	400	432	.5
Nose gear elevator Platform	14	20	25	26	.1
Winches	15	12	12.5	13	.1
Plumbing	16	37	50	59	.3
Heating	17	8	14	21	.7
Compressed air system	18	9	20	67	.9
Fire protection	19	36	75	90	.7
Electrical	20	62	145	197	.6
Design	21	100	140	160	.3
Utilities	22	140	150	160	.1
Routine maintenance	23	180	200	225	.1
Special maintenance	24	500	720	1400	.6
Personnel	25	1500	1700	1800	.1

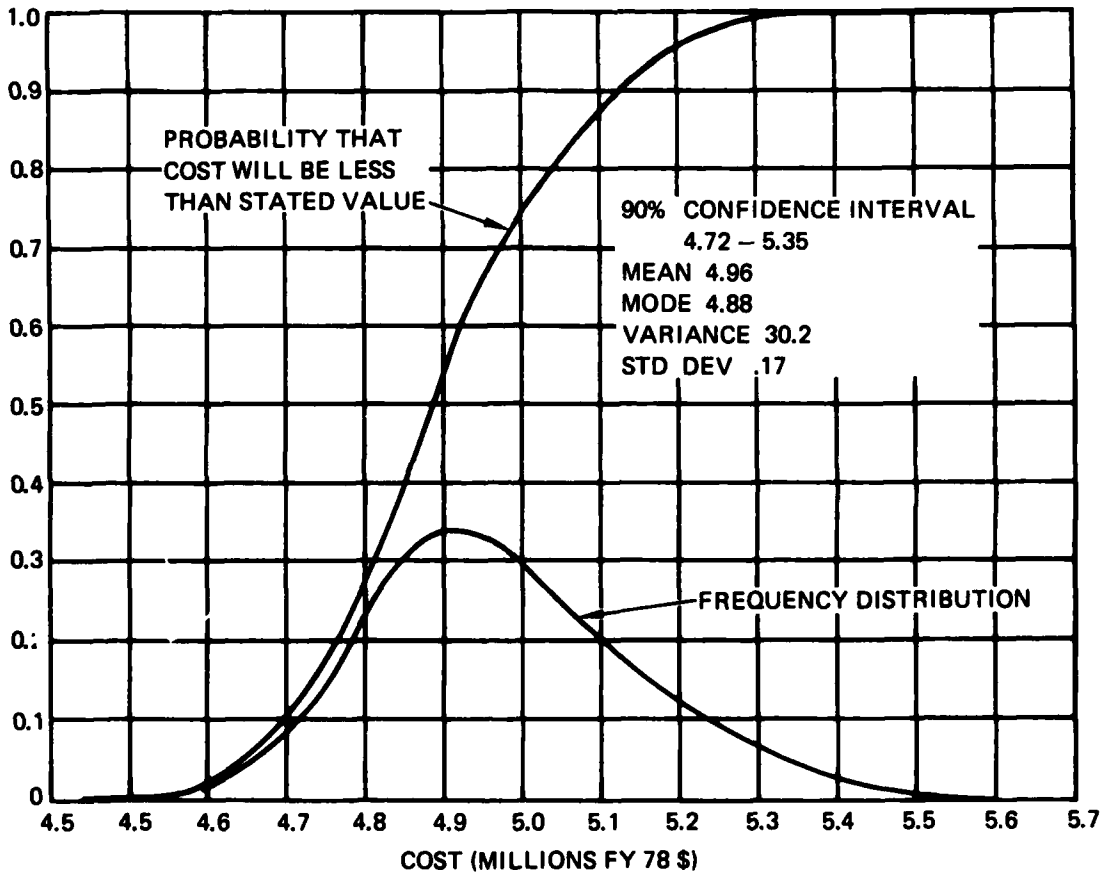

Figure 4-1. Cost uncertainty analysis – acoustical enclosure life cycle cost.

The results of this computer run are shown in figure 4-1 in which life cycle cost is depicted as a probability function. Reference 23 provides a more detailed treatment of the method.

The Coanda alternative to the augmenter requires further economic/design tradeoffs since the current Coanda data base (both cost and design performance) does not support a clear cut decision between these options. Preliminary uncertainty analysis of the Coanda cost was conducted in reference 23. The results of this are shown in figure 4-2. Additional study is required to update this type of analysis to determine the cost/benefit of the Coanda vis-a-vis the augmenter tube approach to sound suppression.

J. RECOMMENDATIONS

Three major technologies are available for in-airframe and out-of-airframe jet engine testing: the air-cooled augmenter tube, air-cooled Coanda/refraction and the water-cooled suppressor. Recommendations are grouped into three areas: in-frame, out-of-frame, and material tradeoffs.

1. In-Frame Testing. For in-frame testing, Fleet operating data only exist for the dry augmenter tube acoustical enclosure and the water-cooled suppressor. As shown in table 4-5, the dry augmenter tube acoustical enclosure, which can accommodate various aircraft types, is more cost beneficial than the one aircraft design of the wet suppressor. If there are at least three different aircraft types at a facility, it is more cost effective to build one acoustical enclosure than three sound suppressors. If there are at least two different aircraft types at a facility, it is 60% possible that the acoustical enclosure is still cost effective.

2. Out-of-Frame Testing. For out-of-frame testing, Fleet operating data exist only for the water-cooled test cells. On the basis of probable construction and energy costs for test cells using the dry augmenter tube, the dry Coanda, or the wet suppressor, the Coanda may be the most cost effective design. This must still be verified by actual Fleet operating data.

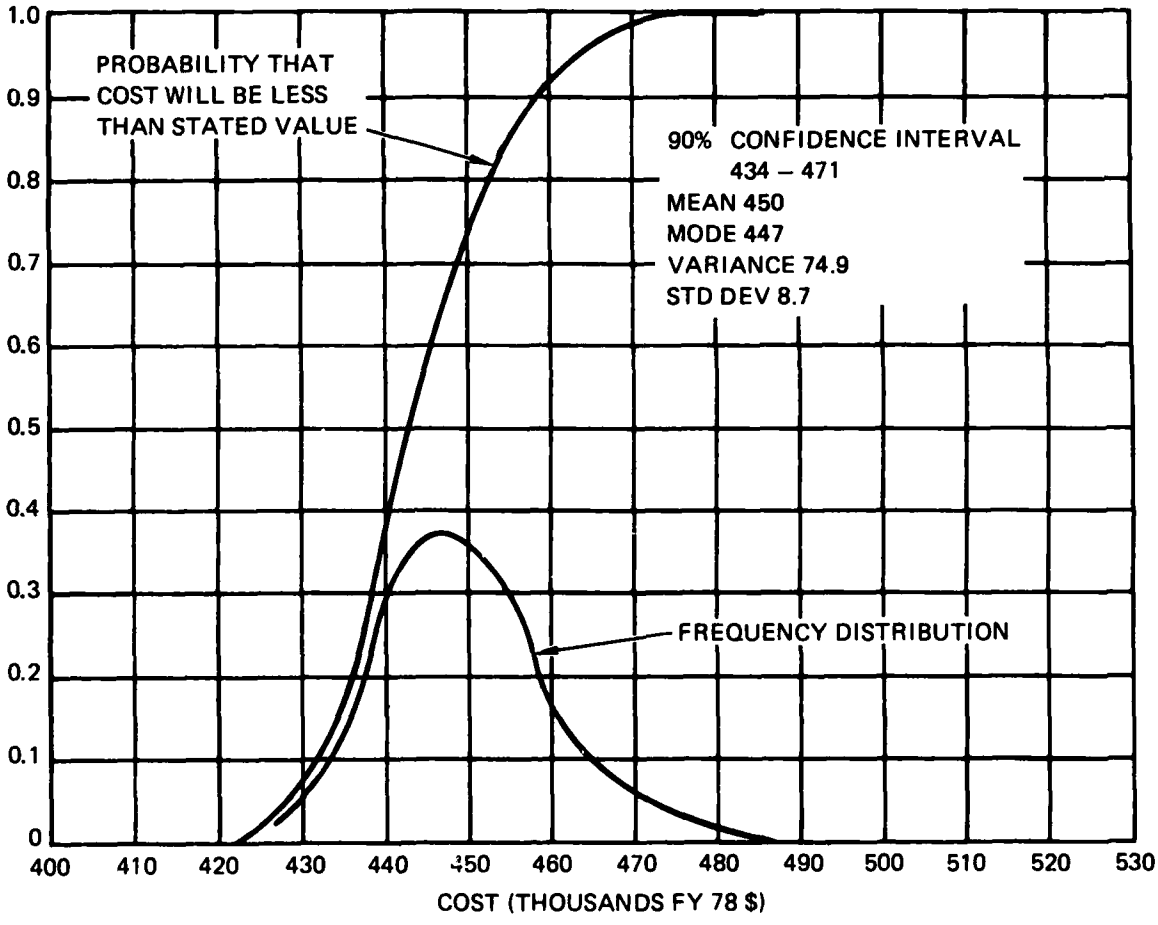

Figure 4-2. Cost uncertainty analysis – Coanada/refraction modification.

3. Material Tradeoff Studies. For all three technologies, the tradeoffs for various construction materials; especially acoustic liner material, should be performed. Specific examples include: use of less expensive (less than 321 S.S.) metals (low temperature) which have shorter life cycles, use of more expensive (more than 321 S.S.) metals with longer life cycles, use of combinations of metals depending on the expected heat exposure at various locations in the suppressor and use of shorter augmenter tube lengths with various acoustic treatments which have more attenuation. These efforts would provide technical data for more cost effective design decisions.

REFERENCES

1. Fluidyne Engineering Report, Aerodynamic and Acoustic Tests of a 1/15 Scale Model Dry Cooled Jet Aircraft Runup Noise Suppression System, October 1975

2. Fluidyne Engineering Report, Reducing the Acoustic Treatment Exposure Temperature in a Dry Cooled Augmenter During F-14A Operation, December 1976 - reproduced as NOSC TN 125, April 1977

3. Western Electro-Acoustic Laboratory Report, 1/15 Scale Model Testing of Dry Cooled Jet Engine Noise Suppressor Using a Hot Jet Simulating the TF-30-P-412 Fan Jet Engine, August 1980

4. Fluidyne Engineering Report, 1/15 Scale Cold Flow Model Tests of the Patuxent River Hush House Configuration, December 1977

5. Naval Air Engineering Center, report number NAEC-65ED-96, Experimental Evaluation of NAS Miramar Hush House (Project P-114), February 1976

6. Fluidyne Engineering Report, Aero-Thermo and Acoustical Data from the Post-Construction Checkout of the Miramar #2 and El Toro Hush Houses, April 1979

7. Gustav Getter Associates Engineers Report, Aircraft Noise Suppression Study, July 1973

8. Civil Engineering Laboratory; G Warren, Ambient Excitation of Hush House Acoustical Enclosure During F-8 Tests, TM-51-78-19, August 1978

9. Rohr Industries Report, An Analytical Study on Acoustical Performance of Perforated Plate Liner for the Augmenter of a Stationary Jet Noise Suppressor, reproduced as NOSC TN 124, April 1977

10. Civil Engineering Laboratory; JF Jenkins, Heat Tint Colors on Stainless Steel, TM-52-77-2, February 1977

11. Rohr Industries Report, Investigation and Testing of High Temperature Fatigue-Resistant Materials for Ground Noise Suppression, November 1978

12. Civil Engineering Laboratory; T Roe Jr, Investigation of High Temperature-Resistant Materials for Acoustical Insulation in Jet Engine Test Facilities, TM-52-77-12, July 1977

13. Civil Engineering Laboratory; Edward Skillman, Test and Evaluation of Candidate Demister Hush House Assemblies, TM-54-77-5, September 1977

14. Naval Air Engineering Center, Final Technical Report-Feasibility/Initial Model Studies Coanda/Refraction Noise Suppression Concept Exploratory Development, NAEC-GSED-80, May 1974

15. Naval Air Engineering Center, Final Technical Report Configuration Scale-Model Studies Coanda/Refraction Noise Suppression Concept Exploratory Development, NAEC-GSED-81, May 1974

16. Naval Air Engineering Center, Final Technical Report - Test Cell Experimental Program-Coanda/Refraction Noise Suppression Concept Advanced Development, NAEC-GSED-97, March 1976

17. Naval Air Engineering Center, Design Configuration Handbook Test Cell System Coanda/Refraction Noise Suppression Concept, NAEC Design Data 92-136, 30 March 1979

18. Naval Air Engineering Center, Jet Engine Demountable Test Cell Exhaust System Phase - Coanda/Refractor Noise Suppression Concept Advanced Development, NAEC-92-112, April 1979

19. Naval Air Engineering Center, Jet Engine Class "C" Test Cell Exhaust System Phase - Coanda/Refraction Noise Suppression Concept Advanced Development, NAEC-92-113, May 1979

20. Naval Air Engineering Center, Coanda Design/Performance Program Set, NAEC Design Data 92-194, November 1979

21. Naval Air Engineering Center, Reliability Analysis for the Coanda/Refraction Noise Suppression Test Cell System, NAEC Design Data 92-211, 23 May 1980

22. Science Applications Inc, Report, Benefit/Cost Analysis of U.S. Navy Jet Engine Test Facilities, Stephen Kornish, November 1976-reproduced as NOSC TN 126, April 1977

23. Science Applications Inc, Report Study of Noise Suppression Systems: A Cost/Benefit Analysis, Stephen Kornish and David Jordan, October 1978

24. Chief of Naval Operations, An Application of Subjective Probabilities to the Problem of Uncertainty in Cost Analysis, Resource Analysis Group, System Analysis Division, HR Jordan and MR Klein

APPENDIX A

COANDA APPLICATION
AIR FLOW FUNCTIONS
(SPECIFIC HEAT RATIO = 1.4)

M	M*	$\frac{A}{A^*}$	$\frac{P}{P_t}$	$\frac{\rho}{\rho_0}$	$\frac{T}{T_t}$	W_T	W_S
0.000	0.00000	***.*****	1.000000	1.000000	1.000000	0.000000	0.000000
0.001	0.00110	578.70360	1.000000	1.000000	1.000000	0.000019	0.000019
0.002	0.00219	289.35180	1.000000	1.000000	1.000000	0.001838	0.001838
0.003	0.00329	192.90170	0.999997	0.999998	0.999999	0.002757	0.002757
0.004	0.00438	144.67720	0.999990	0.999993	0.999997	0.003675	0.003675
0.005	0.00548	115.74230	0.999984	0.999989	0.999995	0.004594	0.004594
0.006	0.00657	96.45256	0.999977	0.999984	0.999993	0.005513	0.005513
0.007	0.00767	82.67432	0.999967	0.999976	0.999990	0.006432	0.006432
0.008	0.00876	72.34065	0.999957	0.999969	0.999988	0.007350	0.007351
0.009	0.00986	64.30336	0.999947	0.999962	0.999985	0.008269	0.008270
0.010	0.01095	57.87367	0.999933	0.999952	0.999981	0.009188	0.009188
0.011	0.01205	52.61319	0.999917	0.999941	0.999976	0.010107	0.010107
0.012	0.01315	48.22945	0.999900	0.999928	0.999971	0.011025	0.011026
0.013	0.01424	44.52013	0.999884	0.999917	0.999967	0.011944	0.011945
0.014	0.01534	41.34082	0.999864	0.999903	0.999961	0.012862	0.012864
0.015	0.01643	38.58542	0.999844	0.999888	0.999955	0.013781	0.013783
0.016	0.01753	36.17445	0.999824	0.999874	0.999949	0.014699	0.014702
0.017	0.01862	34.04723	0.999800	0.999857	0.999943	0.015618	0.015621
0.018	0.01972	32.15636	0.999777	0.999841	0.999936	0.016536	0.016540
0.019	0.02081	30.46461	0.999750	0.999822	0.999928	0.017454	0.017459
0.020	0.02191	28.94205	0.999723	0.999803	0.999921	0.018372	0.018378
0.021	0.02300	27.56456	0.999693	0.999781	0.999912	0.019291	0.019296
0.022	0.02410	26.31230	0.999663	0.999760	0.999904	0.020209	0.020215
0.023	0.02519	25.16893	0.999633	0.999738	0.999895	0.021127	0.021134
0.024	0.02629	24.12093	0.999600	0.999714	0.999886	0.022045	0.022053
0.025	0.02738	23.15681	0.999563	0.999688	0.999875	0.022962	0.022972
0.026	0.02848	22.26680	0.999530	0.999664	0.999866	0.023880	0.023891
0.027	0.02957	21.44278	0.999493	0.999638	0.999855	0.024798	0.024810
0.028	0.03067	20.67767	0.999453	0.999609	0.999844	0.025715	0.025729
0.029	0.03177	19.96533	0.999413	0.999581	0.999832	0.026633	0.026649
0.030	0.03286	19.30049	0.999373	0.999552	0.999821	0.027550	0.027568
0.031	0.03396	18.67858	0.999330	0.999521	0.999808	0.028468	0.028487
0.032	0.03505	18.09555	0.999286	0.999490	0.999796	0.029385	0.029406
0.033	0.03615	17.54791	0.999240	0.999457	0.999783	0.030302	0.030325
0.034	0.03724	17.03247	0.999193	0.999423	0.999769	0.031218	0.031244
0.035	0.03834	16.54649	0.999146	0.999390	0.999756	0.032136	0.032163
0.036	0.03943	16.08755	0.999097	0.999355	0.999742	0.033053	0.033082
0.037	0.04053	15.65348	0.999043	0.999317	0.999726	0.033969	0.034002
0.038	0.04162	15.24220	0.998993	0.999280	0.999712	0.034886	0.034921
0.039	0.04272	14.85206	0.998940	0.999242	0.999697	0.035802	0.035840
0.040	0.04381	14.48146	0.998883	0.999202	0.999681	0.036718	0.036759
0.041	0.04491	14.12894	0.998826	0.999161	0.999664	0.037635	0.037679
0.042	0.04600	13.79321	0.998769	0.999121	0.999648	0.038551	0.038598
0.043	0.04710	13.47313	0.998709	0.999079	0.999631	0.039466	0.039517
0.044	0.04819	13.16763	0.998647	0.999033	0.999613	0.040382	0.040437
0.045	0.04929	12.87568	0.998587	0.998990	0.999596	0.041298	0.041356
0.046	0.05038	12.59646	0.998523	0.998945	0.999578	0.042213	0.042276
0.047	0.05147	12.32916	0.998456	0.998898	0.999559	0.043128	0.043195
0.048	0.05257	12.07299	0.998390	0.998850	0.999540	0.044043	0.044114
0.049	0.05366	11.82728	0.998323	0.998803	0.999520	0.044958	0.045034

M	M*	$\frac{A}{A^*}$	$\frac{P}{P_t}$	$\frac{\rho}{\rho_0}$	$\frac{T}{T_t}$	W_T	W_S
0.050	0.05476	11.58143	0.998253	0.998752	0.999501	0.045873	0.045953
0.051	0.05585	11.36483	0.998184	0.998702	0.999480	0.046788	0.046878
0.052	0.05695	11.14897	0.998111	0.998649	0.999460	0.047702	0.047793
0.053	0.05804	10.93734	0.998037	0.998597	0.999439	0.048617	0.048712
0.054	0.05914	10.73547	0.997963	0.998545	0.999418	0.049531	0.049632
0.055	0.06023	10.54098	0.997887	0.998491	0.999396	0.050445	0.050551
0.056	0.06133	10.35347	0.997810	0.998436	0.999374	0.051358	0.051471
0.057	0.06242	10.17249	0.997731	0.998379	0.999351	0.052272	0.052391
0.058	0.06351	9.99779	0.997651	0.998321	0.999328	0.053185	0.053311
0.059	0.06461	9.82903	0.997567	0.998263	0.999304	0.054098	0.054230
0.060	0.06570	9.66588	0.997488	0.998205	0.999281	0.055012	0.055150
0.061	0.06680	9.50813	0.997401	0.998143	0.999257	0.055924	0.056070
0.062	0.06789	9.35547	0.997315	0.998081	0.999232	0.056837	0.056990
0.063	0.06899	9.20766	0.997229	0.998019	0.999207	0.057749	0.057910
0.064	0.07008	9.06447	0.997141	0.997958	0.999182	0.058662	0.058830
0.065	0.07117	8.92573	0.997048	0.997891	0.999156	0.059573	0.059750
0.066	0.07227	8.78116	0.996959	0.997827	0.999130	0.060485	0.060670
0.067	0.07336	8.66064	0.996866	0.997760	0.999103	0.061397	0.061590
0.068	0.07446	8.53397	0.996773	0.997694	0.999077	0.062308	0.062510
0.069	0.07555	8.41098	0.996676	0.997625	0.999049	0.063219	0.063430
0.070	0.07664	8.29151	0.996580	0.997556	0.999022	0.064130	0.064350
0.071	0.07774	8.17543	0.996480	0.997485	0.998993	0.065041	0.065270
0.072	0.07883	8.06258	0.996381	0.997414	0.998964	0.065951	0.066191
0.073	0.07992	7.95281	0.996281	0.997342	0.998936	0.066861	0.067111
0.074	0.08102	7.84604	0.996178	0.997268	0.998906	0.067771	0.068031
0.075	0.08211	7.74211	0.996075	0.997195	0.998877	0.068681	0.068952
0.076	0.08321	7.64094	0.995969	0.997119	0.998846	0.069590	0.069872
0.077	0.08430	7.54239	0.995863	0.997043	0.998816	0.070500	0.070792
0.078	0.08539	7.44638	0.995756	0.996967	0.998785	0.071409	0.071713
0.079	0.08649	7.35282	0.995646	0.996888	0.998754	0.072317	0.072633
0.080	0.08758	7.26161	0.995534	0.996808	0.998722	0.073226	0.073554
0.081	0.08867	7.17263	0.995424	0.996730	0.998690	0.074134	0.074475
0.082	0.08977	7.08587	0.995308	0.996647	0.998657	0.075042	0.075395
0.083	0.09086	7.00118	0.995196	0.996568	0.998625	0.075949	0.076316
0.084	0.09195	6.91852	0.995080	0.996483	0.998591	0.076857	0.077237
0.085	0.09305	6.83783	0.994960	0.996398	0.998557	0.077764	0.078158
0.086	0.09414	6.75902	0.994841	0.996312	0.998523	0.078671	0.079078
0.087	0.09523	6.68202	0.994721	0.996226	0.998489	0.079577	0.079999
0.088	0.09632	6.60678	0.994598	0.996139	0.998454	0.080483	0.080920
0.089	0.09742	6.53324	0.994475	0.996051	0.998418	0.081389	0.081841
0.090	0.09851	6.46133	0.994353	0.995963	0.998383	0.082295	0.082762
0.091	0.09960	6.39102	0.994228	0.995873	0.998347	0.083200	0.083683
0.092	0.10070	6.32226	0.994098	0.995781	0.998310	0.084105	0.084605
0.093	0.10179	6.25496	0.993972	0.995691	0.998274	0.085010	0.085526
0.094	0.10288	6.18912	0.993840	0.995596	0.998236	0.085915	0.086447
0.095	0.10397	6.12465	0.993711	0.995504	0.998199	0.086819	0.087368
0.096	0.10507	6.06155	0.993578	0.995409	0.998161	0.087723	0.088290
0.097	0.10616	5.99976	0.993443	0.995312	0.998122	0.088626	0.089211
0.098	0.10725	5.93923	0.993307	0.995215	0.998083	0.089529	0.090133
0.099	0.10834	5.87993	0.993171	0.995117	0.998044	0.090432	0.091054

M	M*	$\frac{A}{A^*}$	$\frac{P}{P_t}$	$\frac{\rho}{\rho_o}$	$\frac{T}{T_t}$	W_T	W_S
0.100	0.10944	5.82183	0.993033	0.995018	0.998004	0.091335	0.091976
0.101	0.11053	5.76488	0.992894	0.994819	0.997964	0.092237	0.092897
0.102	0.11162	5.70904	0.992754	0.994619	0.997924	0.093139	0.093819
0.103	0.11271	5.65431	0.992612	0.994718	0.997883	0.094041	0.094741
0.104	0.11380	5.60064	0.992467	0.994613	0.997842	0.094942	0.095663
0.105	0.11490	5.54800	0.992321	0.994509	0.997800	0.095843	0.096584
0.106	0.11599	5.49635	0.992176	0.994406	0.997758	0.096743	0.097506
0.107	0.11708	5.44569	0.992027	0.994299	0.997715	0.097643	0.098428
0.108	0.11817	5.39595	0.991879	0.994193	0.997673	0.098543	0.099350
0.109	0.11926	5.34714	0.991730	0.994086	0.997630	0.099443	0.100272
0.110	0.12035	5.29922	0.991578	0.993977	0.997586	0.100342	0.101194
0.111	0.12144	5.25217	0.991426	0.993868	0.997543	0.101241	0.102117
0.112	0.12254	5.20597	0.991272	0.993757	0.997498	0.102140	0.103039
0.113	0.12363	5.16059	0.991116	0.993646	0.997454	0.103038	0.103961
0.114	0.12472	5.11603	0.990958	0.993533	0.997408	0.103935	0.104884
0.115	0.12581	5.07224	0.990799	0.993419	0.997362	0.104833	0.105806
0.116	0.12690	5.02920	0.990641	0.993306	0.997317	0.105730	0.106728
0.117	0.12799	4.98691	0.990479	0.993191	0.997270	0.106626	0.107651
0.118	0.12908	4.94535	0.990315	0.993072	0.997223	0.107522	0.108574
0.119	0.13017	4.90448	0.990153	0.992957	0.997177	0.108418	0.109496
0.120	0.13126	4.86431	0.989988	0.992839	0.997129	0.109314	0.110419
0.121	0.13236	4.82481	0.989820	0.992719	0.997081	0.110209	0.111342
0.122	0.13345	4.78595	0.989652	0.992598	0.997032	0.111103	0.112265
0.123	0.13454	4.74774	0.989484	0.992477	0.996984	0.111998	0.113188
0.124	0.13563	4.71015	0.989313	0.992355	0.996935	0.112892	0.114111
0.125	0.13672	4.67316	0.989142	0.992232	0.996885	0.113785	0.115034
0.126	0.13781	4.63677	0.988968	0.992107	0.996835	0.114678	0.115957
0.127	0.13890	4.60096	0.988793	0.991982	0.996785	0.115571	0.116881
0.128	0.13999	4.56570	0.988619	0.991858	0.996735	0.116463	0.117804
0.129	0.14108	4.53101	0.988441	0.991730	0.996684	0.117355	0.118727
0.130	0.14217	4.49686	0.988260	0.991601	0.996632	0.118246	0.119651
0.131	0.14326	4.46322	0.988083	0.991473	0.996580	0.119137	0.120574
0.132	0.14435	4.43011	0.987899	0.991342	0.996527	0.120028	0.121498
0.133	0.14544	4.39749	0.987718	0.991212	0.996475	0.120918	0.122421
0.134	0.14653	4.36537	0.987534	0.991080	0.996422	0.121808	0.123345
0.135	0.14762	4.33374	0.987347	0.990946	0.996368	0.122697	0.124269
0.136	0.14871	4.30256	0.987164	0.990814	0.996315	0.123586	0.125193
0.137	0.14979	4.27186	0.986973	0.990678	0.996260	0.124474	0.126117
0.138	0.15088	4.24160	0.986785	0.990543	0.996206	0.125362	0.127041
0.139	0.15197	4.21178	0.986595	0.990407	0.996152	0.126250	0.127965
0.140	0.15306	4.18239	0.986402	0.990268	0.996096	0.127137	0.128889
0.141	0.15415	4.15343	0.986208	0.990130	0.996040	0.128023	0.129814
0.142	0.15524	4.12488	0.986015	0.989991	0.995984	0.128910	0.130738
0.143	0.15633	4.09673	0.985819	0.989850	0.995927	0.129795	0.131662
0.144	0.15742	4.06898	0.985621	0.989709	0.995871	0.130680	0.132587
0.145	0.15851	4.04162	0.985422	0.989565	0.995813	0.131565	0.133511
0.146	0.15960	4.01463	0.985222	0.989422	0.995755	0.132449	0.134436
0.147	0.16068	3.98801	0.985022	0.989279	0.995697	0.133334	0.135361
0.148	0.16177	3.96177	0.984820	0.989133	0.995639	0.134217	0.136286
0.149	0.16286	3.93587	0.984616	0.988988	0.995580	0.135100	0.137210

M	M*	$\frac{A}{A^*}$	$\frac{P}{P_t}$	$\frac{\rho}{\rho_o}$	$\frac{T}{T_t}$	W_T	W_S
0.150	0.16395	3.81833	0.984410	0.988840	0.995521	0.135982	0.138136
0.151	0.16504	3.88514	0.984204	0.988692	0.995461	0.136884	0.139060
0.152	0.16612	3.86028	0.983995	0.988542	0.995401	0.137745	0.139986
0.153	0.16721	3.83575	0.983786	0.988392	0.995340	0.138626	0.140911
0.154	0.16830	3.81153	0.983577	0.988242	0.995280	0.139507	0.141836
0.155	0.16939	3.78765	0.983364	0.988089	0.995218	0.140387	0.142762
0.156	0.17048	3.76406	0.983152	0.987936	0.995157	0.141268	0.143687
0.157	0.17156	3.74079	0.982936	0.987782	0.995095	0.142145	0.144613
0.158	0.17265	3.71781	0.982721	0.987628	0.995032	0.143024	0.145538
0.159	0.17374	3.69512	0.982505	0.987473	0.994970	0.143902	0.146464
0.160	0.17482	3.67273	0.982287	0.987318	0.994907	0.144779	0.147390
0.161	0.17591	3.65063	0.982066	0.987157	0.994843	0.145656	0.148316
0.162	0.17700	3.62878	0.981847	0.987000	0.994779	0.146533	0.149242
0.163	0.17809	3.60722	0.981625	0.986840	0.994715	0.147409	0.150168
0.164	0.17917	3.58593	0.981400	0.986680	0.994650	0.148284	0.151094
0.165	0.18026	3.56489	0.981176	0.986518	0.994585	0.149159	0.152021
0.166	0.18134	3.54412	0.980951	0.986357	0.994520	0.150034	0.152947
0.167	0.18243	3.52359	0.980723	0.986192	0.994454	0.150907	0.153873
0.168	0.18352	3.50332	0.980495	0.986029	0.994388	0.151781	0.154800
0.169	0.18460	3.48329	0.980264	0.985863	0.994321	0.152653	0.155727
0.170	0.18569	3.46350	0.980033	0.985697	0.994254	0.153525	0.156653
0.171	0.18678	3.44395	0.979799	0.985529	0.994186	0.154397	0.157580
0.172	0.18786	3.42463	0.979565	0.985361	0.994118	0.155268	0.158507
0.173	0.18895	3.40553	0.979331	0.985193	0.994050	0.156139	0.159434
0.174	0.19003	3.38666	0.979094	0.985022	0.993982	0.157008	0.160361
0.175	0.19112	3.36801	0.978857	0.984852	0.993913	0.157878	0.161288
0.176	0.19220	3.34958	0.978617	0.984679	0.993843	0.158747	0.162216
0.177	0.19329	3.33136	0.978376	0.984506	0.993773	0.159616	0.163143
0.178	0.19437	3.31334	0.978136	0.984333	0.993704	0.160484	0.164071
0.179	0.19546	3.29553	0.977893	0.984159	0.993633	0.161351	0.164998
0.180	0.19654	3.27797	0.977649	0.983984	0.993562	0.162217	0.165926
0.181	0.19763	3.26051	0.977403	0.983807	0.993491	0.163083	0.166854
0.182	0.19871	3.24330	0.977157	0.983630	0.993419	0.163949	0.167782
0.183	0.19980	3.22628	0.976908	0.983451	0.993347	0.164814	0.168710
0.184	0.20088	3.20945	0.976658	0.983271	0.993274	0.165678	0.169638
0.185	0.20197	3.19280	0.976409	0.983092	0.993202	0.166542	0.170566
0.186	0.20305	3.17634	0.976157	0.982911	0.993129	0.167405	0.171494
0.187	0.20414	3.16005	0.975904	0.982729	0.993055	0.168268	0.172423
0.188	0.20522	3.14395	0.975648	0.982545	0.992981	0.169130	0.173351
0.189	0.20630	3.12802	0.975393	0.982362	0.992907	0.169991	0.174280
0.190	0.20739	3.11225	0.975138	0.982178	0.992832	0.170852	0.175208
0.191	0.20847	3.09666	0.974879	0.981992	0.992757	0.171713	0.176137
0.192	0.20955	3.08123	0.974621	0.981806	0.992682	0.172572	0.177066
0.193	0.21064	3.06597	0.974360	0.981618	0.992606	0.173431	0.177995
0.194	0.21172	3.05087	0.974098	0.981430	0.992530	0.174290	0.178924
0.195	0.21280	3.03593	0.973833	0.981239	0.992453	0.175147	0.179853
0.196	0.21389	3.02115	0.973569	0.981048	0.992376	0.176005	0.180783
0.197	0.21497	3.00651	0.973305	0.980859	0.992299	0.176862	0.181712
0.198	0.21605	2.99203	0.973037	0.980666	0.992221	0.177717	0.182642
0.199	0.21714	2.97770	0.972770	0.980473	0.992143	0.178573	0.183571

M	M*	$\frac{A}{A^*}$	$\frac{P}{P_t}$	$\frac{\rho}{\rho_o}$	$\frac{T}{T_t}$	W_T	W_S
0.200	0.21822	2.96352	0.972499	0.980279	0.992064	0.179428	0.184501
0.201	0.21930	2.94947	0.972229	0.980084	0.991985	0.180282	0.185431
0.202	0.22038	2.93558	0.971955	0.979887	0.991905	0.181135	0.186361
0.203	0.22146	2.92182	0.971682	0.979690	0.991826	0.181988	0.187291
0.204	0.22255	2.90820	0.971408	0.979493	0.991746	0.182840	0.188222
0.205	0.22363	2.89472	0.971132	0.979294	0.991665	0.183692	0.189152
0.206	0.22471	2.88137	0.970855	0.979095	0.991585	0.184542	0.190082
0.207	0.22579	2.86816	0.970578	0.978893	0.991503	0.185393	0.191013
0.208	0.22687	2.85508	0.970296	0.978692	0.991422	0.186242	0.191944
0.209	0.22795	2.84212	0.970017	0.978491	0.991340	0.187091	0.192874
0.210	0.22904	2.82929	0.969735	0.978287	0.991257	0.187940	0.193805
0.211	0.23012	2.81658	0.969452	0.978084	0.991175	0.188787	0.194736
0.212	0.23120	2.80401	0.969167	0.977878	0.991092	0.189634	0.195667
0.213	0.23228	2.79155	0.968882	0.977672	0.991008	0.190481	0.196599
0.214	0.23336	2.77921	0.968593	0.977464	0.990924	0.191328	0.197530
0.215	0.23444	2.76699	0.968305	0.977257	0.990840	0.192171	0.198461
0.216	0.23552	2.75488	0.968017	0.977049	0.990755	0.193016	0.199393
0.217	0.23660	2.74289	0.967725	0.976839	0.990670	0.193860	0.200325
0.218	0.23768	2.73102	0.967434	0.976630	0.990585	0.194702	0.201257
0.219	0.23876	2.71925	0.967140	0.976417	0.990499	0.195545	0.202188
0.220	0.23984	2.70760	0.966847	0.976205	0.990413	0.196386	0.203121
0.221	0.24092	2.69605	0.966552	0.975993	0.990327	0.197228	0.204053
0.222	0.24200	2.68461	0.966255	0.975779	0.990240	0.198068	0.204985
0.223	0.24308	2.67328	0.965958	0.975565	0.990153	0.198908	0.205917
0.224	0.24416	2.66205	0.965658	0.975348	0.990065	0.199748	0.206850
0.225	0.24524	2.65093	0.965358	0.975132	0.989977	0.200585	0.207783
0.226	0.24632	2.63991	0.965055	0.974913	0.989888	0.201422	0.208715
0.227	0.24739	2.62899	0.964752	0.974694	0.989800	0.202259	0.209648
0.228	0.24847	2.61816	0.964450	0.974476	0.989711	0.203095	0.210581
0.229	0.24955	2.60744	0.964144	0.974255	0.989621	0.203930	0.211515
0.230	0.25063	2.59680	0.963838	0.974035	0.989532	0.204765	0.212448
0.231	0.25171	2.58627	0.963529	0.973812	0.989441	0.205599	0.213381
0.232	0.25279	2.57583	0.963221	0.973589	0.989350	0.206433	0.214315
0.233	0.25386	2.56549	0.962909	0.973364	0.989259	0.207265	0.215249
0.234	0.25494	2.55523	0.962598	0.973139	0.989168	0.208097	0.216182
0.235	0.25602	2.54507	0.962286	0.972914	0.989076	0.208928	0.217116
0.236	0.25710	2.53499	0.961972	0.972687	0.988984	0.209758	0.218050
0.237	0.25817	2.52500	0.961658	0.972460	0.988891	0.210588	0.218985
0.238	0.25925	2.51511	0.961340	0.972231	0.988798	0.211417	0.219919
0.239	0.26033	2.50529	0.961023	0.972002	0.988705	0.212245	0.220853
0.240	0.26141	2.49556	0.960706	0.971773	0.988612	0.213073	0.221788
0.241	0.26248	2.48591	0.960386	0.971541	0.988518	0.213899	0.222723
0.242	0.26356	2.47635	0.960066	0.971310	0.988423	0.214726	0.223657
0.243	0.26463	2.46687	0.959742	0.971076	0.988328	0.215551	0.224592
0.244	0.26571	2.45747	0.959420	0.970843	0.988233	0.216376	0.225528
0.245	0.26679	2.44815	0.959094	0.970608	0.988138	0.217199	0.226463
0.246	0.26786	2.43891	0.958768	0.970372	0.988042	0.218022	0.227398
0.247	0.26894	2.42974	0.958442	0.970137	0.987946	0.218845	0.228334
0.248	0.27001	2.42065	0.958114	0.969899	0.987849	0.219666	0.229269
0.249	0.27109	2.41164	0.957786	0.969662	0.987752	0.220497	0.230205

APPENDIX B

NOISE SUPPRESSOR MODELS

The design data presented in the text of this document were based in large part on scale-model testing. In order to provide access to these models during future efforts, this appendix presents the location of the models at the time of this writing, a description of model capability, and at least one Navy activity with knowledge of the model.

AUGMENTER TUBE TECHNOLOGY MODELS

1/15 Scale NAS Miramar - located at Fluidyne Engineering Corporation

This model hardware was built to scale the initial NAS, Miramar full-scale acoustic enclosure. The model hardware consisted of the forward enclosure, augmenter tube, and exhaust stack. The model hardware is useful for cold (500°R) to hot (3300°R) flow tests.

NAVFAC (0452) is a cognizant Navy contact

1/15 Scale Augmenter Tube Sections - located at NOSC, San Diego

This model hardware was built of metal and consisted of various round and obround augmenter tube sections as well as exhaust stack extensions and turning vane hardware. These augmenter tube sections are useful for testing of alternate temperature/pressure response, alternate acoustic response, and alternate pumping ratio response. The model is useful for cold (500°R) to hot (3300°R) flow tests.

NOSC 5134 is a cognizant Navy Contact

1/15 Scale NAS Patuxent River Hush House - located at Fluidyne Engineering Corporation

This model hardware was constructed of wood and plexiglass to evaluate the flow conditions of the secondary inlet configuration of the NAS, Patuxent River Hush House design.

The model hardware is designed for cold flow (500°R) evaluations. These are useful for aerodynamic evaluations but not acoustic evaluations.

NAVFAC 0452 is a cognizant Navy contact

1/15 Scale Plexiglass of NAS, Miramar - located at Fluidyne Engineering Corporation

This model hardware was constructed of Plexiglass to evaluate methods for reducing visible emissions. This model is designed for cold flow (500°R) evaluations.

NAVFAC 0452 is a cognizant Navy contact

COANDA/REFRACTION TECHNOLOGY MODELS

1/6 Scale Model - Demountable - located at NAEC, Lakehurst, New Jersey

This model hardware was built of metal and consists of a single engine ejector system, Coanda turning system, the exhaust plenum enclosure, and a forward enclosure. The model is capable of cold (500°R) and hot (3300°R) flow testing. There are stack extension sections, as well as pressure and temperature taps available.

NAEC 92724 is a cognizant Navy contact

1/6 Scale Model-C-Cell - located at NAEC, Lakehurst, New Jersey

This model hardware was built of metal and consists of a single engine ejector system, Coanda turning system, and exhaust plenum enclosure. The model is capable of cold (500°R) and hot (3300°R) flow testing. There are stack extensions, as well as pressure and temperature taps available.

NAEC 92724 is cognizant Navy Contact

1/20 Scale Plexiglass - located at NAEC, Lakehurst, New Jersey

This model hardware consists of metal ejector and turning surfaces with plexiglass forward (demountable) enclosure and plexiglass exhaust plenum. The model is capable of cold (500°R) flow testing. The plexiglass allows observation of flow conditions.

NAEC 92724 is a cognizant Navy contact

Full-Scale Demonstration Unit

The only remaining section of the demonstration unit is the IRIS assembly which is used at NARF, Jacksonville, Florida. This unit is the adjustable inlet to the Coanda ejector system. The unit is being used on a conventional C-cell at this time.

The remainder of the demonstration unit hardware has been scrapped.

NAEC 92724 is cognizant Navy contact

STANDARD WET TEST CELL

1/8 Scale C-Cell - located at the Naval Postgraduate School, Monterey, California

This model hardware is built of metal with plexiglass view ports. The model consists of the ram-jet burner, forward enclosure, conventional wet cell augmenter, and conventional demountable exhaust stack. The model can accommodate (cold (500°R) and hot (2100°R) flow testing.

Dr Dave Netzer or NAPC PE: AFK:71 are cognizant Navy contacts.

DEFINITION OF AUGMENTER TUBE TECHNOLOGY AERODYNAMIC/ THERMODYNAMIC SYMBOLS

A	Area
A^*	Choked throat area (M = 1.0)
A_A	Augmenter cross-sectional area
A_{AM}	Primary burner air meter throat area
A_D	Subsonic diffuser exit area
A_{NT}	Jet nozzle throat area
A_{PM}	Pilot burner air meter throat area
A_{SM}	Secondary air meter throat area
A/R	Aspect ratio of augmenter cross section
ARP	Augmentation ratio parameter
D	Diameter
D_A	Augmenter cross-sectional diameter
D_{AM}	Effective diameter of obround augmenter = $\sqrt{4A_A/\pi}$
D_N	Jet nozzle exit diameter
D_{NT}	Jet nozzle throat diameter
L	Length
L_A	Augmenter length

AD-A122 025 GROUND RUNUP NOISE SUPPRESSION PROGRAM PART 3 DRY SUPPRESSOR TECHNOLOGY BASE(U) NAVAL OCEAN SYSTEMS CENTER SAN DIEGO CA R GLASS ET AL. 20 JUN 82 3/3

UNCLASSIFIED NOSC/TR-674 F/G 20/1 NL

END

FILMED

DTIC

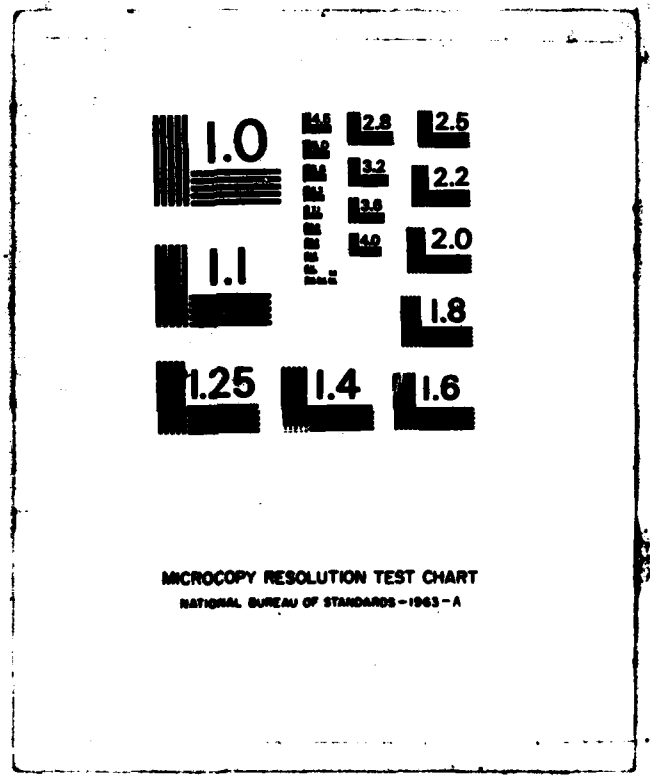
1.0
1.1
1.25
1.4
1.6
2.8
2.5
3.2
2.2
3.6
2.0
4.0
1.8
MICROCOPY RESOLUTION TEST CHART
NATIONAL BUREAU OF STANDARDS-1963-A

DEFINITION OF AUGMENTER TUBE TECHNOLOGY AERODYNAMIC/ THERMODYNAMIC SYMBOLS (Continued)

L_D	Subsonic diffuser length
mw	Molecular weight
mw_{air}	Molecular weight of air
mw_N	Jet exhaust molecular weight
P	Absolute pressure
P_{amb}	(PA) Static pressure outside of Hush House
P_{bar}	(BARO) Local barometric pressure during model tests
P_{BE}	(PSEC) Burner enclosure interior pressure during model tests corresponding to Hush House interior pressure
P_{EE}	(PAMB) Exhaust enclosure pressure during model tests corresponding to Hush House outside ambient pressure
P_{inlet}	Hush House air inlet static pressure
$P_{interior}$	Hush House interior static pressure
P_{NB}	Jet nozzle base pressure
P_{NBp}	Jet nozzle base pressure parameter
P_p	Pressure parameter
P_{shell}	Augmenter shell static pressure

DEFINITION OF AUGMENTER TUBE TECHNOLOGY AERODYNAMIC/ THERMODYNAMIC SYMBOLS (Continued)

P_{SM}	(PSSM) Secondary air meter throat static pressure
P_{wall}	Augmenter wall static pressure
P_T	Total pressure (absolute pressure)
$P_{T_{AM}}$	(PTAM) Primary burner air meter total pressure
$P_{T_{exit}}$	Augmenter plus ramp or augmenter plus diffuser exit total pressure (usually equal to $P_{ambient}$)
$P_{T_{flow}}$	Hush House interior flow total pressure
P_{T_N}	(PTN) Jet nozzle inlet total pressure
$P_{T_{PM}}$	(PTPM) Pilot burner air meter inlet total pressure
$P_{T_{ramp}}$	Ramp exit total pressure
$P_{T_{sec}}$	(PSEC) Secondary (pumped) air flow total pressure
$P_{T_{SM}}$	(PTSM) Secondary air meter inlet total pressure
r	Radius
r_{NT}	Jet nozzle throat radius
T	Absolute temperature

DEFINITION OF AUGMENTER TUBE TECHNOLOGY AERODYNAMIC/ THERMODYNAMIC SYMBOLS (Continued)

T_{amb}	Hush House external ambient temperature
T_{BE}	(TAMB) Burner enclosure air temperature during model tests corresponding to Hush House external ambient temperature
T_{EE}	Exhaust enclosure air temperature during model tests (used in the analysis of acoustical data)
T_{mix}	Average mixed temperature of jet and pumped flows
T_{mix_p}	Average mixed temperature parameter
T_{ramp}	Ramp surface temperature
T_{wall}	Augmenter wall temperature
T_{wall_p}	Augmenter wall temperature parameter
T_T	Total temperature
$T_{T_{AM}}$	(TTAM) Primary burner air meter inlet total temperature
T_{T_N}	(TTN) Jet nozzle total temperature
$T_{T_{PM}}$	Pilot burner air meter inlet total temperature
$T_{T_{SM}}$	(TTSM) Secondary air meter inlet total temperature velocity
V	Velocity

DEFINITION OF AUGMENTER TUBE TECHNOLOGY AERODYNAMIC/ THERMODYNAMIC SYMBOLS (Continued)

V_{av}	Average Velocity
V_{jet}	Ideal jet velocity expanded from P_{T_N} to P_{amb}
$V_{mix\ avg}$	Average mixed velocity in augmenter
$V_{mix\ max}$	Maximum measured core velocity some distance from jet nozzle exit
W	Mass flow rate
$W_{aircraft}$	Aircraft engine exhaust mass flow rate
$W_{air\ meters}$	Sum of primary and pilot air meter mass flow rates during model tests
W_{fuel}	Fuel mass flow rate during model tests
W_{inlet}	Total Hush House inlet mass flow rate
W_N	(WN) Jet nozzle mass flow rate from model tests corresponding to aircraft engine exhaust mass flow rate
W_{pumped}	(WS) Secondary (pumped) air mass flow rate
X	Axial location
X_A	Axial location in augmenter
X_N	Axial distance between jet nozzle exit and augmenter entrance
Y	Lateral distance from jet nozzle centerline at nozzle exit to nearest augmenter wall
Y_{CTR}	Lateral distance from augmenter center to augmenter wall
Y_p	Nozzle centerline lateral position parameter = $\frac{Y - r_{NT}}{Y_{CTR} - r_{NT}}$

DEFINITION OF AUGMENTER TUBE TECHNOLOGY AERODYNAMIC/ THERMODYNAMIC SYMBOLS (Continued)

Z	Vertical distance from jet nozzle centerline at nozzle exit to nearest augmenter wall
Z_{CTR}	Vertical distance from augmenter center to augmenter wall
Z_p	Nozzle centerline vertical position parameter = $\frac{Z - r_{WT}}{Z_{CTR} - r_{WT}}$
α	Angle
α_S	Angle of lateral (sidewise) jet deflection
α_V	Angle of vertical jet deflection
λ_N	Jet nozzle pressure ratio

DEFINITION OF AUGMENTER TUBE TECHNOLOGY
ACOUSTIC SYMBOLS

α	Sound absorption coefficient
c	Wavelength
ρ_{EXIT}	Density of jet exhaust gas at exit plane
ρ_{AMB}	Density of ambient temperature air
δ	Boundary layer thickness
dB	Decibel
dBA	A-weighted sound level
DI	Directivity correction in dB for sound propagation parallel to the ground
f	Frequency of sound
f_F	Full-scale frequency
f_M	Model-scale frequency
f_p	Frequency at which a spectrum of sound power level peaks
Hz	Hertz, unit of frequency
ΔL_{NF}	No-flow attenuation of lined augmenter measured with loudspeaker excitation
ΔL	Total attenuation of jet noise by the lined augmenter, dB
λ_N	Jet nozzle pressure ratio

DEFINITION OF AUGMENTER TUBE TECHNOLOGY AERODYNAMIC/ THERMODYNAMIC SYMBOLS (Continued)

n	Scale factor (full scale dimension/model-scale dimension)
ϕ	Directivity angle: 0° in downstream direction along centerline of exhaust stack
NR	Noise reduction for sound propagating from one room into an adjacent room, dB
PWL	Sound power level, dB re 10^{-12} watt
PWL_{AJ}	Attenuated sound power level of the jet
PWL_{free}	Unattenuated sound power level of the free jet
PWL_{F}	Sound power level of a full-scale jet
PWL_{M}	Measured sound power level of a model jet
PWL_{NF}	Normalized sound power level of a full-scale jet
PWL_{NM}	Normalized sound power level of a model jet
PWL_{outlet}	Sound power level exiting from downstream end of augmenter (with ramp)
PWL_{SN}	Sound power level of self-generated noise of augmenter (ie, noise generated by flow of air; not primary jet noise)
ΔPWL	Measured difference between total free jet sound power level PWL_{free} and sound power level at the augmenter exit PWL_{outlet}, dB

DEFINITION OF AUGMENTER TUBE TECHNOLOGY AERODYNAMIC/ THERMODYNAMIC SYMBOLS (Continued)

ΔPWL_0	Baseline PWL in dB for the condition S_N=4 in; nozzle at F-14 position (Y_p=0.45); 72-in. BBN lined obround augmenter with lined 45° exit ramp; effective obround augmenter diameter of 12 in; T_T=520, 2300, and 3300°R; and T_N=2 and 3.
ΔPWL_s	Shift of sound power level spectrum
ΔPWL_1	Correction to ΔPWL in dB for length of lined augmenter different from 72 in (model-scale)
ΔPWL_2	Correction to ΔPWL in dB for effective diameter of obround augmenter different from 12 in (model-scale)
ΔPWL_3	Correction to ΔPWL in dB for center position of jet nozzle
ΔPWL_4	Correction to ΔPWL in dB for radial or lateral position of the nozzle different from the F-14 position (Y_p=0.45, or model-scale nozzle 3.6 in right of the centerline)
ΔPWL_5	Correction to ΔPWL in dB for angular alignments
R	Distance from augmenter exit, ft
S	Strouhal number = $\frac{fD_N}{U_j}$
S_p	Peak Strouhal number = $\frac{f_p D_N}{U_j}$
SPL	Sound pressure level, dB re 0.0002 dyne/cm^2
$\overline{SPL}$	Room-average SPL

DEFINITION OF AUGMENTER TUBE TECHNOLOGY AERODYNAMIC/ THERMODYNAMIC SYMBOLS (Continued)

$\overline{SPL}'$	Room-average SPL produced by the reference sound source
T_{T_N}	Total jet nozzle temperature in degrees Rankine
T_{60}	Reverberation time; time in seconds for SPL in a room to decay 60 dB
U_{eff}	Effective ramp flow velocity
U_j	Jet exit velocity
V	Velocity
V_O	Arbitrary reference velocity
V_{EX}	Velocity of flow from augmenter exit
$V_{mix\ max}$	Maximum velocity of mixed jet flow at exit
V_j	Jet velocity
Vol	Room volume, m^3
W	Acoustic power, watts
W_{AJ}	Acoustic power of attenuated jet noise at augmenter exit
W_{EXH}	Acoustic power at augmenter exit = $W_{AJ} + W_{SN}$
W_{SN}	Acoustic power of self-generated noise at augmenter exit

DEFINITION OF COANDA/REFRACTION TECHNOLOGY SYMBOLS

A/B	Afterburner
A_{cell}	Cellroom cross-sectional area
A_m	Ejector exit area
A_p	Engine exhaust nozzle area
A_{pi}	Primary air inlet area
AR	Ejector exit aspect ratio
A_{se}	Exhaust stack exit area
A_{si}	Secondary air inlet flow area
A_x	Occupied flow area at engine inlet
A_y	Occupied flow area at engine exhaust
a	Defined quantity for cubic equation solution
b	Defined quantity for cubic equation solution
b_o	Ejector exit height
D_m	Ejector diameter
E	Coanda entrainment ratio
g	Gravitational constant
H	Channel height between acoustic panels

DEFINITION OF COANDA/REFRACTION TECHNOLOGY SYMBOLS (Continued)

H_c	Sudden expansion cavity height
H_o	Ejector exit width
K_t	Sudden expansion loss coefficient
L	Acoustic panel length
L_1	First-stage ejector length
L_2	Second-stage ejector length
L_3	Third stage-ejector length
L_e	Exhaust stack length
M_e	Mach number at acoustic panel exit
M_i	Inlet Mach number
M_o	Ejector exit Mach number (also Mach number incident to Coanda surface)
M_p	Engine exhaust Mach number
M_x	Cellroom Mach number at engine inlet
M_y	Cellroom Mach number at engine exit
P_a	Ambient pressure
P_e	Static pressure at acoustic panel exit

DEFINITION OF COANDA/REFRACTION TECHNOLOGY SYMBOLS (Continued)

P_m	Ejector exit static pressure
P_p	Engine exhaust static pressure
P_{tc}	Total pressure inside enclosure
P_{te}	Total pressure at acoustic panel exit
P_{ti}	Inlet total pressure
P_{tp}	Engine exhaust total pressure
P_x	External engine static pressure at inlet
P_y	External engine static pressure at exit
P	Defined quantity for cubic equation solution
q	Defined quantity for cubic equation solution
R	Ejector pumping ratio
R_1	First-stage ejector equivalent radius
R_2	Second-stage ejector equivalent radius
R_3	Third-stage ejector equivalent radius
R_a	Gas constant for air
R_m	Ejector radius
R_o	Coanda surface radius

DEFINITION OF COANDA/REFRACTION TECHNOLOGY SYMBOLS (Continued)

R_p	Engine exhaust nozzle radius
r	Defined quantity for cubic equation solution
S_{ew}	Exhaust stack width
T_a	Ambient temperature
T_m	Ejector exit static pressure
T_{te}	Exit temperature
T_{tm}	Ejector exit total temperature
T_{tp}	Engine exhaust total temperature
V_{cell}	Cellroom velocity
V_{pi}	Primary air inlet velocity
V_{se}	Exhaust stack exit velocity
V_{si}	Secondary air inlet velocity
W_{1s}	First-stage ejector entrained flow
W_{2s}	Second-stage ejector entrained flow
W_{3s}	Third-stage ejector entrained flow
W_{cs}	Secondary flow entrained by Coanda surface
W_m	Ejector exit weight flow

DEFINITION OF COANDA/REFRACTION TECHNOLOGY SYMBOLS (Continued)

W_p	Engine exhaust weight flow
W_{pi}	Primary air inlet weight flow
W_s	Entrained air weight flow
W_{se}	Total Coanda exit flow
W_{si}	Secondary air inlet weight flow
X	Defined quantity for cubic equation solution
XLE	Ejector length
ϕ	Angle used in cubic equation solution
θ_o	Coanda turn angle
η	Ejector pumping efficiency
γ	Ratio of specific heats